LONG-TERM ATMOSPHERIC MEASUREMENT AND INTERPRETATION

(OF RADIATIVELY ACTIVE TRACE GASES)

Date: April 2012

DECC contract numbers: GA0201

University of Bristol: Simon O'Doherty, Aoife Grant

Met Office: Alistair J. Manning, Maria Athanassiadou

rdscientific: Richard G. Derwent

INSCON: Peter Simmonds

Terra Modus: Dickon Young

Contents

1 Executive Summary

This report details the work undertaken in year one of the DECC contract GA0201 that runs from March 2011 until March 2014. In this first year, one additional site, Ridge Hill near Hereford, has become operational, and a second at Tacolneston, near Norwich, is close to completion. The main site, Mace Head on the east coast of Ireland, has continued to produce high-frequency, high-quality observations. Chapter 3 describes in detail the four measurement sites and the instrumentation employed at each.

Chapters 4 and 5 of this report focus on the on-going analysis of the Mace Head observations. The first of these two chapters describes how they are used to estimate a northern hemisphere baseline concentration for of the observed gases. For each gas a monthly and annual baseline concentration is estimated along with an annual growth rate. The recent rise in nitrous oxide (N_2O), one of the most important greenhouse gases, is cause for some concern as it is also seen across the AGAGE network. The reason for the rise is currently unknown and is under investigation. The concentrations of the CFCs continue to decline whereas the concentrations of their replacements, the HFCs, continue to rise rapidly.

Chapter 5 describes the NAME-Inversion method for estimating regional emissions of trace gases. The method uses above-baseline observed 'pollution' events and knowledge of where the air has recently traversed and how emissions would have diluted, to estimate the emission distribution that would best describe the observations. The NAME (Numerical Atmospheric dispersion Modelling Environment) model is used, coupled to the 3-D meteorology, to describe the dispersion from source to observation point. Where appropriate, for each of the gases observed at Mace Head, UK and North West European (NWEU) emissions are estimated for each year. For some of the principle gases, such as methane and nitrous oxide, observations are available from 1989 and have been used to estimate annual UK emissions from 1990 to 2011 inclusive. The agreement between the UK inventory, as reported to the UNFCCC as part of the Kyoto Protocol, are compared to the NAME-Inversion results. Of particular note is the current agreement between the inventory and the inversion results for methane, unlike in the early 1990s where the inventory is significantly above the inversion estimates.

Chapter 6 describes how vertical profiles of methane concentrations from aircraft measurements over three European locations were used along with modelled profiles to validate surface European emissions of methane both from bottom-up and estimated through inversion modelling. The comparison shows a reasonable agreement overall giving us further confidence both in the modelling approach and the estimated surface emissions. Discrepancies between the modelled and observed profiles highlight possible areas of future improvement. Main areas identified as such, relate to: (a) upper level (stratospheric) intrusions and associated mixing influencing methane profiles in the free troposphere many days and 100's of km away from the intrusion (b) orographic and other processes associated with complex flow not captured in the transport model (c) errors or biases in the background field and (d) transient emissions not captured in the estimated annual averages.

2 Introduction

Monitoring of atmospheric concentrations of gases is important in assessing the impact of international policies related to the atmospheric environment. The effects of control measures on chlorofluorocarbons (CFCs), halons and HCFCs introduced under the 'Montreal Protocol of Substances that Deplete the Ozone Layer' are now being observed. Continued monitoring is required to assess the overall success of the Protocol and the implication for atmospheric levels of replacement compounds such as HFCs. Similar analysis of gases regulated by the Kyoto Protocol on greenhouse gases will likewise assist policy makers.

Since 1987, high-frequency, real time measurements of the principal halocarbons and radiatively active trace gases have been made as part of the Global Atmospheric Gases Experiment (GAGE) and Advanced Global Atmospheric Gases Experiment (AGAGE) at Mace Head, County Galway, Ireland. For much of the time, the measurement station, which is situated on the Atlantic coast, monitors clean westerly air that has travelled across the North Atlantic Ocean. However, when the winds are easterly, Mace Head receives substantial regional scale pollution in air that has travelled from the industrial regions of Europe. The site is therefore uniquely situated to record trace gas concentrations associated with both the mid-latitude Northern Hemisphere background levels and with the more polluted air arising from Europe.

The observation network in the UK is now being expanded to include three additional stations; Angus Tower near Dundee, Tacolneston near Norwich and Ridge Hill near Hereford. Ridge Hill became operational on 1st March 2012, Tacolneston should be operational by the summer 2012. Angus Tower, run by Edinburgh University, has been making measurements since late 2005.

The Met Office's Lagrangian atmospheric dispersion model, NAME (**N**umerical **A**tmospheric dispersion **M**odelling **E**nvironment), has been run for each 2-hour period of each year from 1989 so as to understand the recent history of the air arriving at Mace Head at the time of each observation. By identifying when the air is unpolluted at Mace Head, i.e. when the air has travelled across the Atlantic and the air concentration reflects the mid-latitude Northern Hemisphere baseline value, the data collected have been used to estimate baseline concentrations, trends and seasonal cycles of a wide range of ozone-depleting and greenhouse gases for the period 1990-2011 inclusive.

By removing the underlying baseline trends from the observations and by modelling the recent history of the air on a regional scale, estimates of UK, Irish and North West European (UK, Ireland, France, Germany, Denmark, the Netherlands, Belgium, Luxembourg) emissions and their geographical distributions have been made using EMIT (Emission Modelling Inversion Technique). The estimates are presented as yearly averages and are compared to the UNFCCC inventory.

The atmospheric measurements and emission estimates of greenhouse gases provide an important cross-check for the emissions inventories submitted to the United Nations Framework Convention on Climate Change (UNFCCC). This verification work is consistent with good practice guidance issued by the Intergovernmental Panel on Climate Change (IPCC).

2.1 Publications

Carpenter, L.J., Z.L. Fleming, K.A. Read, J.D. Lee, S.J. Moller, J. Hopkins, R. Purvis, A.C. Lewis, K. Müller, B. Heinold, H. Herrmann, K. Wadinga Fomba, D. van Pinxteren, C. Müller, I. Tegen, A. Wiedensohler, T. Müller, N. Niedermeier, E.P. Achterberg, M.D. Patey, E.A. Kozlova, M. Heimann, D.E. Heard, J.M.C. Plane, A.S. Mahajan, H. Oetjen, S. Vaughan, S.R. Arnold, T. Ingham, D. Stone, L.Whalley, M. Evans, M.J. Pilling, R.J. Leigh, P.S. Monks, A. Karunaharan, J. Tschritter, D. Pöhler, U. Frieß, R. Holla, L. Mendes, H. Lopez, B. Faria, A.J. Manning and D.W.R. Wallace. Seasonal characteristics of tropical marine boundary layer air measured at the Cape Verde Atmospheric Observatory. Journal of Atmospheric Chemistry, Online First, 6 December 2011

Corazza M, P. Bergamaschi, A. T. Vermeulen, T. Aalto, L. Haszpra, F. Meinhardt, S. O'Doherty, R. Thompson, J. Moncrieff, E. Popa, M. Steinbacher, A. Jordan, E. Dlugokencky, C. Brühl, M. Krol, and F. Dentener, Inverse modelling of European N2O emissions: Assimilating observations from different networks, Atmos. Chem. Phys., 11, 2381-2398, 2011

Derwent, R.G., Simmonds, P.G., O'Doherty, Grant, A., Young, D., Cooke M.C., Manning, A.J., Utembe, S.R., Jenkin, M.E., Shallcross, D.E., 2011. Seasonal cycles in short-lived hydrocarbons in baseline air masses arriving at Mace Head, Ireland. *Manuscript submitted to Atmospheric Environment.*)

Ebinghaus, R., S.G. Jennings, H.H. Kock , R.G. Derwent, A.J. Manning, T.G. Spain Decreasing trends in total gaseous mercury observations in baseline air at Mace head, Ireland from 1996 to 2009. Accepted Atmospheric Environment, Jan 2011.

Fleming, Z., P.S. Monks, A.J. Manning, Review: Untangling the influence of air-mass history in interpreting observed atmospheric composition. (2012) Atmos. Res., 104-105, pp. 1-39

Giostra, U., F. Furlani, J. Arduini, D. Cava, A.J. Manning, S.J. O'Doherty, S. Reimann, M. Maione, The determination of a "regional" atmospheric background mixing ratio for anthropogenic greenhouse gases: A comparison of two independent methods, Atmospheric Environment, Volume 45, Issue 39, December 2011, Pages 7396-7405.

Grant A, E. Yates, P.G. Simmonds, R.G. Derwent, A.J. Manning, D. Young, D.E. Shallcross, S. O'Doherty, A five year record of high-frequency in-situ measurements of hydrocarbons at Mace Head, Ireland, Atmos. Meas. Tech., 4, 955-964, 2011

Jones C.E, S. J. Andrews, L. J. Carpenter, C. Hogan, F. E. Hopkins, J. C. Laube, A. D. Robinson, T. G. Spain, S. D. Archer, N. R. P. Harris, P. D. Nightingale, S. J. O'Doherty, D. E. Oram, J. A. Pyle, J. H. Butler, and B. D. Hall, Results from the first national UK inter-laboratory calibration for very short-lived halocarbons, Atmos. Meas. Tech., 4, 865-874, 2011

Keller, C.A, D. Brunner, S. Henne, M.K. Vollmer, S. O'Doherty, S. Reimann, Evidence for under-reported Western European emissions of the potent greenhouse gas HFC-23, Geophys. Res. Lett., 38, L15808, doi:10.1029/2011GL047976, 2011

Logan, J.A., Staehelin, J., Megretskaia, A., Cammas, J. –P., Thouret, V., Claude, H., De Backer, H., Steinbacher, M., Scheel, H.E., Stubi, R., Frohlich, M., Derwent, R., 2011. Changes in ozone over Europe since 1990: analysis of ozone measurements from sondes, regular aircraft (MOZAIC) and alpine surface sites. *Submitted to JGR*.

Manning, A. J., S. O'Doherty, A. R. Jones, P. G. Simmonds, and R. G. Derwent (2011), Estimating UK methane and nitrous oxide emissions from 1990 to 2007 using an inversion modeling approach, J. Geophys. Res., 116, D02305, doi:10.1029/2010JD014763.

Manning, A.J.
The challenge of estimating regional trace gas emissions from atmospheric observations.
Phil. Trans. R. Soc. A 2011, 369, 1943-1954. doi: 10.1098/rsta.2010.0321

Nevison, C.D, E. Dlugokencky, G. Dutton, J.W. Elkins, P. Fraser, B. Hall, P.B. Krummel, R.L. Langenfelds, S. O'Doherty, R.G. Prinn, L.P. Steele, R.F. Weiss, Exploring causes of interannual variability in the seasonal cycles of tropospheric nitrous oxide, Atmos. Chem. Phys., 11, 3713-3730, 2011

Polson, D., D. Fowler, E. Nemitz, U. Skiba, A. McDonald, D. Famulari, C. Di Marco, I. Simmons, K. Weston, R. Purvis, H. Coe, A. J. Manning, H. Webster, M Harrison, D O'Sullivan, C Reeves, D Oram.
Estimation of spatial apportionment of greenhouse gas emissions for the UK using boundary layer measurements and inverse modelling technique (2011)
Atmospheric Environment, 45, 4, pp. 1042-1049. doi:10.1016/j.atmosenv.2010.10.011

Pyle, J. A., M. J. Ashfold, N. R. P. Harris, A. D. Robinson, N. J. Warwick, G. D. Carver, B. Gostlow, L. M. O'Brien, A. J. Manning, S. M. Phang, S. E. Yong, K. P. Leong, E. H. Ung, S. Ong (2011), Bromoform in the tropical boundary layer of the maritime continent during OP3. Atmos. Chem. Phys., 11, pp. 529-542, doi:10.5194/acp-11-529-2011.

Pyle, J. A., N. J. Warwick, N. R. P. Harris, Mohd Radzi Abas, A. T. Archibald, M. J. Ashfold, K. Ashworth, M. P. Barkley, G. D. Carver, K. Chance, J. R. Dorsey, D. Fowler, S. Gonzi, B. Gostlow, C. N. Hewitt, T. P. Kurosu, J. D. Lee, S. B. Langford, G. Mills, S. Moller, A. R. MacKenzie, A. J. Manning, P. Misztal, Mohd Shahrul Mohd Nadzir, E. Nemitz, H. M. Newton, L. M. O'Brien, Simon Ong, D. Oram, P. I. Palmer, Leong Kok Peng, Siew Moi Phang, R. Pike, T. A. M. Pugh, Noorsaadah Abdul Rahman, A. D. Robinson, J. Sentian, Azizan Abu Samah, U. Skiba, Huan Eng Ung, Sei Eng Yong, and P. J. Young. The impact of local surface changes in Borneo on atmospheric composition at wider spatial scales: coastal processes, land-use change and air qualityPhil. Trans. R. Soc. B November 27, 2011 366:3210-3224; doi:10.1098/rstb.2011.0060

Rigby, M., Manning, A.J., Prinn, R. G. (2011) Inversion of long-lived trace gas emissions using combined Eulerian and lagrangian chemical transport models. Atmos. Chem. Phys., 11, 9887-9898.

Rigby, M., R. Prinn, A.J. Manning. The value of high-frequency, high-precision methane isotopologue measurements for source and sink estimation, submitted J. Geophys Res. - Atmospheres

Simmonds, P.G., A.J. Manning, M. Athanassiadou, A. Scaife, The amplitude of the seasonal cycle of nitrous oxide and chlorofluorocarbon atmospheric mixing ratios and the Brewer Dobson circulation., 2011JD017206, submitted Journal of Geophysical Research - Atmospheres.

Simmonds, P. G., Derwent, R.G., Manning, A. J., Grant, A., O'Doherty, S. and Spain, G. Estimation of hydrogen deposition velocities from 1995-2008 at Mace Head, Ireland using a simple box model and concurrent ozone depositions (2011), Tellus B, 63, Issue 1, pp. 40-51. doi: 10.1111/j.1600-0889.2010.00518.x

Skiba, U., S.K. Jones, U. Dragosits, J. Drewer, D. Fowler, R.M. Rees, V. Pappa, L. Cardenas, D. Chadwick, S. Yamulki, A. J. Manning (2011). UK emissions of the greenhouse gas nitrous oxide. *Phil. Trans. R. Soc. B 2012* **367***, 1175-1185, doi: 10.1098/rstb.2011.0356*

2.2 Meetings

DECC meeting (London, 13th October 2011) – Presented new network to DECC and Defra

Non-CO_2 Greenhouse Gas Conference (NCGG6), Amsterdam, The Netherlands, 2-4th November 2011. Emission estimates of HFCs presented.

NCAS meeting, Gerrards Cross, 16th November 2011. Inversion methodology and "New DECC Network" presented

InGOS start-up Meeting (Haarlem, Netherlands, 21-22nd November 2011) – Chaired a session relating to halocarbon calibrations in Europe.

NERC Town meeting, Birmingham, 24th November 2011

Medusa 201 (La Jolla, San Diego, November 2011) – Detailed course on Medusa software operation

AGAGE meeting (La Jolla, San Diego, December 2011) – new network and instrumentation, as well as provisional results using Angus data in the inversion methodology were presented

NERC GHG proposal meeting (Edinburgh, 26th January 2012)

ICOS workshop (France, 16-17th February 2012 – Invited talk about the AGAGE network

DECC meeting (London, 14th March 2012) – Progress meeting

Met Office meeting (Exeter, 29th March 2012) - Progress Meeting

3 Instrumental

The map in figure 1 shows the location of the three new sites, Angus, Ridge Hill and Tacolneston and Mace Head, which has been operational since 1987. Two of the three new sites are currently operational, Angus and Ridge Hill. The site at Ridge Hill was set-up in February with instrumentation installed on the 22nd and 23rd of February. Angus data has been collected since late 2005 and the University of Edinburgh, as collaborators in the project, have provided data from the beginning of March 2011. Problems with the GC-ECD at Angus from the beginning of the project contract have meant N_2O data for the whole of 2011 is unusable in calculating emission estimates using the inversion methodology EMIT (discussed in detail in Part 2 of this report). We anticipate Tacolneston will be operational by summer 2012. The movement of the mobile lab, which houses instrumentation, to the site was not possible due to unforeseen planning applications which have now been approved. Table 1 gives an overview of the gases which are measured at each of the operational sites and specifies which instrument each gas is measured on.

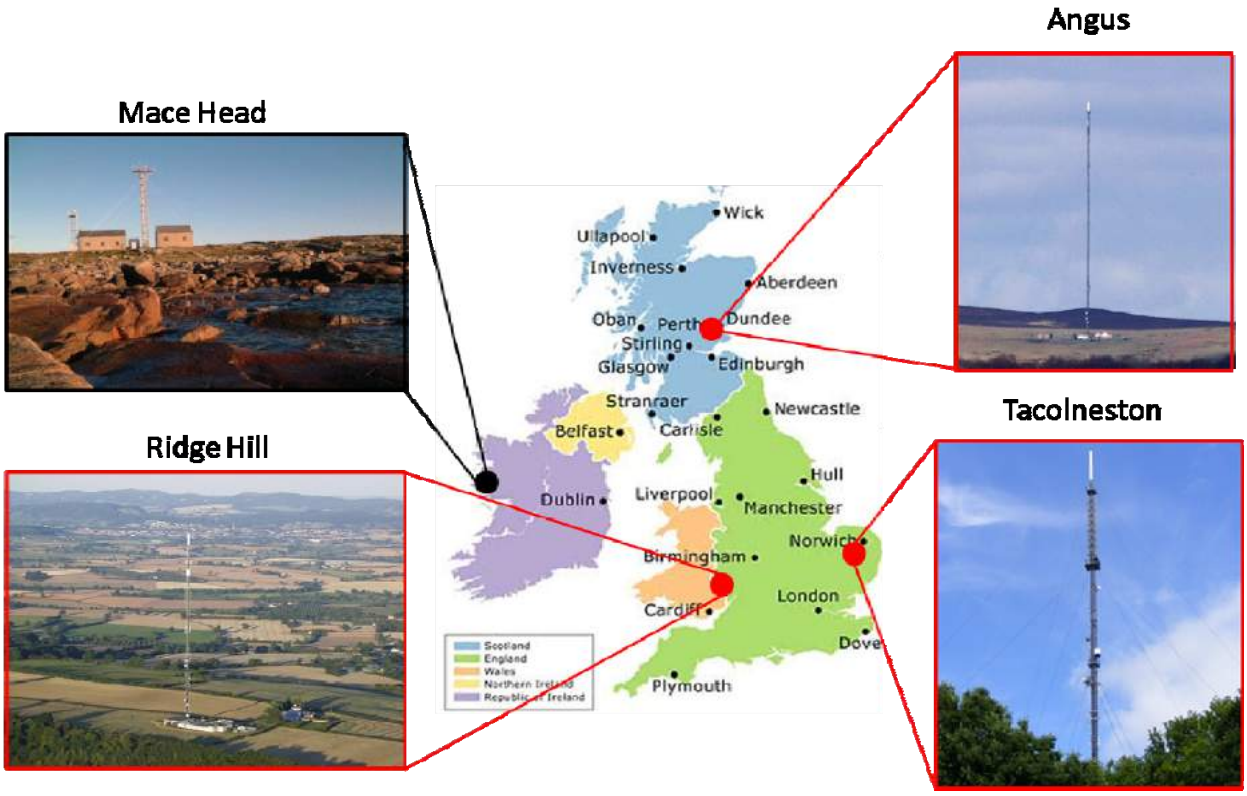

Figure 1: The location of Mace Head and the three new sites in the greenhouse gas measurement network.

Instruments	Mace Head – MHD		Ridge Hill - RGL	Tall Tower Angus - TTA	Tacolneston - TAC
Picarro	CO_2 CH_4 (Also on GC-MD)		CO_2 CH_4		CO_2 CH_4
LiCor	CO_2 (historic data)			CO_2	
GC-ECD	N_2O CFC-12 CFC-11 CFC-113	$CHCl_3$ CH_3CCl_3 CCl_4	N_2O SF_6	N_2O SF_6	N_2O SF_6
GC-FID	CH_4			CH_4	
RGA3/PP1	H_2 CO			H_2 CO	H_2 CO
Medusa	SF_6 CF_4 C_2F_6 C_3F_8 c-C_4F_8 HFC-23 HFC-32 HFC-134a HFC-152a HFC-125 HFC-143a HFC-227ea HFC-236fa HFC-43-10mee HFC-365mfc HFC-245fa HCFC-22 HCFC-141b HCFC-142b HCFC-124	CFC-11 CFC-12 CFC-13 CFC-113 CFC-114 CFC-115 H-1211 H-1301 H-2402 CH_3Cl CH_3Br CH_3I CH_2Cl_2 CH_2Br_2 $CHCl_3$ $CHBr_3$ CCl_4 CH_3CCl_3 $CHCl=CCl_2$ $CCl_2=CCl_2$			All Species measured on the Mace Head Medusa

Table 1: Measurement sites in the new network with gases monitored at each site and the instrument on which they are measured.

3.1 New Sites

3.1.1 Angus

A visit to the Tall Tower at Angus,10 km north of Dundee, was made on Monday the 9th of May 2011 to see how the tower lines and instrumentation were set-up. Figure 2 shows the team that visited the site (top left) and the tower itself which is 230 m high (top right). The sampling inlet is at 222 m up the tower. The bottom half of the image shows the instrumentation set up inside the building next to the tall tower. The centre image shows sampling valves for the GC-FID and ECD which measure CH_4, and N_2O and SF_6 respectively. The lower right image shows where the sample from the line up the tower is split off into the three different instruments.
Measurements made from the Angus tower will enable improved resolution of greenhouse gas emission maps, particularly over Scotland.

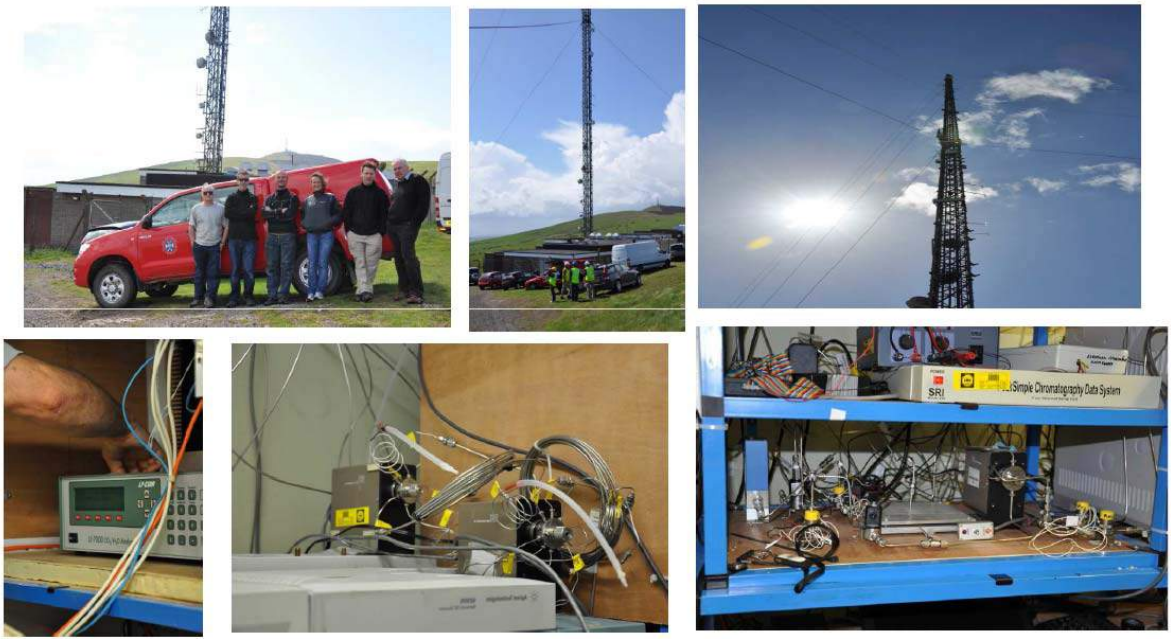

Figure 2: Picture of the tall tower at Angus, Dundee run by the University of Edinburgh (above) with instrumentation set-up (below).

3.1.2 Ridge Hill

Figure 3: The 166.4 metre Tall tower at Ridge Hill (right) with a view of the surrounding countryside (top centre). The grey cabin houses instrumentation and the images on the left show the first measurements of CO_2 and CH_4 taken from the new site at Ridge Hill.

The site at Ridge Hill in Herefordshire has been operational since the 23rd of February (Figure 3). Sampling lines were installed in the first and second weeks of February and civil works were completed on the 12th of February. Equipment was transported from the research lab at the University of Bristol on the 22nd of February and installation of measurement equipment was

completed on the 23rd of February. The site is operating without problems and two weekly site visits are begin made to ensure all instrumentation is running well and there is sufficient calibration and carrier gases.

3.1.3 Tacolneston

Tacolneston will be operational during the summer of 2012.

Part 1 of the installation at Tacolneston was completed in November. The three sample lines up the tall tower at Tacolneston were installed on the 17th and 18th of November. These lines had to be installed in a hurry as the radiofrequency for the tower transmission was being switched on the following week which would mean riggers would not be able to climb the tower above a certain height. The air sampling lines were installed at 50, 100 and 180 meters up the tower and lead down to the base of the tower. Figure 4 shows the top of the 100 m and 180 m sample lines attached to upside down cups. These cups cover the inlet lines to prevent water ingress.

Part 2 of the installation at Tacolneston will involve: Bringing the air sampling lines back along the gantry feeder to the mobile lab which will house instrumentation; Building a concrete plinth for the mobile lab to sit on; and bringing a 32 amp power supply to the mobile lab from the closest power supply in the adjacent building. We were informed by Arqiva in the first week of January that they would need to apply for planning permission to put the mobile lab on the site. This is because the mobile lab will be in place for over 6 months and it is above a certain size. Planning approval was received on the 28th of March. We are now waiting on a build offer for the civil works to supply power and build a plinth for the mobile lab.

The three instruments which will measure trace gases at Tacolneston have been installed in the Mobile Lab and are operating well. On the week of the 19th of December two instruments, the Tacolneston multiple detector (MD) and Tacolneston Picarro were moved into the Mobile Lab, currently at the University of Bristol, and all consumable gases were plumbed up. The Tacolneston Picarro and MD were set running continuously over the Christmas break. On the 10th of January three Synflex air sampling lines were installed in the mobile lab. These lines will be directly connected to those up the tall tower at Tacolneston once at the site. In the interim one of the lines was set-up as per the tower inlet design, with a stainless steel cup with wire gauze over the inlet, facing downward. This prevents water, large particles and insects from entering the tubing. Both instruments ran sampling from this line, as they will at the site, continuously for two months. Instruments were shutdown at the end of February to conserve consumable gases.

On the 10th and 11th of January Stephen Humphrey, the technician from the University of East Anglia who will be maintaining the instruments in the mobile lab, and Dickon Young, who manages the software for all the new sites, came to Bristol to move the Medusa into the Mobile Lab. The move was successful and the Medusa is now operating well. All instruments in the Mobile Lab (Medusa, Picarro and MD) are installed and ready for operation once moved to Tacolneston.


Figure 4: The approximate location of the air sampling lines (180 m, 100 m, 50 m) on the tower at Tacolneston (right). The cups which cover the line inlets at the top of the tower (lower centre) and the mobile lab (bottom left) which will house instrumentation at Tacolneston.

3.2 Instrumentation

3.2.1 Picarro-CRDS

The Picarro G2301 is a cavity ring-down spectrometer (CRDS) which measures concentrations of CO_2 and CH_4 every second. Sample modules were constructed for the two Picarros, one is shown in Figure 5. Air entering the Picarro can then be dried thus minimising the water correction necessary. The sample module also allows calibration standards, a target gas and air samples from different heights of the tower to be measured automatically by the Picarro. A switching valve was fitted in the sampling modules which is plumbed to all the calibration standards and air lines. This valve can then be switched using the Picarro software and the valve position recorded automatically in the Picarro data files.

The G2301 is a wavelength-scanned cavity-ring down spectrometer with a 15-20 km optical path achieved with multiple reflections inside a 35 cm^3 optical cell. It is well suited for automated minimum-maintenance operation at a remote site. For CO_2 and CH_4, the air sample needs to either be dried (achieved e.g. with a Nafion device for CH_4) or corrections applied using the H_2O measurement. Currently one of these is operating at Mace Head, and compares well with the AGAGE Flame Ionisation Detector (FID) measurements made in 2009, after applying water vapour corrections. The sampling scheme consists of an air inlet connected to a primary pump to ensure sufficient flushing of the inlet line. Filters are used to prevent airborne particles from entering the analyser. Calibration is achieved using cylinders with precisely known concentrations spanning the concentration range expected in ambient air. Automatic sampling is achieved using a multi-position valve controlled by the G2301, the sample module. To protect the unit during power a failure, a UPS is used (Figure 5). The G2301 can be

remotely controlled from an external PC, allowing frequent instrument checks from Bristol and timely data retrieval and analysis.

Tanks were purchased for calibration gases. Target gases and calibration standard tanks were filled and calibrated free of change under the Infrastructure for Measurements of the European Carbon Cycle (IMECC) Translational Access at Max Plank Institute Jena by Armin Jordan. This means that all measurements of CO_2 are calibrated under the NOAA X2007 scale and measurements of CH_4 are calibrated under NOAA 2004 scale.

An agreement was setup between the University of Bristol and Integrated Carbon Observing System (ICOS). This enables the data collected at Ridge Hill and Tacolneston to be calibrated using the complex and optimised ICOS database system. Automatic data transfer from the Ridge Hill Picarro to the ICOS server has been setup and the first set of data is being calibrated.

Figure 5: The Picarro installed in the cabin at Ridge Hill with backup power system below (left) and the sample module and Picarro in close up (right).

3.2.2 GC-ECD and Peak Performer 1

The Tacolneston multiple detector (TAC-MD) shown in Figure 6, has two instruemtns measuring from the same sample module. A gas chromatograph with an electron capture detector (GC-ECD) and a Peak Performer 1 (PP1). The PP1 has a mercuric oxide detector which measures H_2 and CO, whilst the electron capture detector (ECD) measures N_2O and SF_6. In this system one sampling module is used with two separate loops for trapping air, these loops filled with air are simultaneously injected onto two set of columns. One set in the GC oven for separating SF_6 and N_2O and the other set in the GC oven of the PP1 to separate H_2 from CO.

The Peak Performer 1 (PP1) is the commercial name for the system optimised to measure H_2 and CO. This ultra-trace level gas detection system monitors low (ppb) concentrations of reducing (combustible) gases with accuracies of ±10 ppb and ±1 ppb for H_2 and CO

respectively. This instrument is fitted with a mercuric oxide bed and, following its reduction, mercury vapour is measured by UV photometry. High instrument sensitivity is attributed to the ease of measurement of mercury vapour at low concentrations, while the instrument shows no response to Ar, He, N_2 or O_2.

Collected gas samples are flowed through a custom made, temperature and pressure controlled sample module before collection in a 1 ml sample loop. Prior to separation samples are dried using a permeation Nafion drier (Permapure, USA) where samples are counter purged with dry air. Gas samples are introduced via electrically actuated gas sampling valves and separated chromatographically within an isothermal mandrel-heated column. Eluted compounds travel directly to the detector which contains a heated bed of mercuric oxide. Following its reduction to mercury vapour ($Hg_{(v)}$) by reducing gas X in the reaction shown below, the resulting vapour is quantitatively determined by precision UV photometry downstream of the reaction bed.

$$X + HgO_{(solid)} \rightarrow XO + Hg_{(vapour)}$$

The detector outlet flow passes through filter for mercury removal before venting. The PP1 is the most popular instrument for making continuous long-term measurements of both H_2 and CO due to its low consumption of inexpensive carrier gas (zero-air) and the low maintenance required. With continuous use of the PP1 mercury lamps only require replacement every 4-6 months and a zero air generator can be run continuously. However a drawback of the PP1 is the detectors non-linear response to increases in concentration of both H_2 and CO. To correct for non-linearity a high concentration standard of accurately known concentration must undergo serial dilution, each of which are run through the PP1 to produce a calibration curve. A quadratic fit can be made through calibration curve which is then used to correct data for non-linearity.

N_2O and SF_6 are separated on three columns (Table 2) before their concentrations are detected using the ECD. This column combination means that O_2 which adversely affects the SF_6 and can be “heart-cut” (i.e. cut out of the sample) and that small SF_6 peak elutes from the column before the large N_2O peak which prevents N_2O tailing into the SF_6.

Pre-Column	1m x 3.7mm I.D., 3/16” O.D. Porapak-Q, 80/100 mesh
Pre-Column Temp. (°C)	90
Main Column	2m x 3.7mm I.D., 3/16” O.D. Porapak-Q, 80/100 mesh
Main-Column Temp. (°C)	90
Post-Column	0.91m x 1/8” O.D. molecular sieve 5A, 40/60 mesh
Post-Column Temp. (°C)	185
Detector	Agilent Electron Capture Detector.
Carrier Gas	Ar/CH_4 5%

Table 2: The specification of the columns, temperatures and carrier gas of the GC-ECD systems at Tacolneston and Ridge Hill.

The ECD is selective to electronegative compounds, especially fluorinated compounds. The ECD detector consists of a stainless steel cylinder containing radioactive nickel-63 in an oven

enclosure that is thermostatically controlled to 350°C. The radioactive nickel-63 in the detector emits electrons (beta particles) which collide with and ionise the make-up gas molecules (argon 95%, methane 5%). This reaction forms a stable cloud of free electrons in the ECD detector. When electronegative compounds enter the ECD cell from the column, they immediately combine with some of the free electrons, temporarily reducing the number remaining in the electron cloud. When the electron population is decreased the pulse rate is increased to maintain a constant current equal to the standing current. This pulse rate is converted to the output signal for the detector. The ECD detector electronics therefore measure the pulse rate needed to maintain the standing current.

Figure 6: The TAC-MD which simultaneously measures SF_6 and N_2O on the ECD (to the right) and CO and H_2 on the PP1 (bottom left).

Figure 7: The GC-ECD installed at Ridge Hill with the compressor and zero air generator below. These provide dry air which in turn dries air samples taken from the tower which are entering the ECD.

3.2.3 Medusa

The Medusa can measure a very wide range of species through pre-concentration techniques. The instrumentation has a unique pre-concentration system coupled with a GCMS (Gas chromatography mass spectrometry) which enables the measurement of a wide range of very high volatility traces gases at low parts per trillion (ppt) levels. It was developed at Scripps Institute of Oceanography with input from the University of Bristol's Atmospheric Chemistry research group and measures the full range of Montreal (ozone depleting) and Kyoto Protocol (global warming) gases. The instrument consists of two traps which trap a 2 litre air sample at very cold temperatures (traps are held at -170°C using specialised equipment). These species are selectively desorbed from the traps and flushed onto the GC columns for separation. On

exiting the GC columns the species are detected via a mass spectrometer, a sophisticated detector which can differentiate between individual gas species unlike ECD and mercuric oxide detectors.

Further detail on the intricate operations of the Medusa is outlined below:

The instrumentation has a unique pre-concentration system coupled with a GCMS (Gas chromatography mass spectrometry) which enables the measurement of a wide range of very high volatility traces gases at low parts per trillion (ppt) levels. Central to the Medusa-GCMS design is the 'Cryotiger' which cools adsorbent traps to -165^{o}C. The use of two traps allows more abundant gases (N_2, O_2, H_2O, CO_2 and CH_4) to be removed prior to further analysis avoiding interference with the lower concentration trace gas species. Trace species are isolated by desorption from the first trap onto a smaller second refocusing trap. The two litre air sample is then injected onto the GC column by flash heating of the second trap to release analytes. The mass spectral detector enables accurate identification of the complex mixtures within the air samples once samples have been separated during chromatography. A sample analysis time of one hour means enables a high measurements frequency of 12 air measurements per day, which are all bracketed by standards. A more in-depth description of the operation of the Medusa follows below. Further details can be found in Miller et al., (2008).

Sample analysis in the Medusa takes place in a number of steps:

- The first valve is a multi-position Valco valve; when selected to take an air sample, the sample flows through two Nafion driers and onto the first trap (T1), held at -65 °C. Analytes are trapped on the Hayesep D adsorbent trap, the rest of the air sample flows through a filter and high precision mass flow controller (MFC) at a rate of 100 scc/min.

- T1 is post-flushed (with helium from EPC4) to remove N_2, O_2, Ar, CH_4

- T1 is heated to 80 °C, CF_4 is transferred to T2.

- T2 is post-flushed at -125 °C to further reduce N_2, O_2, Ar

- T2 heated to 100 °C; CF_4 is back-flushed to the GCMS, through the MS-4A and HiSiv-3000 packed pre-column. This is a micropacked column which separates CF_4 from residual O_2, N_2, N_2O, CO_2, Ar and Kr.

- While CF_4 is analysed, T1 post-flushed at -70 °C to remove CO_2, Xe.

- T1 is heated to 100 °C and back-flushed to transfer analytes to T2, held at -165 °C.

- T2 is post-flushed at -65 °C to further reduce CO_2, Xe.

- T2 is heated to 100 C and back-flushed to transfer analytes to the GCMS (bypassing the pre-column).

- Porabond Q chromatography column programmed from 40 °C to 200 °C at 23 °C/min to separate the flurocarbons, SF_6, halocarbons and NMHCs.

- Custom software under the Linux operating system runs the Medusa and the GCMS in Selective Ion Mode (SIM).

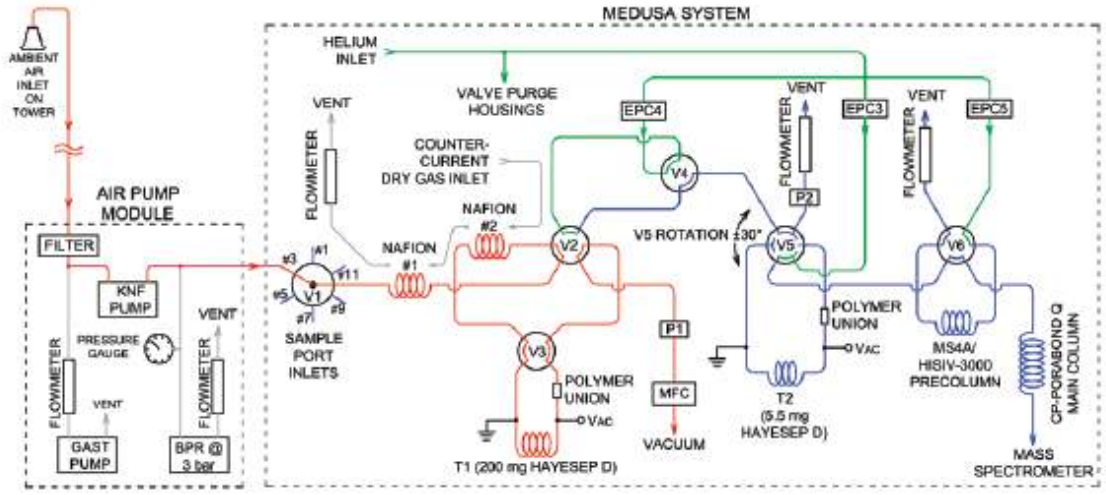

Valve diagram of the Medusa-GCMS setup

4 Atmospheric Northern Hemisphere Baseline Trends

4.1 Introduction

This report presents the results of the analysis of the baseline concentrations of the Mace Head observations from 1990-2011 inclusive. Baseline concentrations are defined here as those that have not been influenced by significant emissions within ten days of the travel, i.e. those that are well mixed and are representative of the mid-latitude Northern Hemisphere background concentrations.

The observations at Mace Head from 1989 to December 2011 have been analysed for each gas measured. The principle tool used to estimate the baseline concentrations is the NAME dispersion model. The methodology used is presented first followed by the analysis of each individual gas. The analysis considers the long term trend of the monthly and annual baseline concentrations, their rate of growth and their seasonal cycle.

4.2 Methodology

This section describes in detail how the monthly baseline concentrations for each gas observed at Mace Head were derived. There are several specific stages to the process and the section is broken down into these segments with examples were possible.

The NAME model is run in backwards mode to estimate the recent history (30 days) of the air en-route to Mace Head. An air history map, such as those shown in figure 8, has been calculated for each 2-hour period from 2003 until Dec. 2011 using UM meteorology and from 1989-2002 using ERA-Interim meteorology, amounting to more than 100000 maps. The model output estimates the 30-day time-integrated air concentration (dosage) at each grid box (40 km horizontal resolution and 0-100m above ground level) from a release of 1 g/s at Mace Head (the receptor). The model is 3-D therefore it is not just surface transport that is modelled, an air parcel can travel from the surface to a high altitude and then back to the surface but only those times when the air parcel is within the lowest 100m above the ground will it be recorded in the maps. The computational domain covers 100^{o}W to 45.125^{o}E longitude and 10^{o}N to 80.125^{o}N latitude and extends to more than 10km vertically (actual height varies depending on version of meteorology used). For each 2-hour period 40,000 inert model particles were used to describe the dispersion. No chemical or deposition processes were modelled, this is realistic given the long atmospheric lifetimes of the vast majority of gases considered.

By dividing the dosage (gs/m^3) by the total mass emitted (3600s/hr x 2hr x 1g/s) and multiplying by the geographical area of each grid box (m^2), the model output is converted into a dilution matrix (s/m). Each element of this matrix *D* dilutes a continuous emission (*e*) of 1 g/m^{2}s from a given grid box over the previous 30 days to an air concentration (g/m^3) at the receptor (*o*) during a 2-hour period.

$$D\,\underline{e} = \underline{o} \qquad \ldots 1$$

Baseline concentrations are defined here as those that have not been influenced by significant emissions within the previous 30-days of travel en-route to Mace Head, i.e. those that are well mixed and are representative of the mid-latitude Northern Hemisphere background concentrations.

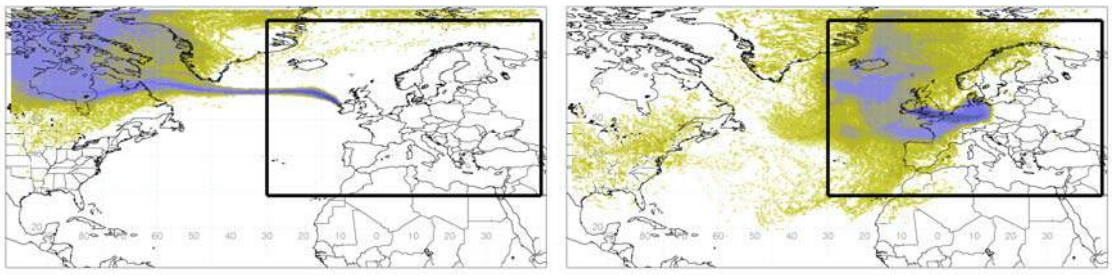

(a) (b)

Figure 8: Examples of 2-hour air history maps derived from NAME (a) baseline period (b) regionally polluted period. The air-history maps describe which surface areas (defined as within 100 m of the surface) in the previous 30-days impact the observation point at a particular time.

A 2-hour period is classed as 'baseline' if it meets the following criteria:

- The total air concentration from the nine grid boxes centred on and surrounding Mace Head is less than ten times the *dilution sensitivity limit* i.e. local emissions do not significantly contribute.
- The total air concentration contribution from the European land mass is less than five times the *dilution sensitivity limit* i.e. European emissions do not significantly contribute.
- The contribution from the southerly latitudes is less than twice the *dilution sensitivity limit* indicating that southerly latitude air is not significantly present.

In order to define a *dilution sensitivity limit* it is necessary to arbitrarily decide on a level of emission that would produce an agreed response at the observation point. In this study we chose an emission of 100 kt CH_4 /yr/grid to produce a 10 ppb impact. As shown later, 10 ppb is approximately the noise found in the baseline signal for methane and an emission of 100 kt/year is about 4% of the estimated UK release of methane in 2006. At a standard temperature of 273.15 K and pressure of 1000 mb, 10 ppb CH_4 is equivalent to ~7 ug/m3. Assuming a horizontal grid resolution of 40 km at a latitude of 50^o N, 100 kt CH_4 /yr/grid is approximately ~2 ug/m^2/s, thus the *dilution sensitivity limit* is calculated, using equation 1, to be 3.4 s/m.

The *dilution sensitivity limit* is attempting to define a threshold above which an emission source would generate a concentration at Mace Head that would be discernible above the baseline noise. The same limit value is used for all of the gases analysed. The chosen limit is arbitrary but the impact of doubling it is small.

Figure 9 shows a three month extract of the methane observations measured at Mace Head. The observations have been colour coded to indicate whether, using the above classification, the air mass they were sampled from was considered baseline. For the baseline analysis all non-baseline observations are removed.

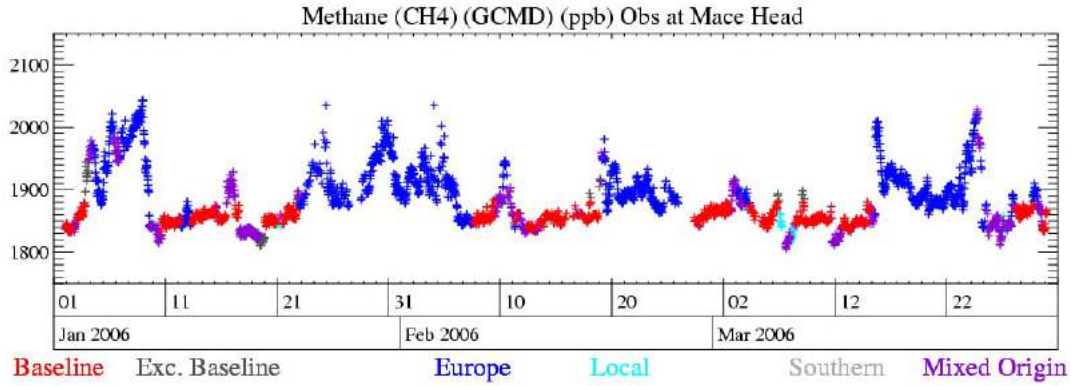

Figure 9: 3-month time-series of Mace Head methane observations showing the impact of the baseline and non-baseline classification. The baseline observations are shown in red.

The points defined as baseline using the above methodology still have a certain level of noise. The principle reasons for this are; emissions from the populated regions of the USA and Canada, unexpected emissions for instance forest fires in Canada or from shipping, local emissions that are not identified using the above criteria above, incorrectly modelled meteorology or transport, i.e. European air defined as baseline by error.

Irrespective of the methodology used to identify these events some will inevitably be classed as baseline when it is inappropriate to do so. To capture such events the baseline data are statistically filtered to isolate and remove these non-baseline observations. For each baseline point in turn, the baseline points in a 40-day window surrounding this central value are considered and, provided that there are sufficient points (>11 with at least 4 in each third of the window or more than 18 in two thirds), a quadratic is fitted to these values. The standard deviation of the actual points and the fitted curve is calculated (*std*) and if the current baseline value is more than *x std* away from the fitted value it is marked for exclusion from the baseline observations. After all baseline points have been considered, those to be excluded are removed. The process is repeated nine times, each time the value for *x* is gradually reduced from 6 to 2, thus ensuring that those points statistically far from the fitted baseline do not unduly affect the points to be excluded by skewing the fitted curve. If there are insufficient baseline points in a 40 day window the values are only included if the spread in the points is small and there are at least 5. The observations removed through this statistical filter are shown in black in figure 9.

For each hour in the time-series the baseline points in a running 40-day window are fitted using a quadratic function and the value extracted for the current hour in question. The process is then advanced by an hour and repeated. If there are insufficient baseline points well spaced within the window (at least 3 in each quarter) it is gradually extended up to 150-days.

For each hour within the observation time record a smoothed baseline concentration is estimated by taking the median of all fitted baseline values within a 20-day time window. If there are fewer than 72 baseline values in the time window then the window is steadily increased up to a maximum of 40 days. If there are still insufficient points then no smoothed baseline concentration is estimated for that hour.

The noise or potential error in the smoothed baseline concentration is estimated to be the standard deviation of the difference between the observations classed as baseline and the smoothed baseline concentrations at the corresponding times. Figure 10 shows, on a much expanded y-axis compared to figure 9, the typical spread of baseline observations about the smoothed continuous baseline estimate.

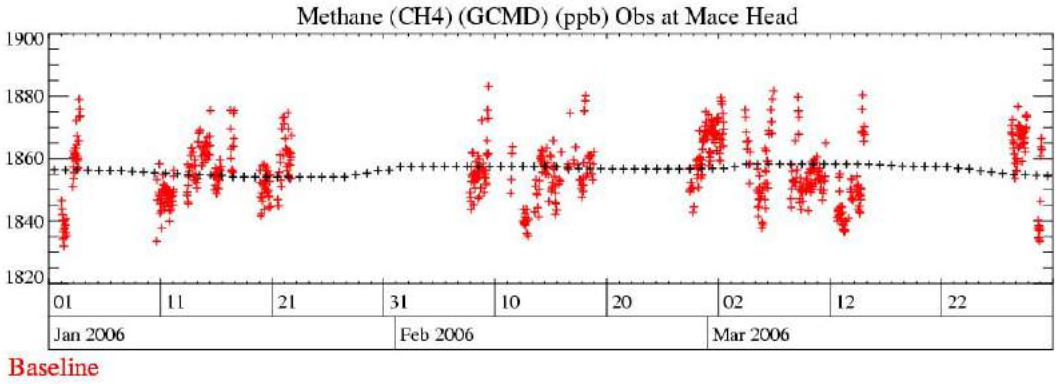

Figure 10: Observations of methane at Mace Head within a 3-month period classed as baseline (red) with the estimated daily baseline concentrations for the same period (black). Note: the y-axis has been expanded compared to figure 9.

Monthly and annual baseline concentrations are estimated by averaging all of the hourly baseline values within the appropriate time window. A monthly value is estimated if there are at least 504 hourly values (21 days) within the month, this ensures a good representation of the whole month.

The annual growth rate on a particular day is defined as the current daily baseline value minus the previous year's value on the same day, e.g. Growth rate for 14th Jan 1996 = (Daily baseline for 14th Jan 1996) – (Daily baseline for 14th Jan 1995). By averaging the annual growth rate values (one per day) within a running 12-month period (6 months either side of the day), a smoothed annual growth rate per day is estimated. Monthly averages of these growth rates for methane and nitrous oxide are shown in figures 49 and 55.

The monthly baseline concentrations were de-trended to produce perturbation values (S_i) for each month and year using equation (**2**):

$$S_i = C_i - a_i \qquad \ldots 2$$

Where C_i is a monthly mean baseline concentration and a_i is the annual average baseline for month i. a_i is calculated by fitting a quadratic function to five consecutive annual averages (a_1 to a_5) centred on the current month of interest and extracting the appropriate value from the quadratic fit. The de-trended perturbation values (S_i) are averaged for each month over the data period studied to produce the mean values shown in figures 11 - 57. The range of values for each month is also shown on the plots.

4.3 Baseline Concentrations

For each gas observed at Mace Head a baseline analysis has been performed. ECMWF meteorology is used from 1989 – 2002 inclusive and Met Office meteorology from 2003-2011 inclusive. The figures that follow illustrate for each gas the monthly and annual baselines, the changing baseline growth rates and the average seasonal cycle seen within the observations. The gases are grouped into similar chemical families; CFC, HCFC, HFC, fluorine compounds (PFCs), chlorine compounds, bromine compounds (halons), hydrocarbons, oxides of carbon and finally nitrous oxide, ozone and hydrogen. Table 1 summaries the annual baseline mass mixing ratios within the observation period for each of the gases considered.

Gas	1990	1991	1992	1993	1994	1995	1996	1997	1998	1999
CFC-11 (GCMD)	264	267	268	269	268	267	266	264	263	261
CFC-12 (GCMD)	496	506	516	522	529	533	537	540	542	544
CFC-13										
CFC-113 (GCMD)	75.4	81	84.2	85	84.6	84.6	84.3	83.8	83.2	82.7
CFC-113										
CFC-114										
CFC-115										8
HCFC-124										1.3
HCFC-141b						5.1	7.2		11.3	13.3
HCFC-142b						8	9.2	10.6	11.3	12.4
HCFC-22										145
HFC-125										1.3
HFC-134a						2.3	4.3	6.3	9.5	13.3
HFC-143a										
HFC-152a						1.2	1.2	1.3	1.9	2.2
HFC-23										
HFC-32										
HFC-227ea										
HFC-236fa										
HFC-245fa										
HFC-365mfc										
PFC-14										
PFC-116										
PFC-218										
SF_6										
SO_2F_2										
CH_3Cl										534
CH_2Cl_2							36.1	36	34.7	31.8
$CHCl_3$ (GCMD)						12.2	12.5	11.9	12	11.4
$CHCl_3$							12.4	11.9	12.5	12.8
CH_3CCl_3 (GCMD)	151	152	150	139	125	111	95	80	66	55
CH_3CCl_3										
CCl_4 (GCMD)			105	104	103	102	101	100	99	98
$CHClCCl_2$										
CCl_2CCl_2										
CH_3Br										10.9
Halon-1211						3.5	3.6		4	4.2
Halon-1301										2.8
Halon-2402										
CH_2Br_2										
$CHBr_3$										
CH_3I										
CH_4 (ppb)	1791	1806	1803	1812	1816	1821	1824	1822	1835	1840
C_2H_6										
C_6H_6										
CO						117	128	117	146	124
CO_2 (ppm)				357	359	361	363	364	367	369
N_2O (ppb)	309	310	310	311	312	312	313	314	314	315
O_3 (ppb)	34.6	36.3	35.4	35.1	36.5	35.4	37.2	37	40.5	41.4
H_2 (ppb)						496	502	494	506	508

Table 3: Annual Northern hemisphere baseline mass mixing ratios for all gases measured at Mace Head 1990-1999 (ppt unless stated).

Gas	2000	2001	2002	2003	2004	2005	2006	2007	2008	2009	2010	2011
CFC-11 (GCMD)	260	259	256	255	253	250	248	246	244	243	241	238
CFC-12 (GCMD)	546	546	546	546	545	544	543	541	539	536	533	531
CFC-13					2.8	2.8	2.9	2.9	2.9	2.9	2.9	3
CFC-113 (GCMD)	82.2	81.5	80.7	79.9	79.3		77.8	77.1	76.6	76	75.3	74.9
CFC-113						78.8	77.9		76.6	76	75.2	74.6
CFC-114					16.6	16.7	16.6	16.5	16.5	16.5	16.4	16.4
CFC-115	8.1	8.2	8.1	8.2	8.4	8.4	8.4	8.3	8.4	8.4	8.4	8.4
HCFC-124	1.4	1.6	1.6	1.6	1.6	1.6	1.6	1.6	1.6	1.6	1.5	1.5
HCFC-141b	15.1	16.3	17.6	18.6	19.1	19.1	19.6	20.4	21	21.3	22	23.1
HCFC-142b	13.6	14.6	15	15.5	16.2	17	18.1	19.3	20.6	21.4	21.9	22.7
HCFC-22	151	158	164	169	175	180	187	195	204	212	219	226
HFC-125	1.6	2.1	2.4	3.1	3.6	4.3	5	5.8	6.9	7.9	9.2	10.8
HFC-134a	17.1	20.7	24.9	29.6	34.6	39.3	43.7	48	53.3	58	63.3	68.4
HFC-143a					5.5	6.4	7.4	8.4	9.6	10.7	11.9	13.2
HFC-152a	2.5	2.9	3.4	4.1	4.8	5.6	6.8	7.9	8.8	8.9	9.4	10
HFC-23									22.5	23.1	23.7	24.6
HFC-32					1	1.6	2.1	2.7	3.4	4.1	5.1	6.5
HFC-227ea								0.4	0.5	0.6	0.6	0.7
HFC-236fa								0.1	0.1	0.1	0.1	0.1
HFC-245fa								0.9	1.1	1.2	1.3	1.5
HFC-365mfc					0.2	0.3	0.4	0.5	0.5	0.6	0.6	0.7
PFC-14					74.9	75.5	76.2	76.9	77.7	78.1	78.7	79.5
PFC-116					3.7	3.7	3.8	3.9	4	4.1	4.1	4.2
PFC-218					0.4	0.5	0.5	0.5	0.5	0.5	0.6	0.6
SF_6					5.6	5.8	6.1	6.3	6.6	6.9	7.2	7.5
SO_2F_2						1.5	1.5	1.6	1.6	1.7	1.7	1.8
CH_3Cl	517	512	511	522	519	526	520	527	532	531	529	519
CH_2Cl_2	30.2	29	29.3	31.1	30.9	30.7	32.2	34.3	36	36.7	40	38.8
$CHCl_3$ (GCMD)	10.9	10.9	11	11.2	11.2	11.1	11.2	11.1	11.4	10.9	11.6	11.5
$CHCl_3$	11.5	10.9	10.4	10.9	10.7	10.8	10.9	10.5	10.4	9.9	10.8	10.9
CH_3CCl_3 (GCMD)	47	39	32	27	23	19	16	13	11	9	8	7
CH_3CCl_3		39.1	31.1	26.8	23	18.8	15.7	13.1	11	9.3	7.8	6.5
CCl_4 (GCMD)	97	96	95	94	93	92	91	90	89	88	87	86
$CHClCCl_2$	1.4	1.4				1	0.9	1	0.8	0.5	0.5	0.4
CCl_2CCl_2		5	4.7	4.7	4.7	3.9	3.8	3.5	3.4	3	3	2.7
CH_3Br	10.5	9.9	9.1	8.8	9.1	10.3	9.5	9.1	9.2	8.6	8.3	8.4
Halon-1211	4.3	4.4	4.4	4.4	4.5	4.5	4.5	4.4	4.4	4.3	4.3	4.2
Halon-1301	2.9	3	3	3.1	3.1	3.2	3.2	3.2	3.3	3.3	3.3	3.3
Halon-2402						0.5	0.5	0.5	0.5	0.5	0.5	0.5
CH_2Br_2							1.5	1.6	1.6	1.6	1.7	1.6
$CHBr_3$						5.7	6	4.6	4.6	4.6	5.2	4.3
CH_3I		1.4	1.5	1.6	1.9	1.9	1.3	1.6	1.4	0.9	0.9	0.9
CH_4 (ppb)	1842	1841	1842	1852	1848	1847	1846	1855	1864	1868	1870	1875
C_2H_6						1266	1305	1337	1342	1066	1059	
C_6H_6						64.7	62.6	61.6	68.1	61.3	58.1	
CO	118	117	126	137	122	123	123	120	119	115	121	117
CO_2 (ppm)	369	371	373	375	377	379	382	384	386	387	390	
N_2O (ppb)	316	317	318	318	319	320	320	321	322	323	323	324
O_3 (ppb)	41	39.1	40	41.2	40.6	39.9	41.1	39.6	40.2	40.5	39.5	40.1
H_2 (ppb)	499	496	497	500	497	500	503	499	501	498	498	504

Table 4: Annual Northern hemisphere baseline mass mixing ratios for all gases measured at Mace Head 2000-2011 (ppt unless stated).

Gas	Growth	Latest Growth
CFC-11 (GCMD)	-1.11	-2.12
CFC-12 (GCMD)	1.92	-2.53
CFC-13	0.02	0.03
CFC-113 (GCMD)	0.05	-0.62
CFC-113	-0.67	-0.71
CFC-114	-0.04	-0.05
CFC-115	0.04	0.01
HCFC-124	0.02	-0.05
HCFC-141b	1.01	0.82
HCFC-142b	0.92	0.6
HCFC-22	6.84	7.13
HFC-125	0.74	1.42
HFC-134a	4.15	5.26
HFC-143a	1.1	1.24
HFC-152a	0.56	0.47
HFC-23	0.67	0.8
HFC-32	0.75	1.22
HFC-227ea	0.07	0.07
HFC-236fa	0.01	0.01
HFC-245fa	0.15	0.16
HFC-365mfc	0.08	0.05
PFC-14	0.65	0.66
PFC-116	0.08	0.08
PFC-218	0.02	0.02
SF_6	0.27	0.28
SO_2F_2	0.06	0.09
CH_3Cl	-1.85	-6.32
CH_2Cl_2	0.22	1.05
$CHCl_3$ (GCMD)	-0.06	0.23
$CHCl_3$	-0.09	0.45
CH_3CCl_3 (GCMD)	-7.13	-1.28
CH_3CCl_3	-3.23	-1.4
CCl_4 (GCMD)	-1.03	-1.06
$CHClCCl_2$	-0.1	-0.07
CCl_2CCl_2	-0.22	-0.12
CH_3Br	-0.23	-0.18
Halon-1211	0.03	-0.07
Halon-1301	0.05	0.01
Halon-2402	-0.01	-0.01
CH_2Br_2	0.01	0.02
$CHBr_3$	-0.22	-0.19
CH_3I	-0.06	0.04
CH_4 (ppb/yr)	4.04	2.68
C_2H_6	-52.11	-149.1
C_6H_6	-0.94	-3.71
CO	0.1	1.36
CO_2 (ppm/yr)	1.93	2.47
N_2O (ppb/yr)	0.71	0.8
O_3 (ppb/yr)	0.26	0.05
H_2 (ppb/yr)	0.36	3.1

Table 5: Northern hemisphere baseline growth rates for all gases measured at Mace Head (ppt/yr unless stated): all years (first column) and current (last column).

4.3.1 CFCs

The time series of baseline selected (i.e. minus pollution events) monthly means for atmospheric chloro-flouro-carbons are shown; CFC-11 (Figure 11), CFC-12 (Figure 12), CFC-113 (Figure 13), CFC-114 (Figure 14) and CFC-115 (Figure 15).

The emissions of all of the CFC compounds have decreased substantially in response to the Montreal Protocol on Substances that Deplete the Ozone Layer, the rate of removal of these compounds by their sinks is limited by their long atmospheric lifetimes.

CFC-11 (45 year lifetime) has also declined over the same period at a rate of 2.1 ppt/yr where its mixing ratio at Mace Head is 237.9 ppt in December 2011 (Figure 11). Similarly, CFC-12, which has a 100 year lifetime, has declined at a rate of 2.5 ppt/yr over 2011 reaching a mixing ratio in December 2011 of 530.9 ppt (Figure 12). It was reported in the 2010 WMO Ozone Assessment, that the decline in these CFCs has been smaller than projected. This is most likely due to releases of these compounds from banks being fairly constant over time rather than declining over time as was originally expected.

As shown in Figure 13, CFC-113 (85 year lifetime) declined at a rate of 0.7 ppt/yr in 2011 to 75.0 ppt in December, 2011. Again the decline is less than had been projected, this time the reason is most likely due to the potential presence of small residual emissions.

The mixing ratios of the two less abundant CFCs, CFC-114 and CFC-115, have not changed appreciably since 2006. Their atmospheric abundances and growth rates are 16.4 and 8.4 ppt, and -0.05 and 0.01 ppt/yr respectively.

4.3.1.1 CFC-11

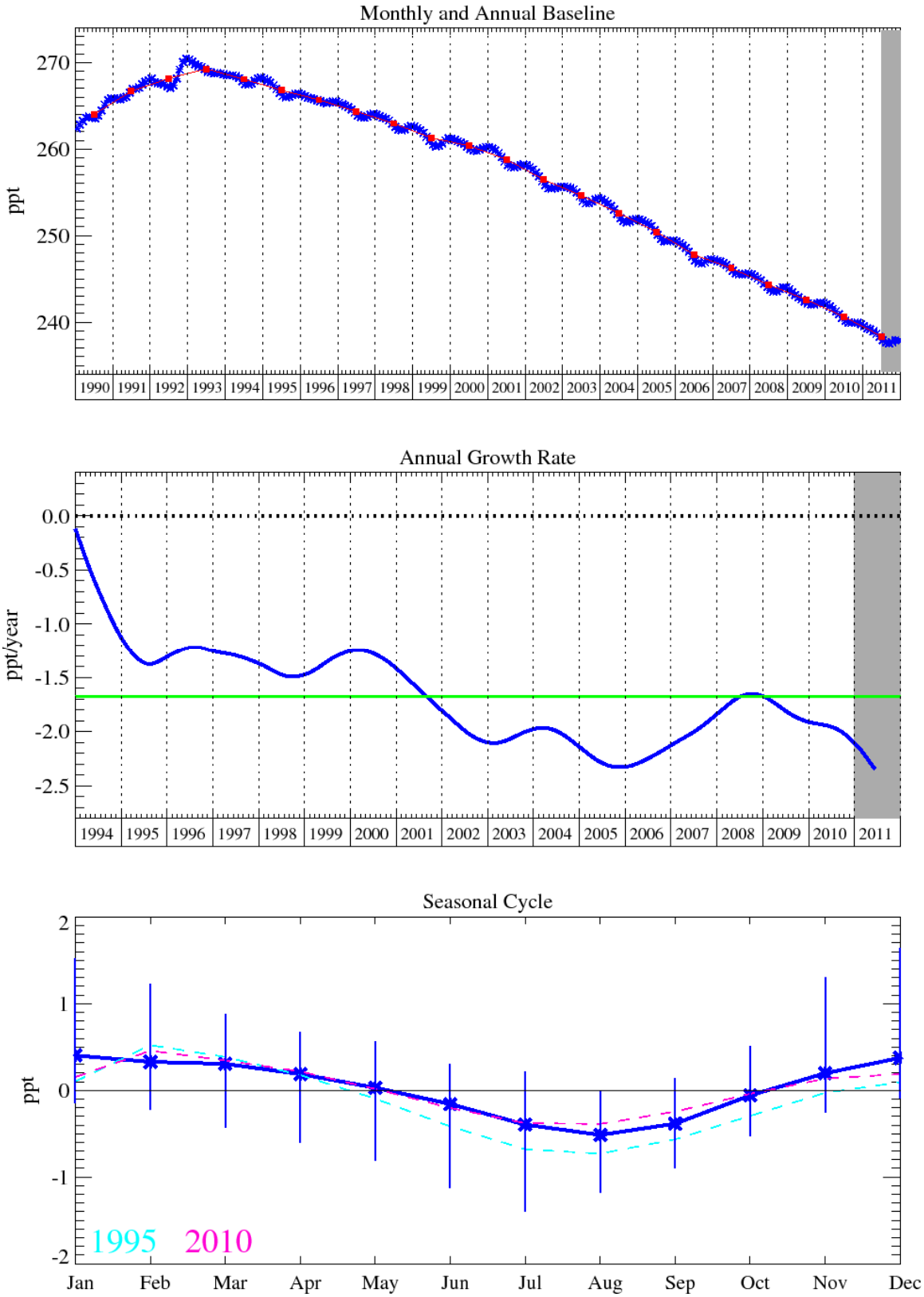

Figure 11: CFC-11: Monthly (blue) and annual (red) baseline (top plot). Annual (blue) and overall average growth rate (green) (middle plot). Seasonal cycle (de-trended) with year to year variability (lower plot).

4.3.1.2 CFC-12

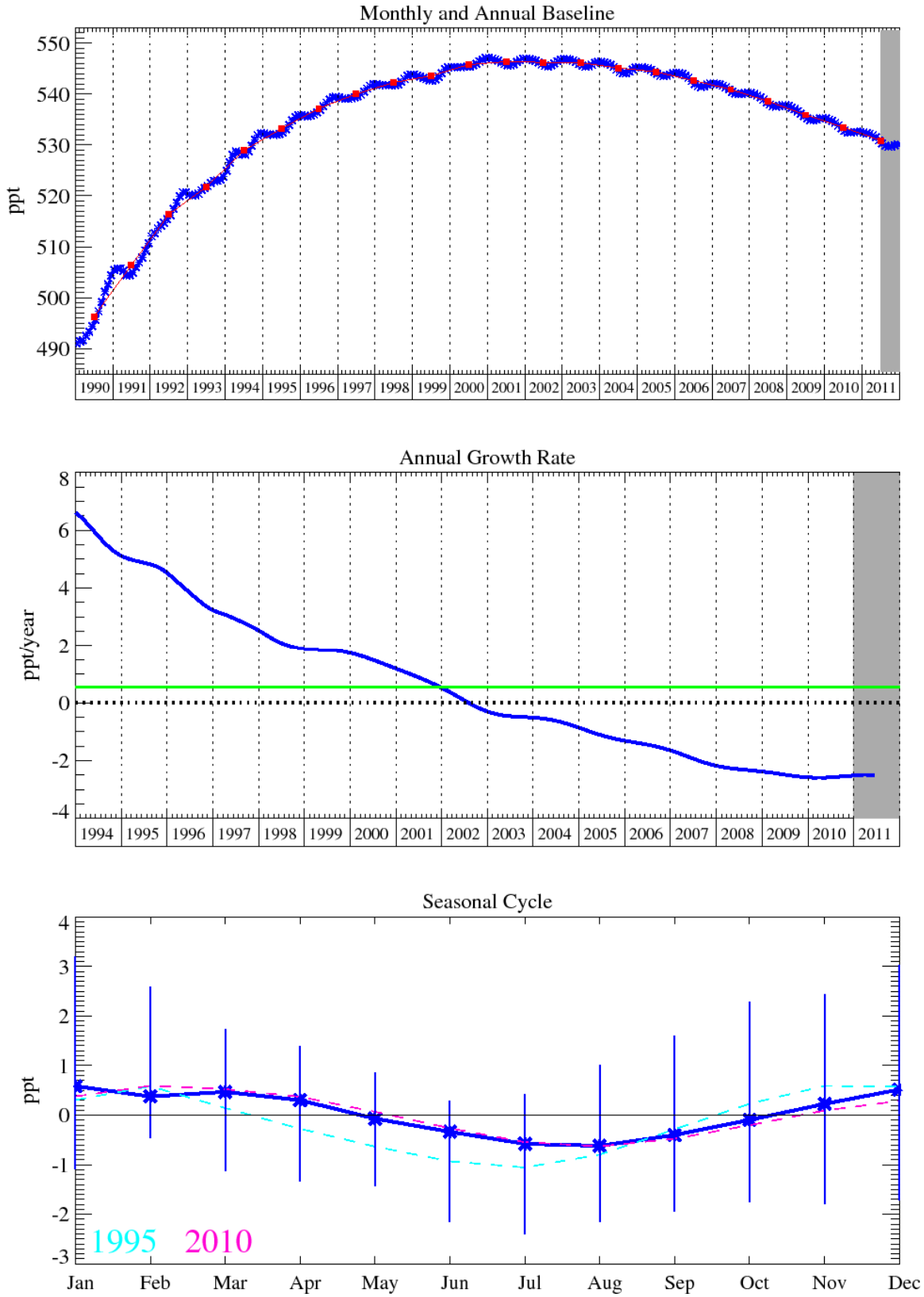

Figure 12: CFC-12: Monthly (blue) and annual (red) baseline (top plot). Annual (blue) and overall average growth rate (green) (middle plot). Seasonal cycle (de-trended) with year to year variability (lower plot).

4.3.1.3 CFC-113

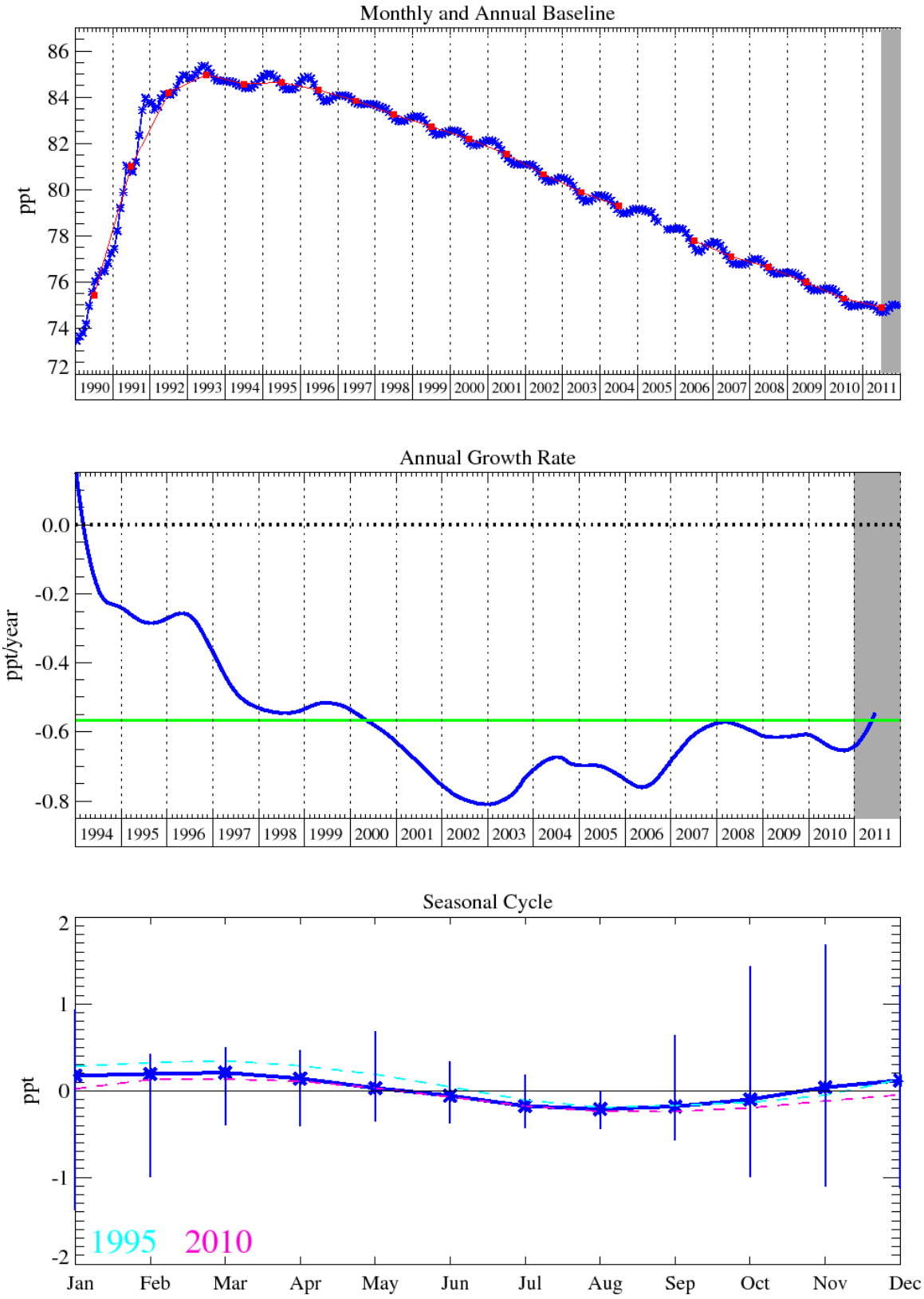

Figure 13: CFC-113: Monthly (blue) and annual (red) baseline concentrations (top plot). Annual (blue) and overall average growth rate (green) (middle plot). Seasonal cycle (de-trended) with year to year variability (lower plot).

4.3.1.4 CFC-114

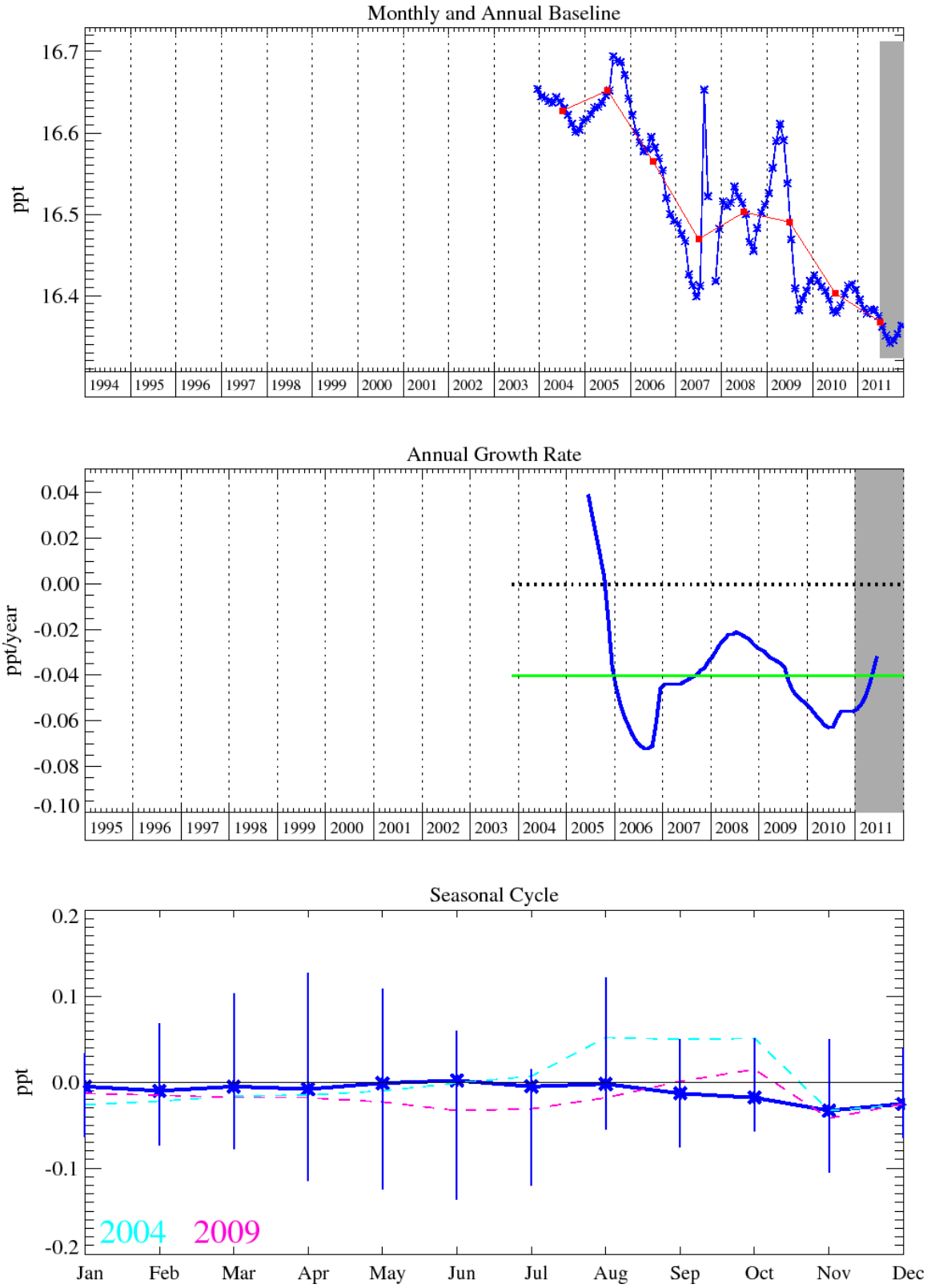

Figure 14: CFC-114: Monthly (blue) and annual (red) baseline concentrations (top plot). Annual (blue) and overall average growth rate (green) (middle plot). Seasonal cycle (de-trended) with year to year variability (lower plot).

4.3.1.5 CFC-115

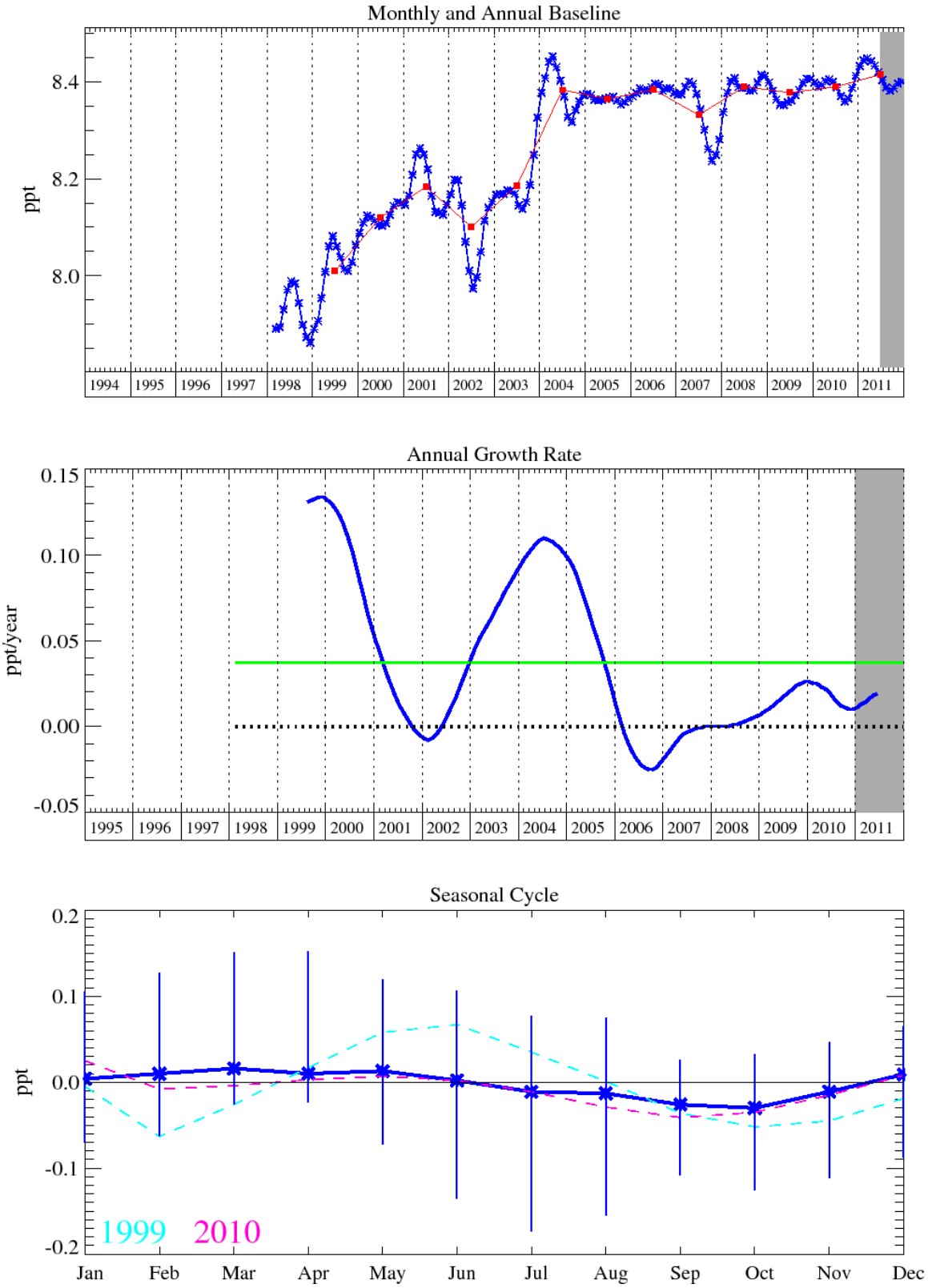

Figure 15: CFC-115: Monthly (blue) and annual (red) baseline concentrations (top plot). Annual (blue) and overall average growth rate (green) (middle plot). Seasonal cycle (de-trended) with year to year variability (lower plot).

4.3.2 HCFCs

Over the past 12-months HCFC-22, the dominant globally produced HCFC compound, has grown at a rate of 7.1 ppt/yr and has currently reached a level at Mace Head of approximately 229.5 ppt (December 2011). This rate of growth has steadily slowed from it's maximum at the end of 2007. HCFC-142b and HCFC-141b have also continued to grow in the atmosphere at increased rates since 2003 and 2005 respectively. Similar to HFCF-22, the rate of growth for HCFC-142b also peaked in 2007 and has declined since then. Prior to these dates HCFC-142b and HFCF-141b showed decreased growth in the atmosphere in line with their expected phase-out. Analysis of the HCFC content of regionally-polluted air arriving at Mace Head from the European continent shows that European emissions reached a peak during 2000-2001 and have subsequently declined following the phase-out in their usage. The reductions are consistent with the phase-out of HCFC production and use from the year 2001 onwards mandated by European regulations designed to exceed the requirements of the Montreal Protocol. In the US implementation of HCFC phase-out through the Clean Air Act Regulations, 2004 resulted in no production or importation of HCFC-141b since 2003, these restriction do not apply to HCFC-142b until 2010. Increasing evidence indicates that increased emissions of these compounds from Asia, in particular China are now offsetting the phase-out in developed countries. The 2011 growth rates of HCFC-141b and 142b are 0.8 and 0.6 ppt/yr respectively. The growth rates of these compounds, calculated from the baseline monthly mean mixing ratios shown in figures 17 and 18, are also presented in Table1c.

4.3.2.1 HCFC-124

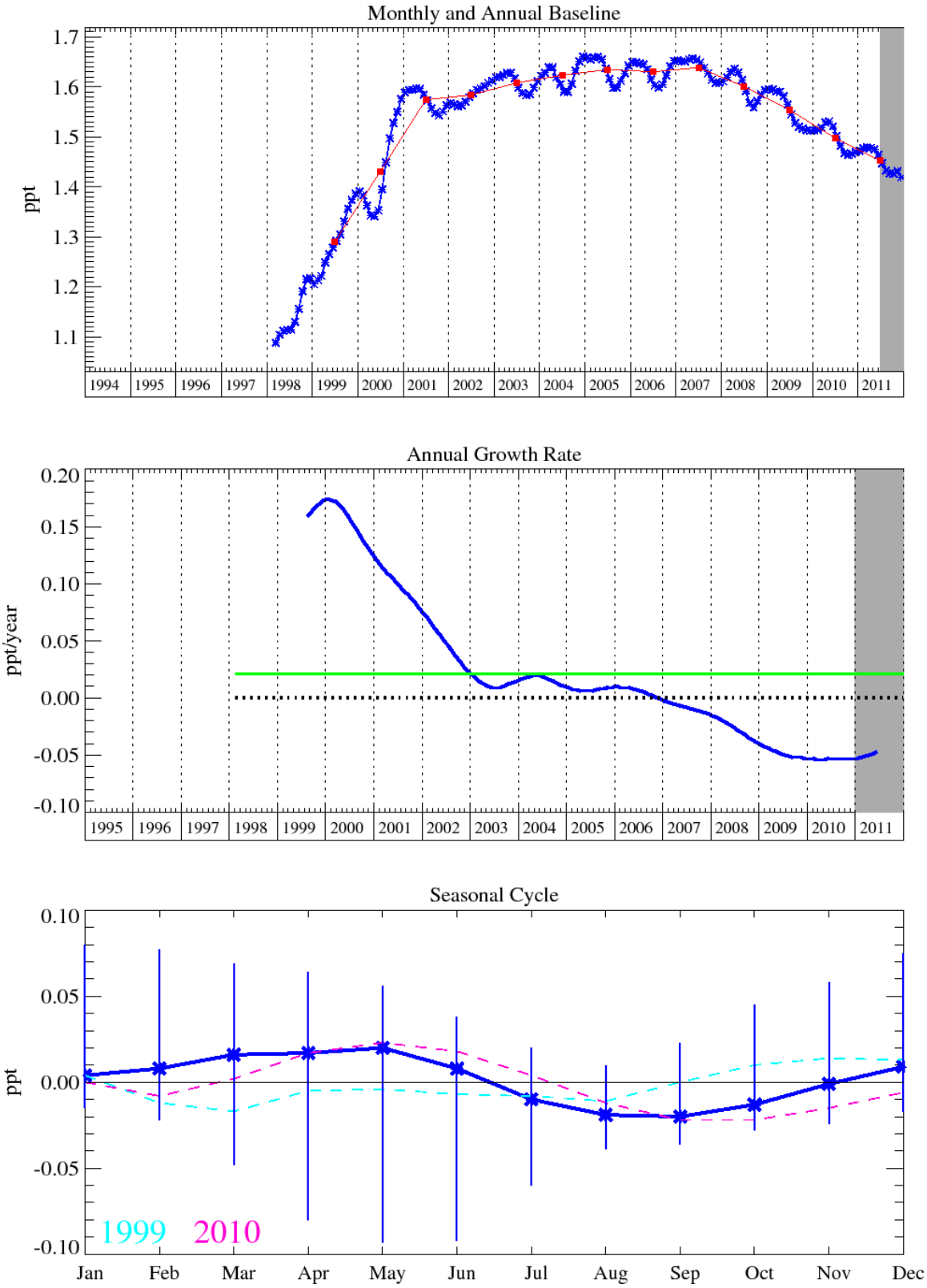

Figure 16: HCFC-124: Monthly (blue) and annual (red) baseline concentrations (top plot). Annual (blue) and overall average growth rate (green) (middle plot). Seasonal cycle (de-trended) with year to year variability (lower plot).

4.3.2.2 HCFC-141b

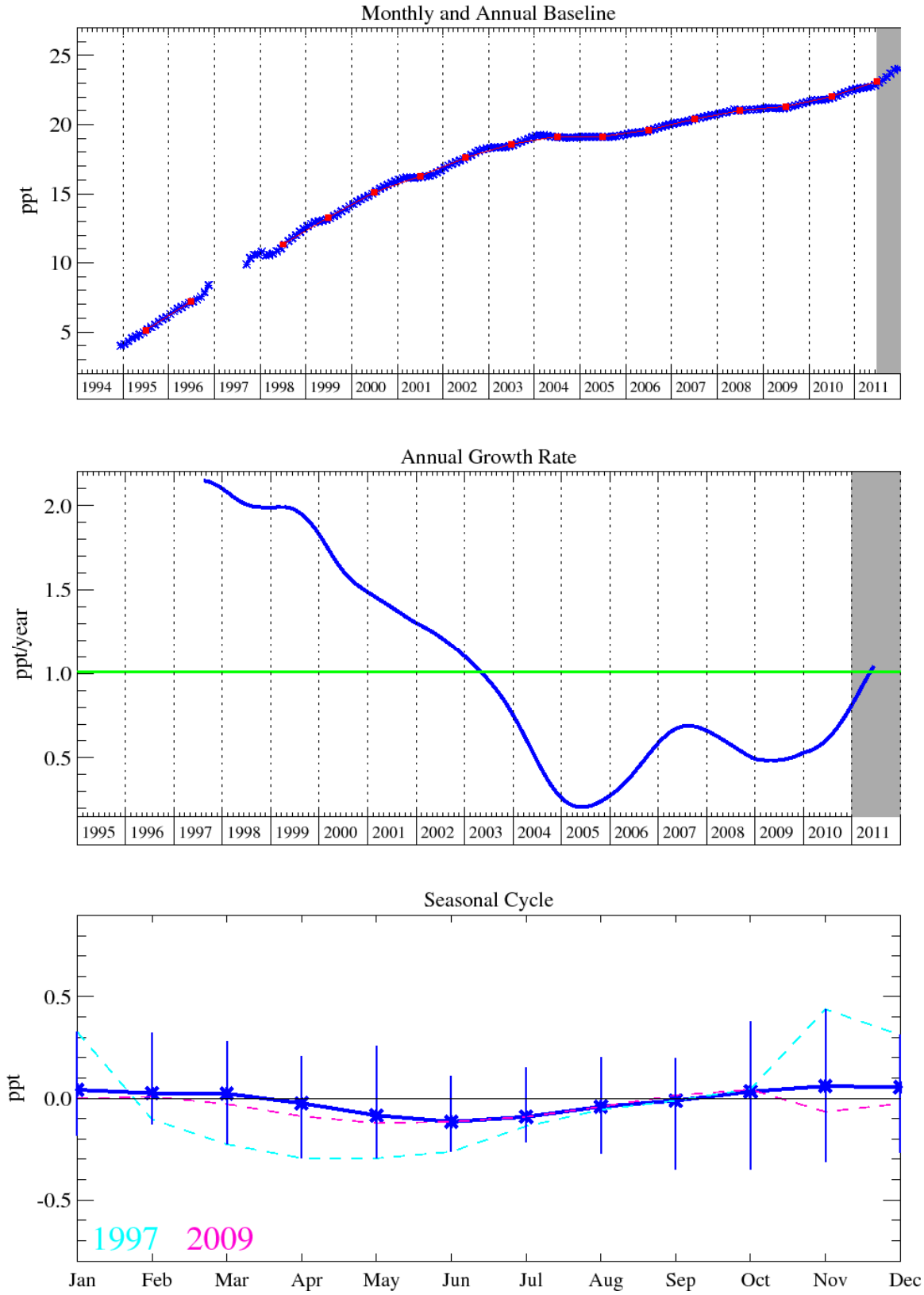

Figure 17: HCFC-141b: Monthly (blue) and annual (red) baseline concentrations (top plot). Annual (blue) and overall average growth rate (green) (middle plot). Seasonal cycle (de-trended) with year to year variability (lower plot).

4.3.2.3 HCFC-142b

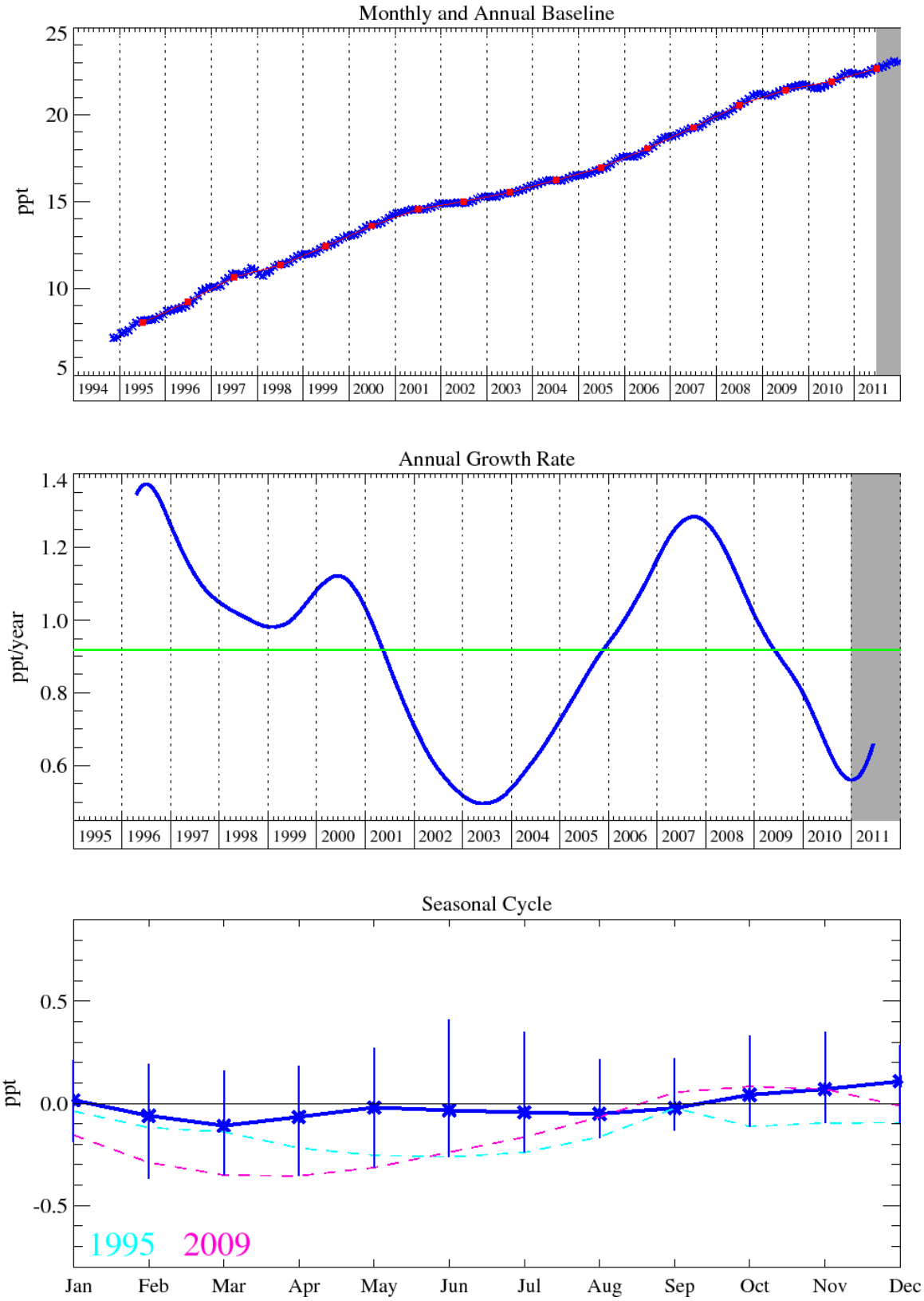

Figure 18: HCFC-142b: Monthly (blue) and annual (red) baseline concentrations (top plot). Annual (blue) and overall average growth rate (green) (middle plot). Seasonal cycle (de-trended) with year to year variability (lower plot).

4.3.2.4 HCFC-22

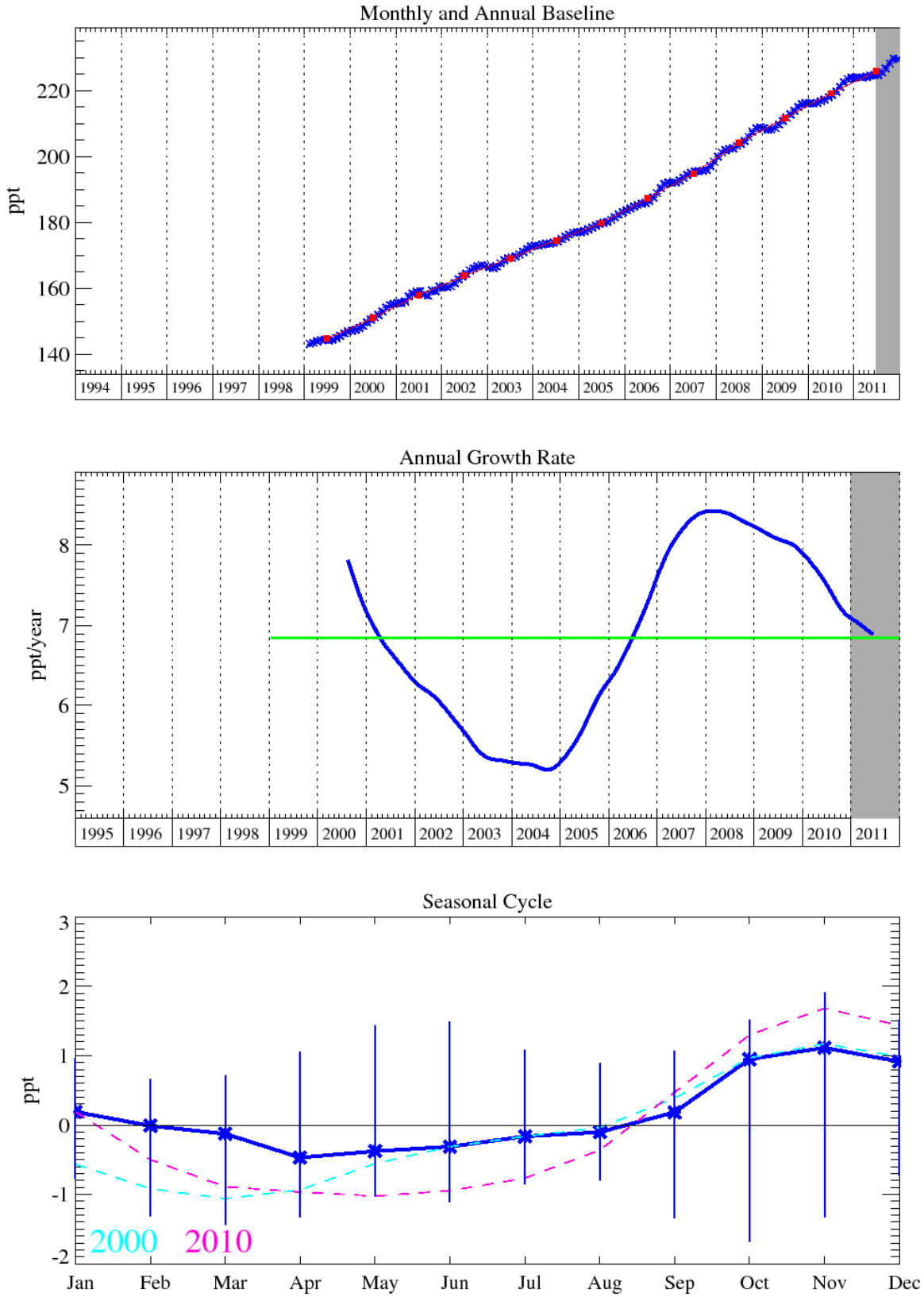

Figure 19: HCFC-22: Monthly (blue) and annual (red) baseline concentrations (top plot). Annual (blue) and overall average growth rate (green) (middle plot). Seasonal cycle (de-trended) with year to year variability (lower plot).

4.3.3 HFCs

Hydrofluorocarbos (HFCs) are replacement chemicals for the long-lived ozone depleting substances in various applications such as refrigeration, fire extinguishers, propellants, and foam blowing. The most recent measurements of the HFCs at Mace Head indicate that the mixing ratios of all HFC compounds continue to grow, as is consistent with sustained emissions of these replacement compounds into the atmosphere. The baseline monthly mean, mixing ratios for all the HFCs are shown in figures 20-2920, and the growth rates of these compounds, calculated from the data are presented in Table1c.

HFC-125 (CHF_2CF_3): This compound is used in refrigeration blends and for fire suppression. It has a GWP_{100} of 3500 and an atmospheric lifetime of 13.4 years. (O'Doherty et al., 2009). This compound is growing rapidly in the atmosphere reaching a level of 11.6 ppt in Dec. 2011 with a growth rate of 1.4 ppt/yr.

HFC-134a (CH_2FCF_3): Globally HFC-134a is the most abundant HFC present in the atmosphere, used predominantly in refrigeration and mobile air conditioning (MAC). Due to its long lifetime 13.4 years and relatively high GWP_{100} 1370 (Forster et al., 2007) the use of HFC-134a (and any other HFCs with a GWP_{100} >150) will be phased out in Europe between 2011 and 2017. It is proposed that a very gradual phase-out of the use of HFC-134a in cars will also take place outside Europe because of the global nature of the car industry. However in developing countries the potential for growth of HFC-134a is still large (Velders et al., 2009). As of Dec. 2011 the atmospheric mole fraction of HFC-134a was 71.2 ppt and growth for 2011 was estimated to be 5.3 ppt/yr.

HFC-143a (CH_3CF_3) is used mainly in refrigerant blends. In Dec 2011 it reached levels of 13.9 ppt. These levels have increased dramatically from the low ppt levels in 1997 at an increasing rate, currently 1.2 ppt/yr. It has a relatively long atmospheric lifetime of 47.1 years

HFC-152a (CH_3CHF_2) has a relatively short lifetime of 1.5 years due to its efficient removal by OH oxidation in the troposphere, consequently it has the smallest GWP_{100} at 133, of all of the major HFCs. It is used as a foam-blowing agent and aerosol propellant, and given its short lifetime has exhibited substantial growth in the atmosphere since measurement began in 1994. However, in the last few years the rate of growth has slowed somewhat to ~0.5 ppt/yr, reaching a mixing ratio in Dec 2011 of 10.4 ppt.

HFC-23 (CHF_3) is primarily a by-product formed during the production of HCFC-22. For this reason it has grown at a rate of 0.8 ppt/yr reached a mixing ratio of 25 ppt by Dec 2011. It is therefore the second most abundant HFC in the atmosphere after HFC-134a, this combined with a long atmospheric lifetime of 222 years makes this compound a potent GHG. Emissions of HFC-23 in developed countries has declined due to the Montreal Protocol phase-out schedule for HCFC-22, however, emissions from developing countries (despite the implementation of HFC-23 incineration through the Clean Development Mechanism) continues to drive global mixing ratios up. A modelling study carried out by Keller et al. (2012) suggests that there are small differences given the uncertainities

Three new HFC compounds have now successfully been added to the Medusa analysis (since 11 January 2008). The atmospheric mole fraction of HFC-245fa is 1.6 ppt and it is growing at a rate of 0.16 ppt/yr. This compounds is used as a foam blowing agent for polyurethane (PUR) foams (atmospheric lifetime 7.6 years and GWP (100 year time horizon) of 1020). HFC-227ea is used as a propellant for medical aerosols and a fire fighting agent (atmospheric lifetime 34.2 years and GWP (100 year time horizon) of 3140). It is has reached a mole fraction of 0.74 ppt with a growth rate of 0.07 ppt/yr. Finally, HFC-236fa, used as a fire fighting agent (atmospheric lifetime 240 years and GWP (100 year time horizon) of 9500) has reached a mixing ratio of 0.10 ppt and is growing at a rate of 0.01 ppt/yr.

4.3.3.1 HFC-125

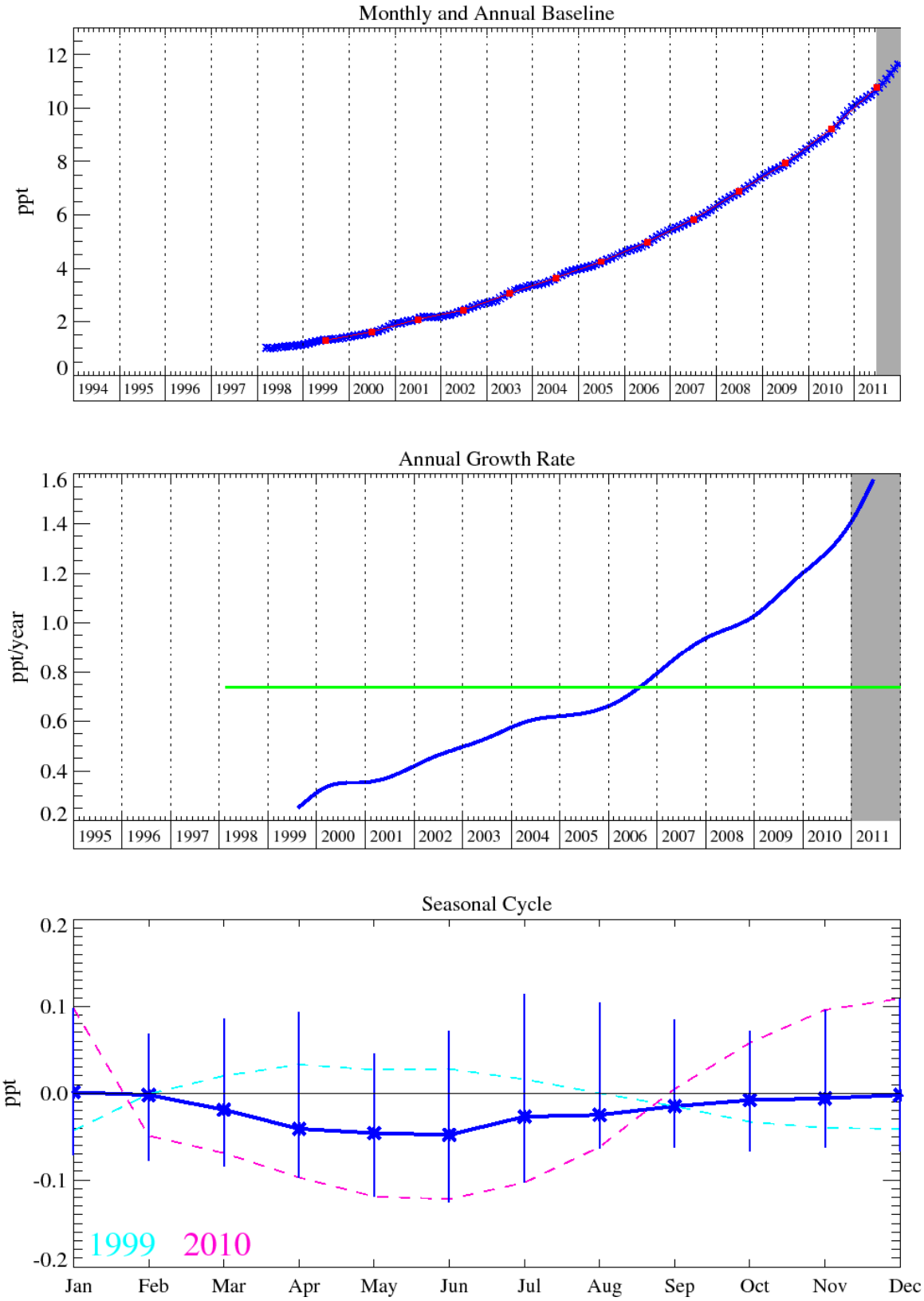

Figure 20: HFC-125: Monthly (blue) and annual (red) baseline concentrations (top plot). Annual (blue) and overall average growth rate (green) (middle plot). Seasonal cycle (de-trended) with year to year variability (lower plot).

4.3.3.2 HFC-134a

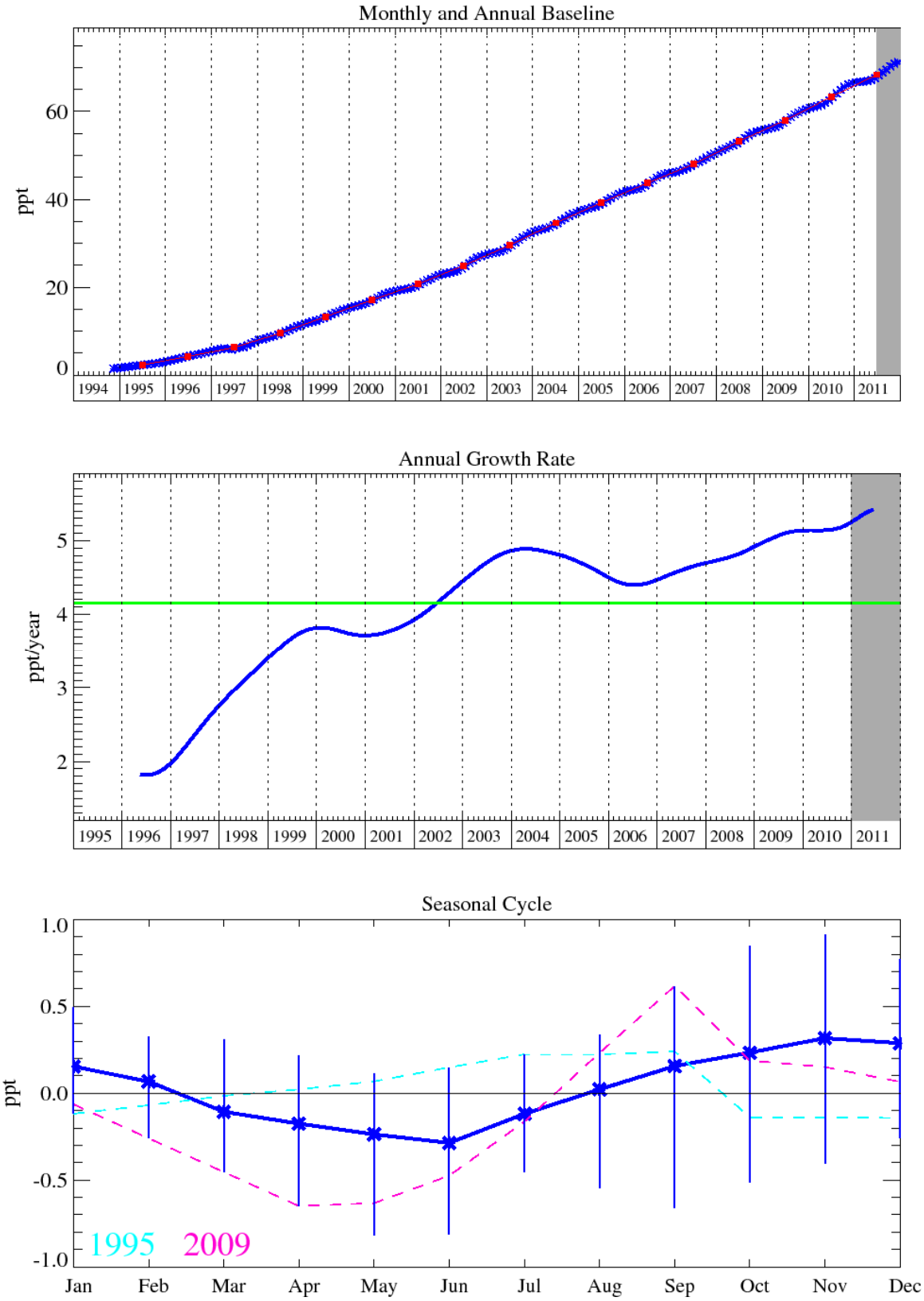

Figure 21: HFC-134a: Monthly (blue) and annual (red) baseline concentrations(top plot). Annual (blue) and overall average growth rate (green) (middle plot). Seasonal cycle (de-trended) with year to year variability (lower plot).

4.3.3.3 HFC-143a

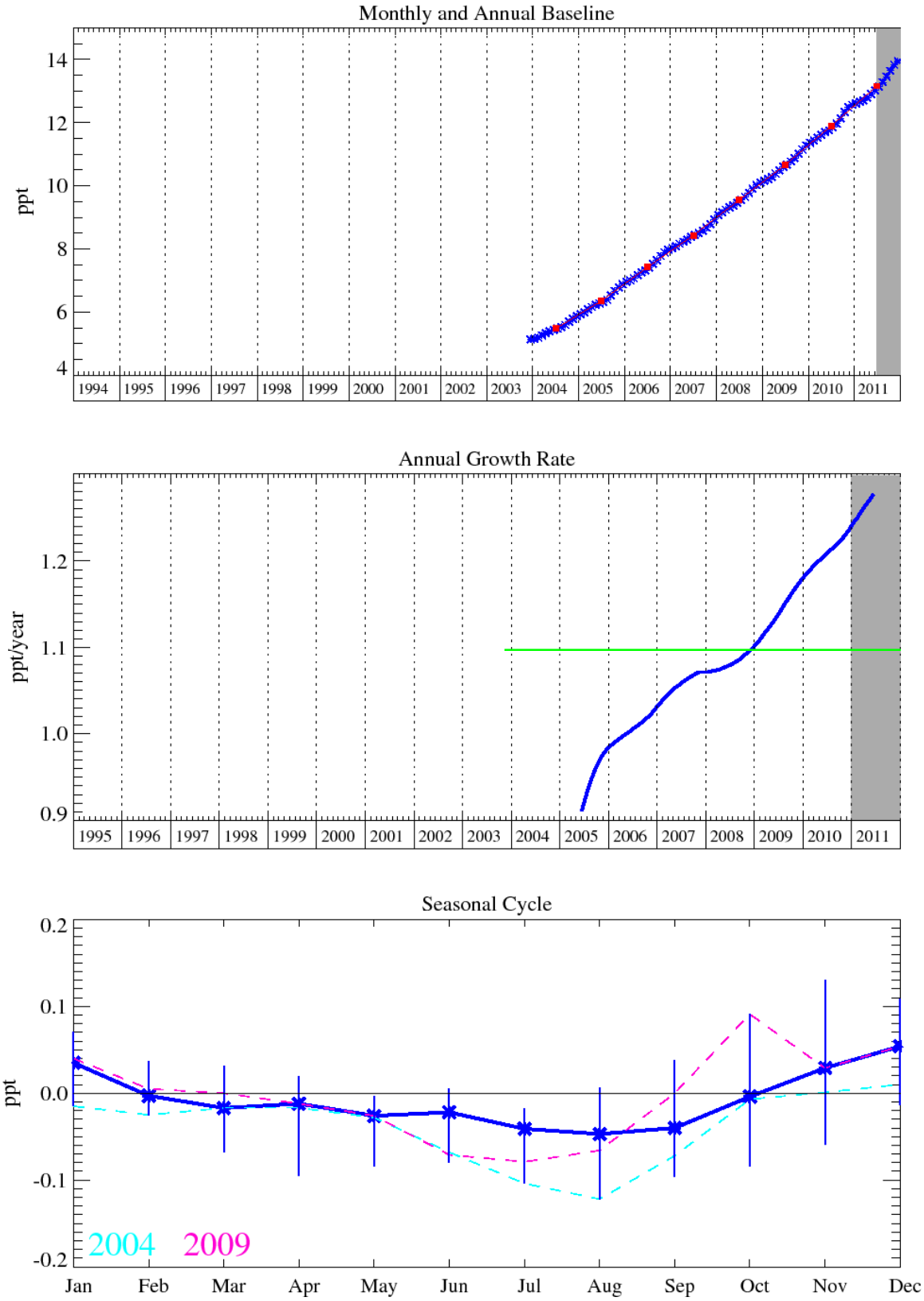

Figure 22: HFC-143a: Monthly (blue) and annual (red) baseline concentrations (top plot). Annual (blue) and overall average growth rate (green) (middle plot). Seasonal cycle (de-trended) with year to year variability (lower plot).

4.3.3.4 HFC-152a

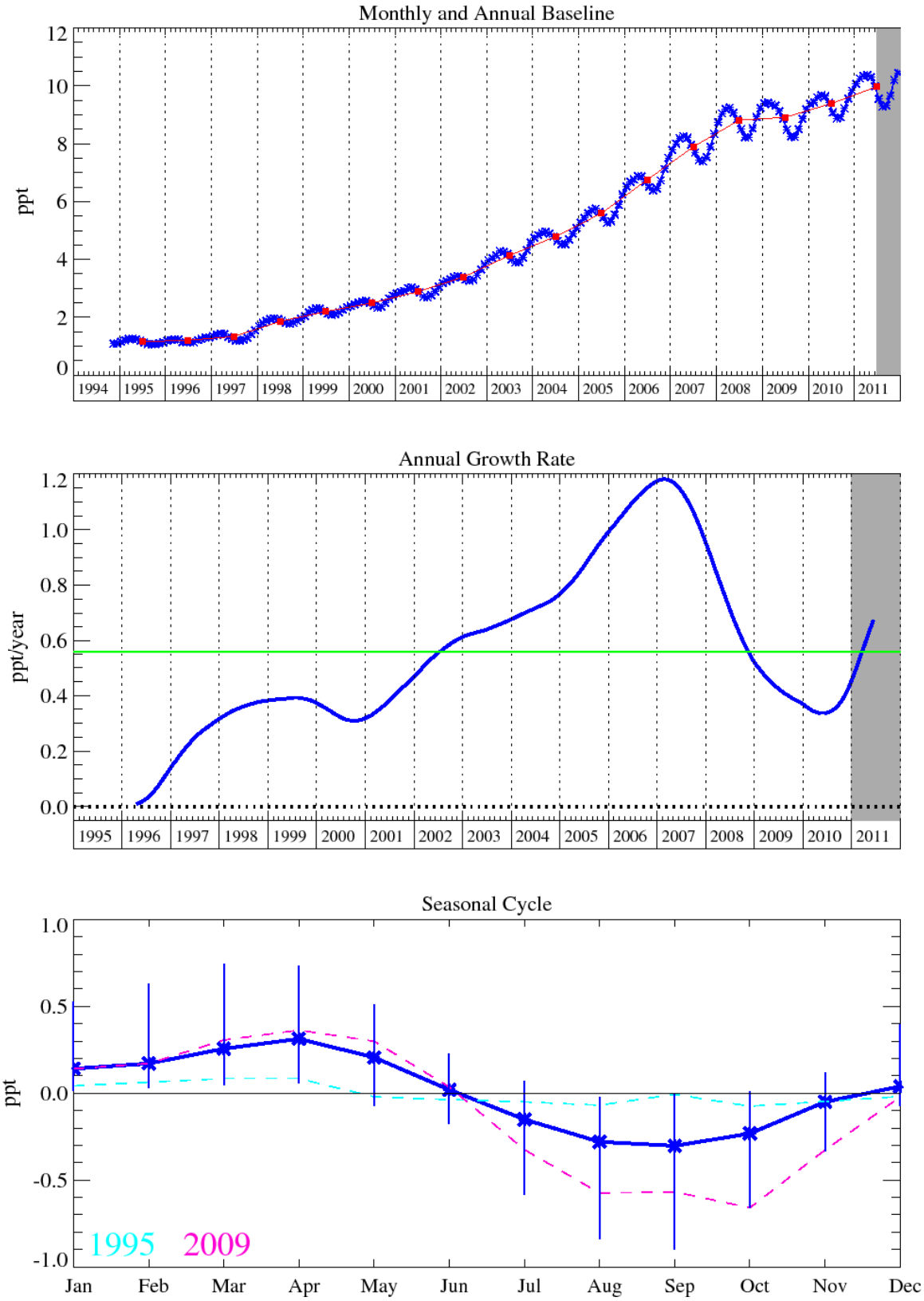

Figure 23: HFC-152a: Monthly (blue) and annual (red) baseline concentrations (top plot). Annual (blue) and overall average growth rate (green) (middle plot). Seasonal cycle (de-trended) with year to year variability (lower plot).

4.3.3.5 HFC-23

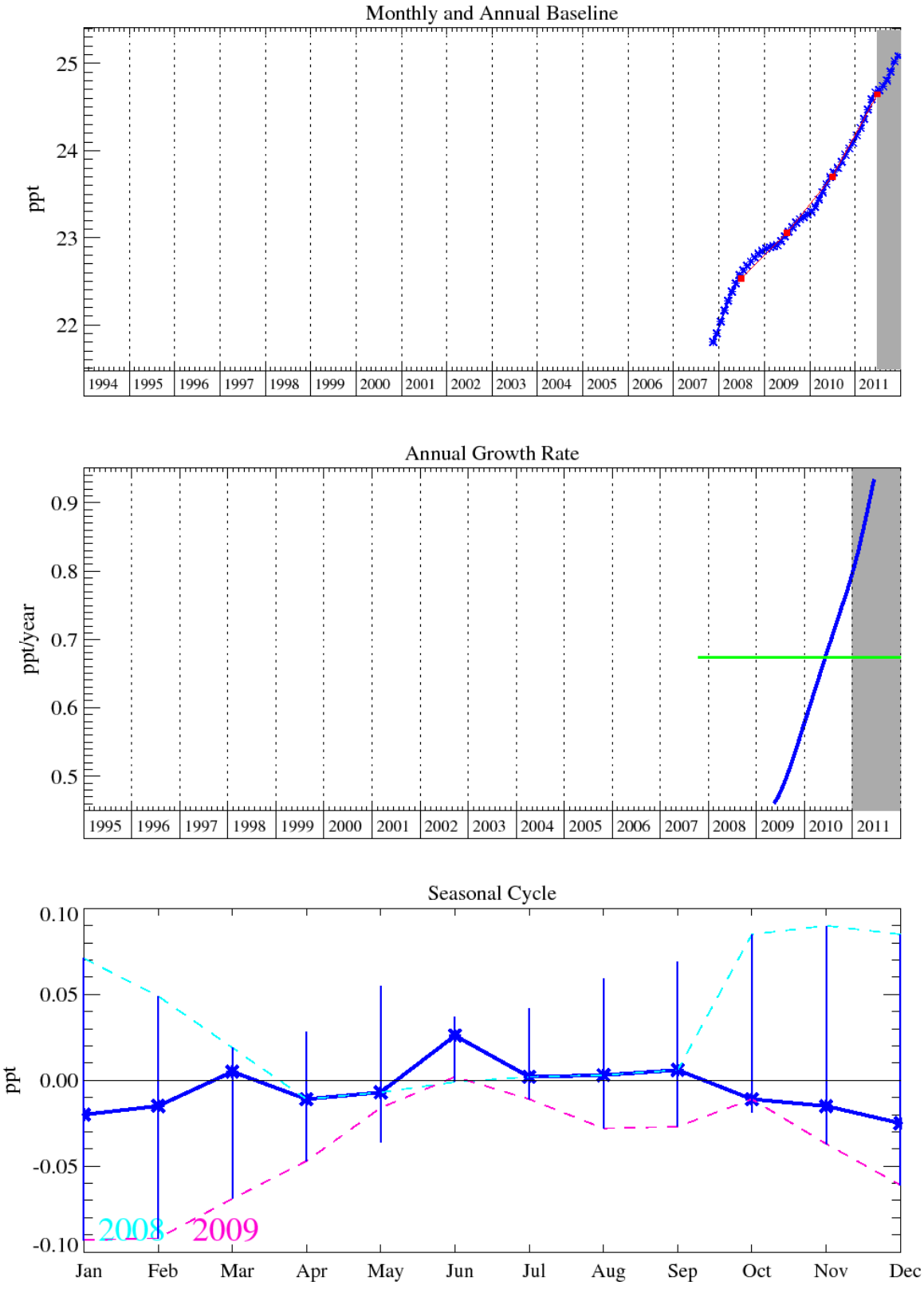

Figure 24: HFC-23: Monthly (blue) and annual (red) baseline concentrations. Annual (blue) and overall average growth rate (green) (lower plot).

4.3.3.6 HFC-32

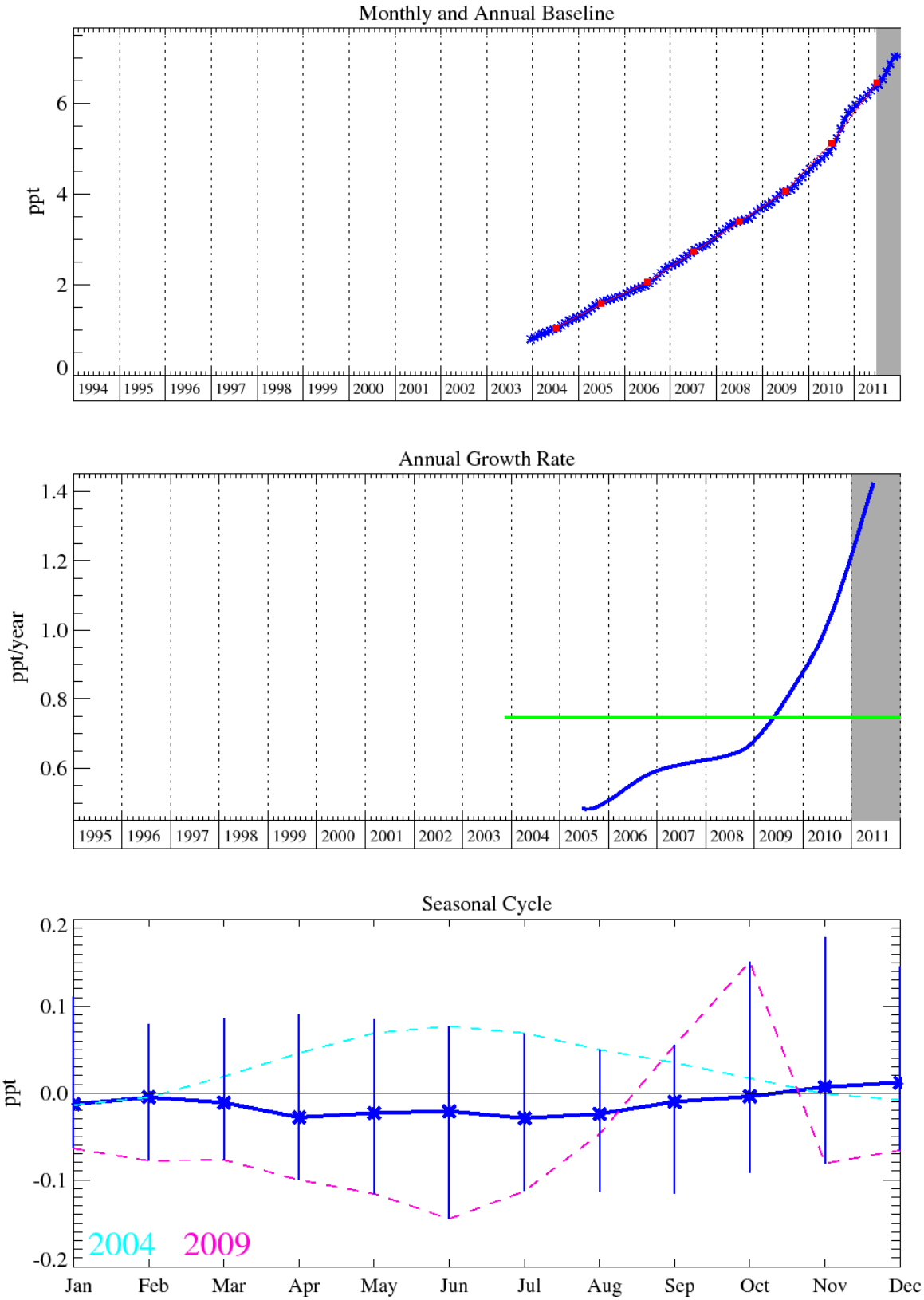

Figure 25: HFC-32: Monthly (blue) and annual (red) baseline concentrations (top plot). Annual (blue) and overall average growth rate (green) (middle plot). Seasonal cycle (de-trended) with year to year variability (lower plot).

4.3.3.7 HFC-227ea

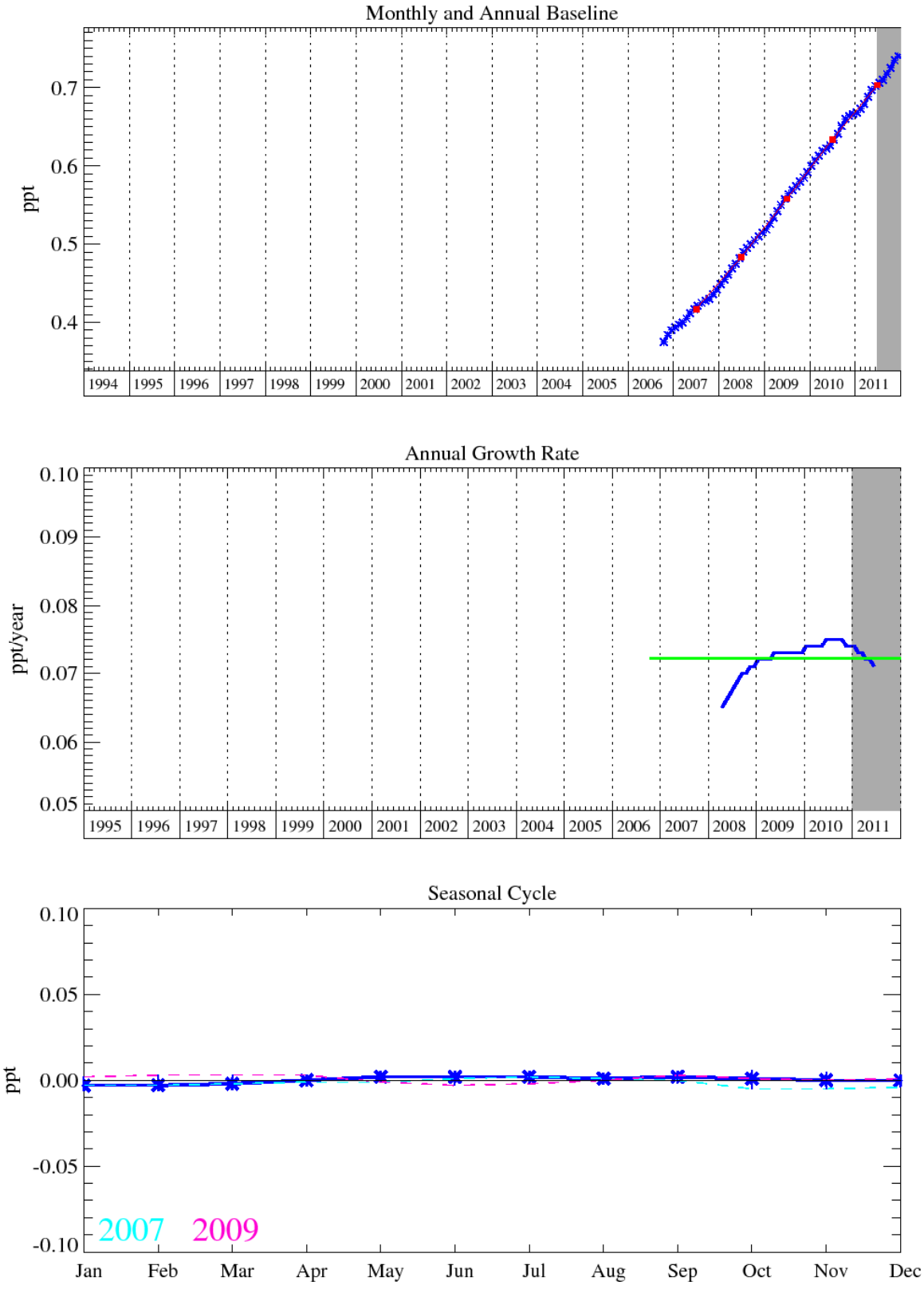

Figure 26: HFC-227ea: Monthly (blue) and annual (red) baseline concentrations (top plot). Annual (blue) and overall average growth rate (green) (middle plot). Seasonal cycle (de-trended) with year to year variability (lower plot).

4.3.3.8 HFC-236fa

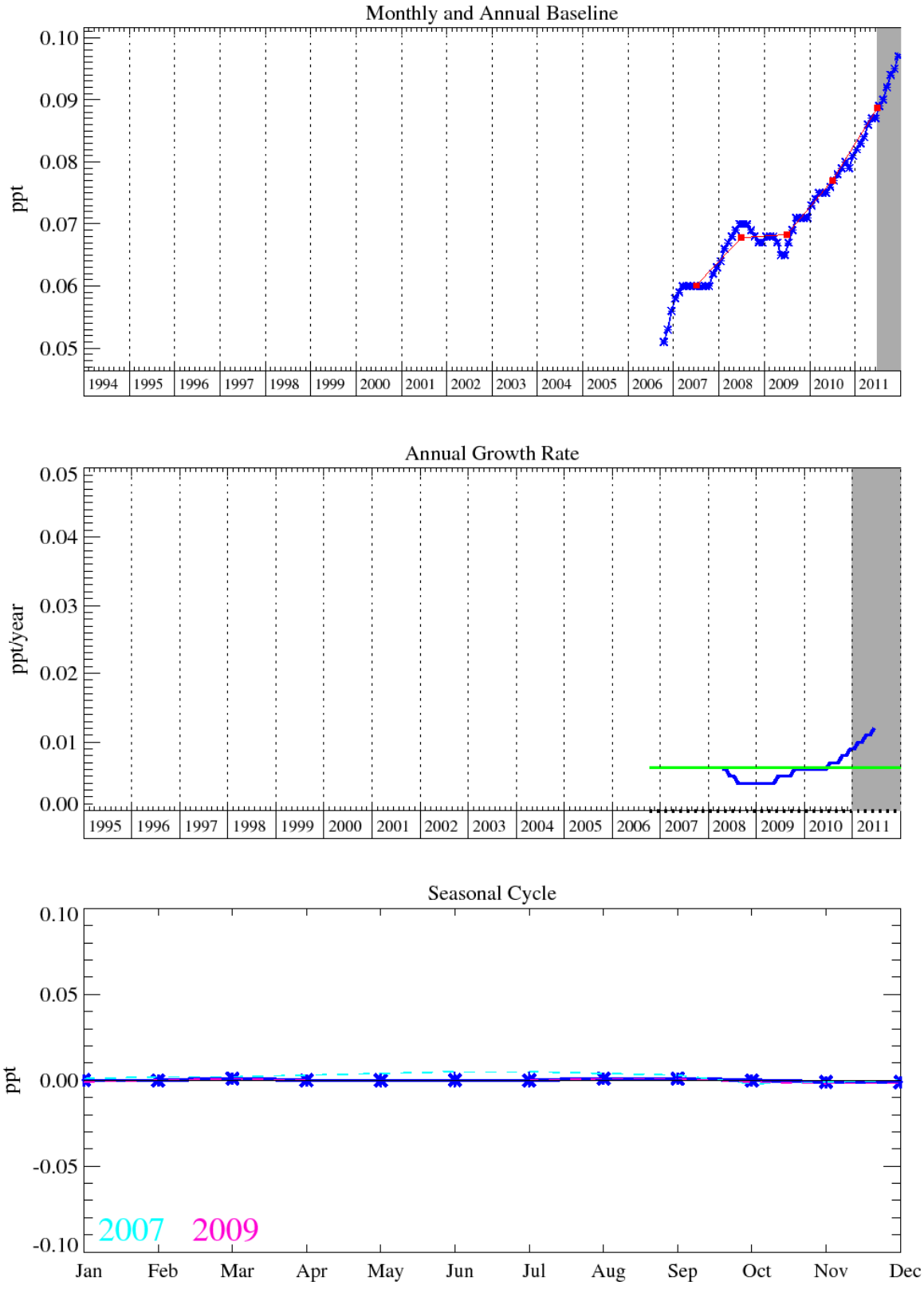

Figure 27: HFC-236fa: Monthly (blue) and annual (red) baseline concentrations (top plot). Annual (blue) and overall average growth rate (green) (middle plot). Seasonal cycle (de-trended) with year to year variability (lower plot).

4.3.3.9 HFC-245fa

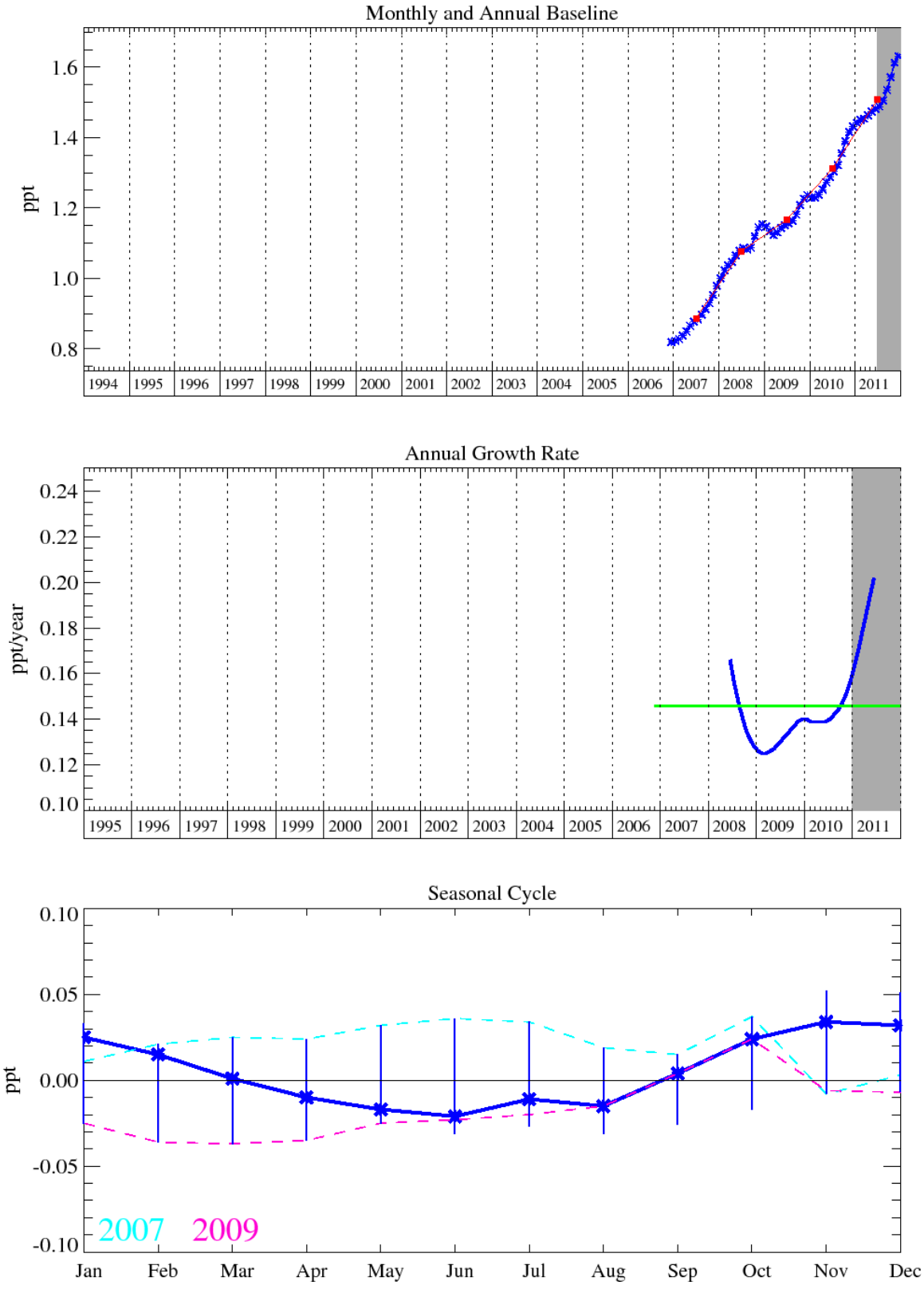

Figure 28: HFC-245fa: Monthly (blue) and annual (red) baseline concentrations (top plot). Annual (blue) and overall average growth rate (green) (middle plot). Seasonal cycle (de-trended) with year to year variability (lower plot).

4.3.3.10 HFC-365mfc

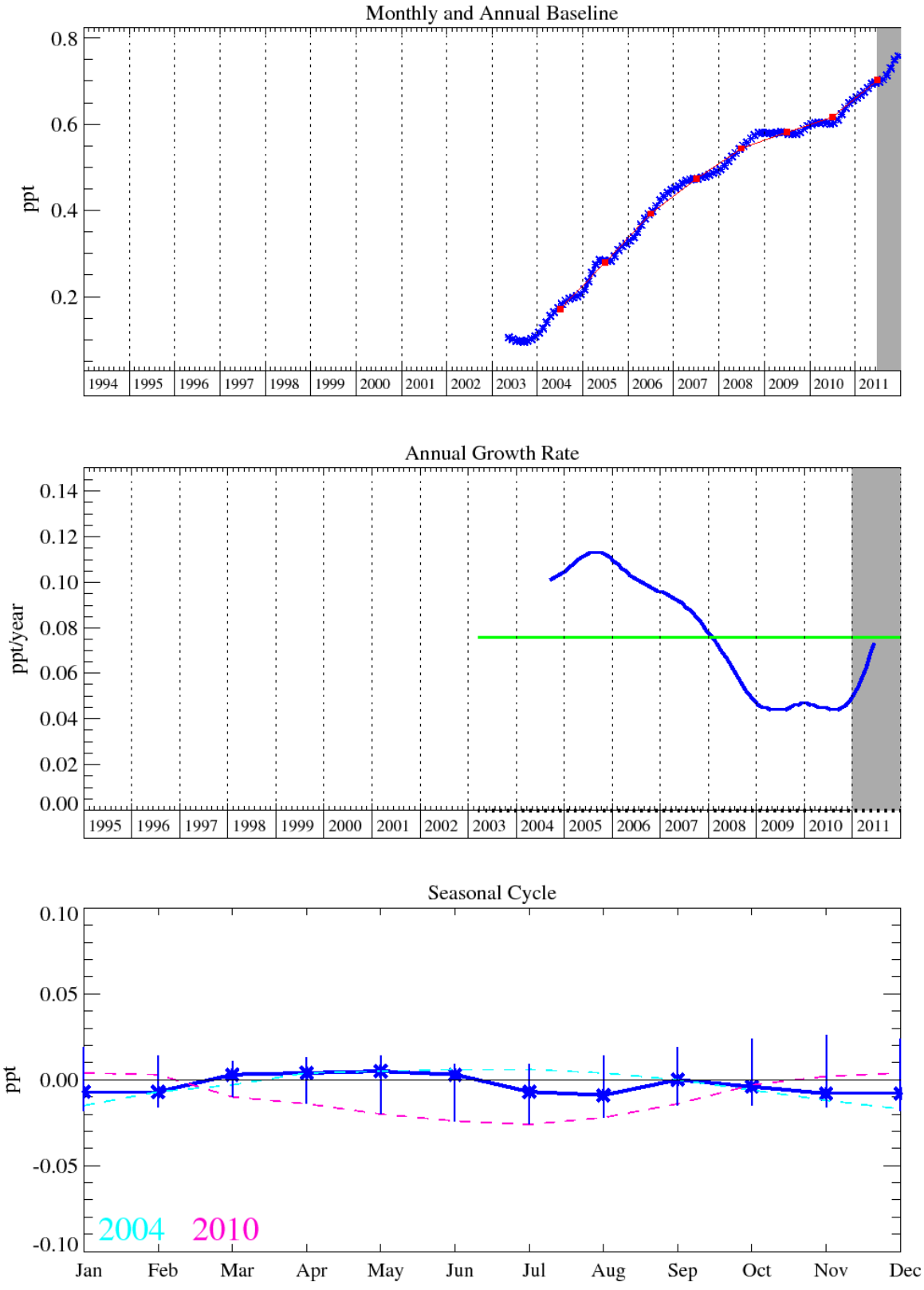

Figure 29: HFC-365mfc: Monthly (blue) and annual (red) baseline concentrations (top plot). Annual (blue) and overall average growth rate (green) (middle plot). Seasonal cycle (de-trended) with year to year variability (lower plot).

4.3.4 Fluorine compounds

The Medusa data record for CF_4, C_2F_6, C_3F_8, and SF_6 are shown in figures 30-33 below. CF_4 possesses the longest known lifetime of anthropogenic molecules (>50,000 yrs), which, when coupled with its high absolute radiative forcing (0.08 W m^{-2} ppb^{-1}, 6500 x eCO_2 (CO_2 equivalent, 100 yr time horizon)), can equate to upwards of 1 % of total radiative forcing. Its primary emission source is as an unwanted by-product of Aluminium smelting during a fault condition known as the Anode Effect. Thus the frequency of occurrence and duration of an Anode Effect event will determine the regional and global CF_4 emission. CF_4 has some additional minor applications in the semiconductor industry (as a source of F radicals), but industry has shied away from using CF_4 knowing that its GWP is so high. The Aluminium industry has recognised the CF_4 (and C_2F_6) emission problem and has been undergoing processes of replacement of older, less efficient Aluminium production cells with more efficient designs, and automated and quicker intervention policies to prevent the occurrence of these Anode Effects. It is also thought that CF_4 has a natural source from crustal degassing.

C_2F_6 is also a potent greenhouse gas with an atmospheric lifetime of >10,000 years. It has common source to CF_4, this serves to help explain why all of the CF_4 above-baseline (pollution) events are usually correlated with those of C_2F_6. However, we note that there are many more frequent and greater magnitude emissions of C_2F_6 relative to CF_4. This is due to the dominant source of C_2F_6 being emitted from semiconductor industries (plasma etching). C_3F_8 (atmospheric lifetime 2600 years) is also used in semiconductor manufacturing, but to a lesser extent to that of C_2F_6.it also has an increasing contribution from refrigeration use. Observations of above-baseline C_3F_8 emissions are less frequent than those of C_2F_6 but are of a higher relative magnitude. The atmospheric trends for CF_4, C_2F_6 and the minor semi-conductor component C_3F_8 are 0.66, 0.08 and 0.02 ppt/yr respectively. These compounds tend to accumulate in the atmosphere due to their very long atmospheric lifetimes, the Dec. 2011 mixing ratio of CF_4 is 79.5 ppt, C_2F_6 is 4.2 ppt and C_3F_8 is 0.6 ppt.

SF_6 is an important greenhouse gas since it has a long atmospheric lifetime of 3,200 years, a high radiative efficiency and a considerable atmospheric trend of 0.28 ppt/yr reaching a mixing ratio of 7.5 ppt by Dec. 2011. Although having minor usage in the semiconductor industry, is predominantly used in heavy duty electrical switchgear. Although the units themselves are hermetically sealed, breakdown and disposal, alongside leakage from wear-and-tear will cause this sector to emit SF_6. A minor use of this gas is also reported in its use as a blanketing (i.e. oxygen inhibiting inert gas) agent during Magnesium production. Hence SF_6 will have many and more diffuse sources relative to the other perfluorinated species. Its atmospheric trend has been predicted to rise at a rate faster than linear, as older electrical switchgear is being switched to higher efficiency units.

4.3.4.1 PFC-14 (CF_4)

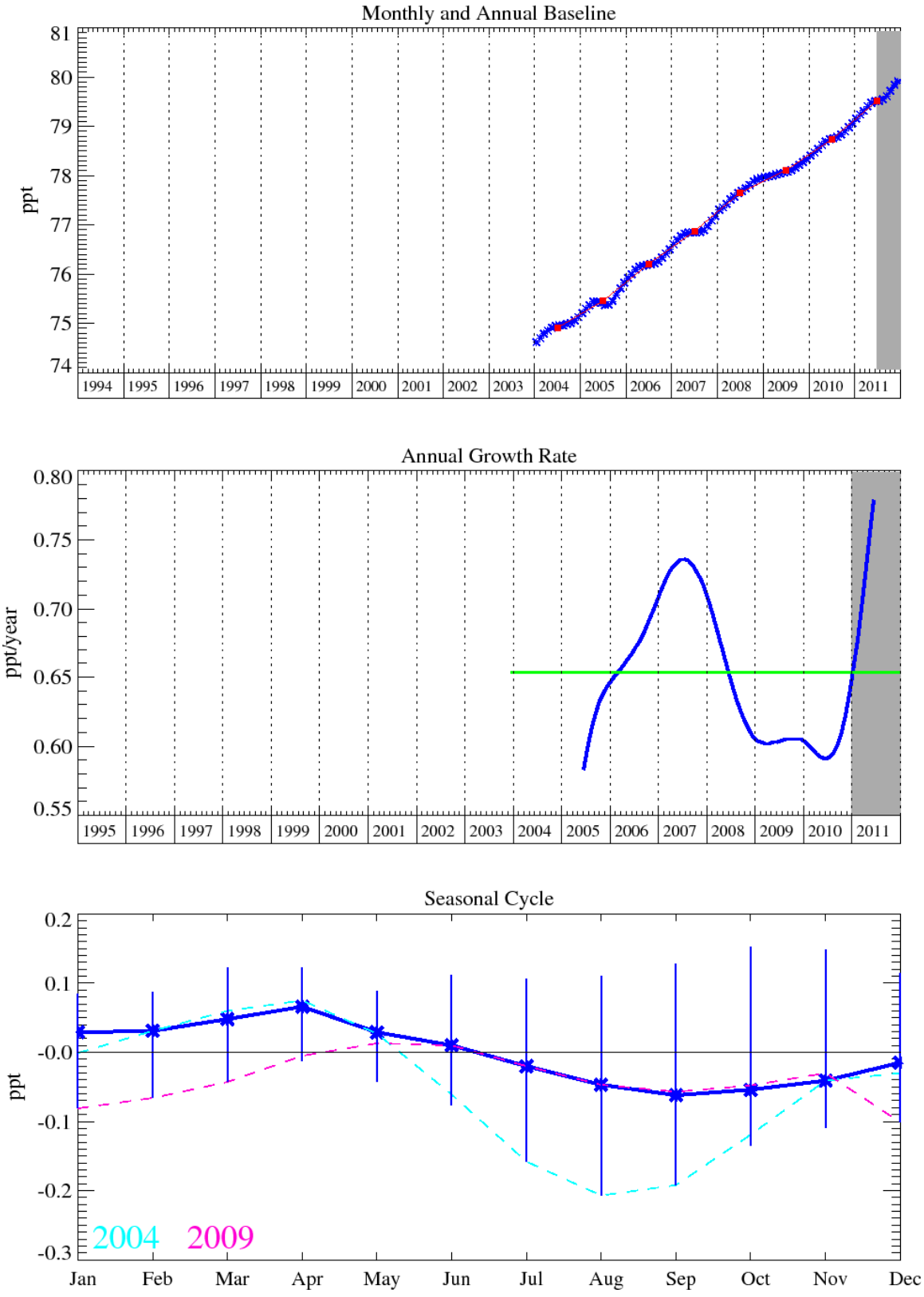

Figure 30: PFC-14: Monthly (blue) and annual (red) baseline concentrations (top plot). Annual (blue) and overall average growth rate (green) (middle plot). Seasonal cycle (de-trended) with year to year variability (lower plot).

4.3.4.2 PFC-116

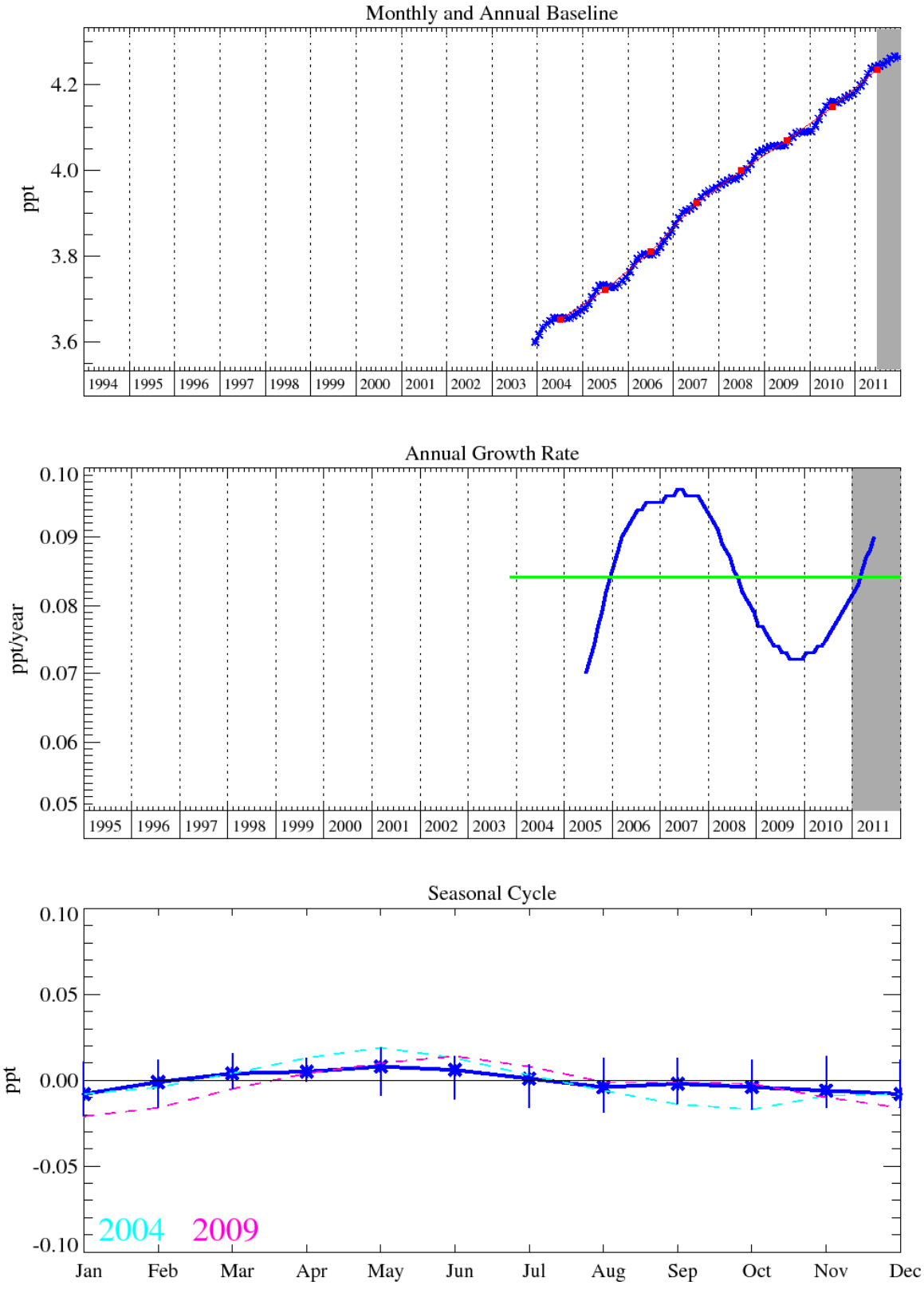

Figure 31: PFC-116: Monthly (blue) and annual (red) baseline concentrations (top plot). Annual (blue) and overall average growth rate (green) (middle plot). Seasonal cycle (de-trended) with year to year variability (lower plot).

4.3.4.3 PFC-218

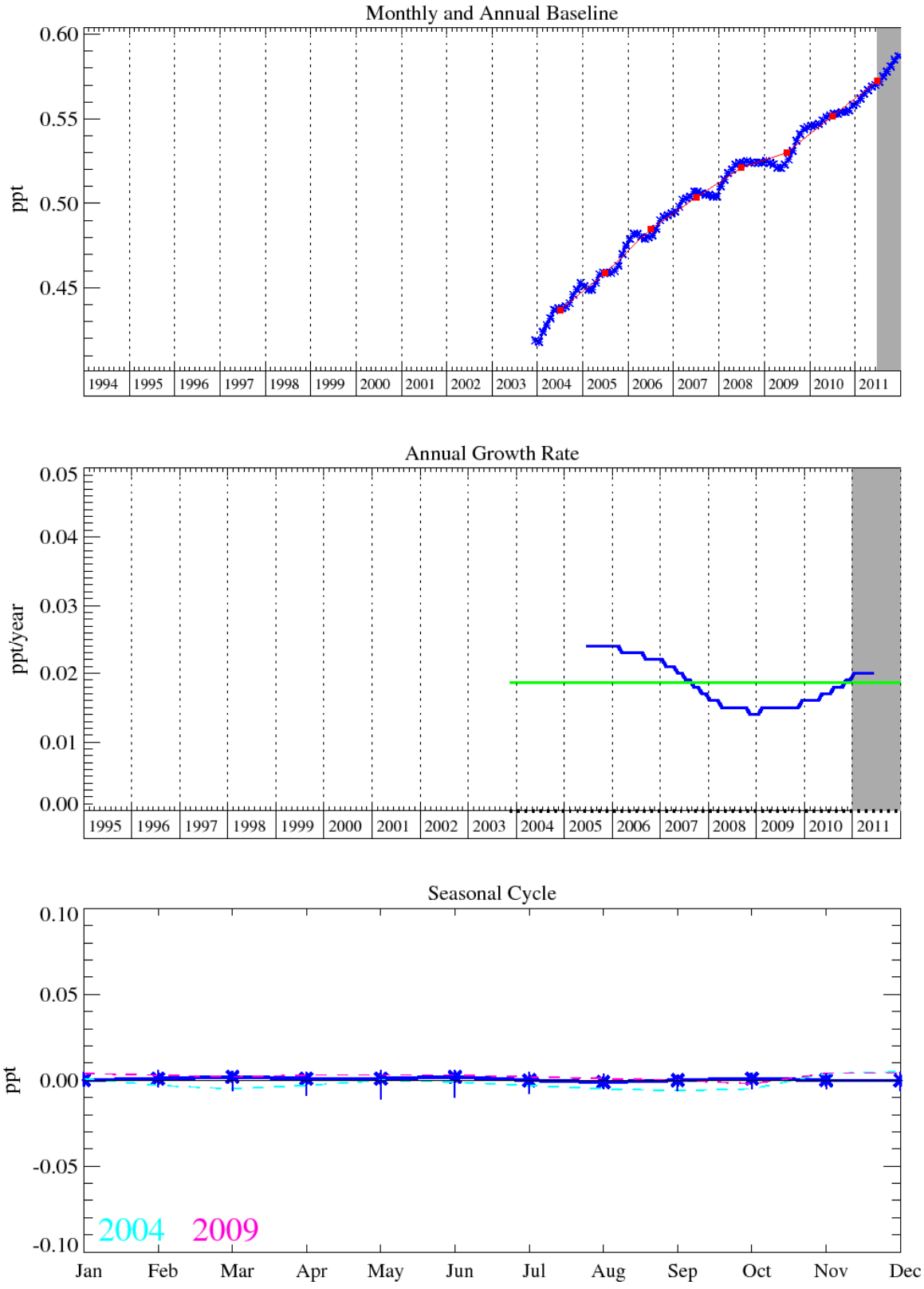

Figure 32: PFC-218: Monthly (blue) and annual (red) baseline concentrations (top plot). Annual (blue) and overall average growth rate (green) (middle plot). Seasonal cycle (de-trended) with year to year variability (lower plot).

4.3.4.4 SF_6

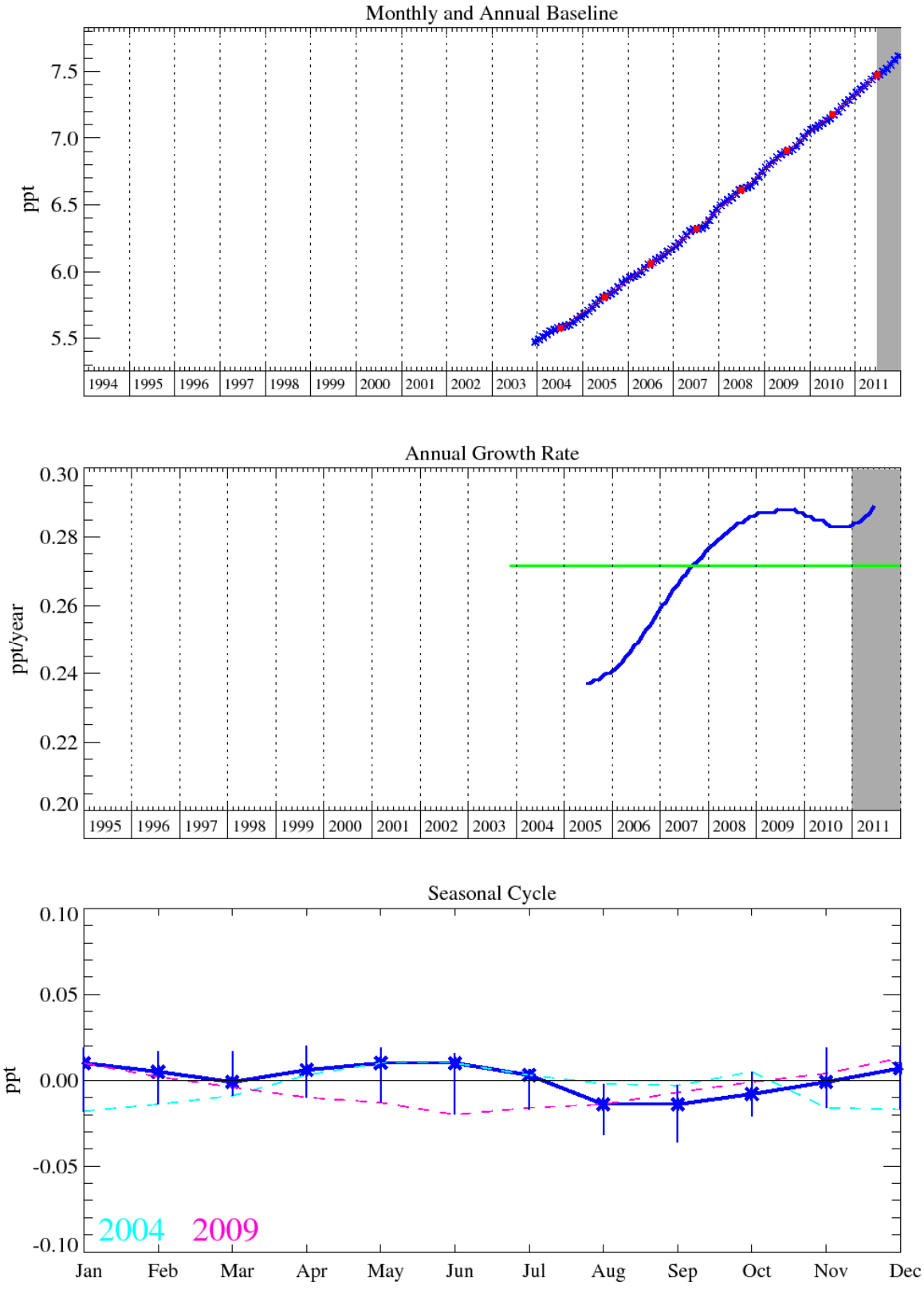

Figure 33: SF_6: Monthly (blue) and annual (red) baseline concentrations (top plot). Annual (blue) and overall average growth rate (green) (middle plot). Seasonal cycle (de-trended) with year to year variability (lower plot).

4.3.4.5 SO_2F_2

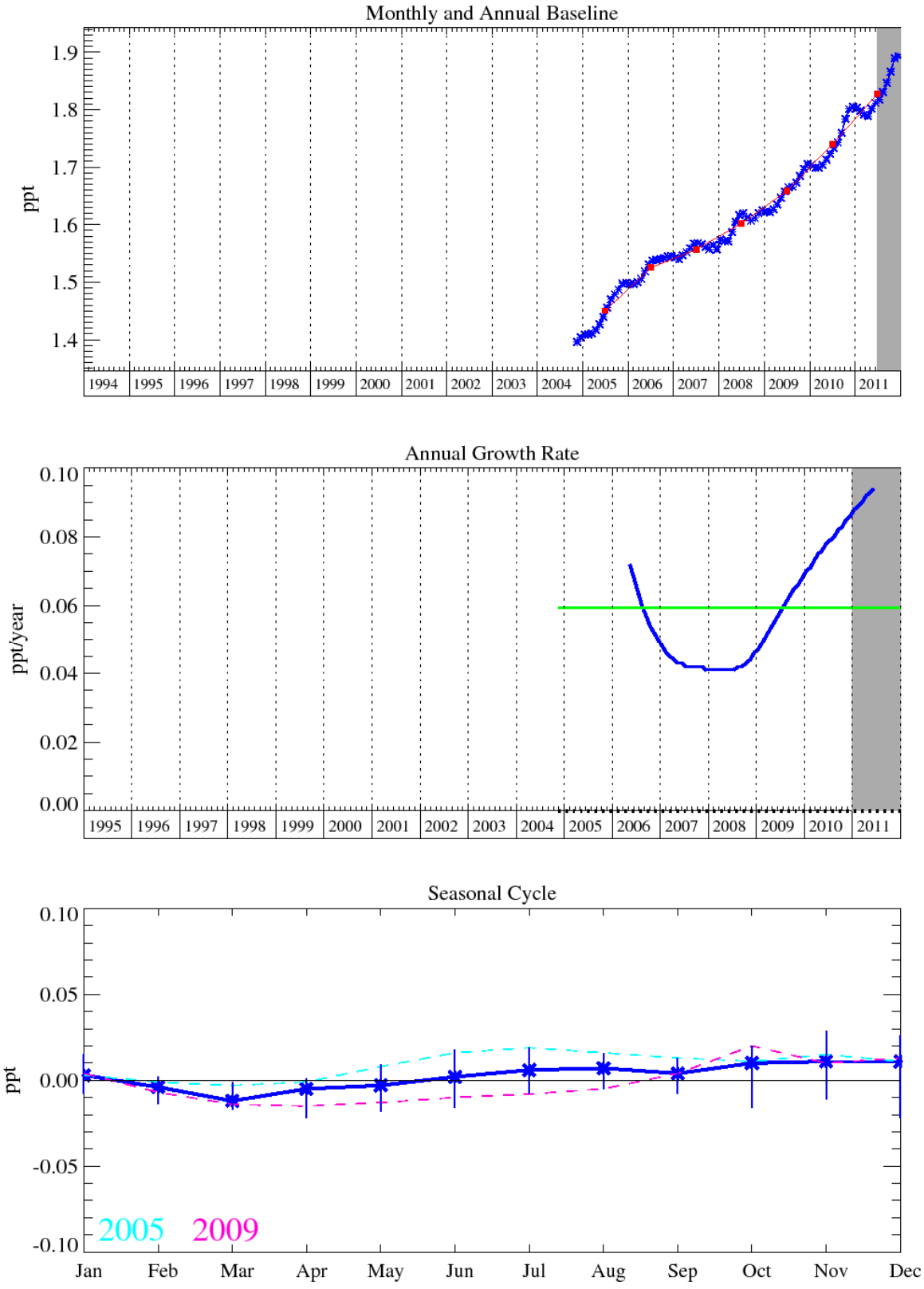

Figure 34: SO_2F_2: Monthly (blue) and annual (red) baseline concentrations (top plot). Annual (green), smoothed through 12-month running filter (red) and overall average growth rate (blue) (middle plot). Seasonal cycle (de-trended) with year to year variability (lower plot).

4.3.5 Chlorine compounds

A number of long lived and very short lived substances (VSLS) halocarbons are measured by the Medusa GC-MS. Previously we reported the recovery of CH_3Cl growth in the atmosphere, this growth abated in 2010 and the trend now shows a decline of 6.3 ppt/yr to 520 ppt (Figure 35). Methyl chloride (CH_3Cl) is not a controlled substance and is emitted from a range of biogenic and anthropogenic sources globally. It is estimated that ~55% of CH_3Cl emissions arise from terrestrial tropical areas with emission rates dependent on global temperature changes. Other major sources are biomass burning, anthropogenic activities and oceans. The atmospheric lifetime of CH_3Cl is 1 year [*Montzka et al.*, 2011] and it has a GWP_{100} of 13 [*Forster et al.*, 2007]. CH_3Cl contributes 16% of the total chlorine loading to the troposphere for long lived species and is thus the most abundant chlorine containing compound in the atmosphere.

Dichloromethane (CH_2Cl_2) global sources are thought to be 70% or greater of anthropogenic origin [*Keene et al.*, 1999; *Cox et al.*, 2003]. It is predominantly used as a paint stripper, degreaser, foam blowing agent and in pharmaceutical production methods. Its use as a paint stripper has been banned since 2010 in the EU [*European Union*, 2009]. CH_2Cl_2 also showed a decline in line with a reduction in the many solvent applications for this compound, however, since around 2003, measurements at Mace Head have shown it to be accumulating in the atmosphere, shown in figure 36, with a growth rate in 2011 of 1.1 ppt/yr, it has a mixing ratio in December 2011 of 41.4 ppt. Emission totals derived using the NAME model and the industry derived inventory suggest that emissions from the NW Europe (and the UK) are decreasing, which implies a source of CH_2Cl_2 to the atmosphere from a location outside of Europe. CH_2Cl_2 has a lifetime of 144 days [*Montzka et al.*, 2011] and a GWP_{100} of 8.7 [*Forster et al.*, 2007].

Figure 38 illustrates the steady downward trend of CCl_4 (26 year lifetime [*Montzka et al.*, 2011]) of 1.1 ppt/yr in 2011, this compound is the second most rapidly decreasing chlorocarbon after CH_3CCl_3. The level of CCl_4 at Mace Head in December 2011 was 85.5 ppt. Its major use was as a feedstock for CFC manufacturing and unlike CH_3CCl_3 a significant inter-hemispheric CCl_4 gradient still exists in 2011, resulting from a persistence of significant NH emissions. It is interesting that atmospheric observations for this compound are decreasing less rapidly than projected in the A1 scenario of the Ozone Assessment (Daniel and Velders et al., 2007). CCl_4 emissions derived from atmospheric observations (top-down) suggest substantially smaller emissions than emissions derived from bottom-up techniques using reported production, feedstock and destruction data. The reason for this discrepancy is not yet fully understood.

The major solvent methyl chloroform (CH_3CCl_3), is an important compound because of its use to estimate concentrations of the hydroxyl radical (OH), which is the major sink species for CH_4, HFCs and HCFCs. The global atmospheric CH_3CCl_3 concentration peaked in 1992 (Prinn et al., 2000) then declined in accordance with its short atmospheric lifetime (5.0 years [*Forster et al.*, 2007]) and phase out under the terms of the Montreal protocol. The average baseline mixing ratio of CH_3CCl_3 at Mace Head (Figure 39) has decreased by 1.3 ppt/yr in 2011 to reach a mixing ratio of 6.4 ppt in December 2011. The GWP_{100} of methyl chloroform is 146.

The major source of trichloroethylene (C_2HCl_3) is from industrial usage as a degreasing agent. It is currently measured with a mole fraction of 0.5 ppt, but is decreasing in the atmosphere at a rate of 0.07 ppt/yr (Figure 40). All but about 2% of the sales are in the NH. The main removal process is with OH. It has an atmospheric lifetime of 4.9 days [*Montzka et al.*, 2011] with this lifetime resulting in a low GWP_{100} of approximately 5 [*UNEP (United Nations Environment Program)*, 2003]. C_2HCl_3 can also undergo reductive de-chlorination to 1,2-dichloroethylene through the activity of soil microbes. Natural sources of C_2HCl_3 are from the oceans and seawater algae. It has been reported that salt lakes are also a natural source of C_2HCl_3 due to the microbial activity of halobacteria [*Weissflog et al.*, 2005].

Perchloroethylene (C_2Cl_4) is mainly used for dry cleaning and as a metal degreasing solvent. Small but significant quantities of C_2Cl_4 are emitted in the flue gas from coal-fired power plants. The atmospheric lifetime of C_2Cl_4 is 90 days [*Montzka et al.*, 2011] and its primary atmospheric sink is reaction with OH. Its December 2011 atmospheric mole fraction is 3.1 with a trend decreasing at the rate of 0.1 ppt/yr (Figure 41). The short lifetime of perchloroethylene results in a GWP_{100} of approximately 15 [*UNEP (United Nations Environment Program)*, 2003].

4.3.5.1 CH_3Cl

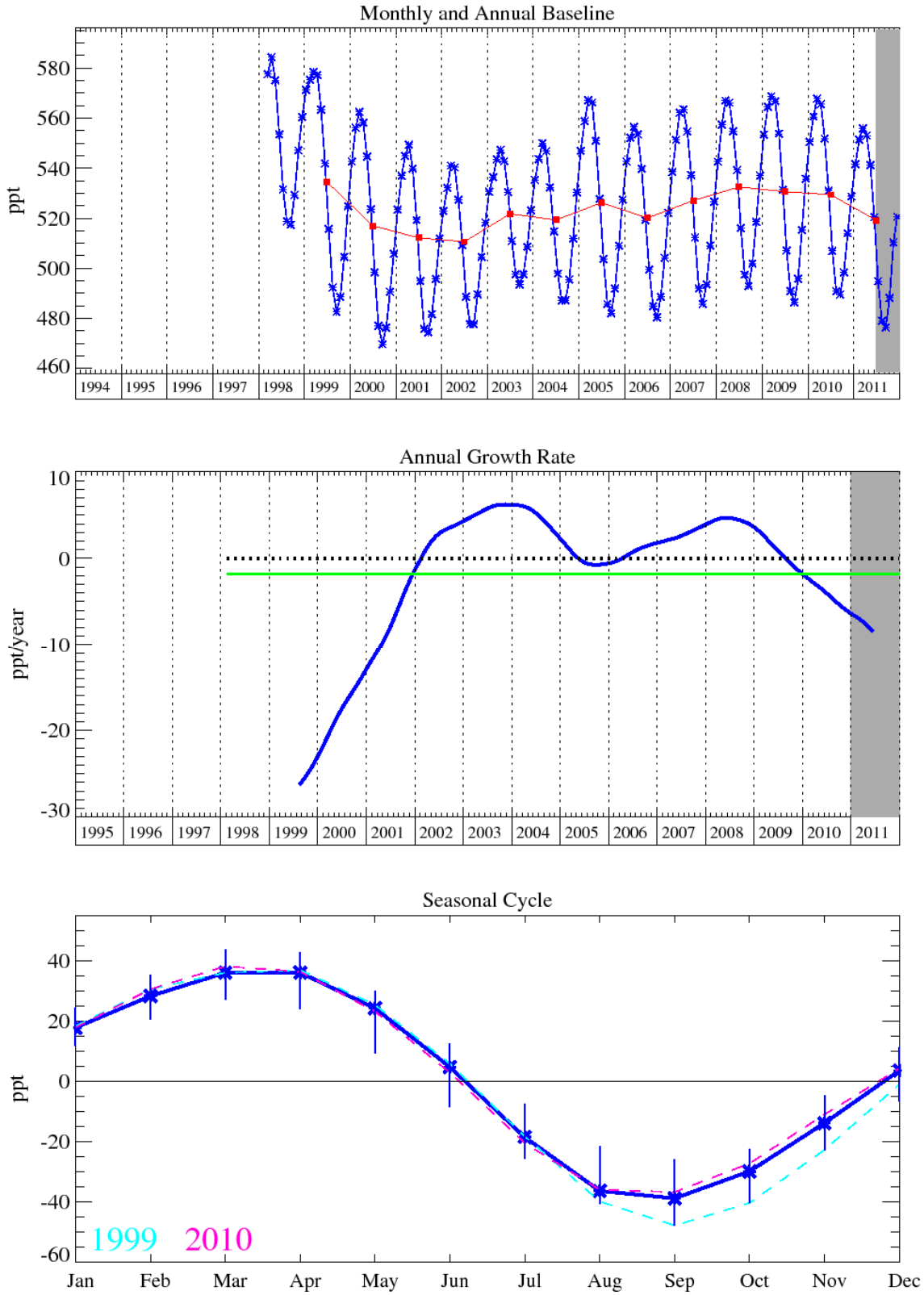

Figure 35: CH_3Cl: Monthly (blue) and annual (red) baseline concentrations (top plot). Annual (blue) and overall average growth rate (green) (middle plot). Seasonal cycle (de-trended) with year to year variability (lower plot).

4.3.5.2 CH_2Cl_2

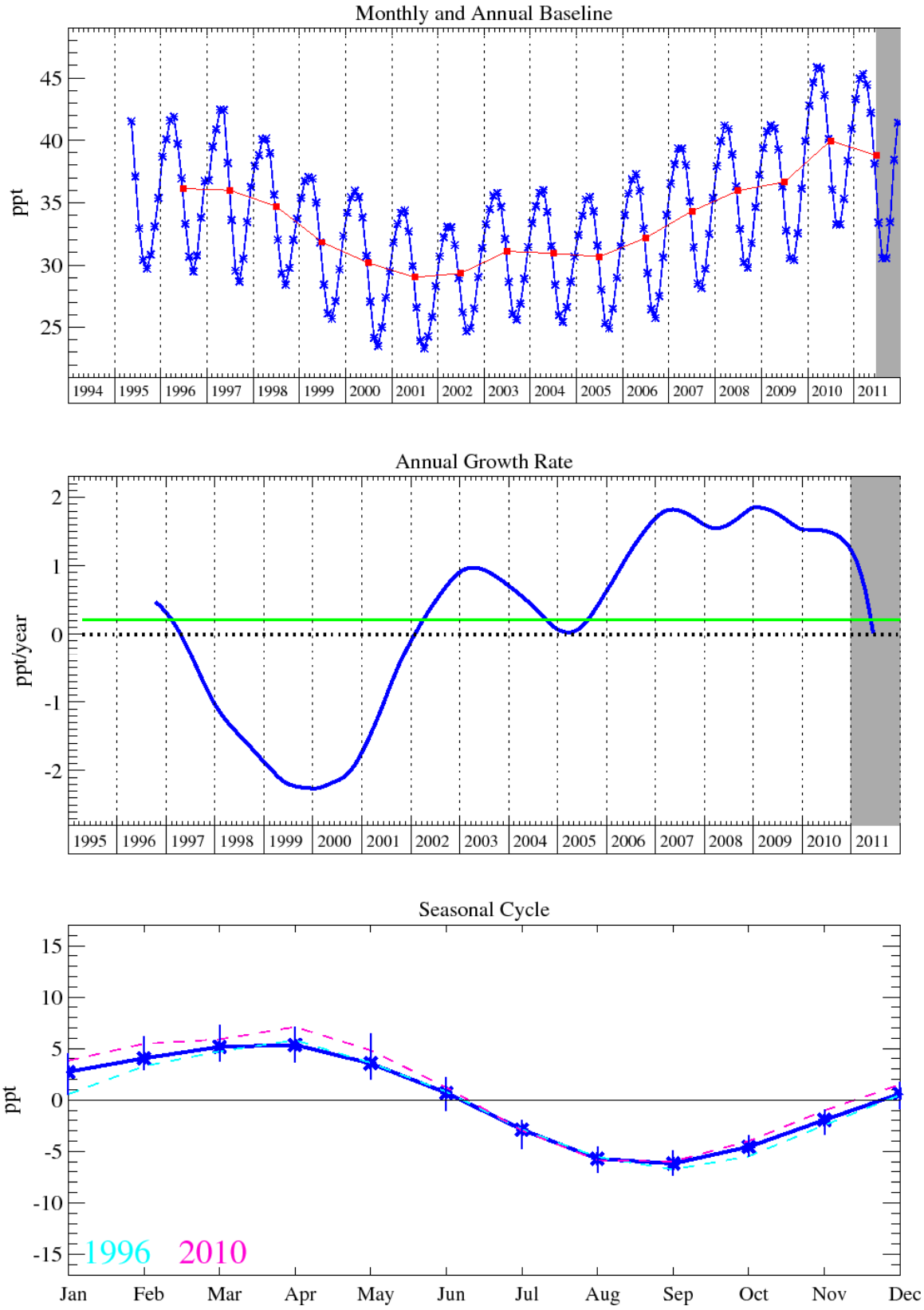

Figure 36: CH_2Cl_2: Monthly (blue) and annual (red) baseline concentrations (top plot). Annual (blue) and overall average growth rate (green) (middle plot). Seasonal cycle (de-trended) with year to year variability (lower plot).

4.3.5.3 $CHCl_3$ (chloroform)

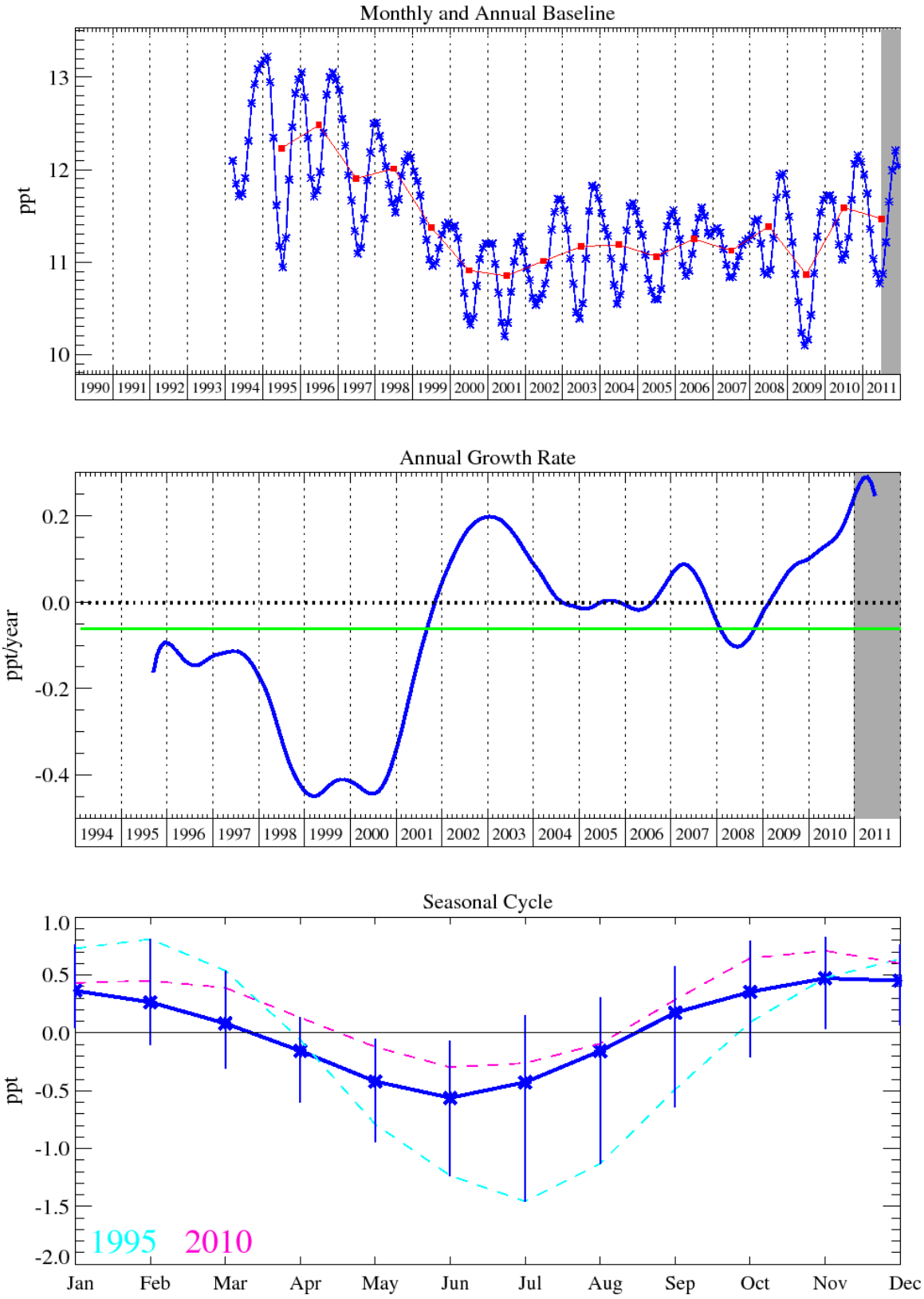

Figure 37: $CHCl_3$: Monthly (blue) and annual (red) baseline concentrations (top plot). Annual (blue) and overall average growth rate (green) (middle plot). Seasonal cycle (de-trended) with year to year variability (lower plot).

4.3.5.4 CCl_4 (carbon tetrachloride)

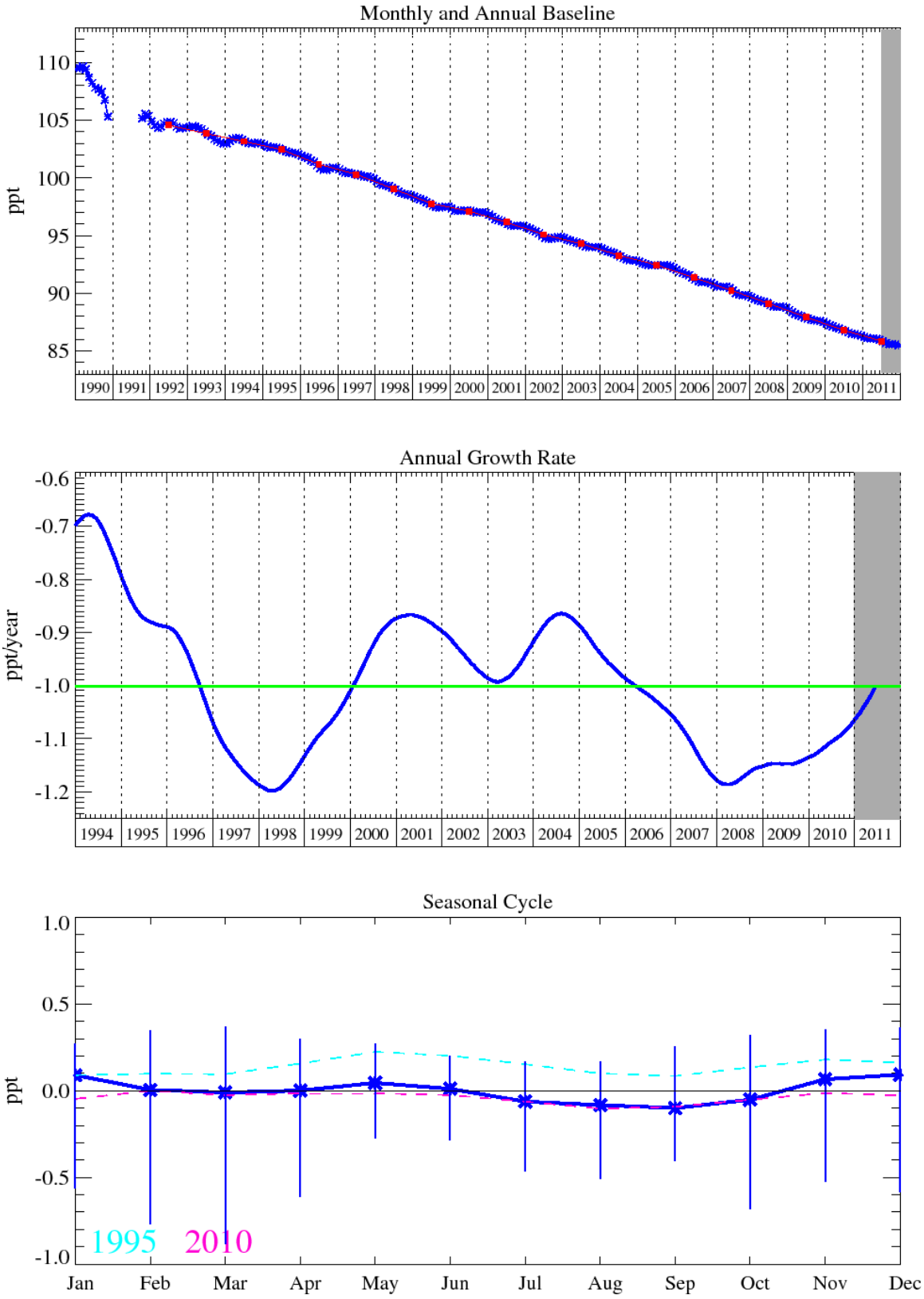

Figure 38: CCl_4: Monthly (blue) and annual (red) baseline concentrations (top plot). Annual (blue) and overall average growth rate (green) (middle plot). Seasonal cycle (de-trended) with year to year variability (lower plot).

4.3.5.5 CH_3CCl_3 (methyl chloroform)

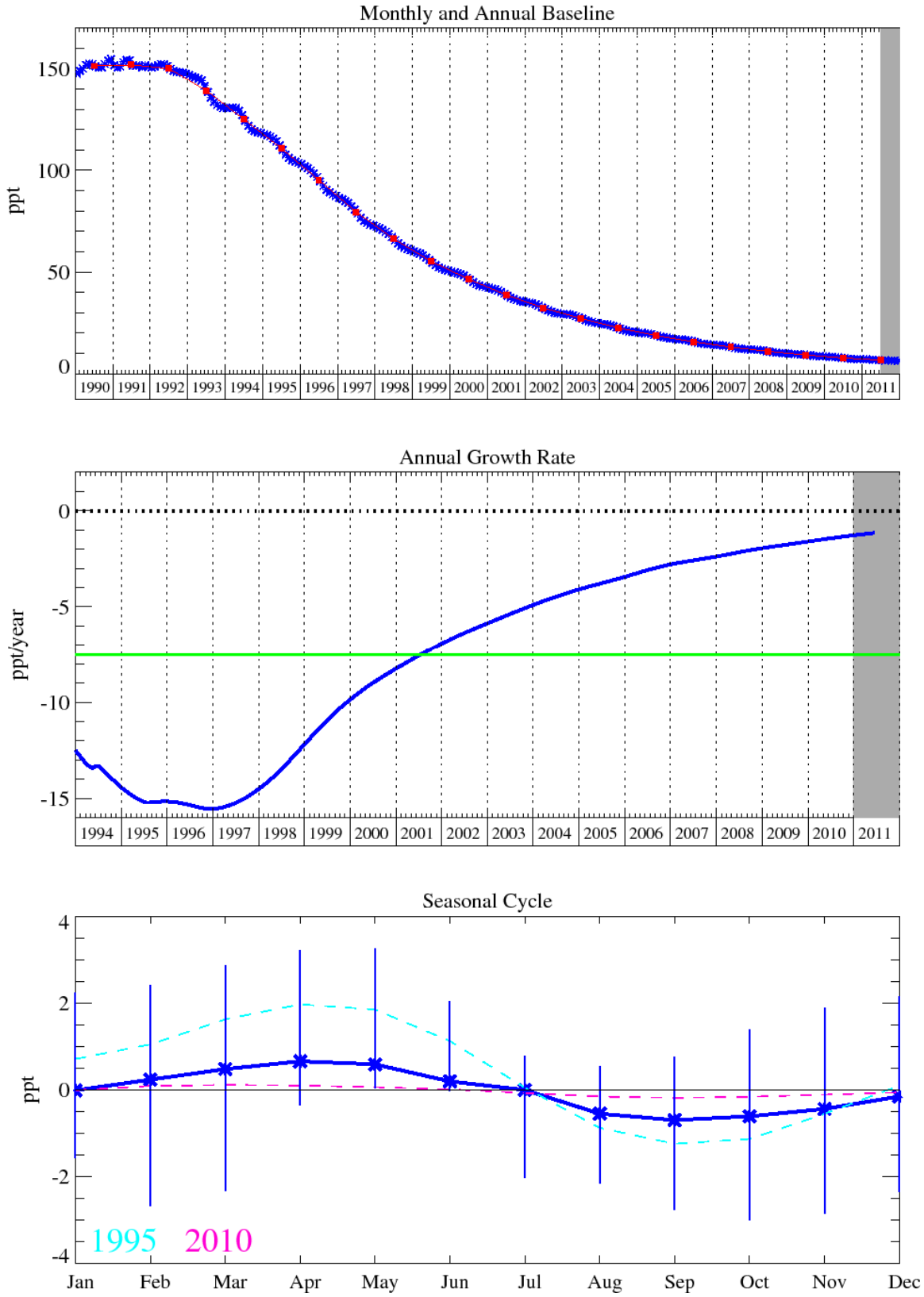

Figure 39: CH_3CCl_3: Monthly (blue) and annual (red) baseline concentrations (top plot). Annual (blue) and overall average growth rate (green) (middle plot). Seasonal cycle (de-trended) with year to year variability (lower plot).

4.3.5.6 $CHClCCl_2$

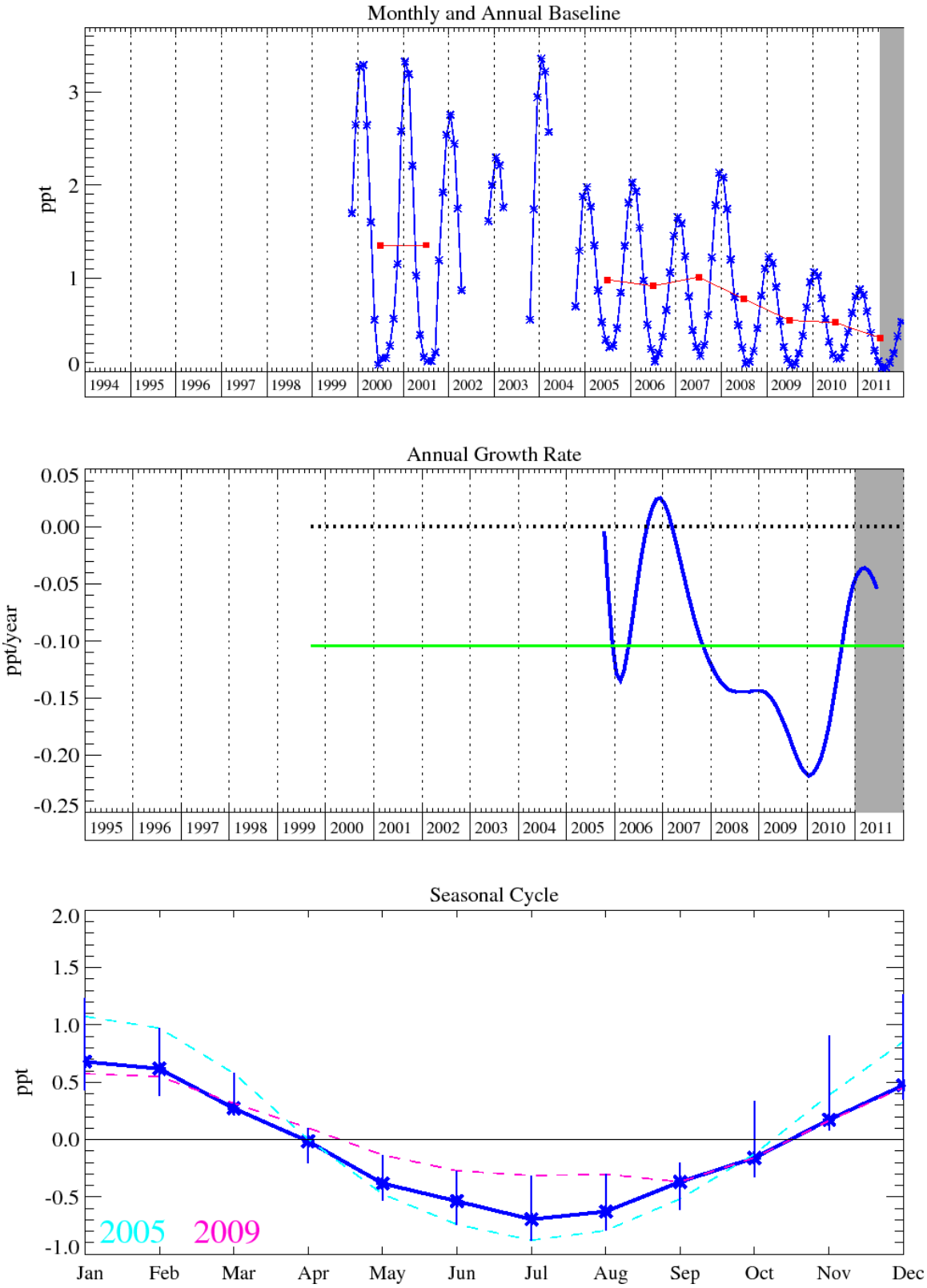

Figure 40: $CHClCCl_2$: Monthly (blue) and annual (red) baseline concentrations (top plot). Annual (blue) and overall average growth rate (green) (middle plot). Seasonal cycle (de-trended) with year to year variability (lower plot).

4.3.5.7 CCl_2CCl_2

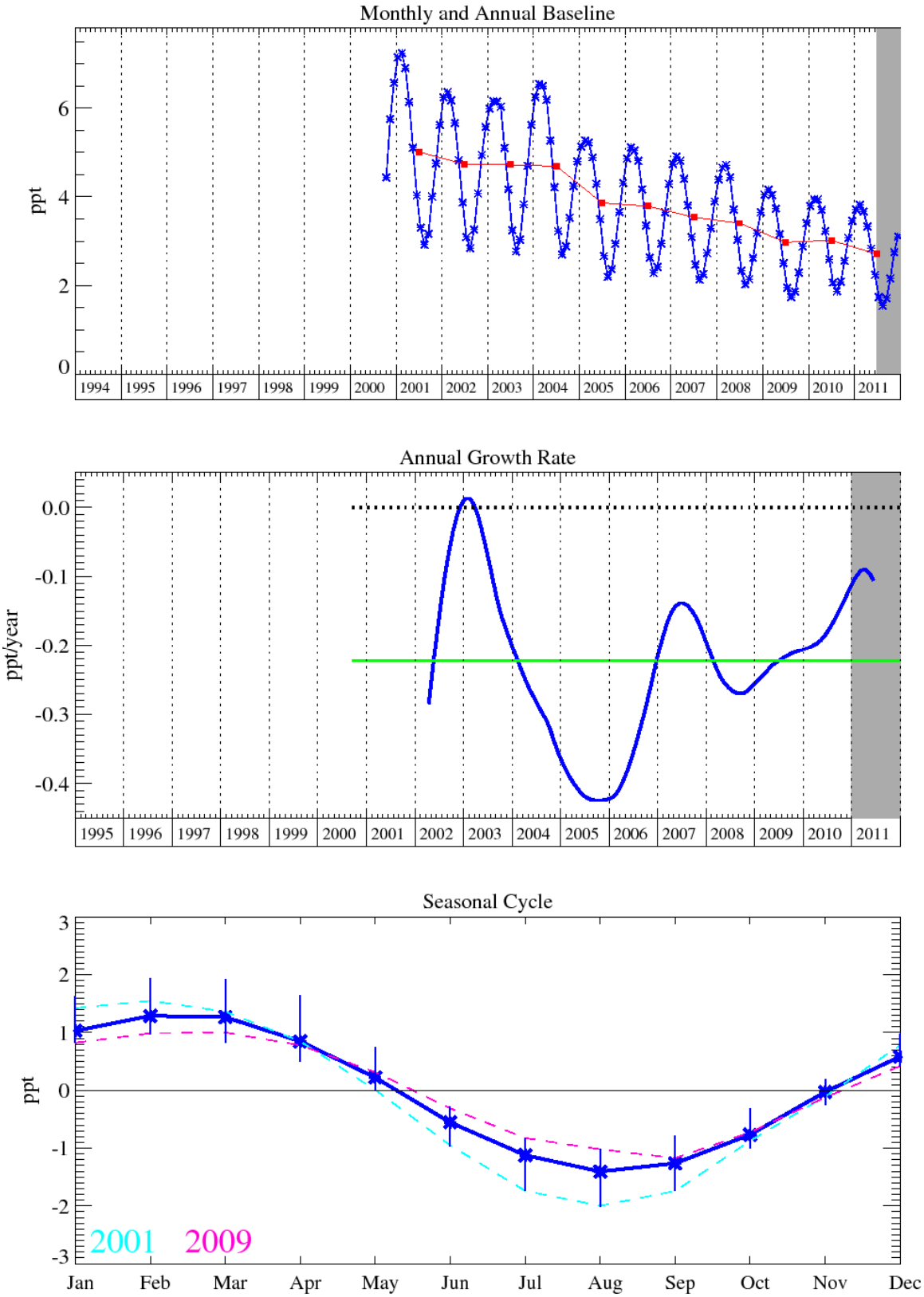

Figure 41: CCl_2CCl_2: Monthly (blue) and annual (red) baseline concentrations (top plot). Annual (blue) and overall average growth rate (green) (middle plot). Seasonal cycle (de-trended) with year to year variability (lower plot).

4.3.6 Bromine compounds

The instrument change in 2005 to the Medusa system produced a discontinuity in the methyl bromide record and should be discounted (Figure 42).

Halon-1211 (Figure 45) continues to show a slight reduction of 0.07 ppt/yr due to limits imposed on halon production in developed nations. Levels at Mace Head are 4.15 ppt for halon-1211 at the end of December 2011. The trend of halon-1301 shown in Figure 46 appears to have reached a plateau at 3.3 ppt in the background atmosphere at Mace Head. The differing rate of decline of the two halons is reflected by their different atmospheric lifetimes; 65 years for halon-1301 and 16 years for halon-1211.

We continue to report trends for the minor halon-2402 (20 year lifetime). This compound was used predominantly in the former Soviet Union. No information on the production of halon-2402 before 1986 has been found. Fraser et al., (1999) developed emission projections for halon-2402 based on atmospheric measurements. They reported that the emissions grew steadily in the 1970s and 1980s, peaking in the 1988-91 timeframe at 1.7 Gg/yr and found these results to be qualitatively consistent with the peak production of 28,000 ODP tonnes reported by the Russian Federation under Article VII of the Montreal Protocol (or assuming all production was halon-2402 and an ODP of 6, a peak production of approximately 4.650 Gg/yr). Measurements at Mace Head indicate that the levels of halon-2402 are fairly stable in the atmosphere (0.46 ppt), the trend estimates are for a reduction of 0.01 ppt/yr in 2011, however the error bars associated with the measurement are large (Figure 47). This magnitude of reduction is consistent with declines in global surface mixing ratios reported in the 2010 WMO Ozone Assessment.

4.3.6.1 Methyl bromide (CH_3Br)

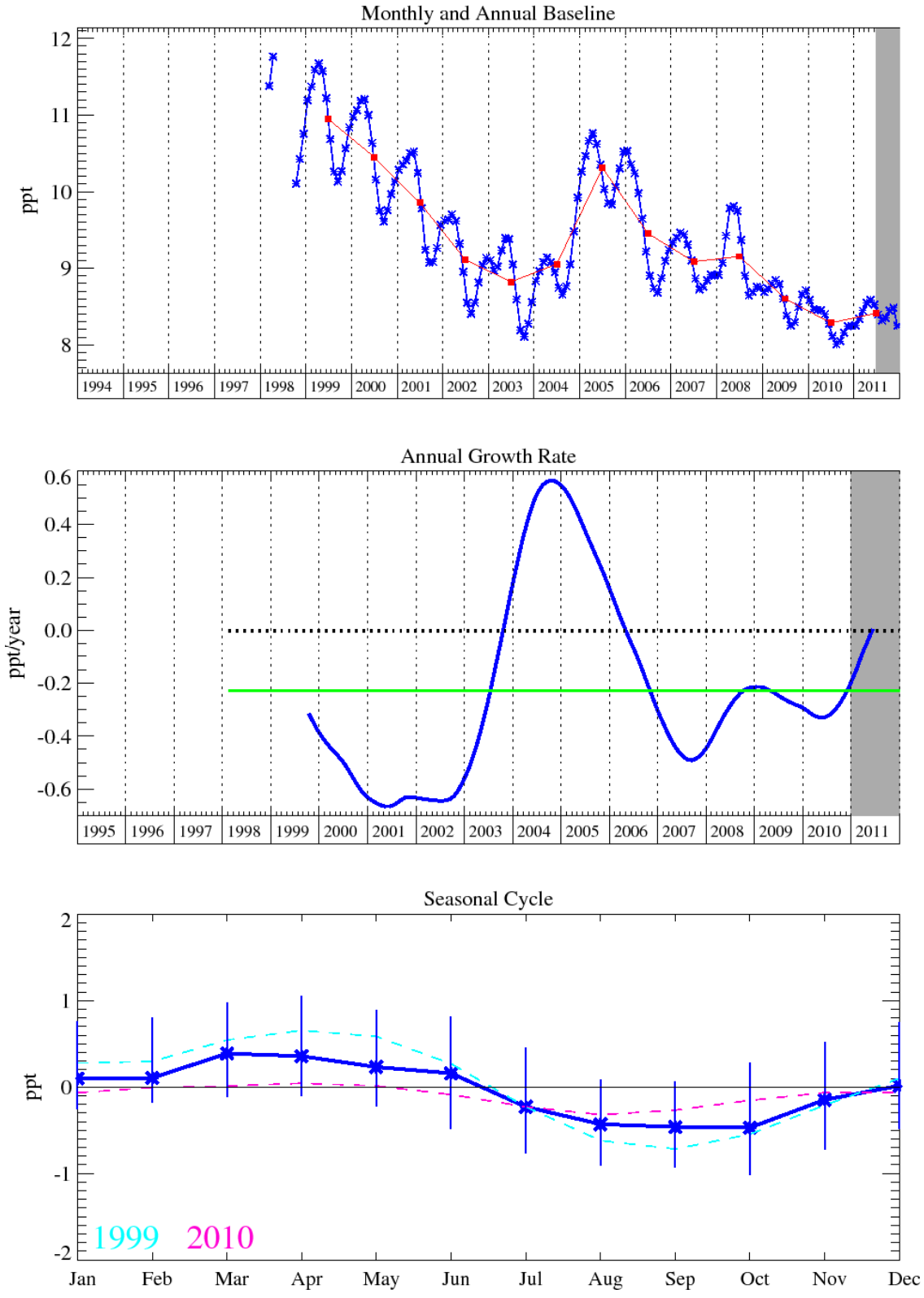

Figure 42: Methyl bromide: Monthly (blue) and annual (red) baseline concentrations (top plot). Annual (blue) and overall average growth rate (green) (middle plot). Seasonal cycle (de-trended) with year to year variability (lower plot).

4.3.6.2 CH_2Br_2

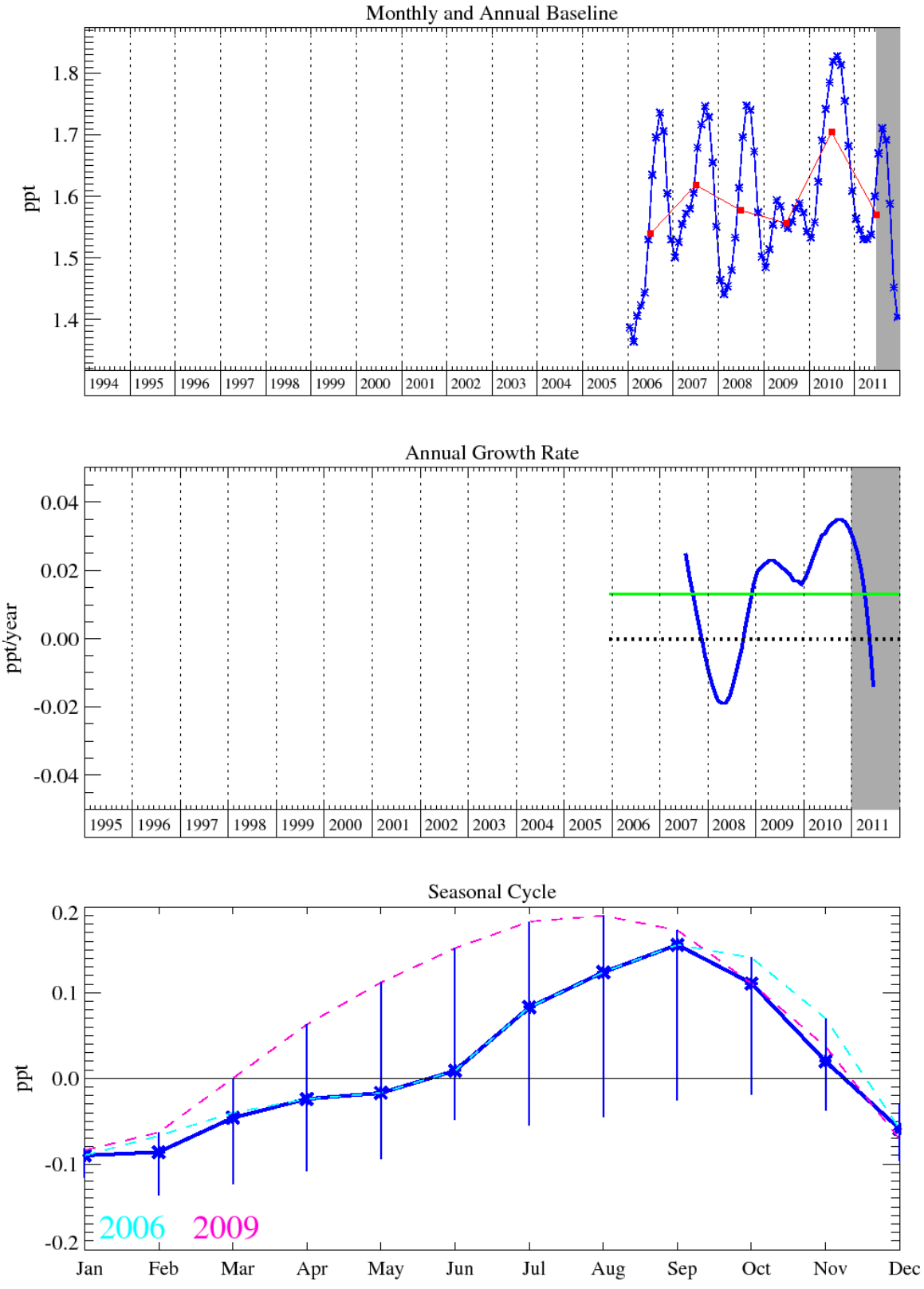

Figure 43: Dibromomethane: Monthly (blue) and annual (red) baseline concentrations (top plot). Annual (blue) and overall average growth rate (green) (middle plot). Seasonal cycle (de-trended) with year to year variability (lower plot).

4.3.6.3 Bromoform ($CHBr_3$)

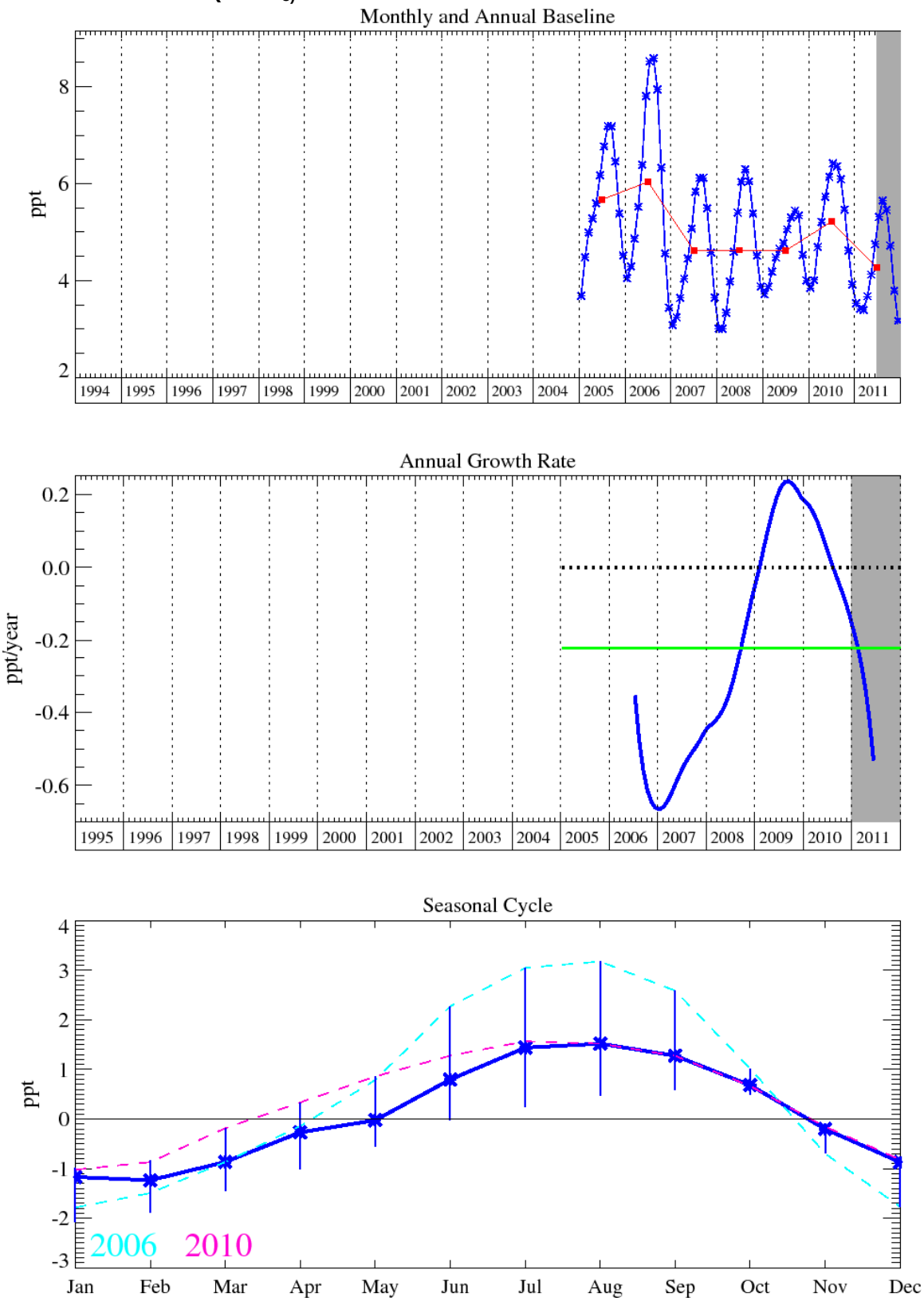

Figure 44: Bromoform: Monthly (blue) and annual (red) baseline concentrations (top plot). Annual (blue) and overall average growth rate (green) (middle plot). Seasonal cycle (de-trended) with year to year variability (lower plot).

4.3.6.4 Halon-1211

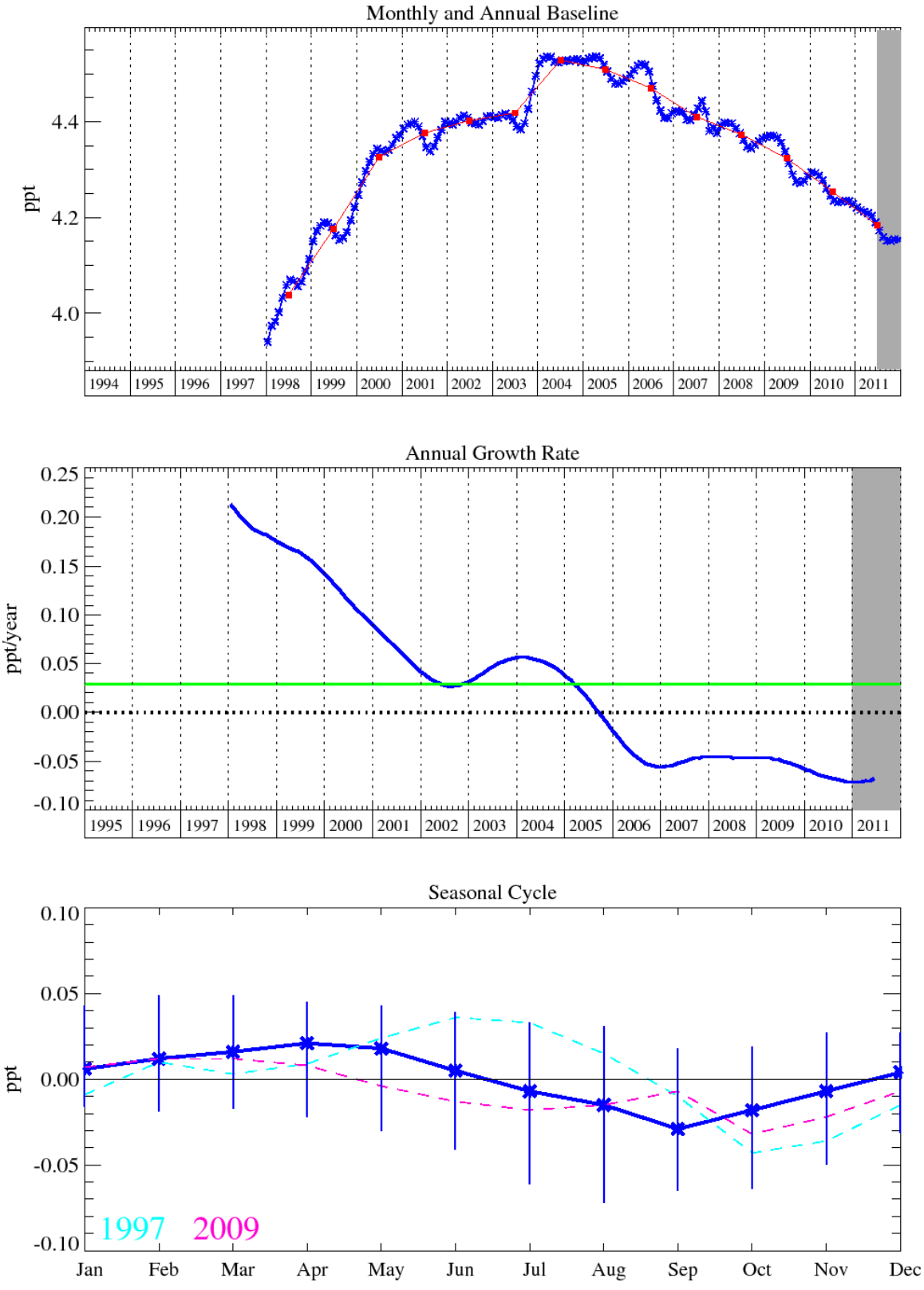

Figure 45: Halon-1211: Monthly (blue) and annual (red) baseline concentrations (top plot). Annual (blue) and overall average growth rate (green) (middle plot). Seasonal cycle (de-trended) with year to year variability (lower plot).

4.3.6.5 Halon-1301

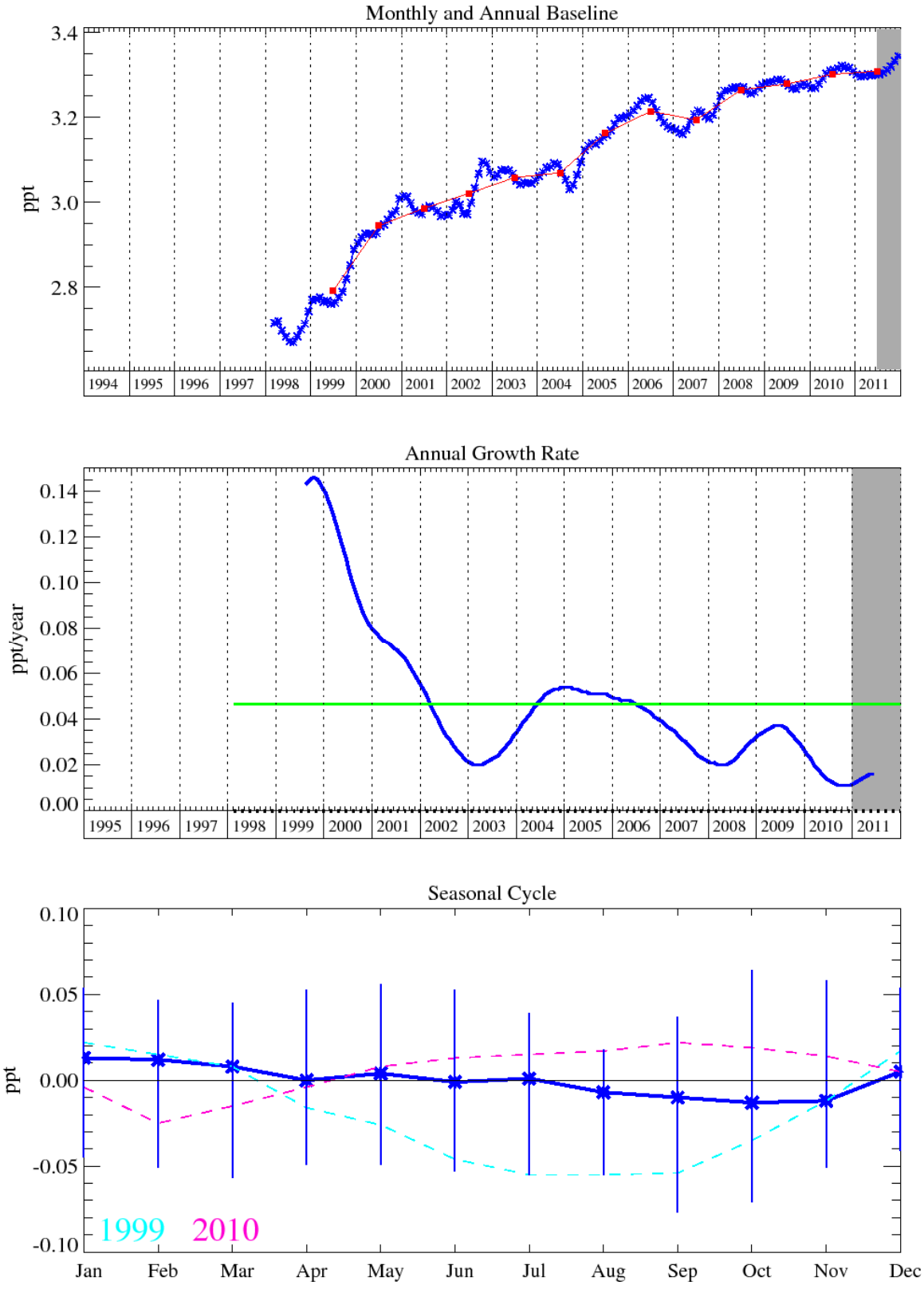

Figure 46: Halon-1301: Monthly (blue) and annual (red) baseline concentrations (top plot). Annual (blue) and overall average growth rate (green) (middle plot). Seasonal cycle (de-trended) with year to year variability (lower plot).

4.3.6.6 Halon-2402

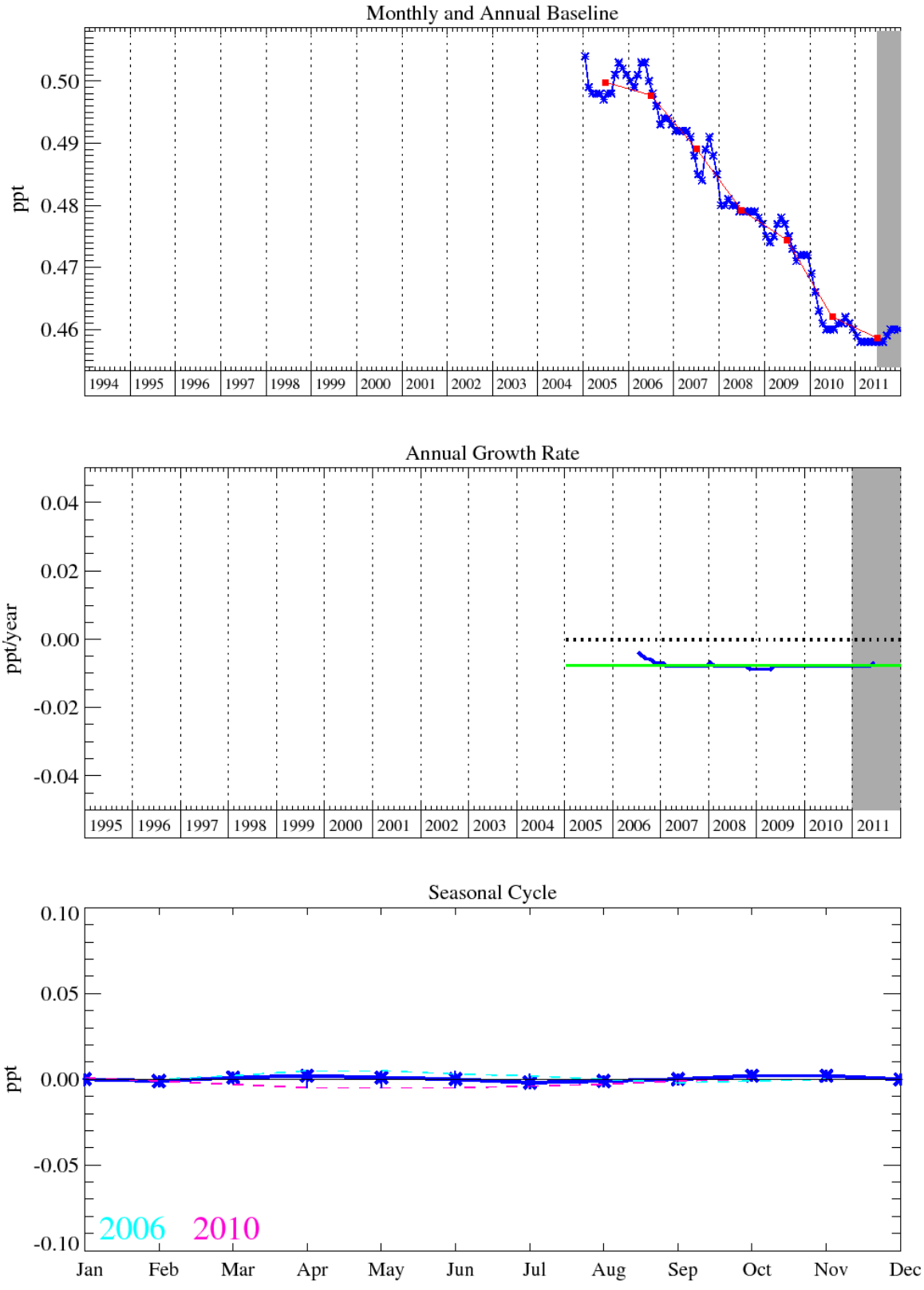

Figure 47: Halon-2402: Monthly (blue) and annual (red) baseline concentrations (top plot). Annual (blue) and overall average growth rate (green) (middle plot). Seasonal cycle (de-trended) with year to year variability (lower plot).

4.3.7 Iodine compounds

Methyl Iodide (CH_3I) is a short lived species with a lifetime of only 7 days [Montzka et al., 2011] and has an insignificant GWP as a result. In common with the majority of iodated gases it is predominantly of biogenic origin with the majority of worldwide emissions occurring from sea/air exchange in open ocean locations [Bassford et al., 1999; Baker et al., 2000; Yokouchi et al., 2001; Cohan et al., 2003]. Due to the close proximity of Mace Head to the Atlantic Ocean a significant variability can be seen in both the baseline measurements and annual growth rates. There are also significant macroalgae sources on the shoreline of the coastal bays to the south and east of Mace Head [Bassford et al., 1999; Baker et al., 2000] which tend to dominate the above baseline measurements

4.3.7.1 CH_3I

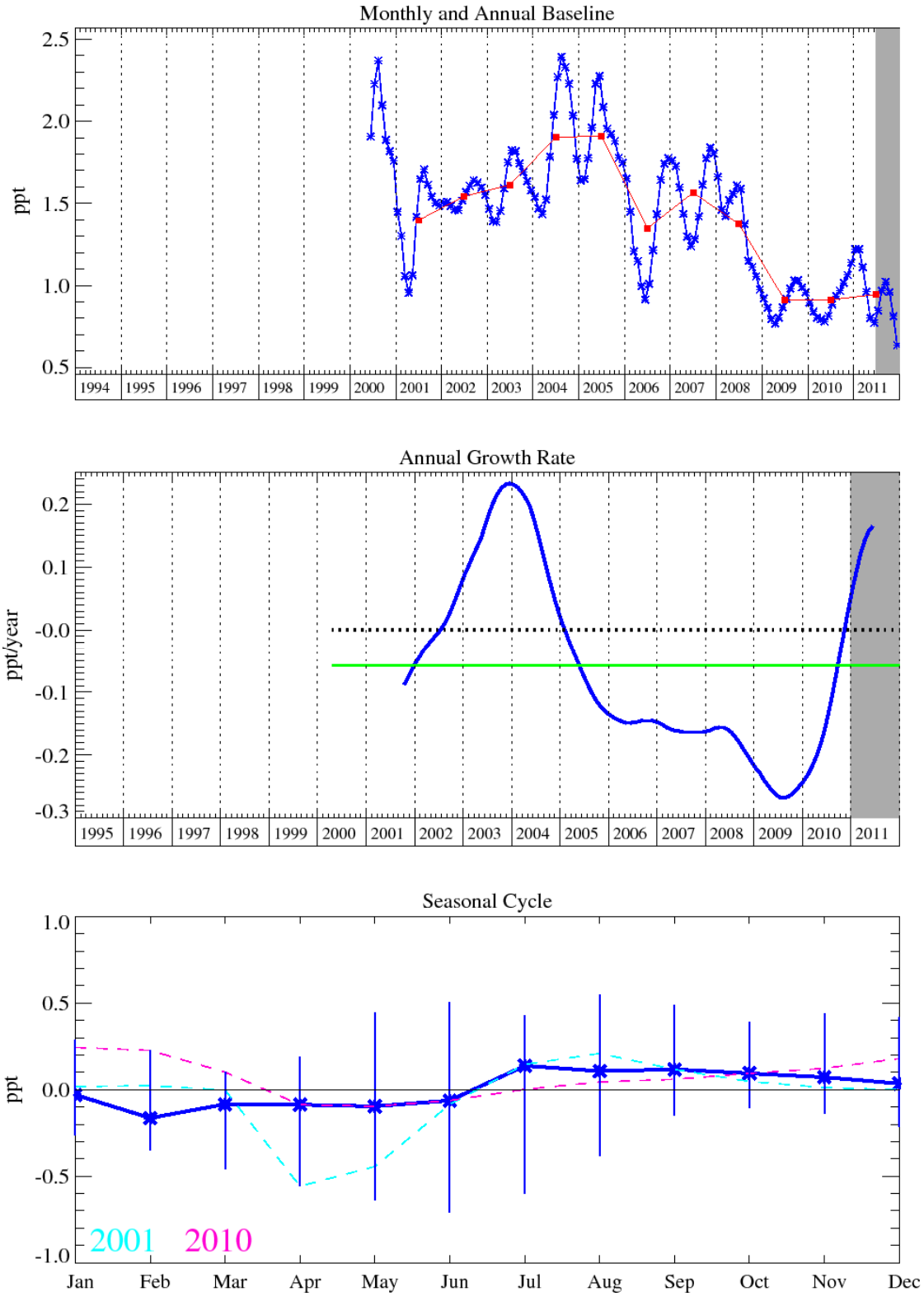

Figure 48: CH_3I: Monthly (blue) and annual (red) baseline concentrations (top plot). Annual (blue) and overall average growth rate (green) (middle plot). Seasonal cycle (de-trended) with year to year variability (lower plot).

4.3.8 Hydrocarbons

The long term trend for CH_4, shown in Figure 49 is of particular interest with a steep rise up to about 2000 followed by a flat period with almost no growth and then most recently a steep rise of 7.5 ppb/yr over the period 2008-2009, 2011 showed growth of 2.7 ppb/yr with a mixing ratio of 1885.9 ppb in December 2011. This most recent growth rate anomaly is unusual in that it occurred almost simultaneously at all of the AGAGE stations in both hemispheres.

In our annual report in 2009 we discussed how the mole fraction of CH_4 in the atmosphere had been rising considerably faster than its long term average growth rate. Several theories were postulated:

(1) Increased emissions from the high latitudes in the Northern hemisphere related to wetlands and reduced permafrost/snow cover.
(2) Increased emissions in the tropics due to increased emissions from wetlands/rice production or biomass burning due to El Niňo conditions.
(3) Reduced levels of OH in the atmosphere. OH is the major sink for atmospheric CH_4.

However each of these theories in isolation does not seem to completely fit the evidence gathered so far. For example, there is no evidence for any link to large scale biomass burning (i.e. no concomitant increase in carbon monoxide), as was the case in 1998 driven by the largest ever El Nino drought. It was therefore our opinion that it is as yet too early to precisely pinpoint the cause for the elevated levels of CH_4 across the globe.

The inferences drawn from the observations were that the CH_4 increase are driven by wetland emissions in the boreal region (driven by a temperature anomaly) and in the tropics (possibly driven by a precipitation anomaly) with a small role for OH changes a possibility in the tropics but not statistically significant. The mole fraction of CH_4 reported from Mace Head (and other AGAGE stations) in 2009 indicate that the rise in CH_4 levelled out (as shown in Figure 49).

4.3.8.1 Methane (CH_4)

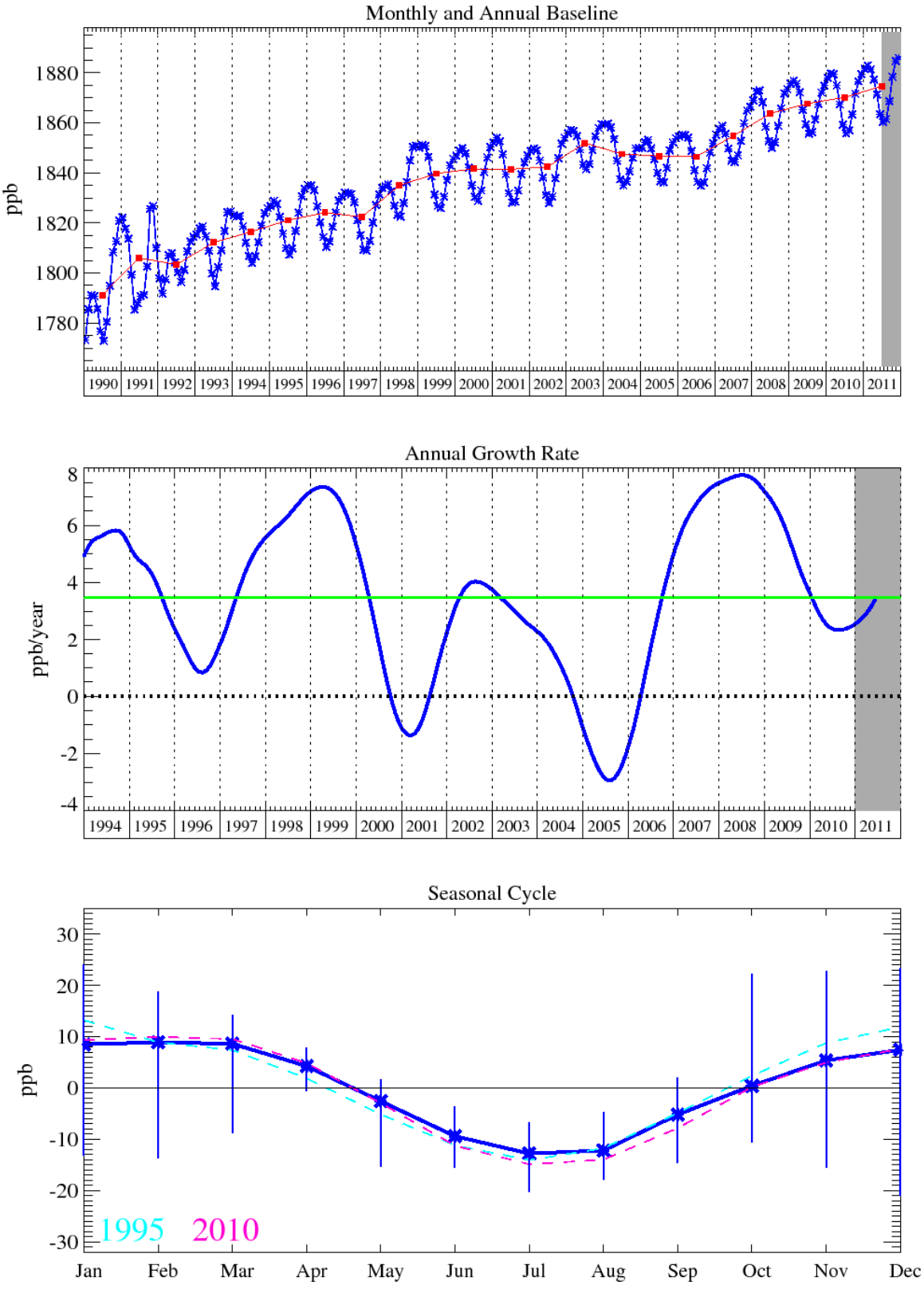

Figure 49: Methane: Monthly (blue) and annual (red) baseline concentrations (top plot). Annual (blue) and overall average growth rate (green) (middle plot). Seasonal cycle (de-trended) with year to year variability (lower plot).

4.3.8.2 Ethane (C_2H_6)

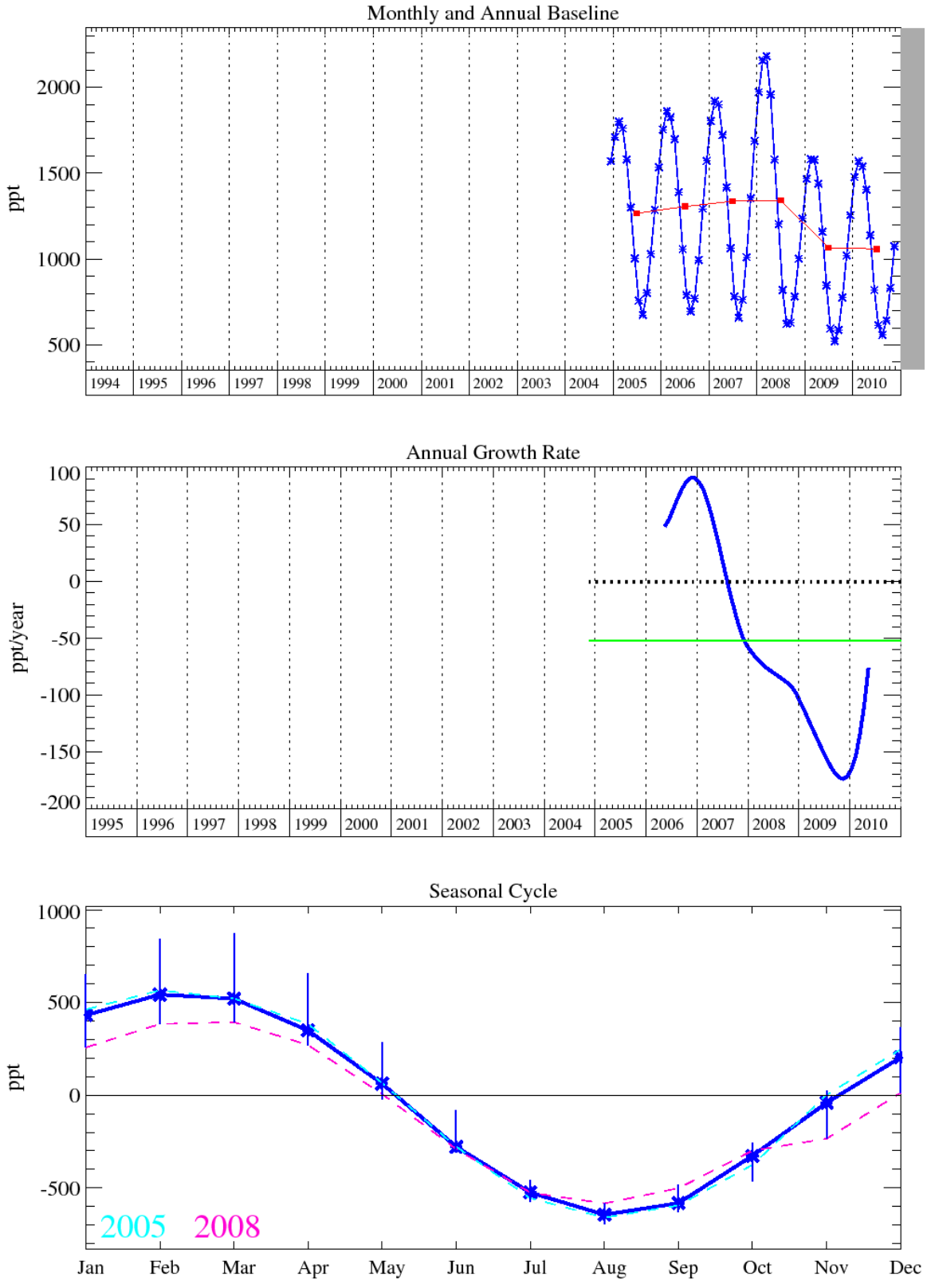

Figure 50: Ethane: Monthly (blue) and annual (red) baseline concentrations (top plot). Annual (blue) and overall average growth rate (green) (middle plot). Seasonal cycle (de-trended) with year to year variability (lower plot).

4.3.8.3 Benzene (C_6H_6)

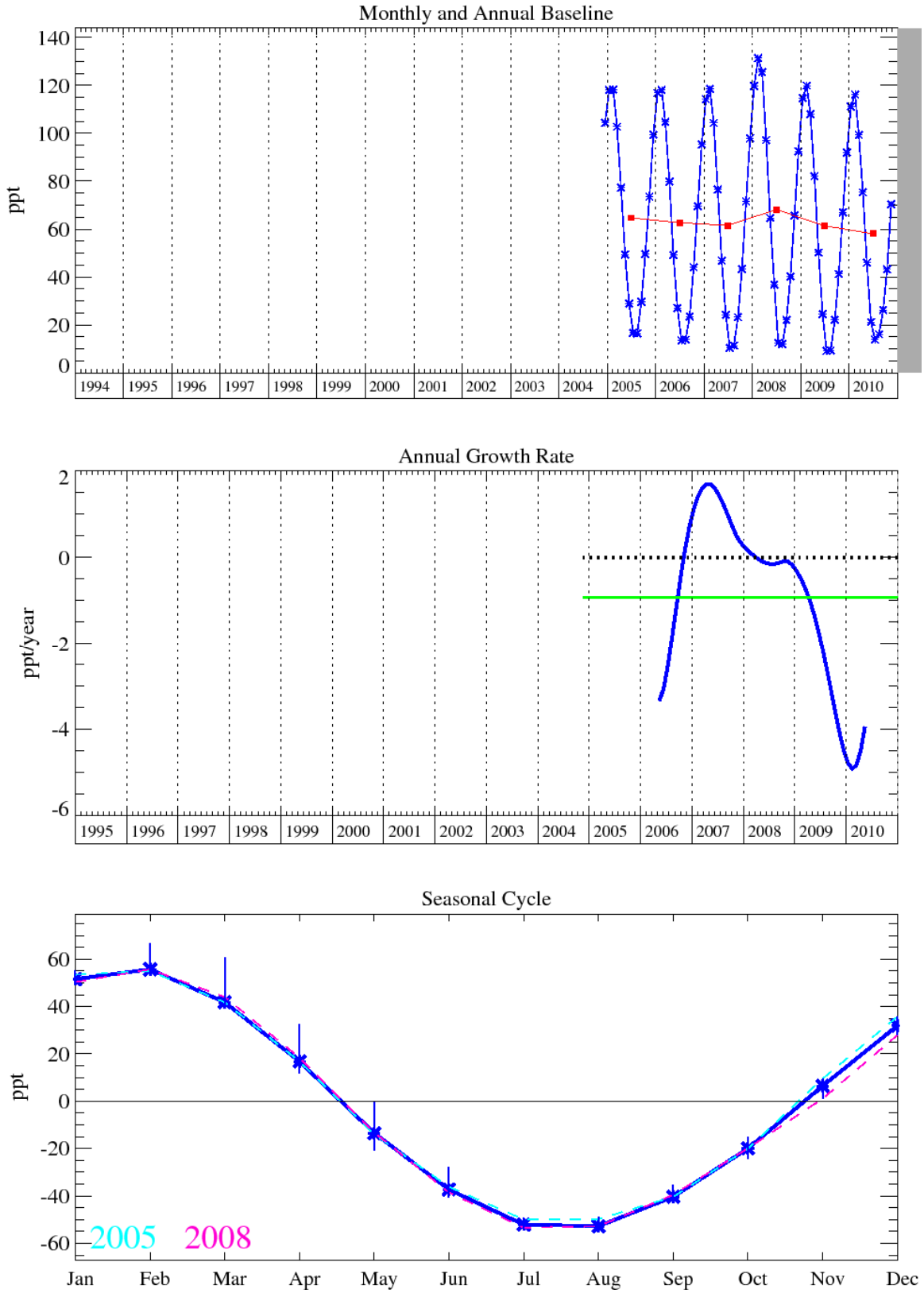

Figure 51: Benzene: Monthly (blue) and annual (red) baseline concentrations (top plot). Annual (blue) and overall average growth rate (green) (middle plot). Seasonal cycle (de-trended) with year to year variability (lower plot).

4.3.8.4 Toluene (C_7H_8)

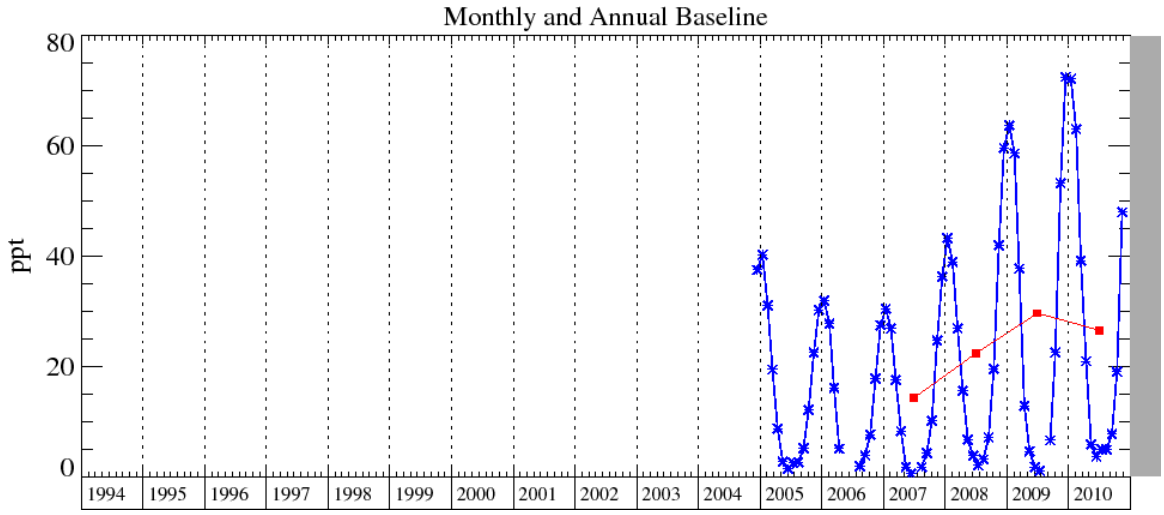

Figure 52: Toluene: Monthly (blue) and annual (red) baseline concentrations (top plot). Annual (blue) and overall average growth rate (green) (middle plot). Seasonal cycle (de-trended) with year to year variability (lower plot).

4.3.9 Oxides of carbon, nitrous oxide, ozone and hydrogen

Annual mean baseline CO levels in 2011 have continued their general downwards trend since 2003. Levels in 2010 showed a small step up relative to those in 2009 and 2011 which is attributed to the forest fires in the Russian Federation (WDCGG, 2012). The baseline mole fraction at the end of 2011 was 122.5 ppb which is significantly lower than its peak values of 147 ppb in 1998 and 137 ppb in 2003.

CO_2 (Figure 54) is the most important greenhouse gas, and has steadily grown at an annual average rate of 1.9 ppm/yr, calculated from the baseline-selected monthly means, it has now reached a mixing ratio of 394 ppm (June 2011) which is the highest yet recorded at Mace Head, Ireland, and has shown significant growth rate anomalies in 1998/99 and 2002/03, which we suggest are a result of the global biomass burning events in those years.

Figure 55 shows the baseline monthly means and trend for N_2O with an almost linear upwards trend of about 0.8 ppb/yr in 2011 and a mixing ratio of 325.0 ppb in December 2011 at Mace Head. The N_2O increase is attributable to human activities, such as fertilizer use and fossil fuel burning, although is also emitted through natural processes occurring in soils and oceans. There are large uncertainties associated with the quantifying the sources of this gas. The global growth anomaly in N_2O is of particular interest with a very substantial increase in 2010-2011. At Mace Head the average historical growth rate of about 0.7 ppb/year has increased to over 0.8 ppb/year. Similarly in the Southern Hemisphere at Cape Grim, Tasmania the growth rate has increased from about 0.6 ppb/year in 2003 to about 1 ppb/year in 2011. From discussions with AGAGE colleagues these increases in N_2O emissions also may be linked to the tropics. Apparently 'wet and warm' microbes in soil can produce bursts in N_2O production, although this is less clear, as very saturated soils can decrease N_2O emissions, However, as noted by Dr R. Weiss of Scripps Institution of Oceanography, there may be different spatial distributions of "wetness" with increased N_2O emissions in some regions and decreases in others. Interestingly, hydrogen has also exhibited a growth spurt in 2011. Here wet soils tend to reduce the normal H_2 deposition velocities due to a reduction in diffusivity. At this stage more global sites need to be carefully assessed to confirm these increases in the N_2O growth rate. We expect AGAGE in collaboration with NOAA to address these issues in a forthcoming paper.

Tropospheric O_3 measurements first started at Mace Head in 1987 and the trends derived from the baseline-selected monthly means, the growth rate and seasonal cycles are shown in figure 56. The Mace Head O_3 measurements exhibited a positive trend (~0.49 ppb) up to about 2003. However, since then there has been no significant growth in ozone and the 12-month moving average of the baseline monthly means in 2011 is 0.05 ppb/yr, its mole fraction at Mace Head was 39.9 in December 2011. Assessment of the long-term trends in tropospheric ozone is difficult due to the scarcity of representative observing sites with long records. The records that do exist vary both in terms of sign and magnitude (Forster *et al.,* 2007). However, The behaviour seen at Mace Head, Ireland is entirely consistent with that reported at two other European baseline stations: Arkona-Zingst and Jungfraujoch (Parrish et al., 2012).

Hydrogen (Figure 57) is an oxidation product of methane and isoprene whose main sink is surface uptake mainly in the northern hemisphere. Annual mean baseline levels have remained roughly constant (within measurement uncertainty) for much of the Mace Head record. It shows a mole fraction of 492.8 ppb in December 2011 which is in the upward phase of its seasonal cycle. There is evidence of anomalous growth in 2010 through the influence of the forest fires in the Russian Federation.

4.3.9.1 Carbon monoxide (CO)

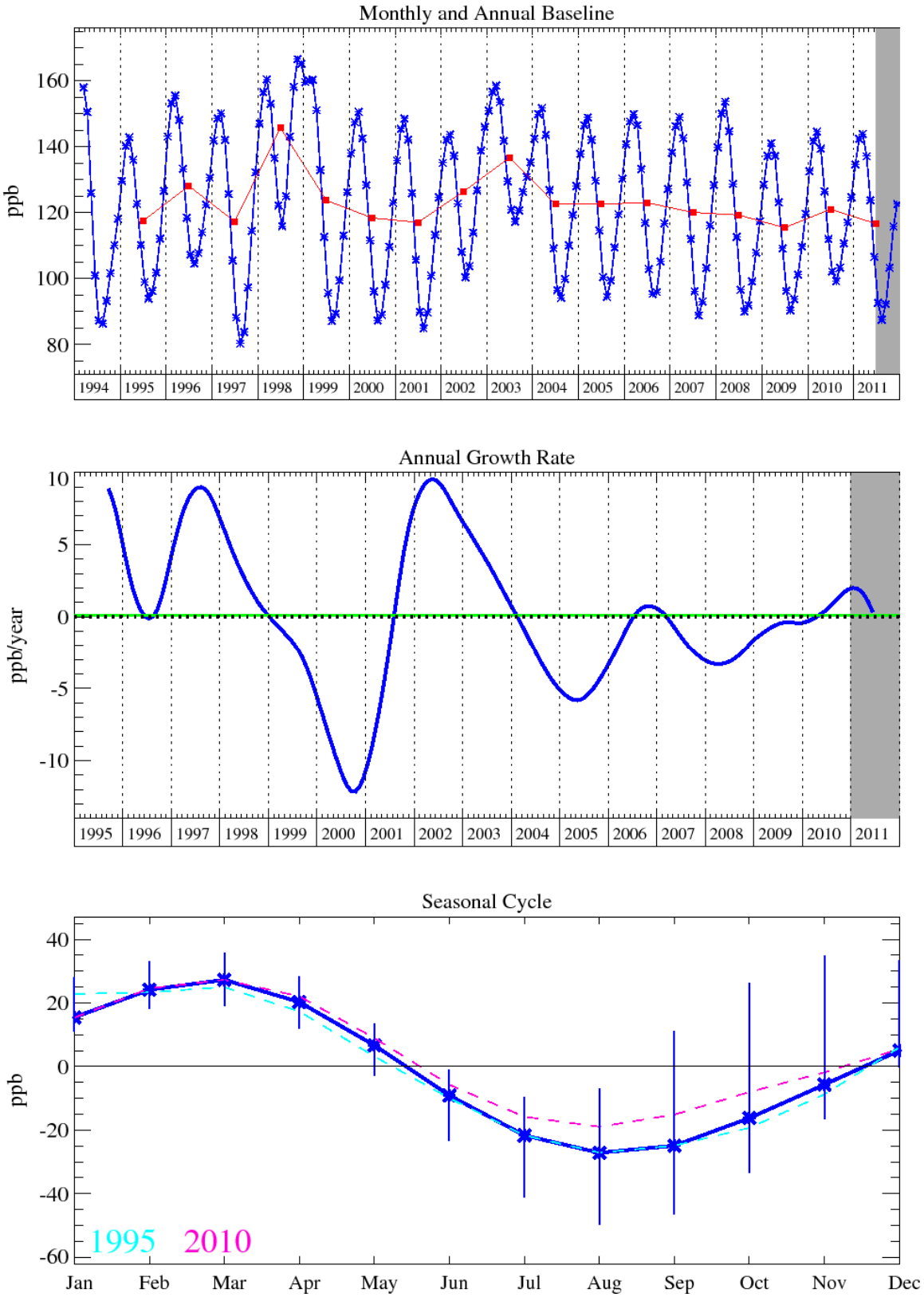

Figure 53: CO: Monthly (blue) and annual (red) baseline concentrations (top plot). Annual (blue) and overall average growth rate (green) (middle plot). Seasonal cycle (de-trended) with year to year variability (lower plot).

4.3.9.2 Carbon dioxide (CO_2)

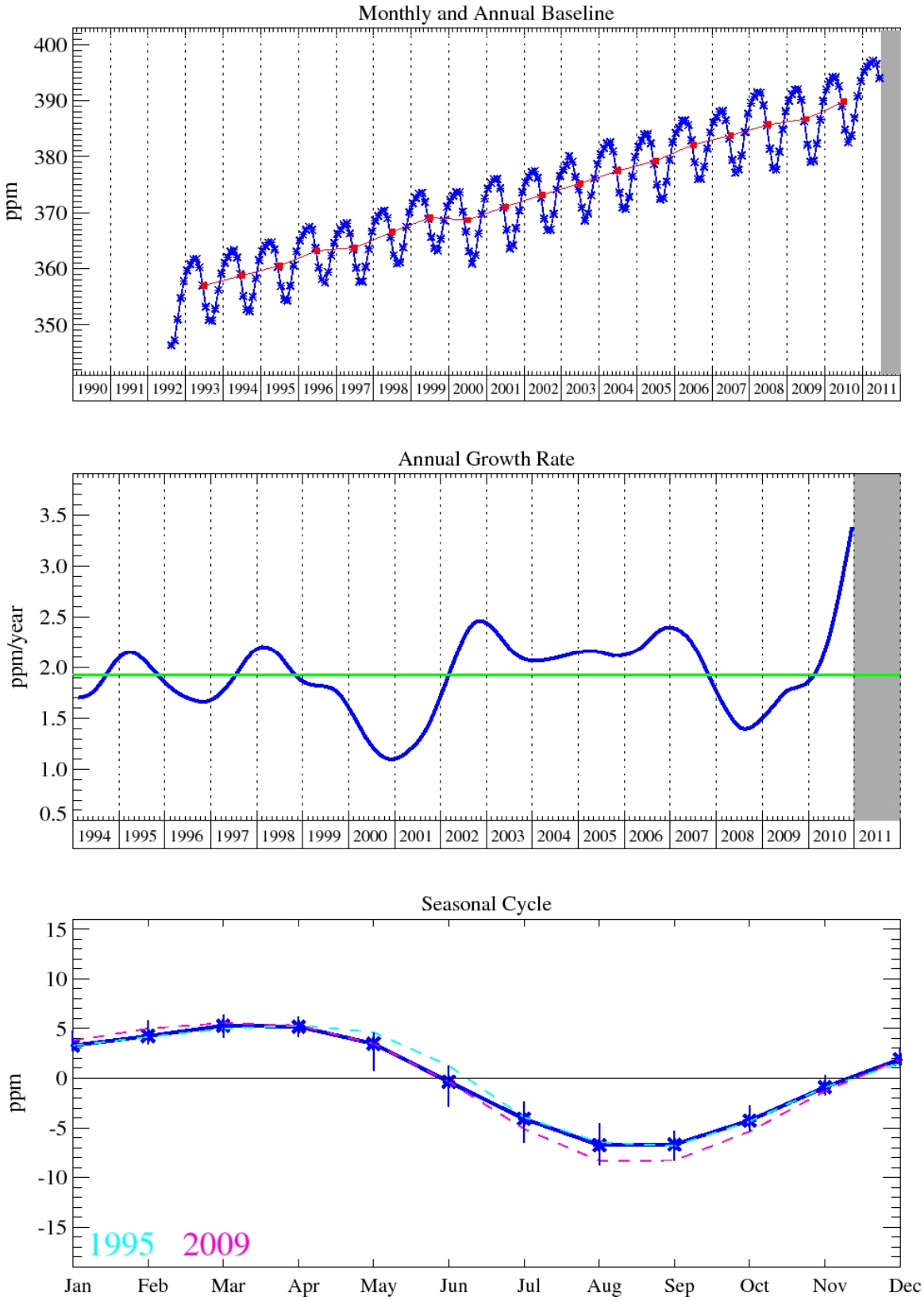

Figure 54: Carbon dioxide: Monthly (blue) and annual (red) baseline concentrations (top plot). Annual (blue) and overall average growth rate (green) (middle plot). Seasonal cycle (de-trended) with year to year variability (lower plot).

Nitrous oxide (N_2O)

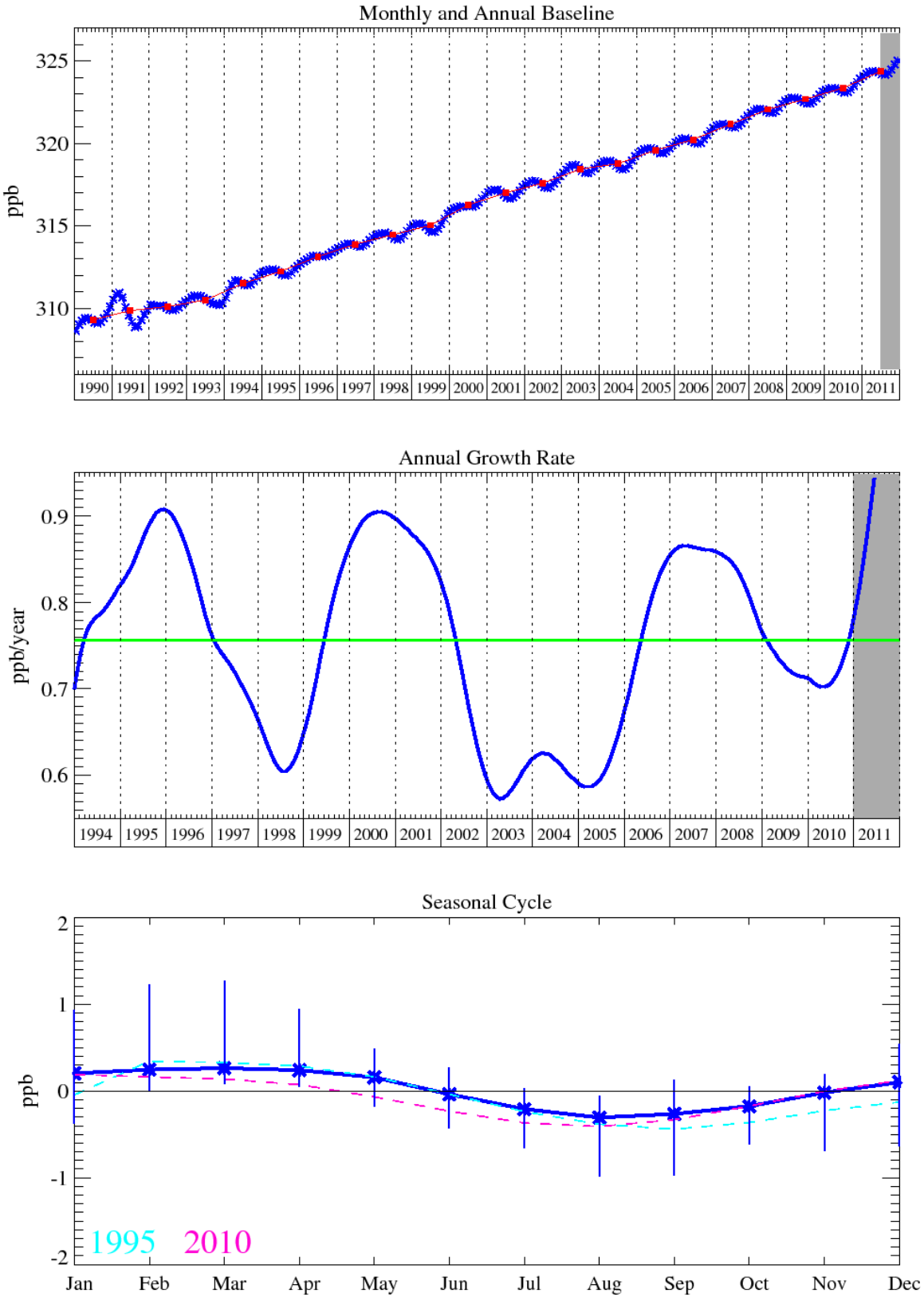

Figure 55: Nitrous oxide: Monthly (blue) and annual (red) baseline concentrations (top plot). Annual (blue) and overall average growth rate (green) (middle plot). Seasonal cycle (de-trended) with year to year variability (lower plot).

4.3.9.3 Ozone (O_3)

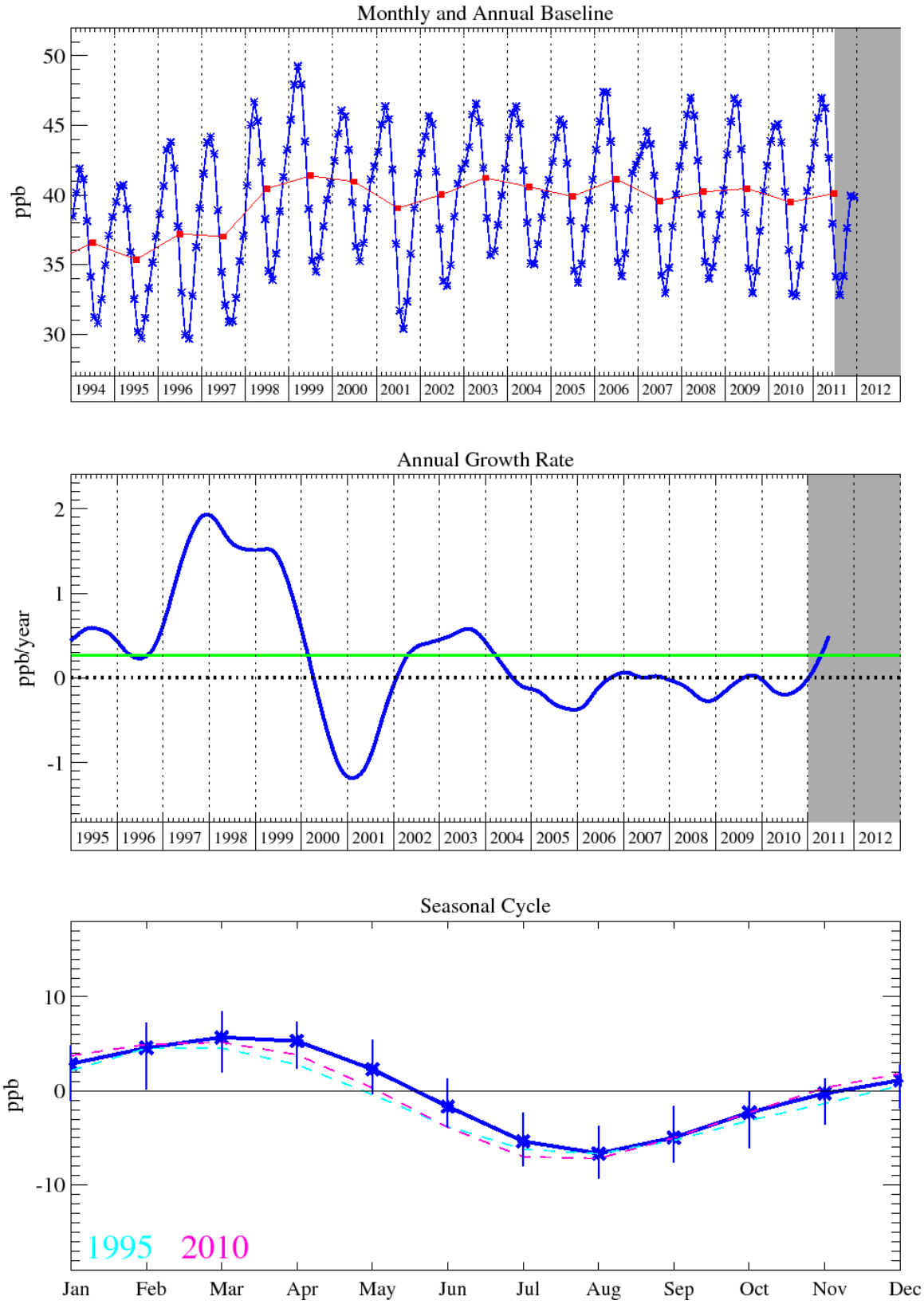

Figure 56: Ozone: Monthly (blue) and annual (red) baseline concentrations (top plot). Annual (blue) and overall average growth rate (green) (middle plot). Seasonal cycle (de-trended) with year to year variability (lower plot).

4.3.9.4 Hydrogen

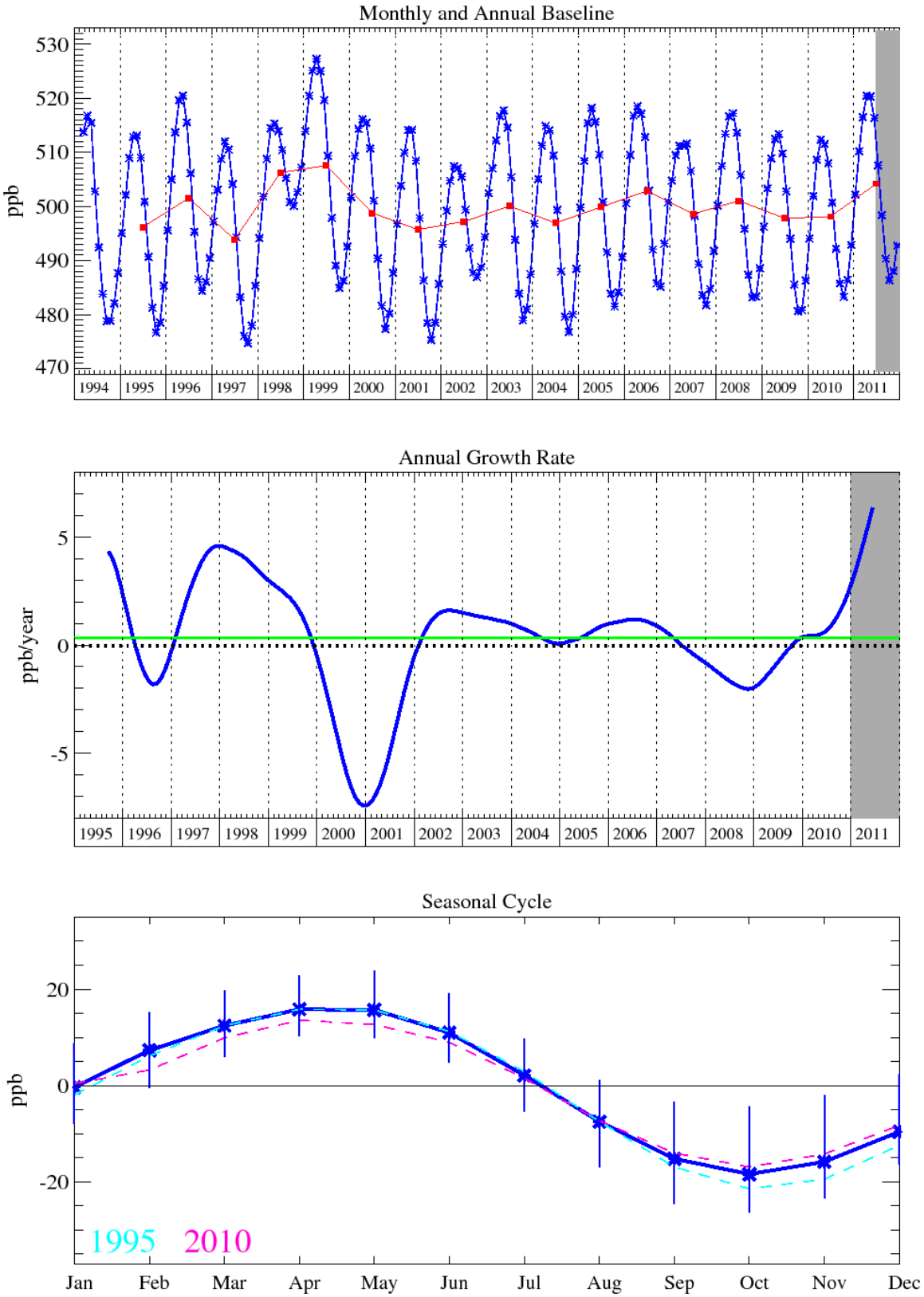

Figure 57: Hydrogen: Monthly (blue) and annual (red) baseline concentrations (top plot). Annual (blue) and overall average growth rate (green) (middle plot). Seasonal cycle (de-trended) with year to year variability (lower plot).

5 Regional Emission Estimates

By removing the time-varying baseline concentrations from the raw measurement data, a time-series of excursions from the baseline for each observed gas has been generated from 1990 onwards or from when observations were started. The observed deviations from baseline are averaged over each two-hour period. These perturbations are driven by emissions on regional scales that have yet to be fully mixed on the hemisphere scale. Henceforth these above-baseline measurements are referred to as simply the observations.

5.1 NAME-Inversion Technique

The observation time-series, together with the NAME model output predicting the recent history of the air, was used to estimate the emission distribution of each gas over NW Europe (NWEU). The iterative best-fit technique, simulated annealing (Press *et al* 1992), was used to derive these regional emission estimates based on a statistical skill score (cost function) comparing the observed and modelled time-series at Mace Head. The technique, referred to as EMIT in figures, starts from a set of random emission maps, it then searches for the emission map that leads to a modelled time series at Mace Head that most accurately mimics the observations.

The aim of the NAME-Inversion method is to estimate the spatial distribution of emissions across a defined geographical area. In the equation to solve (Equation 1) the set of observations (*o*) and the dilution matrix (*D*) as estimated using the NAME model are known. The observations are in volume mixing ratios. The dilution matrix has units (s/m) and is calculated from the time-integrated air concentrations produced by the NAME model. The dilution matrix has *t* rows equal to the number of 2-hour periods considered and has *n* columns equal to the number of grid points in the defined geographical domain. This matrix dilutes a continuous emission of 1 g/m^{2}s over a given grid to an air concentration [g/m^3] at the receptor during a 2-hour period. The observations are converted from volume mixing ratio [ppb] to air concentration [g/m^3] using the modelled temperature and pressure at the observation point.

The inversion domain is chosen to be a smaller subset of the full domain used for the air history maps. It covers 14.30^{o}W – 30.76^{o}E longitude and 36.35^{o}N – 66.30^{o}N latitude and is shown as the black box in figure 8. The smaller domain covers all of Europe and extends into the Atlantic and has an intrinsic horizontal resolution of 0.352^o longitude by 0.234^o latitude. The inversion domain needs to be smaller to ensure re-circulating air masses are fully represented but also because emission sources very distant from Mace Head have little discernible impact on the concentration at the station, i.e. the signal would be too weak to be seen. The inversion method assumes baseline concentration air enters the inversion domain regardless of direction. For the eastern and southern edges in particular this will be incorrect. Emissions in Russia and around the Black Sea would be expected to elevate the atmospheric concentrations along the eastern edge, and due to the latitudinal gradient it would be reasonable to assume below mid-latitudinal baseline concentration air enters from the south. This issue is overcome in the inversion by solving for but not analysing the estimated emissions in any grid on the edge of the inversion domain. It is assumed that the error of above or below baseline concentration air entering the domain will be absorbed into the solutions in these edge grids.

In order for the best-fit algorithm to provide robust solutions for every area within the domain, each region needs to significantly contribute to the air concentration at Mace Head on a reasonable number of time periods. If the signal from an area is only rarely or poorly seen at Mace Head, then its impact on the cost function is minimal and the inversion method has little skill at determining its true emission.

The contribution that different grid boxes make to the air concentration observed varies from grid to grid. Grid boxes that are distant from the observation site contribute little to the observation, whereas those that are close have a large impact. In order to balance the contribution from different grid boxes, those that are more distant are grouped together into increasingly larger blocks. The grouping varies for each time period considered and between the different gases due to varying meteorology and the impact of missing observations respectively. The underlying horizontal grid resolution is 25 km (= *x*) and is equal to the resolution of the NAME output. The grouping creates blocks that have a resolution of *x*, 2*x*, 4*x*, 8*x,* 16*x* and 32x.

An *emission sensitivity* level [g/m^2/s] has been estimated for each gas. Below this level the impact of the emission at the receptor is assumed lost within the baseline noise of the observation. The *dilution sensitivity limit* threshold (3.4 s/m), as derived in the baseline analysis, is used again. Baseline noise is defined as the standard deviation of baseline observations about the defined smoothed baseline value.

For each grid box the number of times it provides a contribution to Mace Head above the *dilution sensitivity limit* threshold is calculated from the dilution matrix. If this is below the minimum number required (arbitrarily defined as 240 2-hour time periods, i.e. 20 days) or the total contribution from the grid box is lower than an arbitrary value (6 x 240 x *dilution sensitivity limit*) then a grid resolution twice as coarse is considered. This process is repeated until the condition is satisfied or until the grid resolution is 32 times the original (32*x*) (Figure 58), where *x* = ~25 km.

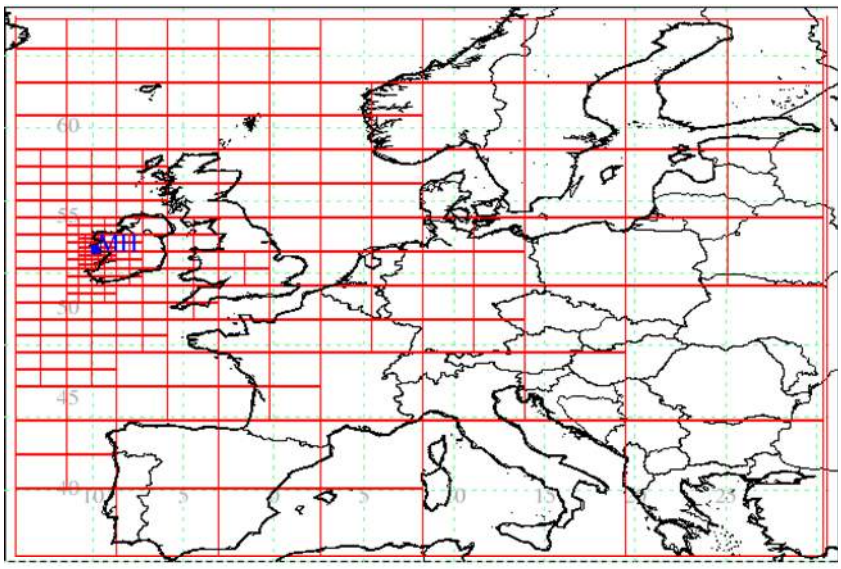

Figure 58: Example of the distribution of the different sized regions used by the inversion method to estimate regional emissions (1*x* by 1*x* through to 32*x* by 32*x*, *x* = ~25 km).

The modelled time-series at the measurement station is calculated by applying the current emission map to the dilution matrix (Equation 1).

The inversion process works by iteratively choosing different emissions, varying the emission magnitudes and distributions, with the aim of minimising the mismatch between the observations and the modelled concentrations. No *a priori* conditions are set. The relative skill of a derived emission map is tested by comparing the modelled and observed time-series by using a cost function that combines four different statistics. Other cost functions have been

investigated, for example *RMSE*, using the pseudo observation test (see below) but were found to be less accurate at recreating a prescribed emission distribution.

Cost function: $\left[5(1-r)\right]+\left[0.5\ NMSE\right]+\left[4(1-\ fac2)\right]+\left[20(1-\ facNoise)\right]$

where,

r = Pearson correlation coefficient

NMSE = Normalised Mean Square Error: $\left(\frac{Mean\ Square\ Error}{AvgObs\ x\ AvgModel}\right)$

fac2 = Fraction within a factor of 2 of observations

facNoise = Fraction of model values within *Noise* of the observations

Noise = Standard deviation of baseline observations within 6-months of the observation about the defined smoothed baseline value. Note observations below the *Noise* level are considered to have a magnitude equal to the *Noise* level with respect to the *fac2* calculation.

The iteration process is repeated until the future potential improvement in skill in the emission map is estimated to be negligible.

To simulate uncertainties in the meteorology, dispersion and observations a time-series of random noise is applied to the observations. The random element is multiplicative and taken from a log-normal distribution with mean 1 and variance one fifth of the *Noise*. Any observations that are negative are considered to be zero.

Any periods that were classed as baseline but were removed by the statistical filtering are removed from the analysis as these are considered to be unrepresentative of air from that sector. Times when the air is classed as 'local' are likewise removed from the analysis. A 2-hour period is classed as 'local' if the contribution from the 9 grids surrounding Mace Head is above fifteen times the *dilution sensitivity limit*. The local times represent periods when the emissions from the local area (75 km x 75 km area centred on Mace Head) would have a dominate effect on the observations. These are typically characterised by low wind speeds, low boundary layer heights and thus poor dispersion conditions. During such times the meteorological models used, with horizontal resolutions of between 25 and 80 km, are poor at correctly resolving the local flows as they are dominated by sub-grid scale processes, e.g. land-sea breezes. For example, 86% (87%) of the CH_4 (N_2O) observations were retained for analysis.

For each time period solved for, the whole inversion process is repeated multiple times (8) to give an indication of the potential uncertainty in the emission solution, each time with a different random starting point and a different time-series of random noise. Solutions are calculated for three-year periods covering the period when observations are available. After solutions have been estimated for a particular three-year period, the period is moved on by one month and the process repeated, e.g. Jan'95 – Dec'97, Feb'95 – Jan '98, etc.

An annual estimate of emission is calculated by averaging all of the solutions that contain a complete calendar year within the solved-for time period. The range for each year for each geographical region is calculated from the same sample of solutions and is taken as the 5th and 95th percentile solutions.

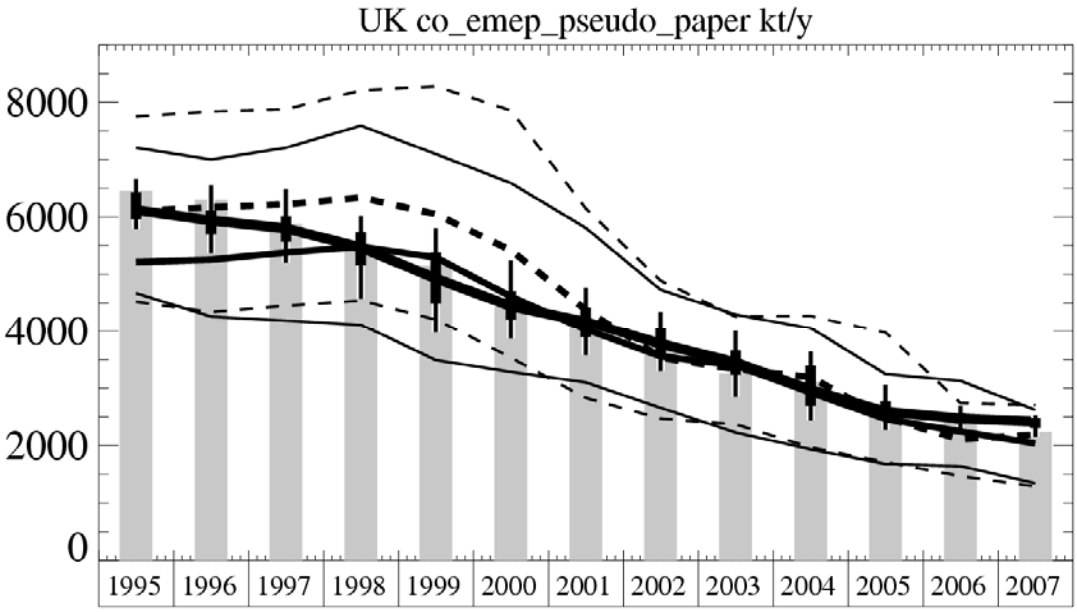

Figure 59: Time-series of annual emission estimates using model-derived pseudo observations. The light grey columns are the EMEP inventory values. The solid line with 5th, 25th, median, 75th and 95th percentiles is the case with no noise and the same meteorology. The solid line is the case with noise and the same meteorology. The dashed line is with noise and different meteorology (UKMO used to create pseudo observations and ERAI dilution matrix used within the inversion). The 5th and 95th estimates provide the uncertainty ranges in each case and are shown as thinner lines with the same style.

To assess the ability of the inversion system to correctly estimate emissions on the regional scale it was first applied to model derived pseudo observations. The carbon monoxide (CO) emissions from the EMEP program (www.emep.int) were used to calculate a model time-series at Mace Head. Time-series' were derived using both ERAI and UKMO. The inversion system was tested using the ERAI dilution matrix applied to, firstly, the pseudo observations derived using ERAI and then to the pseudo observations derived using UKMO. The latter test investigates the ability of the inversion system to estimate emissions with a system that has errors. The impact of applying random noise to the system is investigated by solving with and without noise. Figure 59 shows the time-series of emission estimates and true emissions for NWEU in this idealised case study.

The median emission total when no noise is added to the pseudo observations is excellent and the uncertainty bars are small. When noise is added to the measurements the median fit is still good but the uncertainty range is larger (solid lines). When a different meteorology is used to derive the pseudo observations and noise is added (dashed line) the fit is still good but the uncertainty range is at its largest. However in every case the uncertainty range completely encompasses the true solution and gives confidence that the methodology is able to recreate the correct emission total within the estimated uncertainty range.

Figure 60 is an example of the observed and modelled time series of air concentration for CH_4 for 2010 at Mace Head. The magnitudes and patterns are similar and demonstrate that the inversion process is able to derive an emission map that produces a good match to the observations.

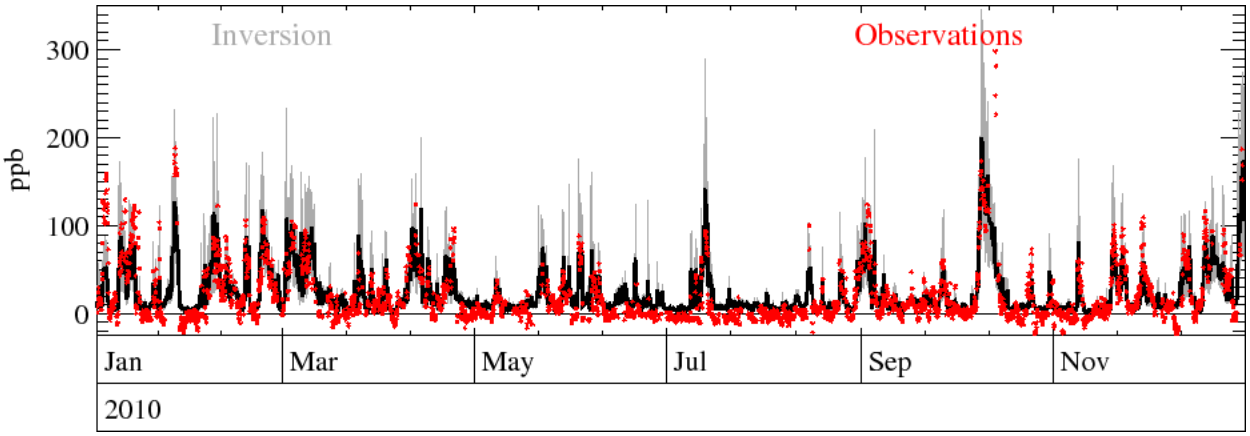

Figure 60: Time series of observed and best-fit modelled CH_4 concentrations (deviation from baseline) at Mace Head for the first three months of 2010 (solid black line = Inversion, grey = uncertainty in inversion, red crosses = observations).

Emission totals from specific geographical areas are calculated by summing the emissions from each 25 km grid box in that region (Figure 61).

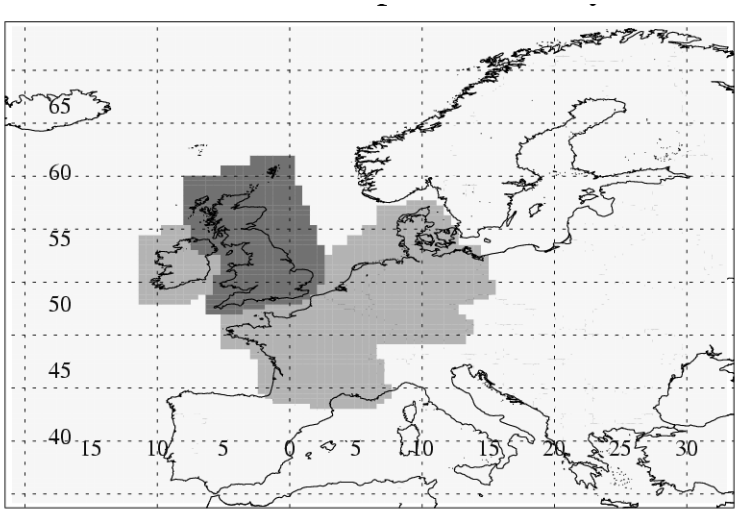

Figure 61: Geographical areas used to define UK and NWEU regional totals

All of the emissions are assumed constant in time and are geographically static within each 3-year study period. This is clearly a significant simplification. A sudden, but subsequently maintained, change in emissions, will be picked up by solving multiple 3-year periods covering slightly different time periods, i.e. solving for a 3-year period and then advancing by one month. Enhanced emissions in any particular season, e.g. increased N_2O emissions in spring following fertilizer application, will not be resolved.

All areas of the domain are assumed to impact reasonably equally on Mace Head. The grouping of grid cells together, so that each area contributes approximately equally to the observations, attempts to ensure this but clearly there will be some variability. Also large grid cells could have significant variability actually within the grid itself especially if there are significant orographic features within the grid, e.g. the Alps. This may lead to errors if certain parts of the grid are more frequently sampled than others. However because of the large travel distances and therefore time elapsed between emission in these large grids and measurement the impact of this will be small. Also by only reporting emissions within NWEU this issue is assumed small.

The inversion method makes no distinction between anthropogenic and natural sources and thus its estimates are for the combined total, making direct comparisons with the UNFCCC inventory difficult. For most of the gases analysed here the natural emissions are estimated to be small in comparison to the anthropogenic emissions. For example, for CH_4 the natural emissions in NWEU are estimated to be 240 kt/yr (Bergamaschi *et al* 2005).

It is also important to recognise that the release of certain gases to the atmosphere, e.g. N_2O released from agricultural practices, may occur many miles from its actual source and therefore adds to the uncertainty of using the maps to attribute emissions to particular regions. The area considered to be the UK includes the waters directly surrounding the UK (Figure 61), so the impact of this is considered to be small for the UK. This would be problematic if the individual contributions of Belgium or The Netherlands for example were presented and is the reason why only the NWEU total is considered. The most significant region in relation to this issue is the border between Northern Ireland and Ireland, however due to the proximity to Mace Head and the corresponding high resolution of the output there the impact is assumed small.

The transport modelling and thus the inversion algorithm also assume that the loss processes associated with each gas are negligible within the regional domain. Given the atmospheric lifetimes of most of the gases studied here this is considered to be a robust assumption.

5.2 Regional Emission Estimates

5.2.1 CFC

5.2.1.1 CFC-11

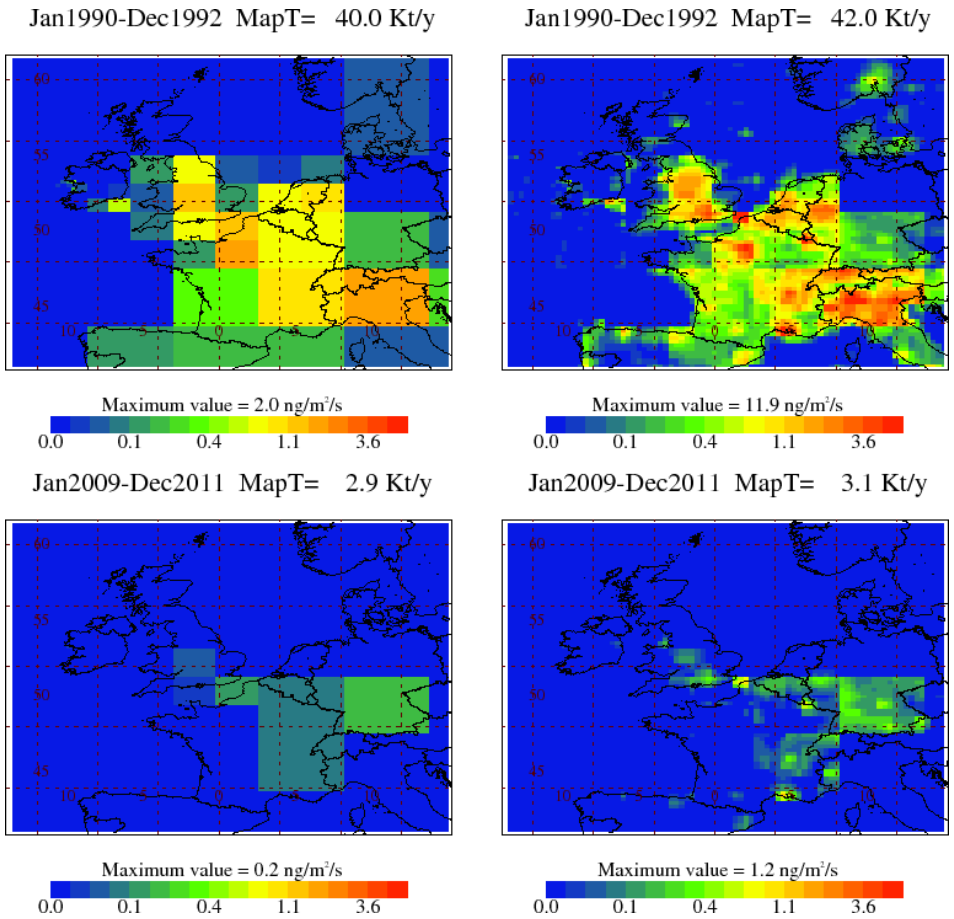

Figure 62: NAME-inversion emission estimates for 1990-92 (upper) and 2009-11 (lower). On the right hand side the emissions per grid box have been re-distributed based on population.

The emissions of CFC-11 in both the UK and NWEU as a whole fell very significantly between 1990 and the late 1990s. This clearly shows the impact of the Montreal Protocol which banned the use of this gas in developed countries from 1995 onwards. The residual emissions reflect the leakage from old appliances e.g. fridges.

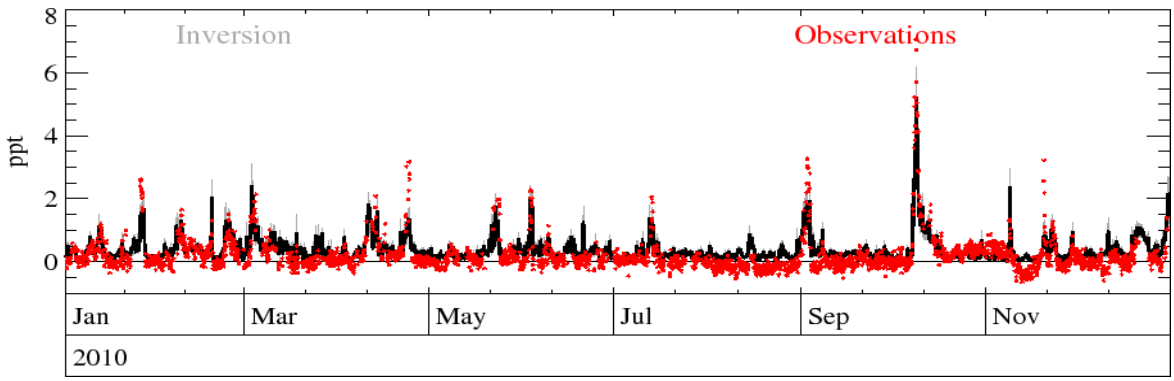

Figure 63: Example time-series of observations Vs. model using best-fit emission estimates.

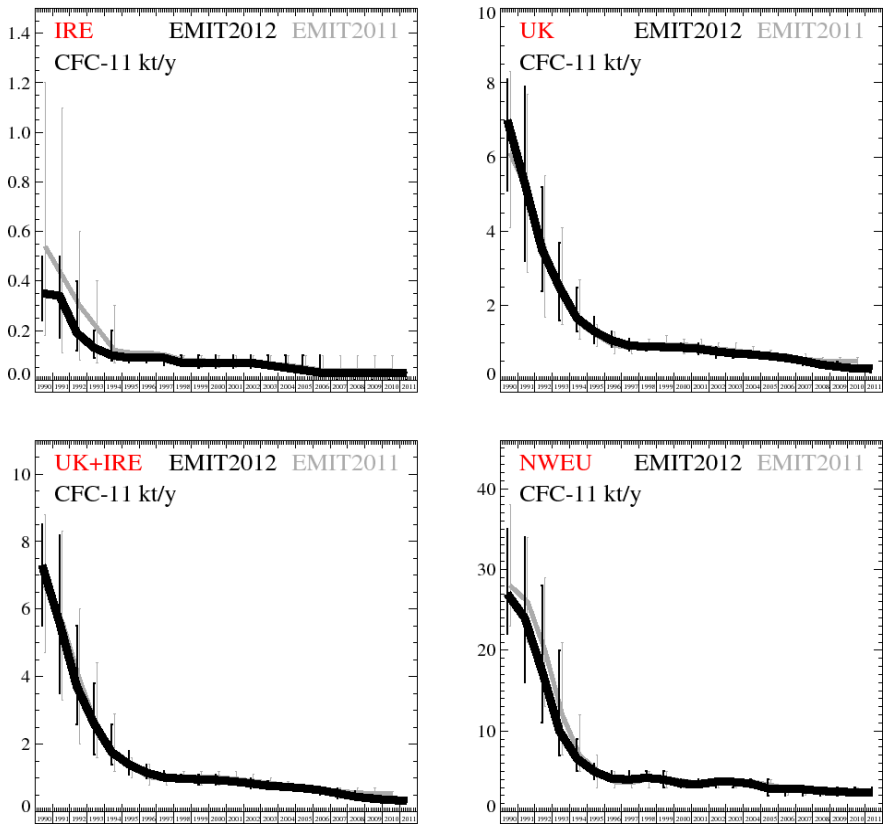

Figure 64: Emission estimates for IRE, UK, IRE+UK and NWEU. The uncertainty bars represent the 5th and 95th percentiles. Grey emissions are estimates from last year.

Unit	Year	IRE	(5th-95th)	UK	(5th-95th)	UK+IRE	(5th-95th)	NWEU	(5th-95th)	Number
kt/y	1990	0.35	(0.24- 0.5)	7	(5.1- 8.1)	7.3	(5.5- 8.5)	27	(22.- 35.)	1920
kt/y	1991	0.34	(0.17- 0.5)	5.3	(3.2- 7.9)	5.6	(3.5- 8.2)	24	(16.- 34.)	3840
kt/y	1992	0.19	(0.12- 0.4)	3.5	(2.4- 5.2)	3.7	(2.6- 5.5)	17.4	(11.- 28.)	4000
kt/y	1993	0.13	(0.09- 0.2)	2.5	(1.6- 3.7)	2.6	(1.7- 3.8)	10	(7.- 20.)	4000
kt/y	1994	0.1	(0.08- 0.2)	1.67	(1.3- 2.5)	1.77	(1.4- 2.6)	6.6	(5.- 9.)	4000
kt/y	1995	0.09	(0.07- 0.1)	1.31	(1.0- 1.7)	1.4	(1.1- 1.8)	5	(4.- 6.)	4000
kt/y	1996	0.09	(0.07- 0.1)	1.07	(0.9- 1.3)	1.16	(1.0- 1.4)	4.1	(4.- 5.)	4000
kt/y	1997	0.09	(0.06- 0.1)	0.93	(0.8- 1.1)	1.02	(0.9- 1.2)	4	(4.- 5.)	4000
kt/y	1998	0.07	(0.06- 0.1)	0.9	(0.8- 1.0)	0.98	(0.9- 1.1)	4.2	(4.- 5.)	4000
kt/y	1999	0.07	(0.05- 0.1)	0.89	(0.8- 1.0)	0.96	(0.8- 1.1)	4	(3.- 5.)	4000
kt/y	2000	0.07	(0.05- 0.1)	0.87	(0.8- 1.0)	0.94	(0.8- 1.1)	3.5	(3.- 4.)	4000
kt/y	2001	0.07	(0.05- 0.1)	0.84	(0.7- 1.0)	0.9	(0.8- 1.0)	3.4	(3.- 4.)	4000
kt/y	2002	0.07	(0.05- 0.1)	0.77	(0.6- 0.9)	0.84	(0.7- 1.0)	3.7	(3.- 4.)	4000
kt/y	2003	0.06	(0.05- 0.1)	0.72	(0.6- 0.8)	0.77	(0.7- 0.9)	3.7	(3.- 4.)	4000
kt/y	2004	0.05	(0.04- 0.1)	0.69	(0.6- 0.8)	0.74	(0.7- 0.8)	3.5	(3.- 4.)	4000
kt/y	2005	0.04	(0.03- 0.1)	0.65	(0.6- 0.7)	0.7	(0.6- 0.8)	2.9	(2.- 4.)	4000
kt/y	2006	0.03	(0.03- 0.1)	0.6	(0.5- 0.7)	0.64	(0.5- 0.7)	2.8	(2.- 3.)	4000
kt/y	2007	0.03	(0.02- 0.0)	0.52	(0.4- 0.6)	0.55	(0.4- 0.7)	2.8	(2.- 3.)	4000
kt/y	2008	0.03	(0.02- 0.0)	0.42	(0.4- 0.5)	0.45	(0.4- 0.6)	2.6	(2.- 3.)	4000
kt/y	2009	0.03	(0.02- 0.0)	0.36	(0.3- 0.5)	0.39	(0.3- 0.5)	2.5	(2.- 3.)	4000
kt/y	2010	0.03	(0.02- 0.0)	0.31	(0.3- 0.4)	0.35	(0.3- 0.4)	2.4	(2.- 3.)	2080
kt/y	2011	0.03	(0.03- 0.0)	0.3	(0.3- 0.3)	0.33	(0.3- 0.4)	2.4	(2.- 3.)	160

Table 6: Emission estimates for UK, IRE and NWEU with uncertainty (5th – 95th %ile).

5.2.1.2 CFC-12

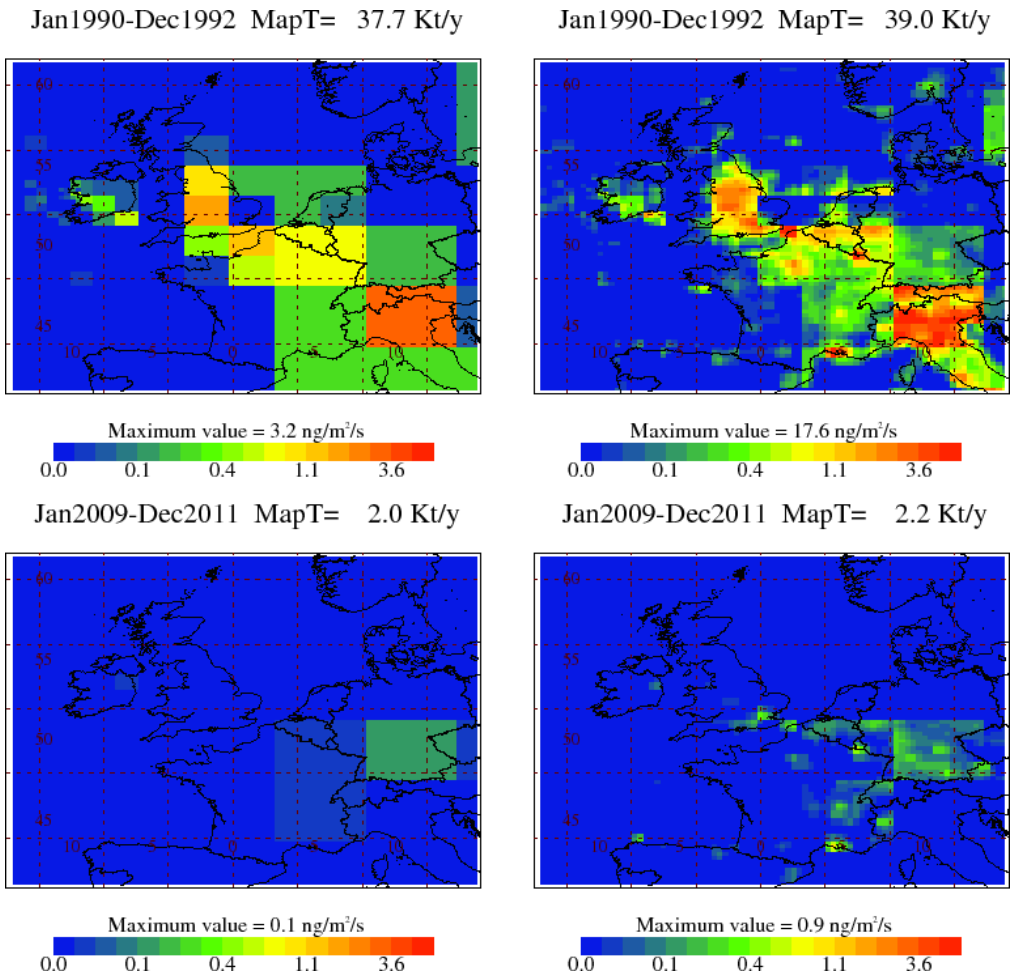

Figure 65: NAME-inversion emission estimates for 1990-92 (upper) and 2009-11 (lower). On the right hand side the emissions per grid box have been re-distributed based on population.

The emissions of CFC-12 in both the UK and NWEU as a whole fell very significantly betwwen1990 and the late 1990s. This clearly shows the impact of the Montreal Protocol which banned the use of this gas in developed countries from 1995 onwards. The residual emissions reflect the leakage from old appliances.

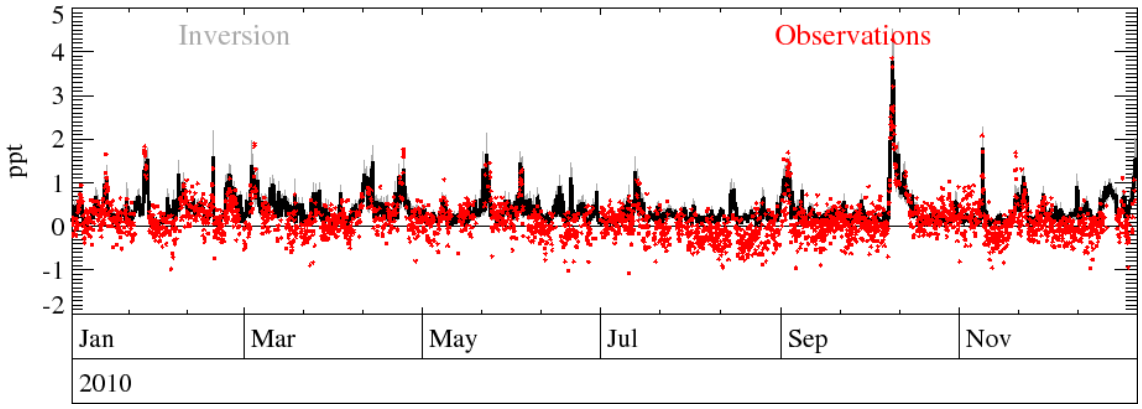

Figure 66: Example time-series of observations Vs. model using best-fit emission estimates.

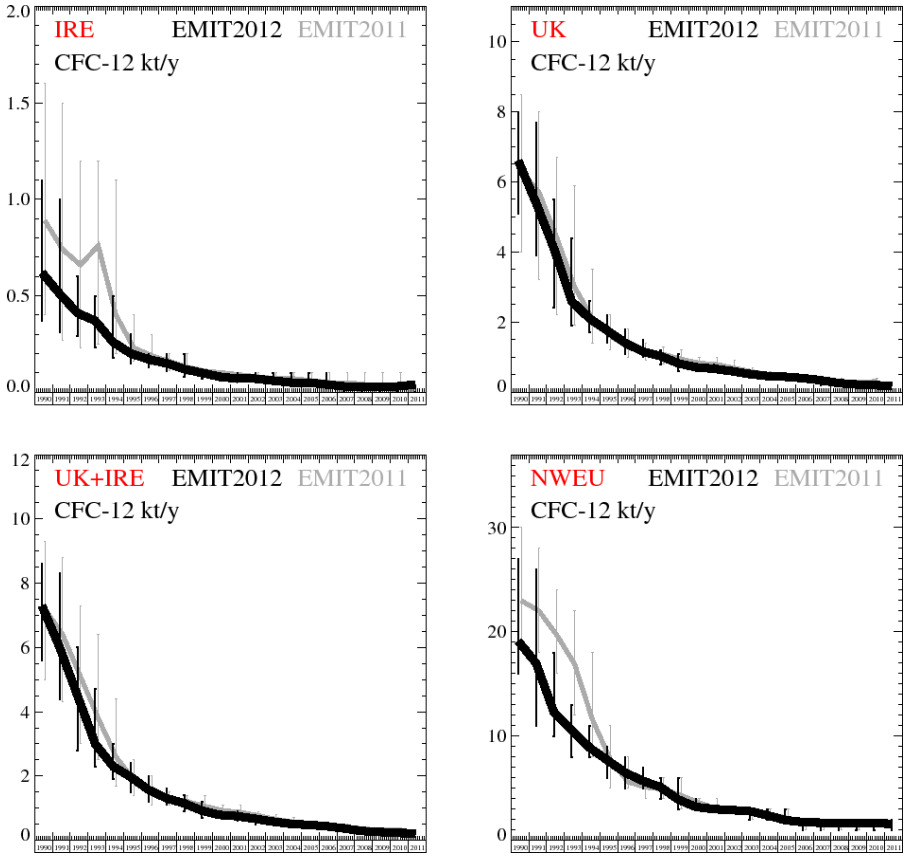

Figure 67: Emission estimates for IRE, UK, IRE+UK and NWEU. The uncertainty bars represent the 5th and 95th percentiles. Grey emissions are estimates from last year.

Unit	Year	IRE	(5th-95th)	UK	(5th-95th)	UK+IRE	(5th-95th)	NWEU	(5th-95th)	Number
kt/y	1990	0.62	(0.37- 1.1)	6.6	(5.1- 8.0)	7.3	(5.6- 8.6)	19.1	(16.- 27.)	1920
kt/y	1991	0.51	(0.31- 1.0)	5.4	(3.9- 7.7)	6	(4.4- 8.3)	17	(11.- 26.)	3840
kt/y	1992	0.41	(0.29- 0.6)	4.1	(2.4- 5.5)	4.5	(2.8- 6.0)	12.3	(10.- 18.)	4000
kt/y	1993	0.37	(0.23- 0.5)	2.6	(1.9- 4.4)	3	(2.3- 4.7)	10.6	(8.- 13.)	4000
kt/y	1994	0.26	(0.18- 0.5)	2.1	(1.7- 2.6)	2.3	(1.9- 3.0)	8.9	(8.- 11.)	4000
kt/y	1995	0.2	(0.15- 0.3)	1.76	(1.4- 2.2)	1.97	(1.5- 2.4)	7.7	(6.- 9.)	4000
kt/y	1996	0.17	(0.13- 0.2)	1.41	(1.1- 1.8)	1.57	(1.2- 2.0)	6.5	(5.- 8.)	4000
kt/y	1997	0.15	(0.11- 0.2)	1.16	(1.0- 1.5)	1.31	(1.1- 1.6)	5.7	(5.- 7.)	4000
kt/y	1998	0.12	(0.08- 0.2)	1.03	(0.8- 1.2)	1.15	(0.9- 1.4)	5.1	(4.- 6.)	4000
kt/y	1999	0.1	(0.07- 0.1)	0.82	(0.6- 1.1)	0.92	(0.7- 1.2)	3.9	(3.- 6.)	4000
kt/y	2000	0.08	(0.06- 0.1)	0.71	(0.6- 0.8)	0.79	(0.7- 0.9)	3.2	(3.- 4.)	4000
kt/y	2001	0.07	(0.06- 0.1)	0.67	(0.6- 0.8)	0.75	(0.6- 0.9)	3	(3.- 3.)	4000
kt/y	2002	0.07	(0.05- 0.1)	0.6	(0.5- 0.7)	0.67	(0.5- 0.8)	2.9	(3.- 3.)	4000
kt/y	2003	0.06	(0.05- 0.1)	0.52	(0.4- 0.6)	0.58	(0.5- 0.7)	2.8	(2.- 3.)	4000
kt/y	2004	0.05	(0.04- 0.1)	0.46	(0.4- 0.5)	0.51	(0.5- 0.6)	2.4	(2.- 3.)	4000
kt/y	2005	0.05	(0.04- 0.1)	0.44	(0.4- 0.5)	0.48	(0.4- 0.5)	1.94	(2.- 3.)	4000
kt/y	2006	0.04	(0.03- 0.1)	0.4	(0.3- 0.5)	0.44	(0.4- 0.5)	1.74	(1.- 2.)	4000
kt/y	2007	0.03	(0.02- 0.0)	0.34	(0.2- 0.4)	0.37	(0.3- 0.5)	1.69	(1.- 2.)	4000
kt/y	2008	0.03	(0.02- 0.0)	0.26	(0.2- 0.3)	0.29	(0.2- 0.4)	1.66	(1.- 2.)	4000
kt/y	2009	0.03	(0.02- 0.0)	0.22	(0.2- 0.3)	0.26	(0.2- 0.3)	1.65	(1.- 2.)	4000
kt/y	2010	0.03	(0.03- 0.0)	0.2	(0.2- 0.3)	0.23	(0.2- 0.3)	1.64	(1.- 2.)	2080
kt/y	2011	0.04	(0.03- 0.0)	0.18	(0.2- 0.2)	0.22	(0.2- 0.3)	1.59	(1.- 2.)	160

Table 7: Emission estimates for UK, IRE and NWEU with uncertainty (5th – 95th %ile).

5.2.1.3 CFC-113

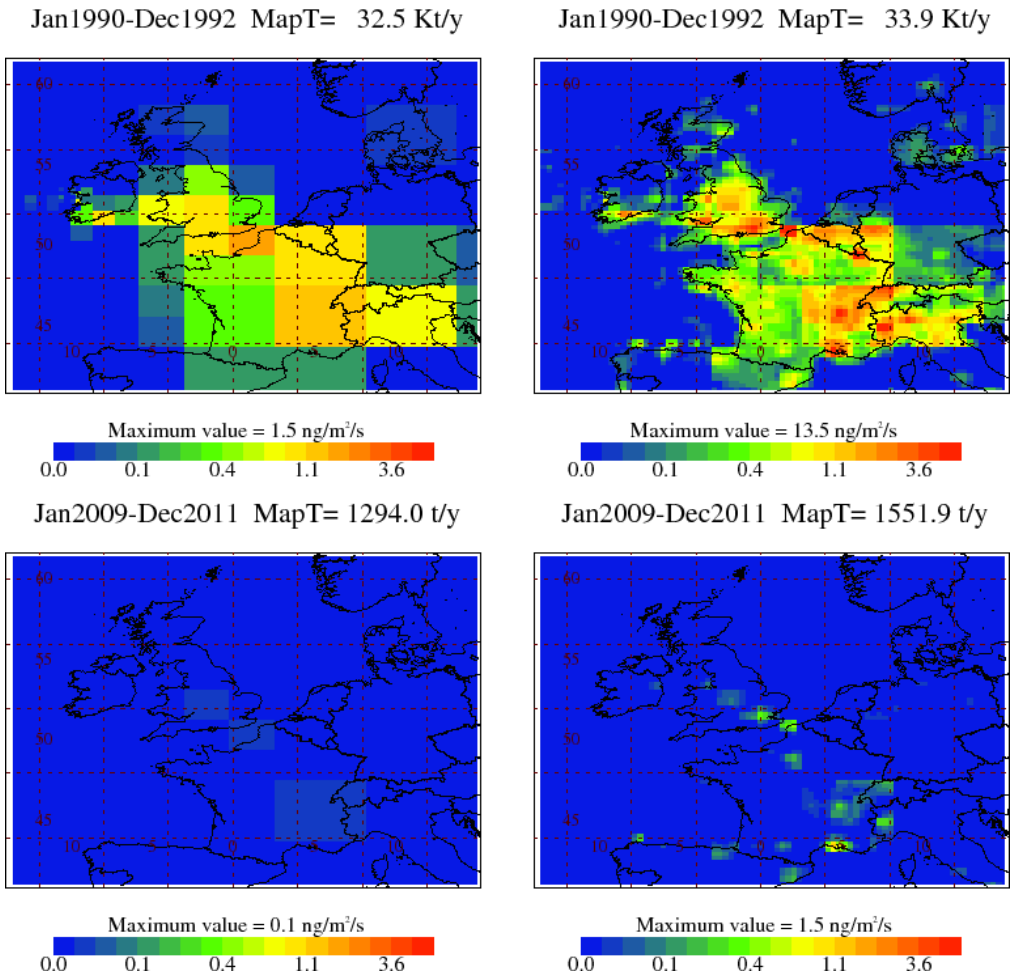

Figure 68: NAME-inversion emission estimates for 1990-92 (upper) and 2009-11 (lower). On the right hand side the emissions per grid box have been re-distributed based on population.

The emissions of CFC-113 in both the UK and NWEU as a whole fell very significantly between 1990 and the mid-1990s. This clearly shows the impact of the Montreal Protocol which banned the use of this gas in developed countries from 1995 onwards. The residual emissions reflect the leakage from old appliances.

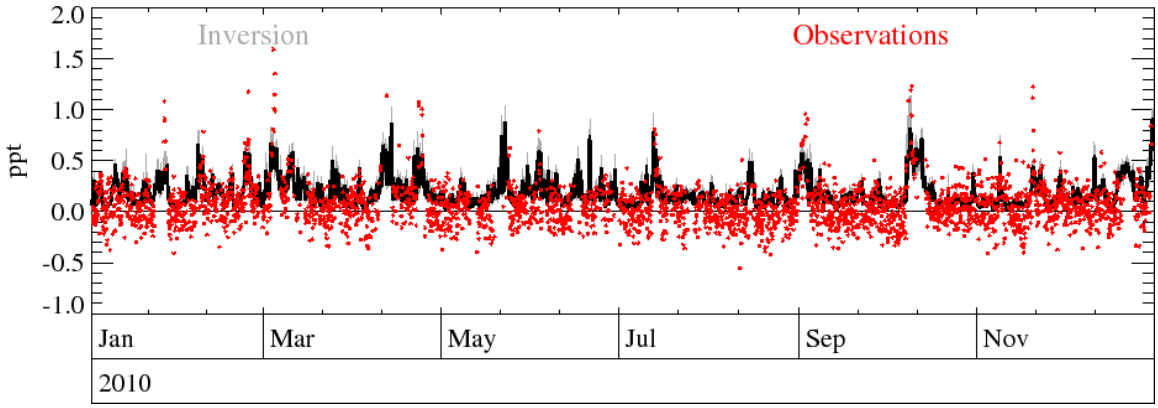

Figure 69: Example time-series of observations Vs. model using best-fit emission estimates.

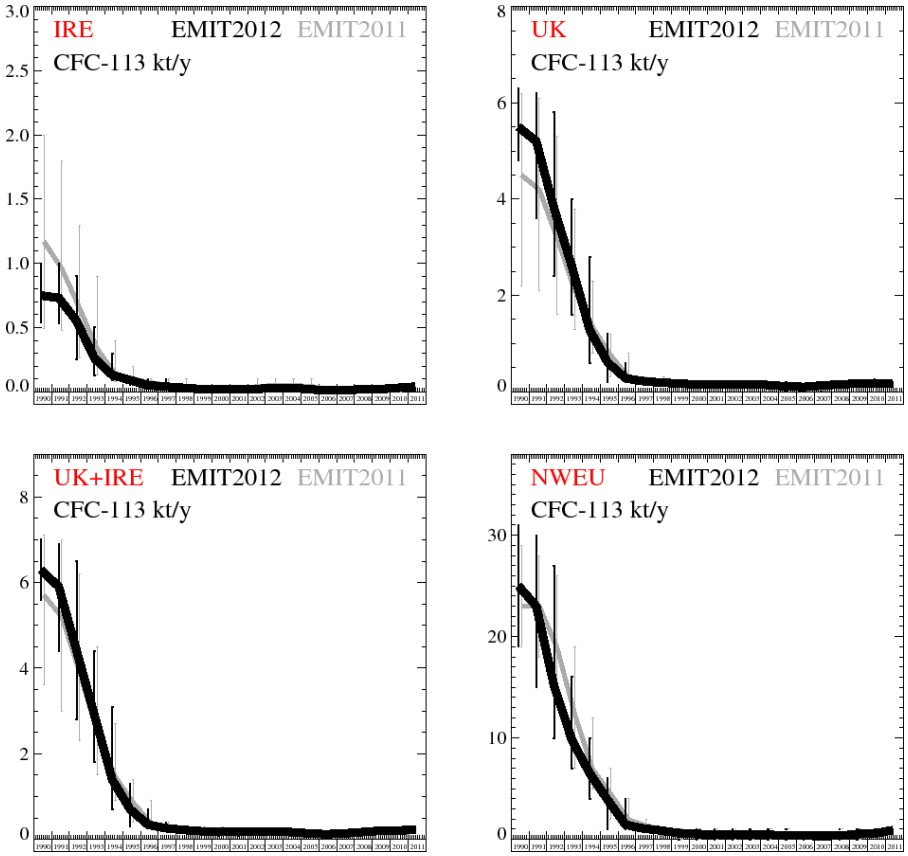

Figure 70: Emission estimates for IRE, UK, IRE+UK and NWEU. The uncertainty bars represent the 5th and 95th percentiles. Grey emissions are estimates from last year.

Unit	Year	IRE	(5th-95th)	UK	(5th-95th)	UK+IRE	(5th-95th)	NWEU	(5th-95th)	Number
kt/y	1990	0.75	(0.54- 1.0)	5.5	(4.8- 6.3)	6.3	(5.6- 7.0)	25	(19.- 31.)	1920
kt/y	1991	0.73	(0.53- 1.0)	5.2	(3.6- 6.2)	5.9	(4.4- 6.9)	23	(15.- 30.)	3840
kt/y	1992	0.55	(0.25- 0.9)	3.8	(2.4- 5.8)	4.4	(2.8- 6.5)	15.1	(10.- 27.)	4000
kt/y	1993	0.26	(0.13- 0.5)	2.6	(1.6- 4.0)	2.9	(1.8- 4.4)	9.8	(7.- 16.)	4000
kt/y	1994	0.13	(0.09- 0.3)	1.28	(0.6- 2.8)	1.39	(0.7- 3.1)	6.5	(4.- 10.)	4000
kt/y	1995	0.09	(0.05- 0.1)	0.61	(0.2- 1.2)	0.7	(0.3- 1.3)	3.9	(1.- 6.)	4000
kt/y	1996	0.05	(0.04- 0.1)	0.28	(0.2- 0.6)	0.34	(0.3- 0.7)	1.44	(1.- 4.)	4000
kt/y	1997	0.04	(0.02- 0.1)	0.22	(0.2- 0.3)	0.26	(0.2- 0.4)	1.07	(1.- 1.)	4000
kt/y	1998	0.03	(0.02- 0.0)	0.19	(0.2- 0.2)	0.22	(0.2- 0.3)	0.87	(1.- 1.)	4000
kt/y	1999	0.02	(0.01- 0.0)	0.17	(0.1- 0.2)	0.19	(0.1- 0.2)	0.61	(0.- 1.)	4000
kt/y	2000	0.02	(0.01- 0.0)	0.15	(0.1- 0.2)	0.17	(0.1- 0.2)	0.53	(0.- 1.)	4000
kt/y	2001	0.02	(0.01- 0.0)	0.15	(0.1- 0.2)	0.17	(0.1- 0.2)	0.5	(0.- 1.)	4000
kt/y	2002	0.02	(0.02- 0.0)	0.16	(0.1- 0.2)	0.18	(0.1- 0.2)	0.48	(0.- 1.)	4000
kt/y	2003	0.03	(0.02- 0.0)	0.16	(0.1- 0.2)	0.18	(0.1- 0.2)	0.47	(0.- 1.)	4000
kt/y	2004	0.03	(0.02- 0.0)	0.14	(0.1- 0.2)	0.17	(0.1- 0.2)	0.45	(0.- 1.)	4000
kt/y	2005	0.02	(0.01- 0.0)	0.11	(0.0- 0.2)	0.14	(0.1- 0.2)	0.38	(0.- 1.)	4000
kt/y	2006	0.01	(0.01- 0.0)	0.1	(0.0- 0.1)	0.12	(0.1- 0.2)	0.35	(0.- 0.)	4000
kt/y	2007	0.01	(0.01- 0.0)	0.13	(0.0- 0.2)	0.14	(0.1- 0.2)	0.34	(0.- 0.)	4000
kt/y	2008	0.02	(0.01- 0.0)	0.15	(0.1- 0.2)	0.17	(0.1- 0.2)	0.35	(0.- 1.)	4000
kt/y	2009	0.02	(0.02- 0.0)	0.17	(0.1- 0.2)	0.2	(0.2- 0.2)	0.52	(0.- 1.)	4000
kt/y	2010	0.03	(0.02- 0.0)	0.18	(0.1- 0.2)	0.21	(0.2- 0.2)	0.59	(1.- 1.)	2080
kt/y	2011	0.04	(0.03- 0.0)	0.18	(0.1- 0.2)	0.22	(0.2- 0.3)	0.91	(1.- 1.)	160

Table 8: Emission estimates for UK, IRE and NWEU with uncertainty (5th – 95th %ile).

5.2.2 HCFC

5.2.2.1 HCFC-124

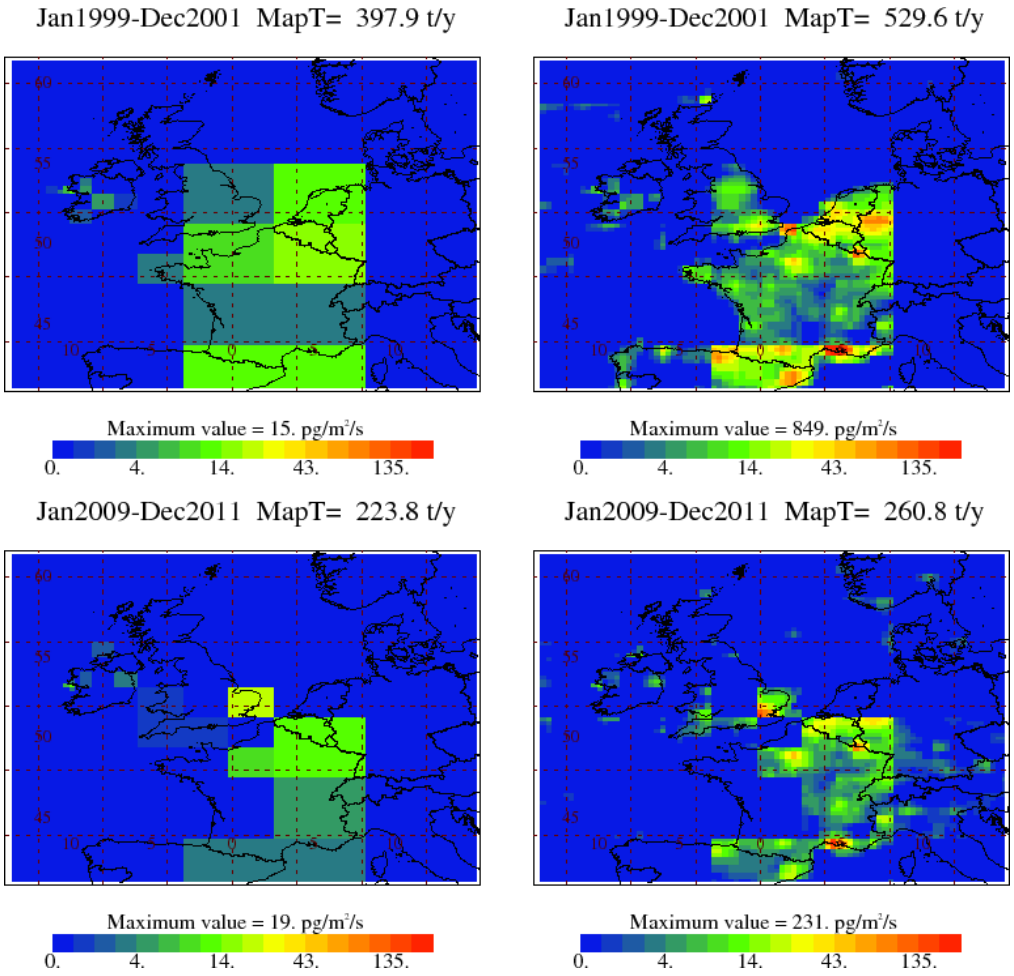

Figure 71: NAME-inversion emission estimates for 1990-92 (upper) and 2009-11 (lower). On the right hand side the emissions per grid box have been re-distributed based on population.

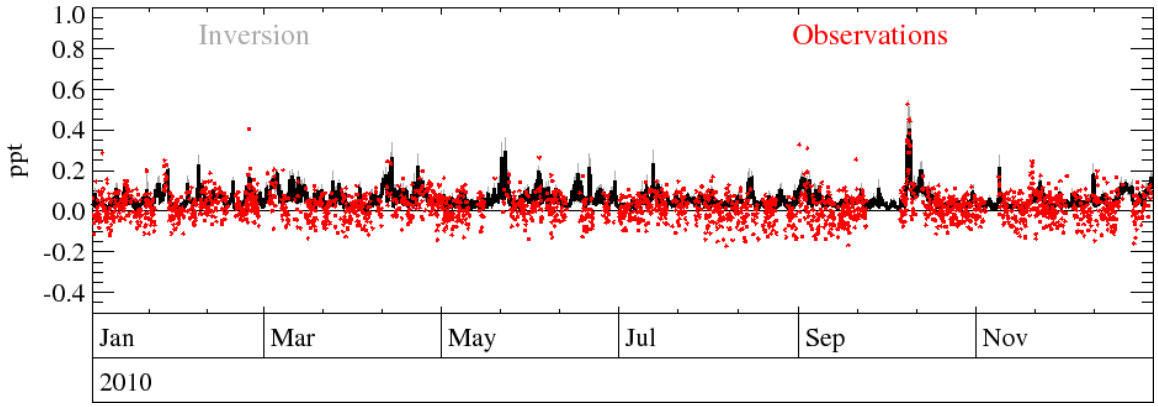

Figure 72: Example time-series of observations Vs. model using best-fit emission estimates.

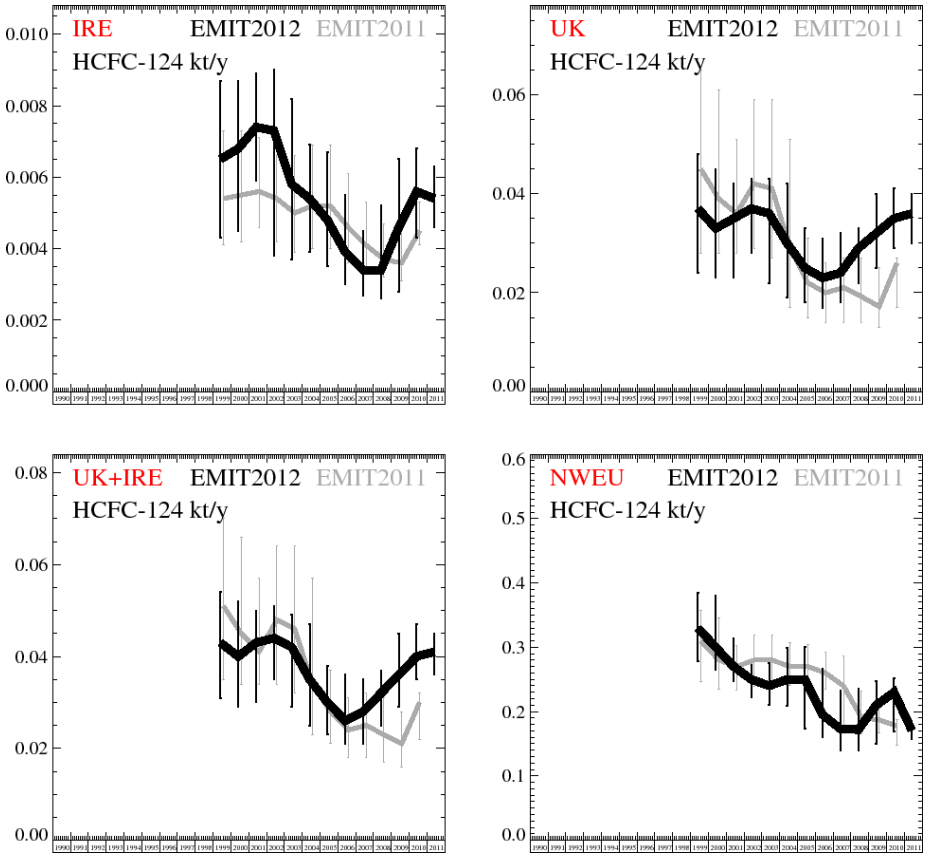

Figure 73: Emission estimates for IRE, UK, IRE+UK and NWEU. The uncertainty bars represent the 5th and 95th percentiles. Grey emissions are estimates from last year.

Unit	Year	IRE	(5th-95th)	UK	(5th-95th)	UK+IRE	(5th-95th)	NWEU	(5th-95th)	Number
t/y	1999	6.5	(4.3- 8.7)	37	(24.- 48.)	43	(31.- 54.)	330	(278.- 385.)	972
t/y	2000	6.8	(4.5- 8.7)	33	(23.- 45.)	40	(29.- 52.)	300	(265.- 380.)	1944
t/y	2001	7.4	(5.9- 8.9)	35	(23.- 42.)	43	(30.- 50.)	270	(247.- 314.)	2025
t/y	2002	7.3	(3.8- 9.0)	37	(28.- 43.)	44	(35.- 51.)	250	(223.- 273.)	2025
t/y	2003	5.8	(3.7- 8.2)	36	(22.- 43.)	42	(29.- 49.)	240	(210.- 276.)	2025
t/y	2004	5.4	(3.9- 6.9)	30	(19.- 42.)	35	(25.- 47.)	250	(209.- 299.)	2025
t/y	2005	4.8	(3.5- 6.7)	25	(18.- 33.)	30	(23.- 38.)	250	(174.- 301.)	2025
t/y	2006	3.9	(3.0- 5.5)	23	(17.- 31.)	26	(21.- 36.)	195	(160.- 266.)	2025
t/y	2007	3.4	(2.7- 4.5)	24	(18.- 32.)	28	(21.- 35.)	173	(140.- 233.)	2025
t/y	2008	3.4	(2.6- 5.2)	29	(22.- 33.)	32	(25.- 37.)	172	(139.- 236.)	1925
t/y	2009	4.6	(2.8- 6.5)	32	(25.- 40.)	36	(29.- 45.)	210	(150.- 248.)	1742
t/y	2010	5.6	(4.3- 6.8)	35	(29.- 41.)	40	(35.- 47.)	230	(169.- 252.)	850
t/y	2011	5.4	(4.6- 6.3)	36	(30.- 40.)	41	(36.- 45.)	171	(158.- 186.)	80

Table 9: Emission estimates for UK, IRE and NWEU with uncertainty (5th – 95th %ile).

5.2.2.2 HCFC-141b

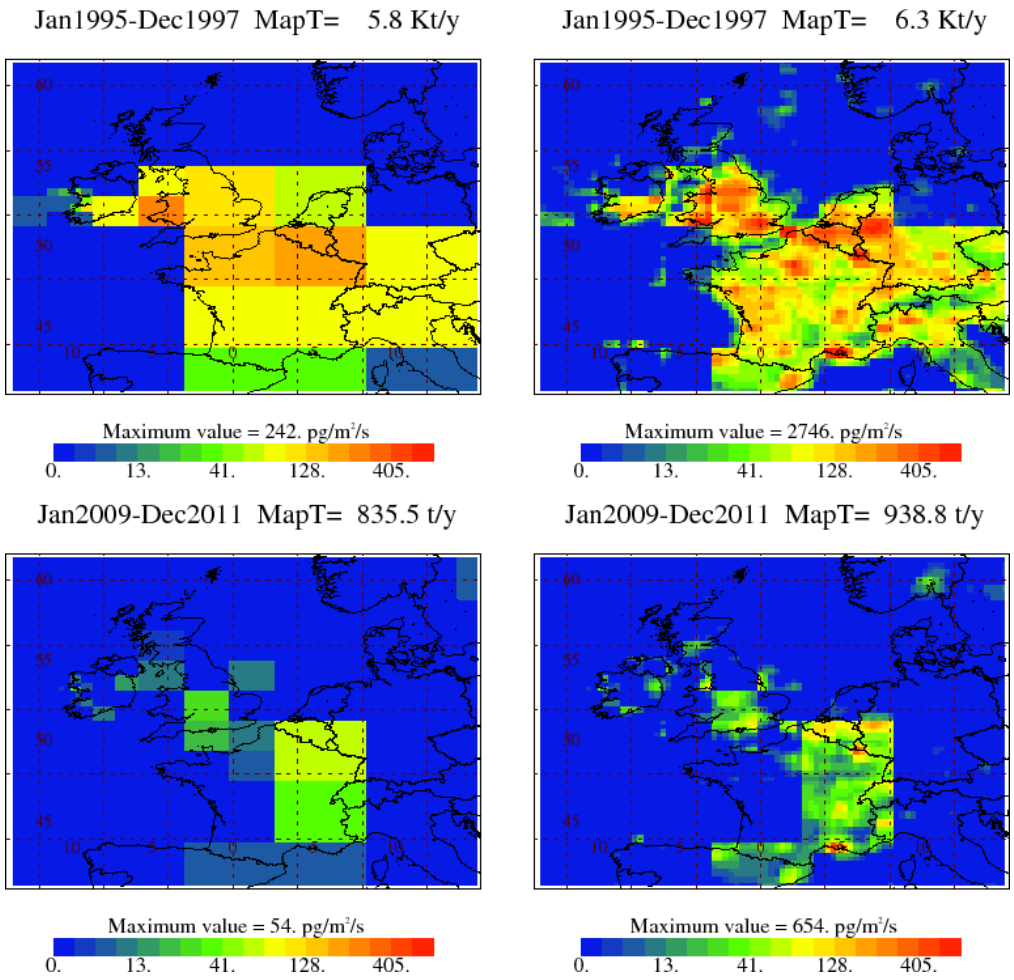

Figure 74: NAME-inversion emission estimates for 1990-92 (upper) and 2009-11 (lower). On the right hand side the emissions per grid box have been re-distributed based on population.

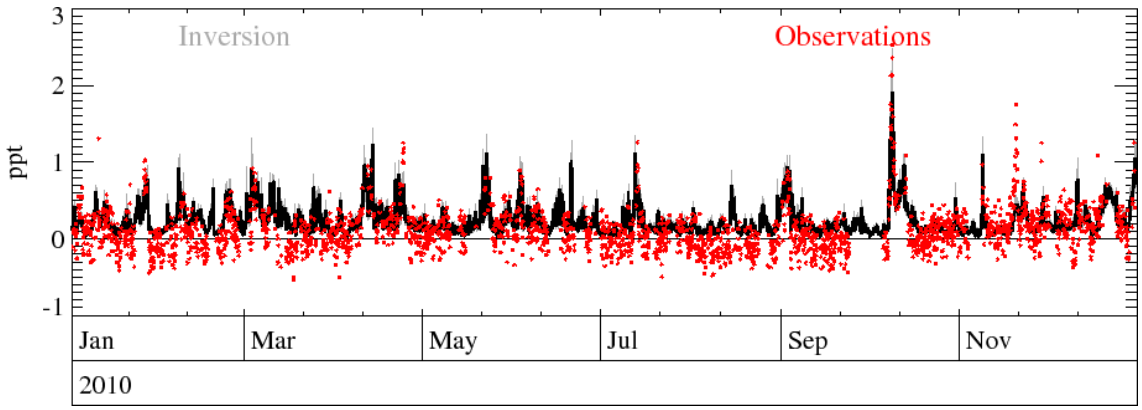

Figure 75: Example time-series of observations Vs. model using best-fit emission estimates.

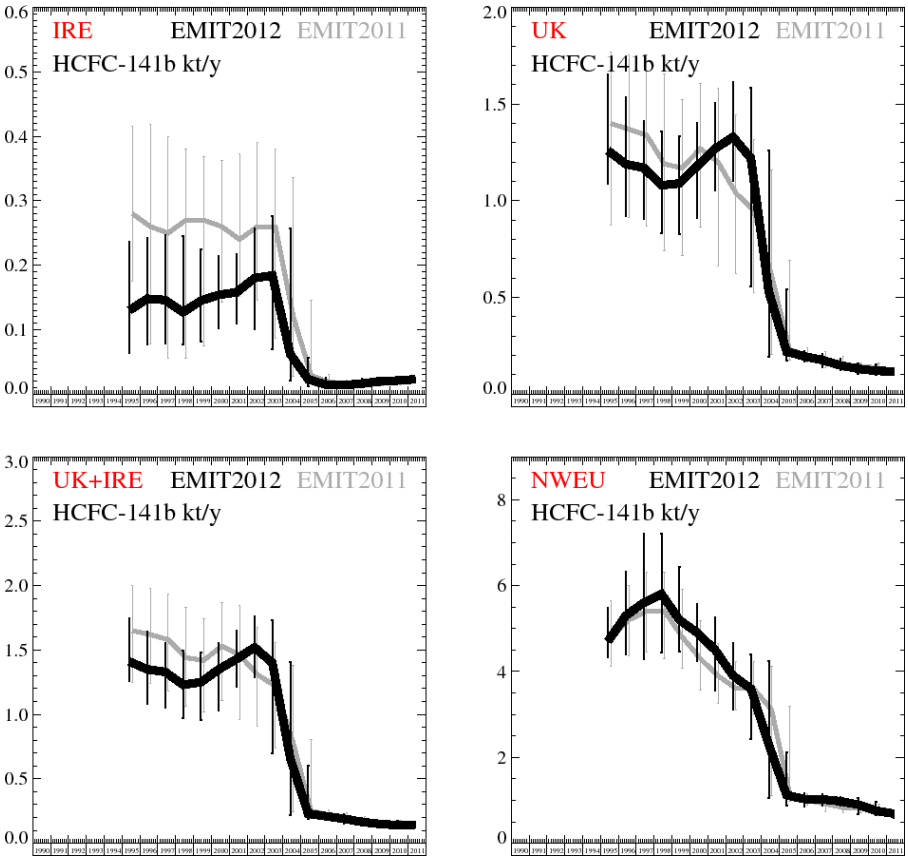

Figure 76: Emission estimates for IRE, UK, IRE+UK and NWEU. The uncertainty bars represent the 5th and 95th percentiles. Grey emissions are estimates from last year.

Unit	Year	IRE	(5th-95th)	UK	(5th-95th)	UK+IRE	(5th-95th)	NWEU	(5th-95th)	Number
t/y	1995	130	(64.- 236.)	1260	(1089.-1655.)	1410	(1257.-1748.)	4700	(4328.-5480.)	480
t/y	1996	148	(77.- 243.)	1190	(922.-1535.)	1350	(1082.-1645.)	5300	(4395.-6326.)	2400
t/y	1997	146	(79.- 247.)	1170	(906.-1415.)	1330	(1053.-1551.)	5600	(4296.-7210.)	4000
t/y	1998	127	(77.- 245.)	1080	(834.-1361.)	1230	(968.-1495.)	5800	(4439.-7210.)	4000
t/y	1999	145	(82.- 225.)	1090	(825.-1333.)	1250	(959.-1483.)	5200	(4470.-6431.)	4000
t/y	2000	154	(102.- 214.)	1180	(913.-1401.)	1350	(1030.-1551.)	4900	(4243.-5578.)	4000
t/y	2001	158	(110.- 217.)	1270	(1052.-1505.)	1430	(1217.-1648.)	4500	(3564.-5264.)	4000
t/y	2002	180	(100.- 257.)	1330	(1101.-1614.)	1520	(1290.-1760.)	3900	(3107.-4656.)	4000
t/y	2003	184	(70.- 276.)	1220	(557.-1584.)	1400	(702.-1733.)	3600	(2433.-4387.)	4000
t/y	2004	62	(21.- 257.)	530	(191.-1261.)	660	(222.-1407.)	2300	(1053.-4250.)	4000
t/y	2005	23	(12.- 57.)	220	(174.- 544.)	230	(190.- 605.)	1120	(878.-2109.)	4000
t/y	2006	14.5	(11.- 25.)	195	(168.- 221.)	210	(181.- 237.)	1030	(861.-1157.)	4000
t/y	2007	14.1	(10.- 20.)	176	(138.- 208.)	191	(153.- 223.)	1020	(888.-1133.)	4000
t/y	2008	16.1	(10.- 24.)	149	(122.- 185.)	166	(140.- 200.)	980	(874.-1084.)	4000
t/y	2009	20	(13.- 26.)	131	(104.- 158.)	150	(126.- 178.)	900	(681.-1053.)	4000
t/y	2010	21	(17.- 27.)	120	(101.- 151.)	141	(124.- 173.)	760	(658.- 968.)	2080
t/y	2011	23	(19.- 26.)	118	(98.- 135.)	139	(122.- 158.)	690	(599.- 747.)	160

Table 10: Emission estimates for UK, IRE and NWEU with uncertainty (5th – 95th %ile).

5.2.2.3 HCFC-142b

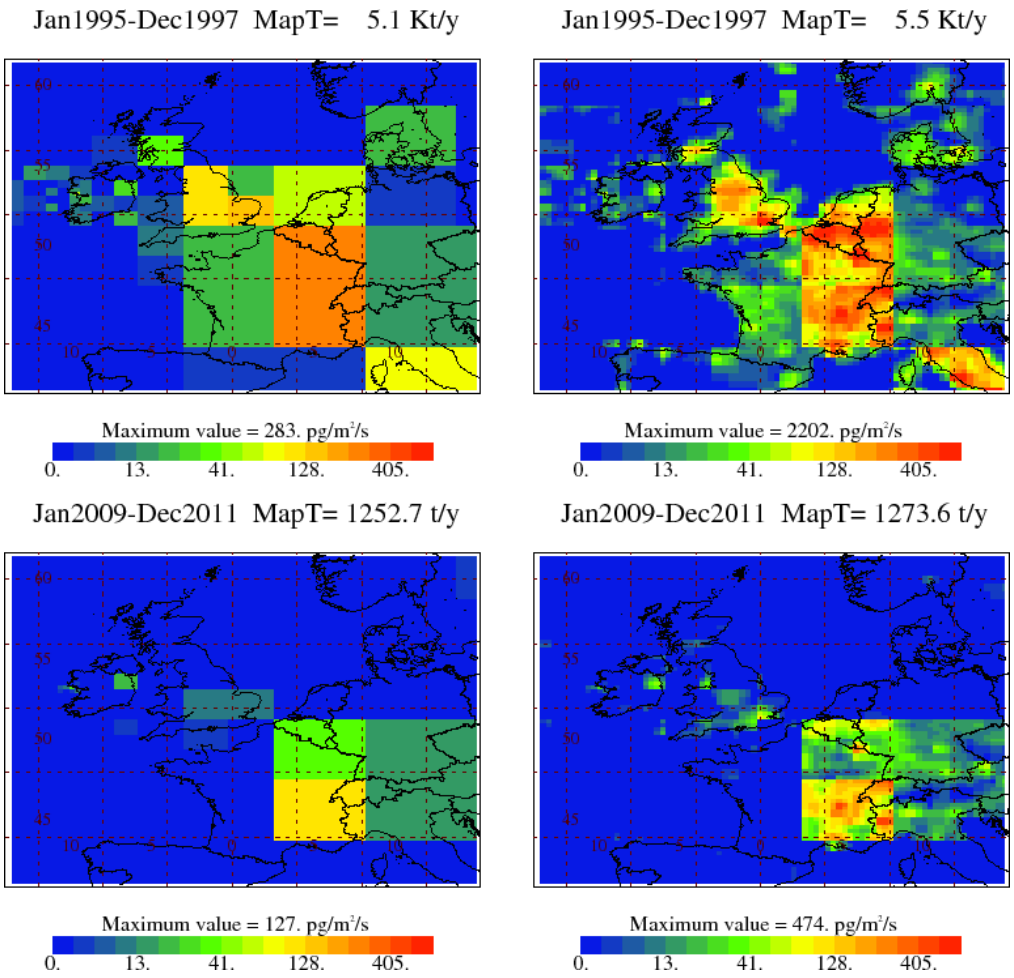

Figure 77: NAME-inversion emission estimates for 1990-92 (upper) and 2009-11 (lower). On the right hand side the emissions per grid box have been re-distributed based on population.

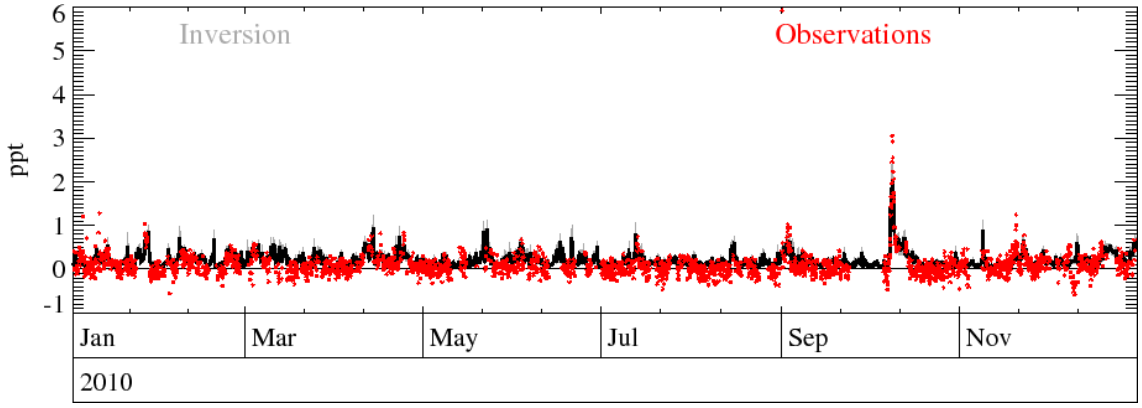

Figure 78: Example time-series of observations Vs. model using best-fit emission estimates.

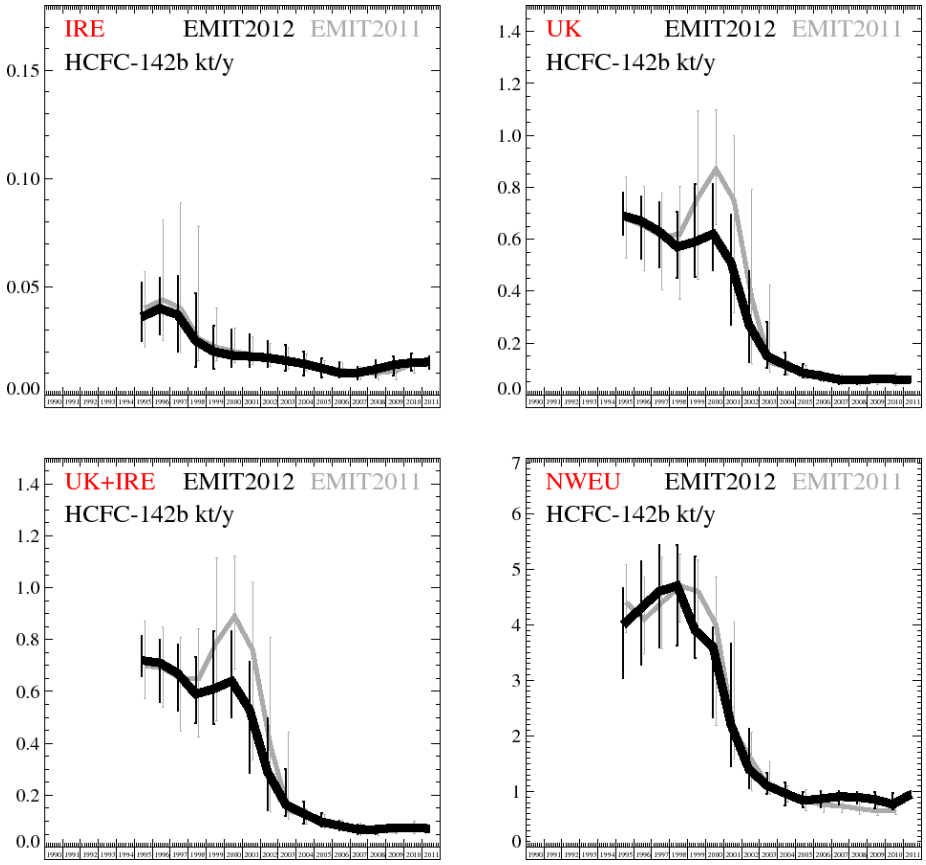

Figure 79: Emission estimates for IRE, UK, IRE+UK and NWEU. The uncertainty bars represent the 5th and 95th percentiles. Grey emissions are estimates from last year.

Unit	Year	IRE	(5th-95th)	UK	(5th-95th)	UK+IRE	(5th-95th)	NWEU	(5th-95th)	Number
t/y	1995	36	(25.- 52.)	690	(615.- 781.)	720	(659.- 813.)	4000	(3035.-4663.)	640
t/y	1996	40	(28.- 54.)	670	(524.- 763.)	710	(561.- 799.)	4300	(3286.-5150.)	2560
t/y	1997	37	(20.- 55.)	630	(493.- 741.)	670	(527.- 781.)	4600	(3601.-5438.)	4000
t/y	1998	25	(13.- 47.)	570	(451.- 707.)	590	(480.- 732.)	4700	(3631.-5437.)	4000
t/y	1999	20	(12.- 32.)	590	(454.- 812.)	610	(476.- 834.)	3900	(3406.-5235.)	4000
t/y	2000	18.3	(13.- 30.)	620	(482.- 812.)	640	(500.- 834.)	3600	(2344.-3952.)	4000
t/y	2001	17.8	(13.- 28.)	510	(269.- 694.)	530	(287.- 714.)	2200	(1458.-3667.)	4000
t/y	2002	17.2	(13.- 25.)	270	(127.- 478.)	290	(142.- 498.)	1400	(1061.-2124.)	4000
t/y	2003	15.8	(11.- 23.)	150	(105.- 283.)	165	(120.- 301.)	1110	(961.-1336.)	4000
t/y	2004	14.4	(9.- 20.)	116	(77.- 162.)	130	(91.- 177.)	970	(757.-1162.)	4000
t/y	2005	12.4	(8.- 17.)	85	(69.- 118.)	97	(79.- 133.)	840	(712.- 993.)	4000
t/y	2006	10.1	(8.- 15.)	73	(55.- 91.)	83	(65.- 102.)	870	(711.-1014.)	4000
t/y	2007	10.2	(7.- 13.)	59	(40.- 76.)	69	(51.- 86.)	910	(776.-1017.)	4000
t/y	2008	11.8	(8.- 16.)	57	(40.- 71.)	68	(51.- 85.)	900	(791.- 996.)	4000
t/y	2009	13.9	(9.- 18.)	61	(49.- 73.)	75	(61.- 88.)	860	(699.- 987.)	4000
t/y	2010	14.9	(11.- 19.)	60	(49.- 73.)	75	(63.- 88.)	770	(683.- 968.)	2080
t/y	2011	15.2	(12.- 18.)	57	(47.- 67.)	72	(59.- 83.)	950	(879.-1016.)	160

Table 11: Emission estimates for UK, IRE and NWEU with uncertainty (5th – 95th %ile).

5.2.2.4 HCFC-22

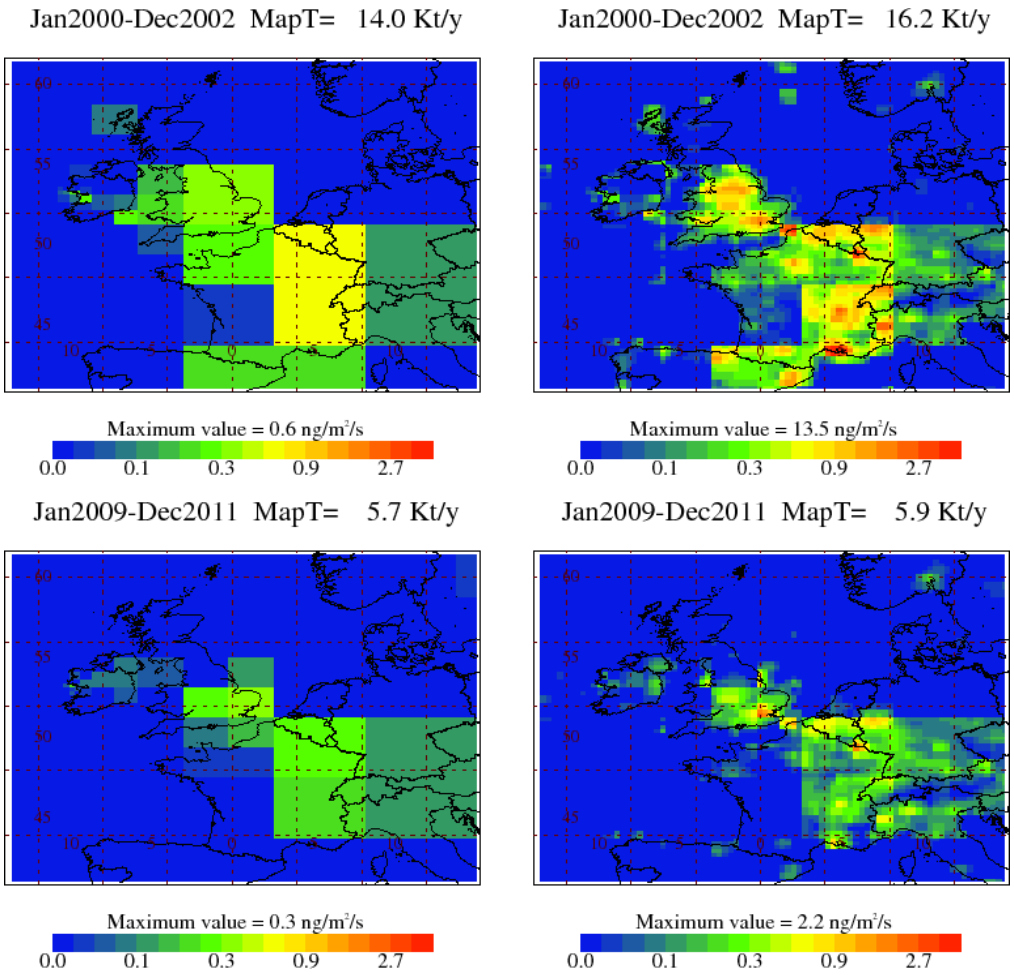

Figure 80: NAME-inversion emission estimates for 1990-92 (upper) and 2009-11 (lower). On the right hand side the emissions per grid box have been re-distributed based on population.

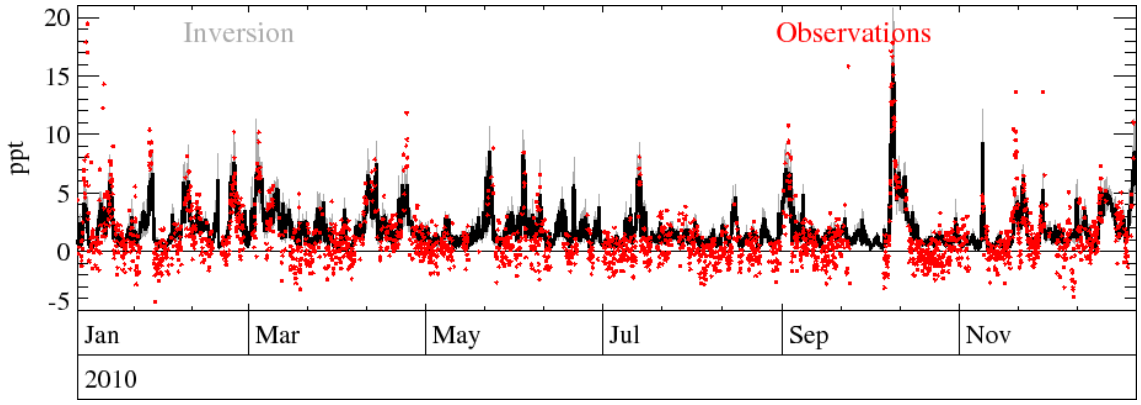

Figure 81: Example time-series of observations Vs. model using best-fit emission estimates.

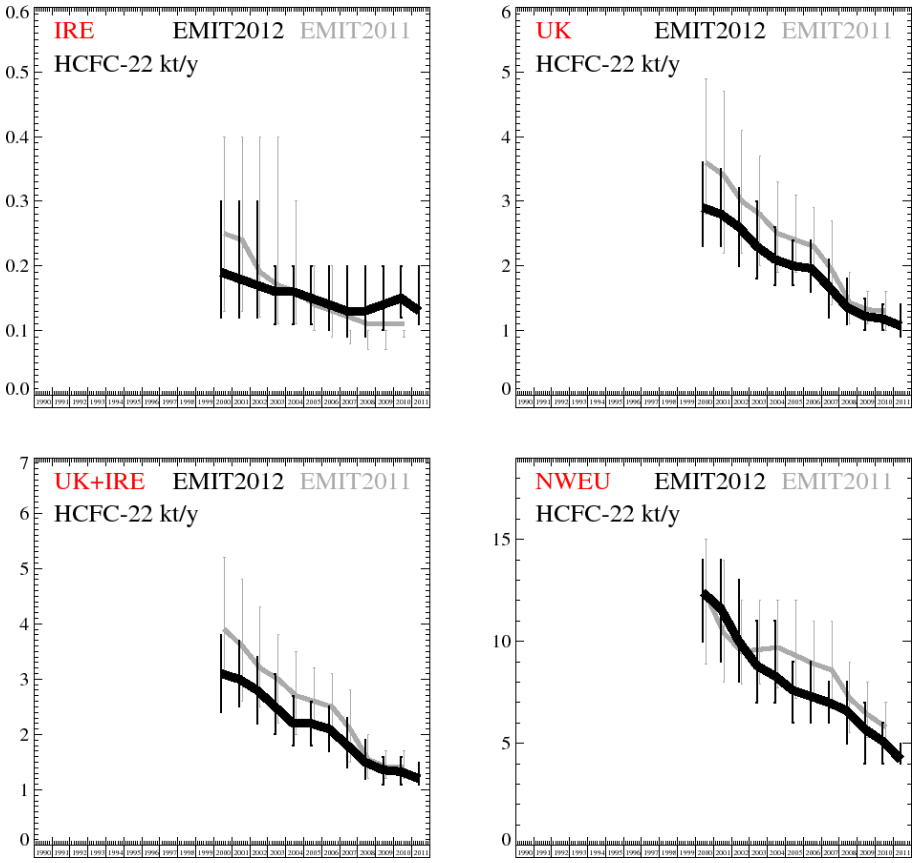

Figure 82: Emission estimates for IRE, UK, IRE+UK and NWEU. The uncertainty bars represent the 5th and 95th percentiles. Grey emissions are estimates from last year.

Unit	Year	IRE	(5th-95th)	UK	(5th-95th)	UK+IRE	(5th-95th)	NWEU	(5th-95th)	Number
kt/y	2000	0.19	(0.12- 0.3)	2.9	(2.3- 3.6)	3.1	(2.4- 3.8)	12.4	(10.- 14.)	1920
kt/y	2001	0.18	(0.12- 0.3)	2.8	(2.3- 3.5)	3	(2.5- 3.7)	11.6	(9.- 14.)	3840
kt/y	2002	0.17	(0.12- 0.3)	2.6	(2.0- 3.2)	2.8	(2.2- 3.4)	10	(8.- 13.)	4000
kt/y	2003	0.16	(0.11- 0.2)	2.3	(1.8- 3.0)	2.5	(2.0- 3.1)	8.8	(7.- 11.)	4000
kt/y	2004	0.16	(0.11- 0.2)	2.1	(1.7- 2.6)	2.2	(1.8- 2.7)	8.3	(7.- 11.)	4000
kt/y	2005	0.15	(0.11- 0.2)	2	(1.7- 2.4)	2.2	(1.8- 2.6)	7.6	(6.- 9.)	4000
kt/y	2006	0.14	(0.10- 0.2)	1.96	(1.6- 2.4)	2.1	(1.7- 2.5)	7.3	(6.- 9.)	4000
kt/y	2007	0.13	(0.09- 0.2)	1.68	(1.2- 2.1)	1.81	(1.4- 2.3)	7	(6.- 8.)	4000
kt/y	2008	0.13	(0.09- 0.2)	1.36	(1.1- 1.8)	1.5	(1.2- 1.9)	6.6	(5.- 8.)	4000
kt/y	2009	0.14	(0.10- 0.2)	1.22	(1.0- 1.5)	1.36	(1.1- 1.6)	5.7	(4.- 7.)	4000
kt/y	2010	0.15	(0.12- 0.2)	1.18	(1.0- 1.4)	1.33	(1.1- 1.6)	5.1	(4.- 6.)	2080
kt/y	2011	0.13	(0.11- 0.2)	1.07	(0.9- 1.4)	1.2	(1.1- 1.5)	4.2	(4.- 5.)	160

Table 12: Emission estimates for UK, IRE and NWEU with uncertainty (5th – 95th %ile).

5.2.3 HFC

5.2.3.1 HFC-125

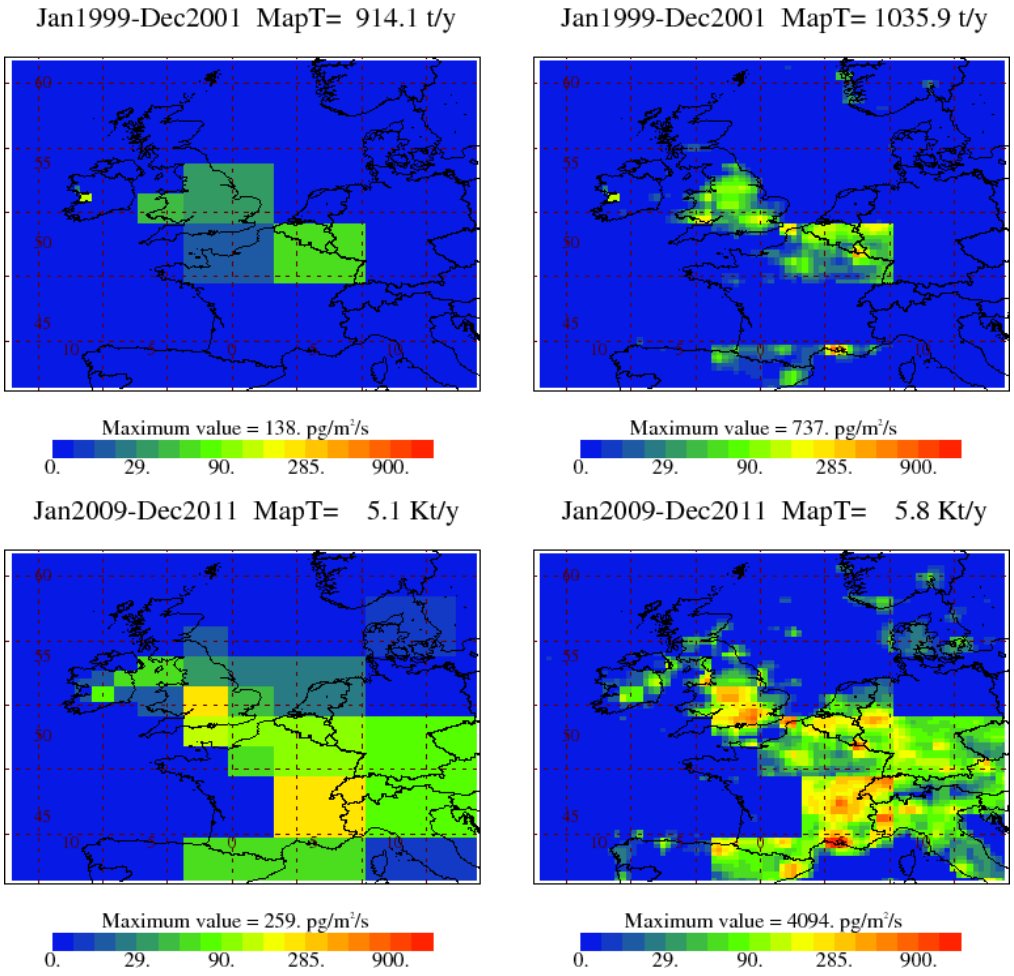

Figure 83: NAME-inversion emission estimates for 1990-92 (upper) and 2009-11 (lower). On the right hand side the emissions per grid box have been re-distributed based on population.

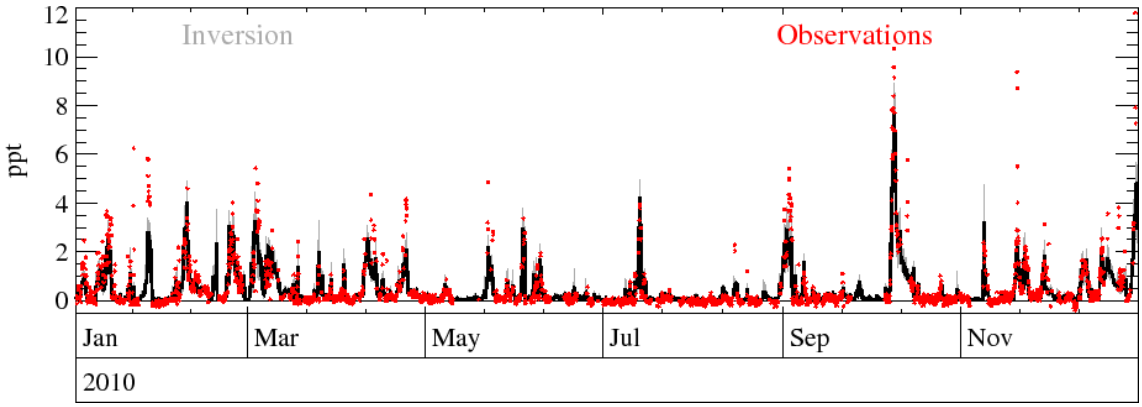

Figure 84: Example time-series of observations Vs. model using best-fit emission estimates.

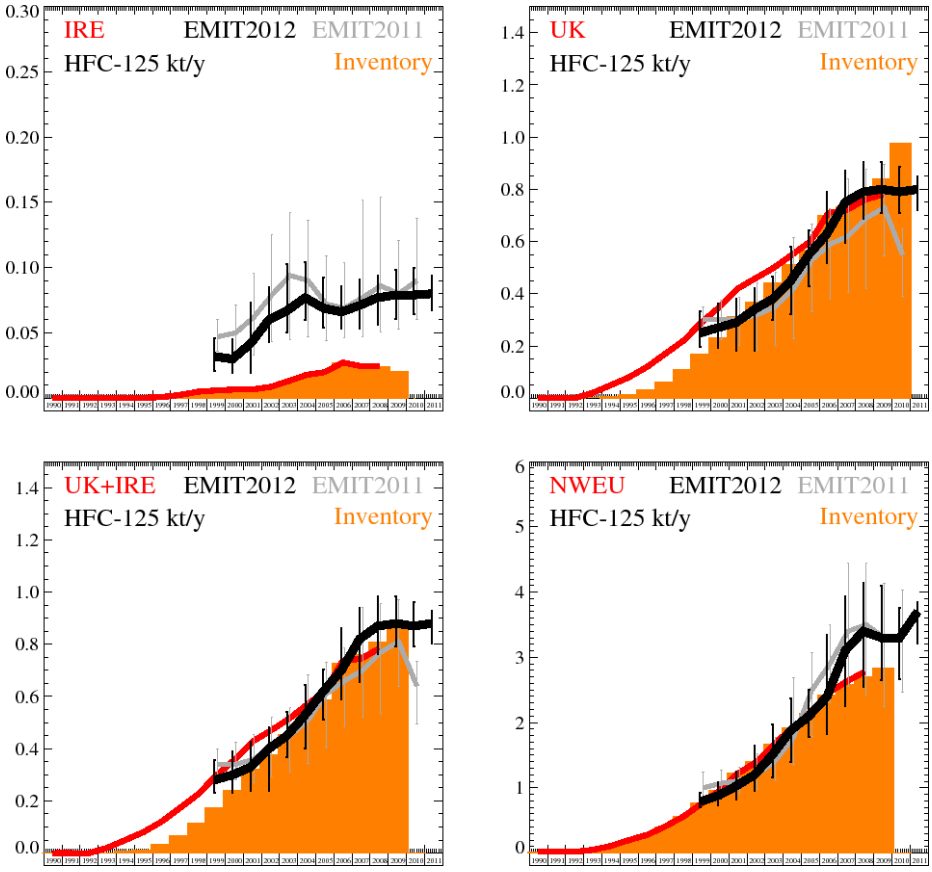

Figure 85: Inversion emission estimates for IRE, UK, IRE+UK and NWEU. Uncertainty bars represent the 5th and 95th percentiles. Orange bars represent UNFCCC emission estimates from the 2012 inventory. Grey (EMIT) and red (UNFCCC) are emissions as estimated last year.

Unit	Year	IRE	(5th-95th)	UK	(5th-95th)	UK+IRE	(5th-95th)	NWEU	(5th-95th)	Number
t/y	1999	32	(21.- 46.)	250	(195.- 332.)	280	(230.- 358.)	790	(704.- 925.)	1920
t/y	2000	30	(19.- 45.)	270	(194.- 363.)	300	(231.- 391.)	880	(726.-1086.)	3840
t/y	2001	42	(19.- 73.)	290	(182.- 381.)	330	(237.- 426.)	1030	(825.-1246.)	4000
t/y	2002	60	(43.- 85.)	340	(183.- 421.)	400	(240.- 483.)	1200	(954.-1651.)	4000
t/y	2003	67	(50.- 103.)	380	(299.- 465.)	450	(368.- 542.)	1510	(1163.-1968.)	4000
t/y	2004	77	(60.- 104.)	450	(323.- 579.)	530	(400.- 646.)	1880	(1402.-2377.)	4000
t/y	2005	69	(54.- 92.)	550	(430.- 643.)	620	(512.- 705.)	2100	(1782.-2506.)	4000
t/y	2006	66	(53.- 86.)	630	(519.- 790.)	700	(588.- 862.)	2400	(1825.-3348.)	4000
t/y	2007	71	(53.- 91.)	750	(596.- 872.)	820	(654.- 941.)	3100	(2253.-3941.)	4000
t/y	2008	77	(56.- 94.)	790	(686.- 906.)	870	(764.- 983.)	3400	(2545.-4140.)	4000
t/y	2009	79	(61.- 98.)	800	(709.- 905.)	880	(791.- 982.)	3300	(2651.-4096.)	4000
t/y	2010	79	(64.- 100.)	790	(710.- 885.)	870	(791.- 962.)	3300	(2671.-3756.)	2080
t/y	2011	80	(67.- 94.)	800	(720.- 851.)	880	(804.- 928.)	3700	(3214.-3844.)	160

Table 13: Emission estimates for UK, IRE and NWEU with uncertainty (5th – 95th %ile).

5.2.3.2 HFC-134a

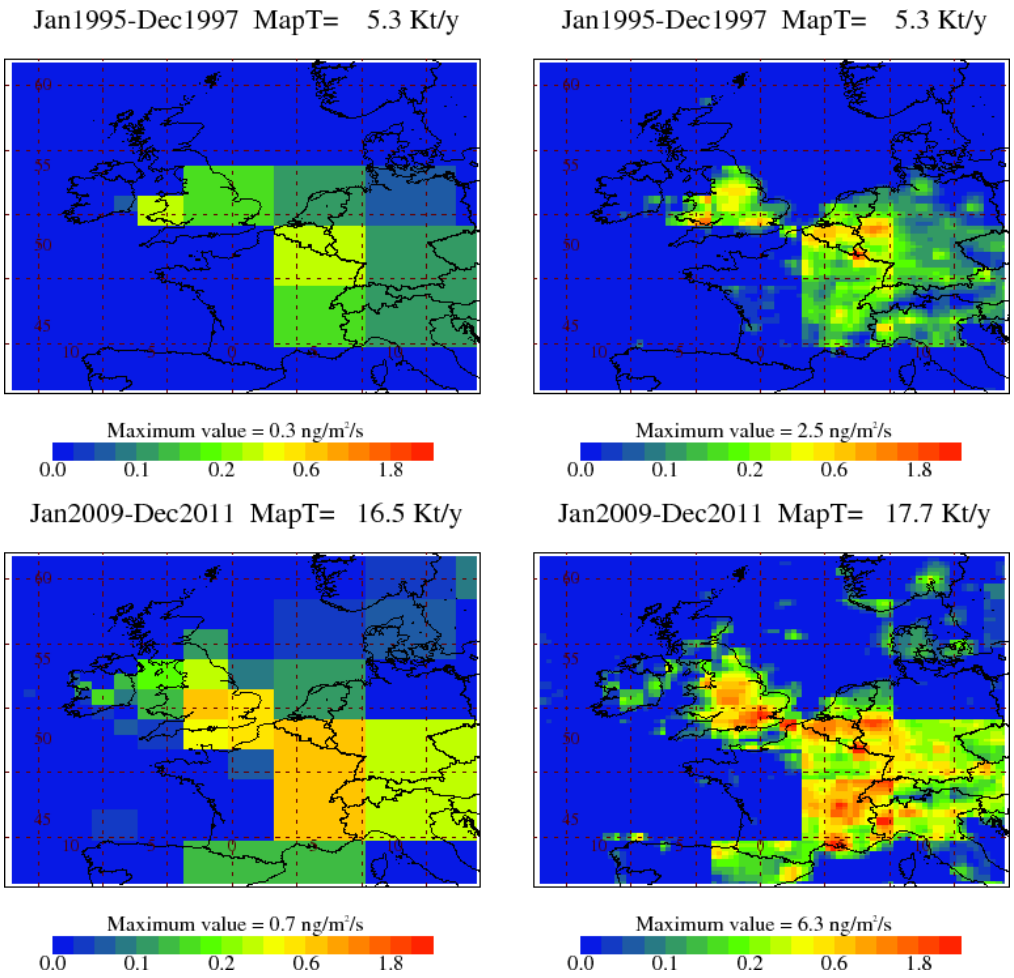

Figure 86: NAME-inversion emission estimates for 1990-92 (upper) and 2009-11 (lower). On the right hand side the emissions per grid box have been re-distributed based on population.

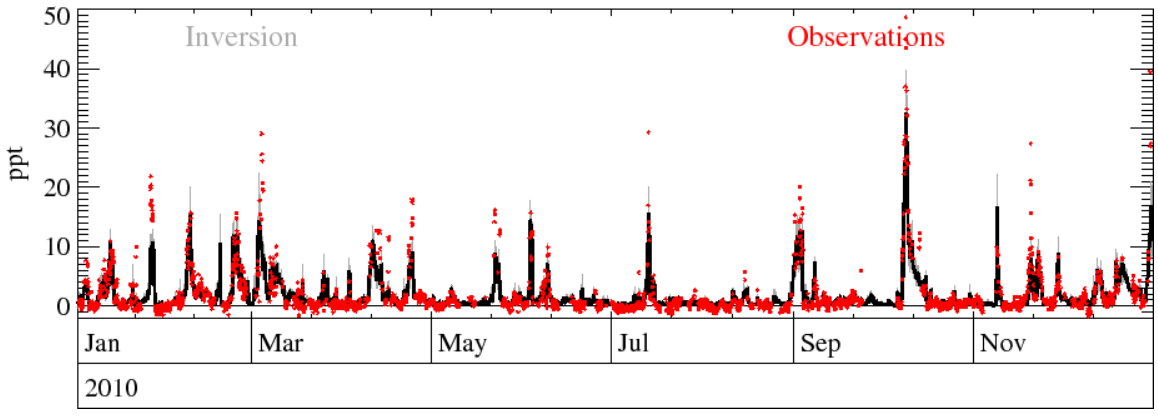

Figure 87: Example time-series of observations Vs. model using best-fit emission estimates.

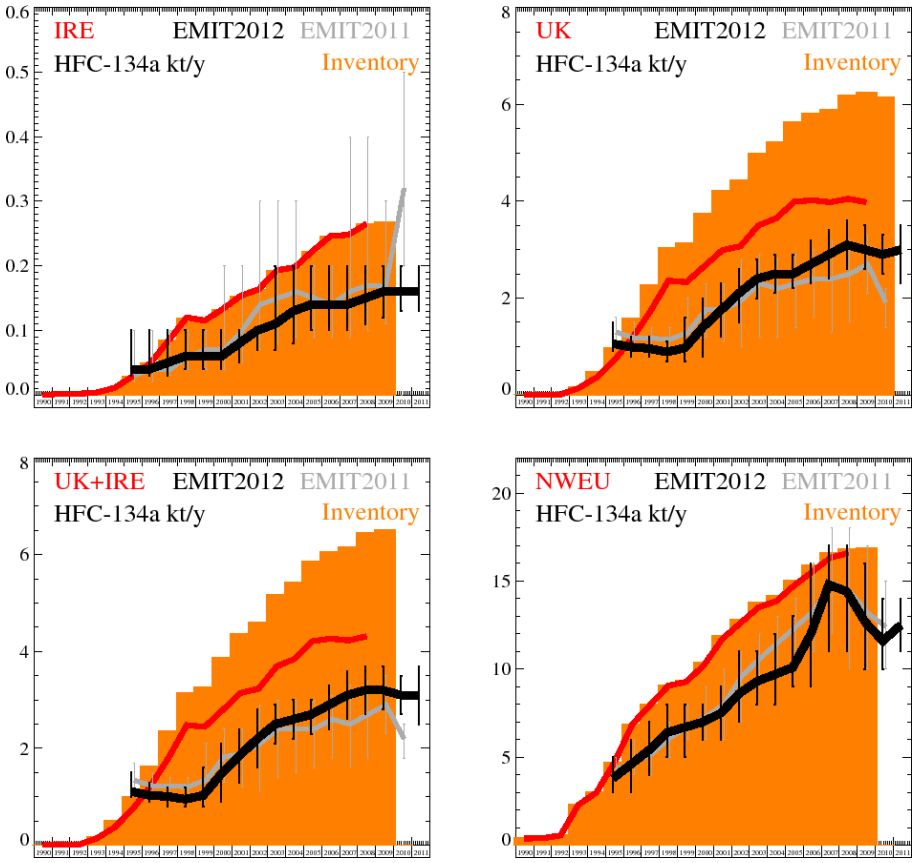

Figure 88: Inversion emission estimates for IRE, UK, IRE+UK and NWEU. Uncertainty bars represent the 5th and 95th percentiles. Orange bars represent UNFCCC emission estimates from the 2012 inventory. Grey (EMIT) and red (UNFCCC) are emissions as estimated last year.

Unit	Year	IRE	(5th-95th)	UK	(5th-95th)	UK+IRE	(5th-95th)	NWEU	(5th-95th)	Number
kt/y	1995	0.04	(0.03- 0.1)	1.06	(0.9- 1.5)	1.11	(1.0- 1.5)	3.8	(3.- 5.)	640
kt/y	1996	0.04	(0.03- 0.1)	0.99	(0.8- 1.2)	1.03	(0.9- 1.3)	4.6	(3.- 6.)	2560
kt/y	1997	0.05	(0.03- 0.1)	0.96	(0.8- 1.2)	1.01	(0.8- 1.2)	5.4	(4.- 7.)	4000
kt/y	1998	0.06	(0.04- 0.1)	0.89	(0.7- 1.1)	0.95	(0.8- 1.2)	6.4	(5.- 8.)	4000
kt/y	1999	0.06	(0.04- 0.1)	0.97	(0.7- 1.6)	1.03	(0.8- 1.6)	6.7	(5.- 8.)	4000
kt/y	2000	0.06	(0.04- 0.1)	1.4	(0.8- 2.0)	1.47	(0.9- 2.1)	7	(6.- 8.)	4000
kt/y	2001	0.08	(0.05- 0.1)	1.75	(1.2- 2.3)	1.84	(1.3- 2.4)	7.5	(6.- 9.)	4000
kt/y	2002	0.1	(0.07- 0.1)	2.1	(1.5- 2.6)	2.2	(1.6- 2.8)	8.6	(7.- 11.)	4000
kt/y	2003	0.11	(0.07- 0.2)	2.4	(2.0- 2.8)	2.5	(2.1- 2.9)	9.3	(8.- 11.)	4000
kt/y	2004	0.13	(0.08- 0.2)	2.5	(2.1- 2.9)	2.6	(2.2- 3.0)	9.7	(8.- 12.)	4000
kt/y	2005	0.14	(0.10- 0.2)	2.5	(2.2- 2.9)	2.7	(2.3- 3.0)	10.1	(9.- 13.)	4000
kt/y	2006	0.14	(0.10- 0.2)	2.7	(2.3- 3.2)	2.9	(2.4- 3.3)	12	(9.- 16.)	4000
kt/y	2007	0.14	(0.10- 0.2)	2.9	(2.4- 3.4)	3.1	(2.6- 3.6)	14.8	(11.- 17.)	4000
kt/y	2008	0.15	(0.11- 0.2)	3.1	(2.6- 3.6)	3.2	(2.7- 3.7)	14.4	(11.- 17.)	4000
kt/y	2009	0.16	(0.12- 0.2)	3	(2.6- 3.5)	3.2	(2.8- 3.7)	12.7	(10.- 16.)	4000
kt/y	2010	0.16	(0.13- 0.2)	2.9	(2.5- 3.3)	3.1	(2.7- 3.5)	11.6	(10.- 14.)	2080
kt/y	2011	0.16	(0.13- 0.2)	3	(2.3- 3.5)	3.1	(2.5- 3.7)	12.5	(11.- 14.)	160

Table 14: Emission estimates for UK, IRE and NWEU with uncertainty (5th – 95th %ile).

5.2.3.3 HFC-143a

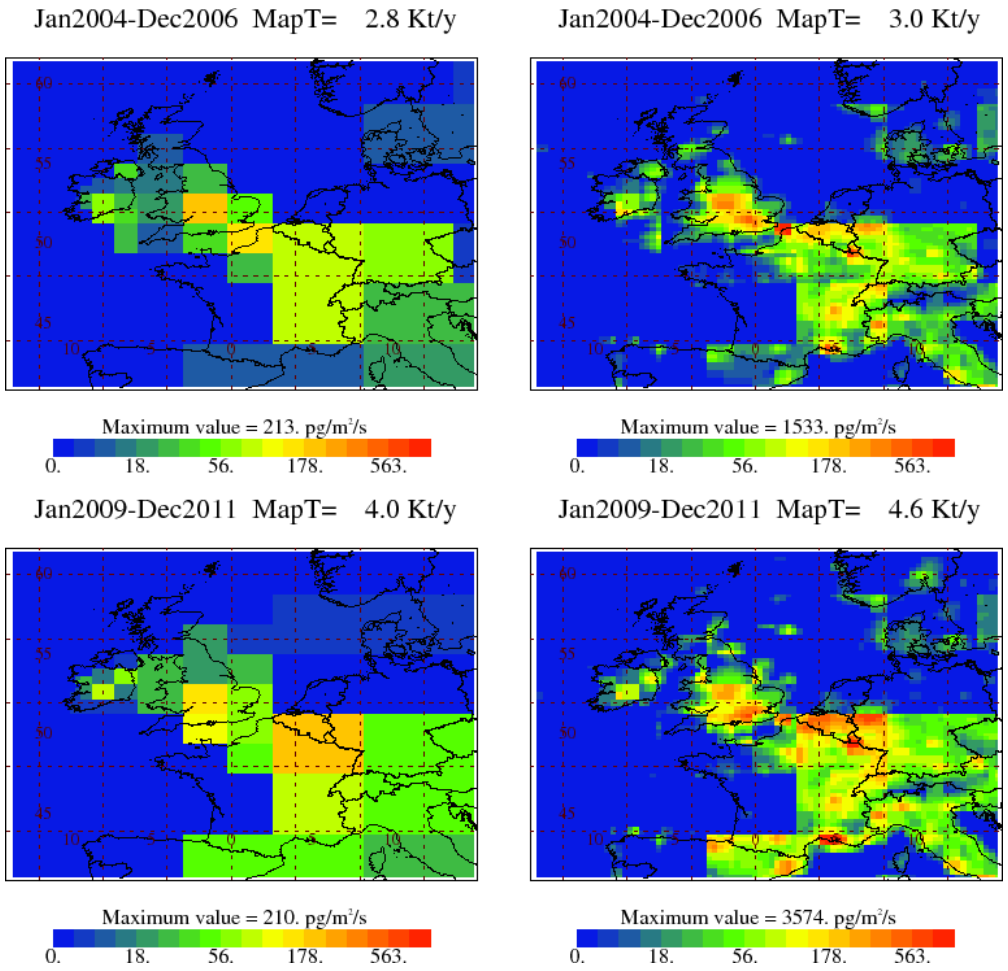

Figure 89: NAME-inversion emission estimates for 1990-92 (upper) and 2009-11 (lower). On the right hand side the emissions per grid box have been re-distributed based on population.

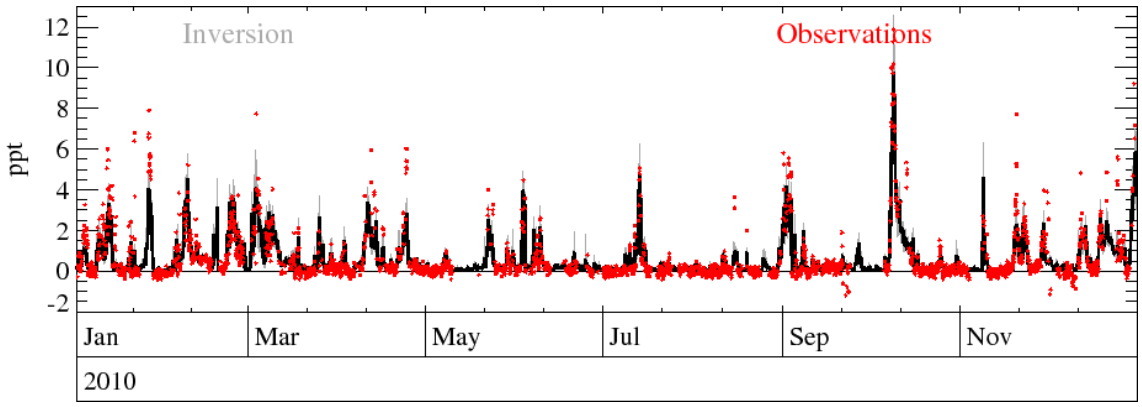

Figure 90: Example time-series of observations Vs. model using best-fit emission estimates.

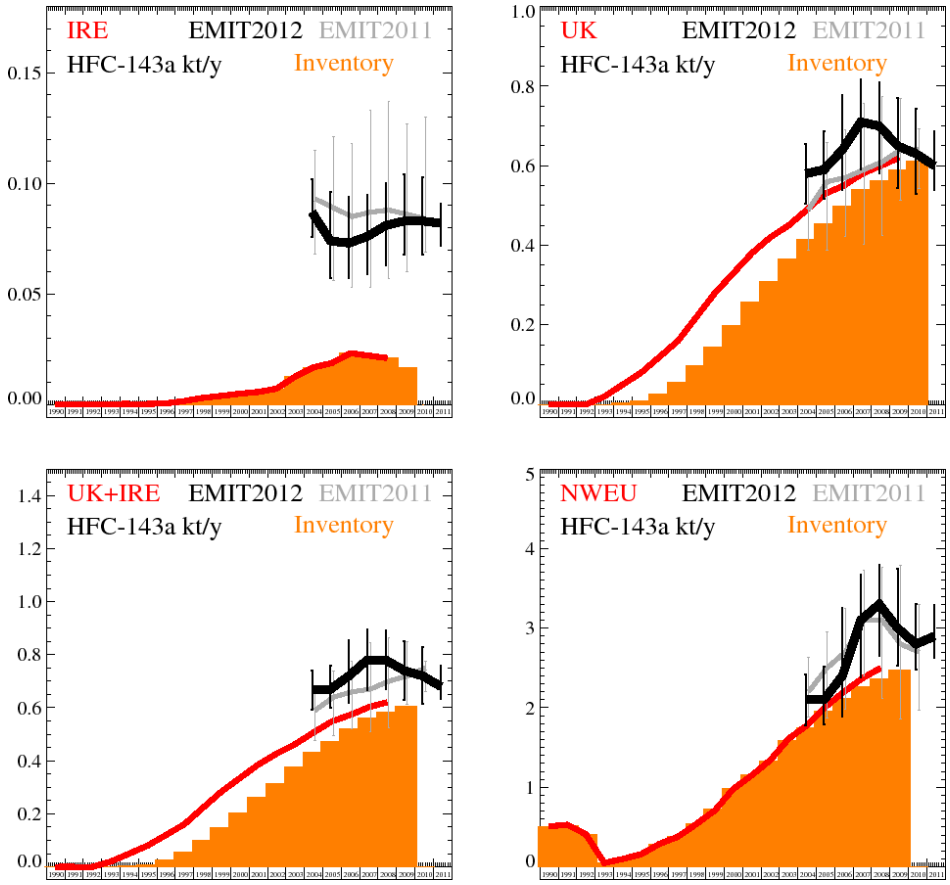

Figure 91: Inversion emission estimates for IRE, UK, IRE+UK and NWEU. Uncertainty bars represent the 5th and 95th percentiles. Orange bars represent UNFCCC emission estimates from the 2012 inventory. Grey (EMIT) and red (UNFCCC) are emissions as estimated last year.

Unit	Year	IRE	(5th-95th)	UK	(5th-95th)	UK+IRE	(5th-95th)	NWEU	(5th-95th)	Number
t/y	2004	87	(76.- 102.)	580	(505.- 655.)	670	(594.- 740.)	2100	(1785.-2414.)	480
t/y	2005	74	(57.- 96.)	590	(517.- 687.)	670	(601.- 757.)	2100	(1790.-2521.)	2400
t/y	2006	73	(57.- 94.)	640	(538.- 778.)	720	(618.- 855.)	2400	(1887.-3255.)	4000
t/y	2007	76	(59.- 95.)	710	(590.- 818.)	780	(668.- 895.)	3100	(2376.-3672.)	4000
t/y	2008	81	(63.- 100.)	700	(580.- 809.)	780	(669.- 891.)	3300	(2649.-3796.)	4000
t/y	2009	83	(68.- 104.)	650	(545.- 770.)	740	(629.- 850.)	3000	(2524.-3742.)	4000
t/y	2010	83	(68.- 103.)	630	(530.- 742.)	720	(616.- 827.)	2800	(2481.-3303.)	2080
t/y	2011	82	(72.- 91.)	600	(539.- 686.)	680	(632.- 760.)	2900	(2629.-3287.)	160

Table 15: Emission estimates for UK, IRE and NWEU with uncertainty (5th – 95th %ile).

5.2.3.4 HFC-152a

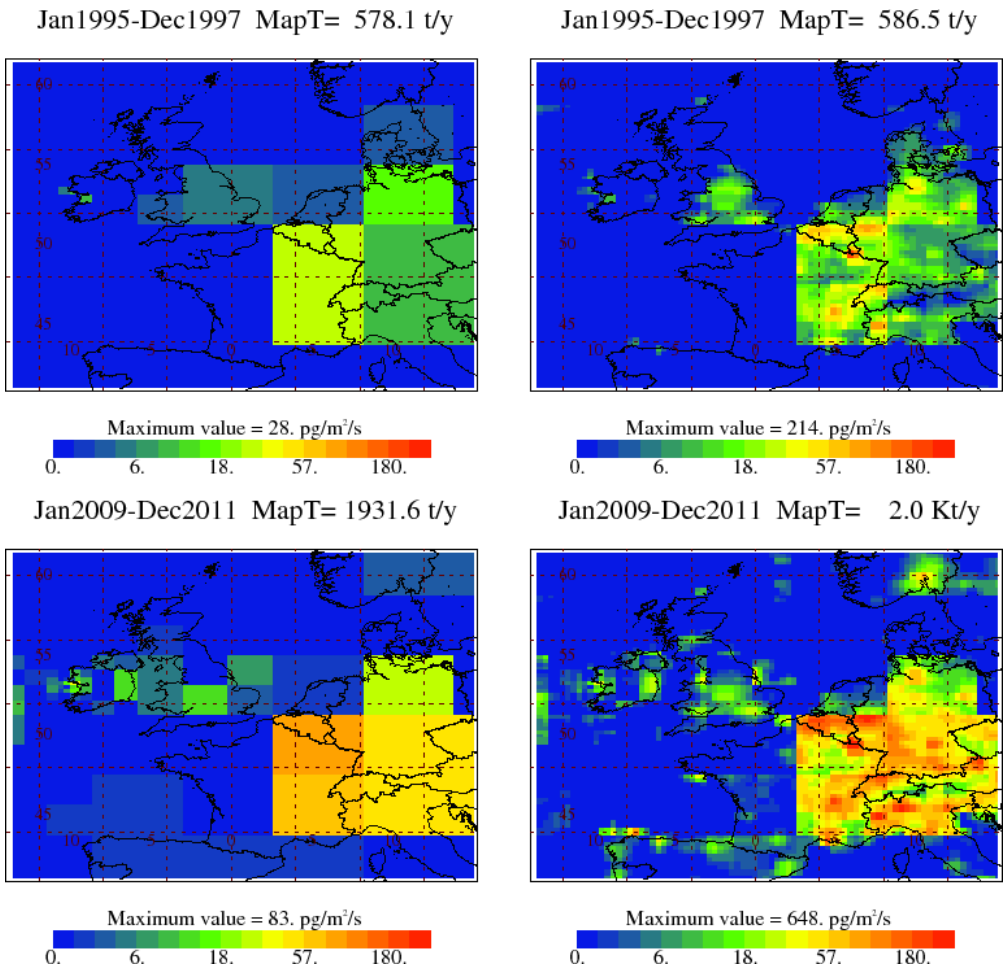

Figure 92: NAME-inversion emission estimates for 1990-92 (upper) and 2009-11 (lower). On the right hand side the emissions per grid box have been re-distributed based on population.

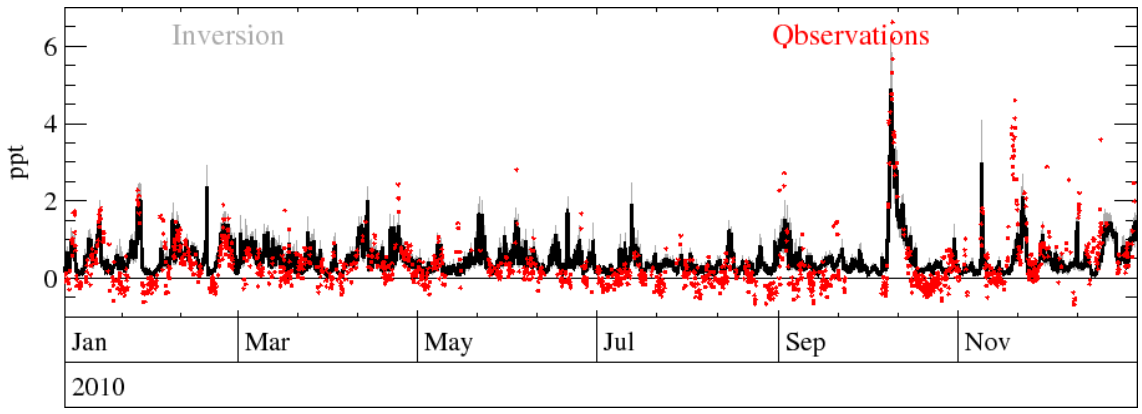

Figure 93: Example time-series of observations Vs. model using best-fit emission estimates.

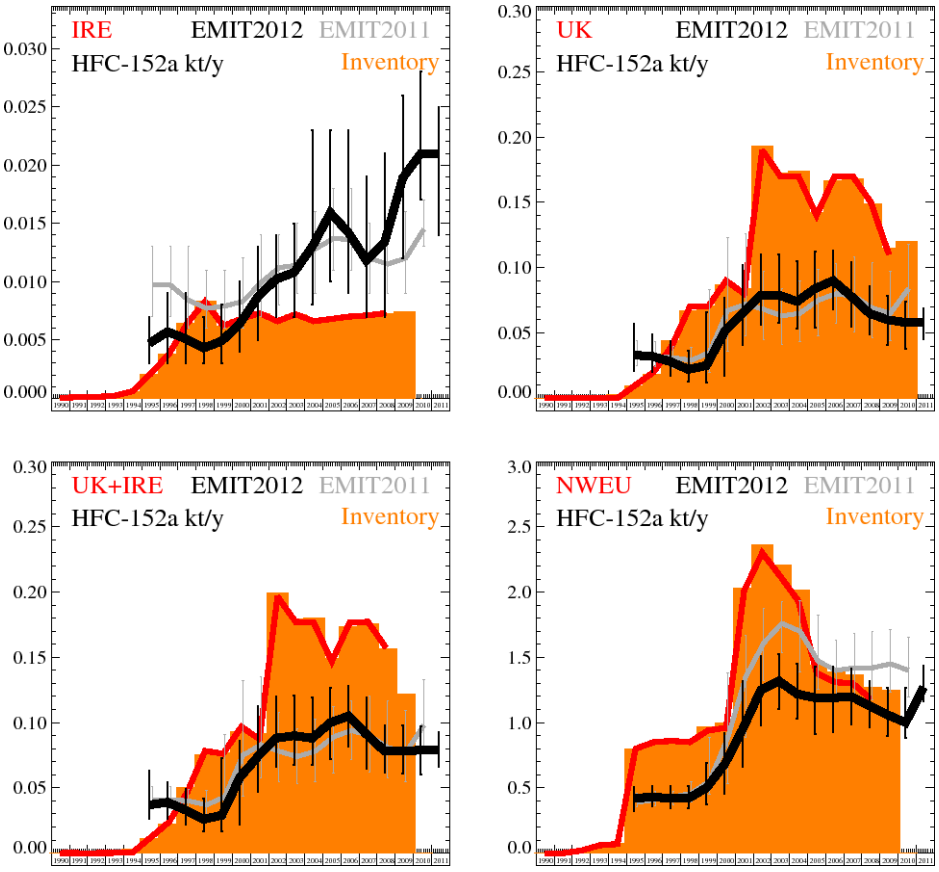

Figure 94: Inversion emission estimates for IRE, UK, IRE+UK and NWEU. Uncertainty bars represent the 5th and 95th percentiles. Orange bars represent UNFCCC emission estimates from the 2012 inventory. Grey (EMIT) and red (UNFCCC) are emissions as estimated last year.

Unit	Year	IRE	(5th-95th)	UK	(5th-95th)	UK+IRE	(5th-95th)	NWEU	(5th-95th)	Number
t/y	1995	4.7	(3.- 7.)	33	(21.- 57.)	37	(26.- 63.)	420	(323.- 510.)	640
t/y	1996	5.7	(3.- 9.)	32	(20.- 49.)	39	(26.- 54.)	430	(356.- 517.)	2560
t/y	1997	5.1	(3.- 9.)	28	(17.- 44.)	33	(22.- 49.)	420	(342.- 514.)	4000
t/y	1998	4.3	(3.- 7.)	22	(13.- 36.)	26	(17.- 42.)	420	(343.- 516.)	4000
t/y	1999	4.9	(3.- 8.)	25	(12.- 66.)	29	(17.- 73.)	500	(373.- 690.)	4000
t/y	2000	6.4	(4.- 10.)	51	(17.- 77.)	58	(22.- 86.)	680	(452.- 921.)	4000
t/y	2001	8.7	(5.- 13.)	65	(41.- 102.)	74	(47.- 113.)	950	(665.-1316.)	4000
t/y	2002	10.2	(7.- 14.)	79	(56.- 110.)	88	(66.- 120.)	1250	(981.-1510.)	4000
t/y	2003	10.8	(7.- 15.)	79	(58.- 110.)	90	(68.- 121.)	1320	(1101.-1525.)	4000
t/y	2004	13	(8.- 23.)	74	(53.- 105.)	88	(68.- 119.)	1220	(1030.-1451.)	4000
t/y	2005	15.9	(10.- 23.)	84	(54.- 112.)	100	(72.- 127.)	1190	(914.-1426.)	4000
t/y	2006	14.2	(9.- 23.)	90	(68.- 113.)	105	(82.- 128.)	1190	(926.-1428.)	4000
t/y	2007	11.8	(7.- 19.)	78	(55.- 104.)	91	(65.- 119.)	1200	(985.-1412.)	4000
t/y	2008	13.4	(7.- 21.)	65	(49.- 86.)	78	(62.- 98.)	1130	(962.-1317.)	4000
t/y	2009	18.9	(12.- 26.)	60	(41.- 78.)	78	(61.- 98.)	1060	(901.-1267.)	4000
t/y	2010	21	(17.- 28.)	58	(38.- 74.)	79	(60.- 97.)	1000	(880.-1268.)	2080
t/y	2011	21	(14.- 25.)	58	(45.- 69.)	79	(66.- 93.)	1270	(1166.-1434.)	160

Table 16: Emission estimates for UK, IRE and NWEU with uncertainty (5th – 95th %ile).

5.2.3.5 HFC-23

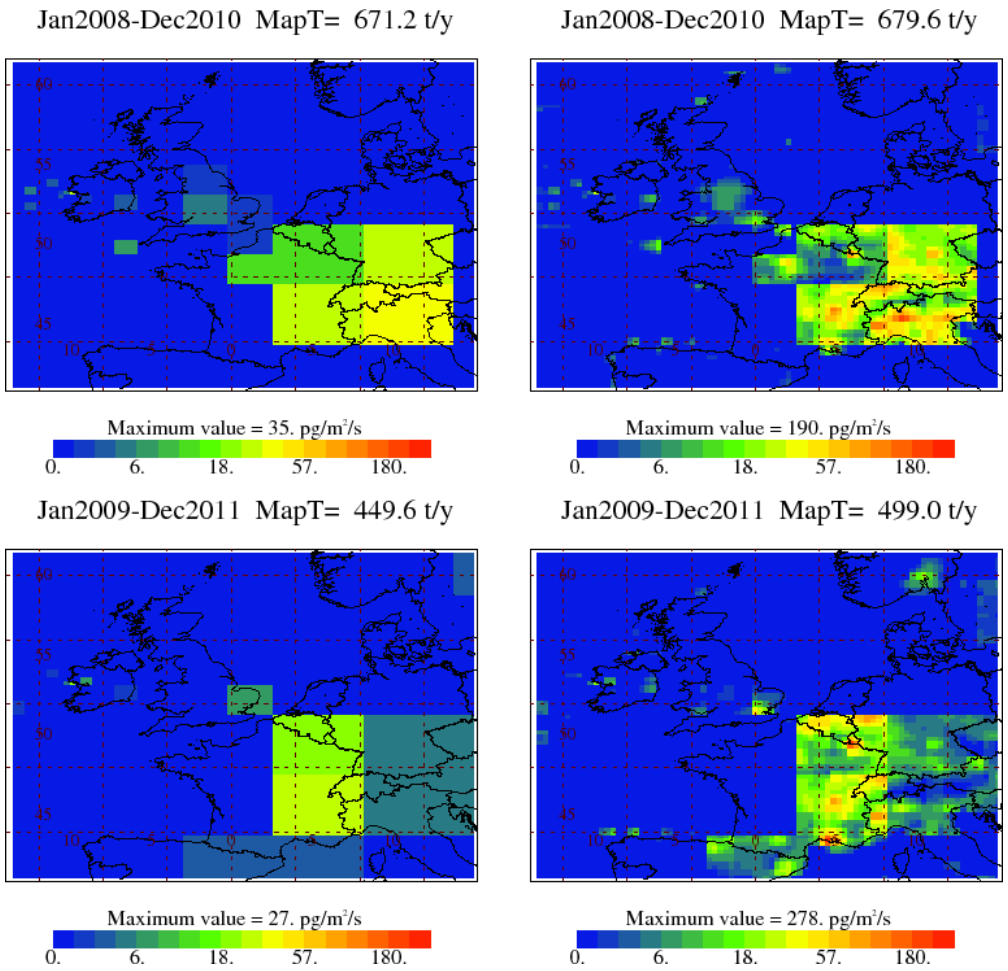

Figure 95: NAME-inversion emission estimates for 1990-92 (upper) and 2009-11 (lower). On the right hand side the emissions per grid box have been re-distributed based on population.

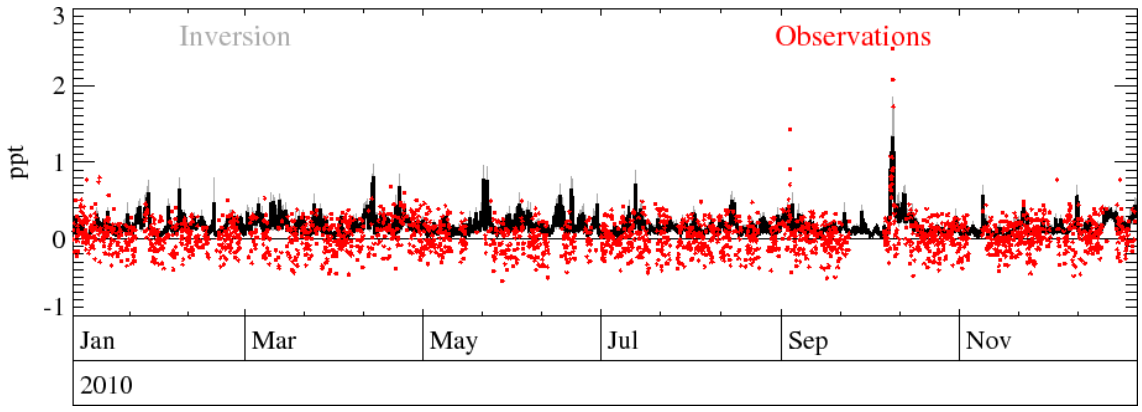

Figure 96: Example time-series of observations Vs. model using best-fit emission estimates.

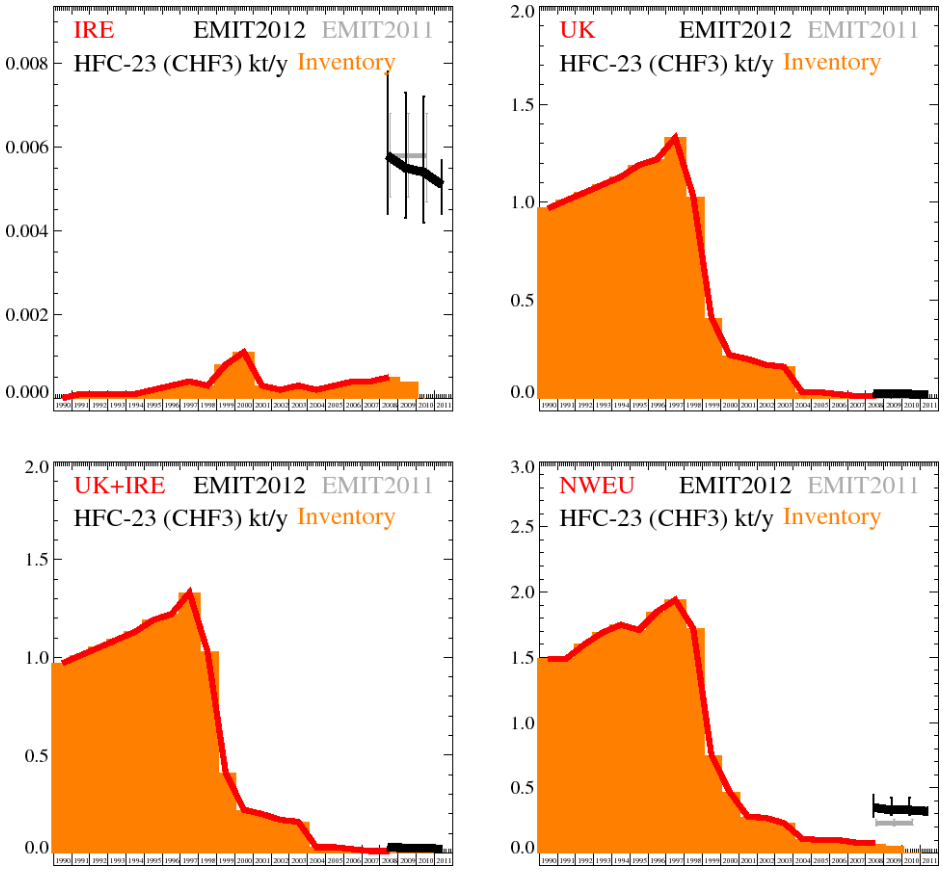

Figure 97: Inversion emission estimates for IRE, UK, IRE+UK and NWEU. Uncertainty bars represent the 5th and 95th percentiles. Orange bars represent UNFCCC emission estimates from the 2012 inventory. Grey (EMIT) and red (UNFCCC) are emissions as estimated last year.

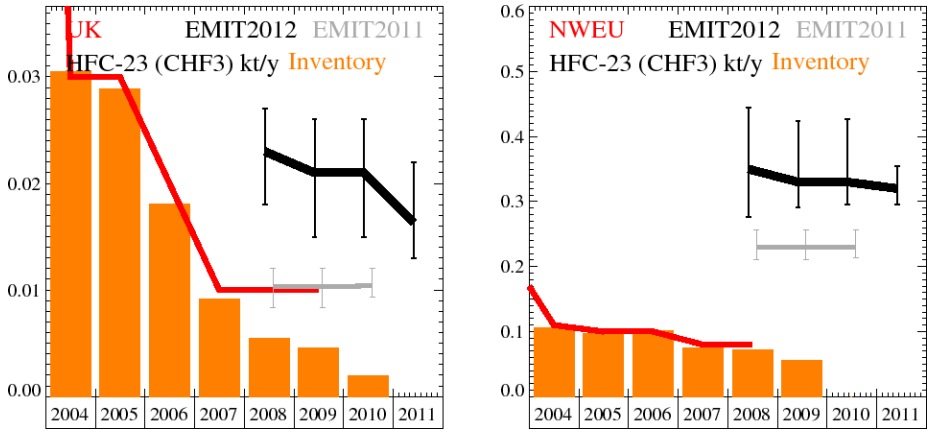

Figure 98: EMIT emission estimates for UK and NWEU (2004-2011). Uncertainty bars represent the 5th and 95th percentiles. Orange bars represent UNFCCC emission estimates from the 2012 inventory. Grey (EMIT) and red (UNFCCC) are emissions as estimated last year.

Unit	Year	IRE	(5th-95th)	UK	(5th-95th)	UK+IRE	(5th-95th)	NWEU	(5th-95th)	Number
t/y	2008	5.8	(4.4- 7.8)	23	(18.- 27.)	29	(23.- 34.)	350	(277.- 445.)	480
t/y	2009	5.5	(4.3- 7.3)	21	(15.- 26.)	27	(21.- 32.)	330	(291.- 424.)	2400
t/y	2010	5.4	(4.2- 7.2)	21	(15.- 26.)	26	(20.- 32.)	330	(295.- 427.)	2080
t/y	2011	5.1	(4.4- 5.7)	16.3	(13.- 22.)	21	(18.- 27.)	320	(295.- 355.)	160

Table 17: Emission estimates for UK, IRE and NWEU with uncertainty (5th – 95th %ile).

5.2.3.6 HFC-32

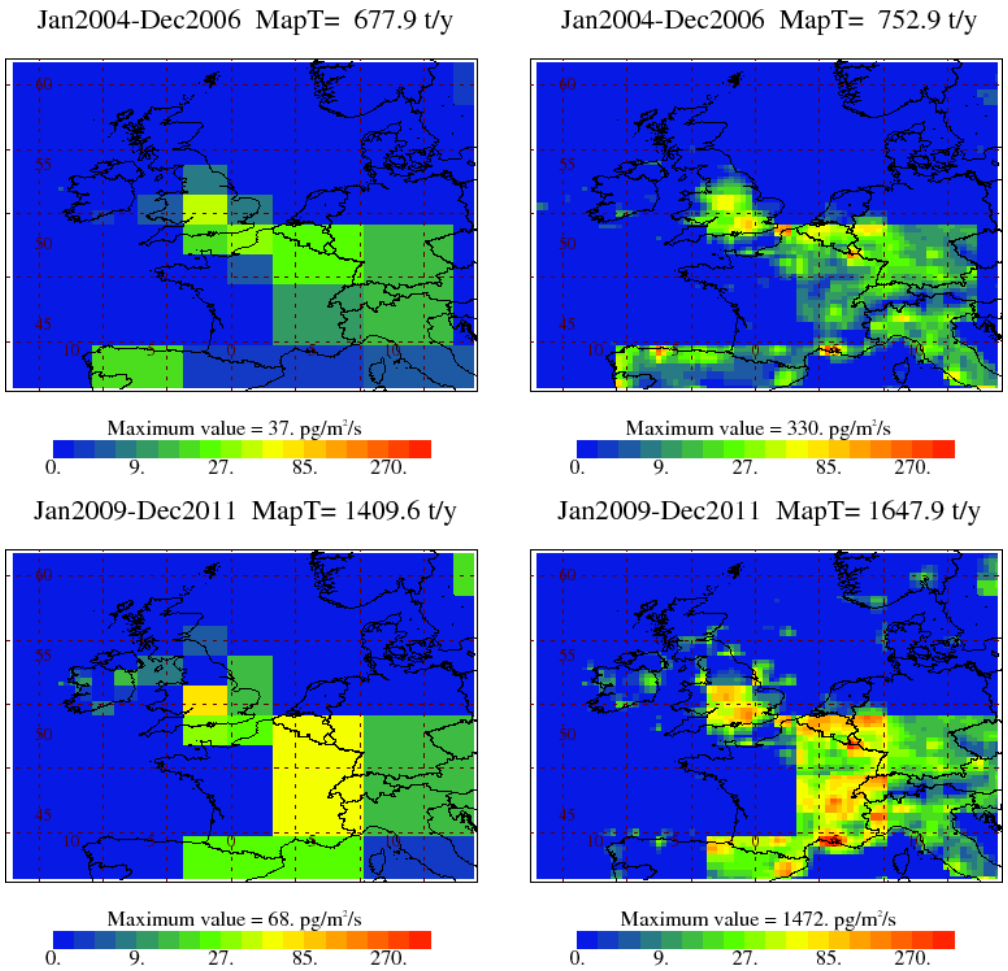

Figure 99: NAME-inversion emission estimates for 1990-92 (upper) and 2009-11 (lower). On the right hand side the emissions per grid box have been re-distributed based on population.

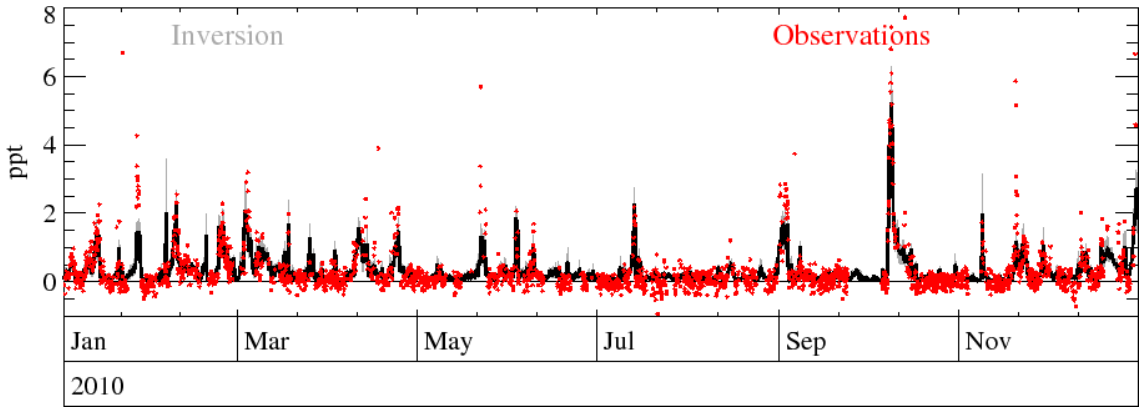

Figure 100: Example time-series of observations Vs. model using best-fit emission estimates.

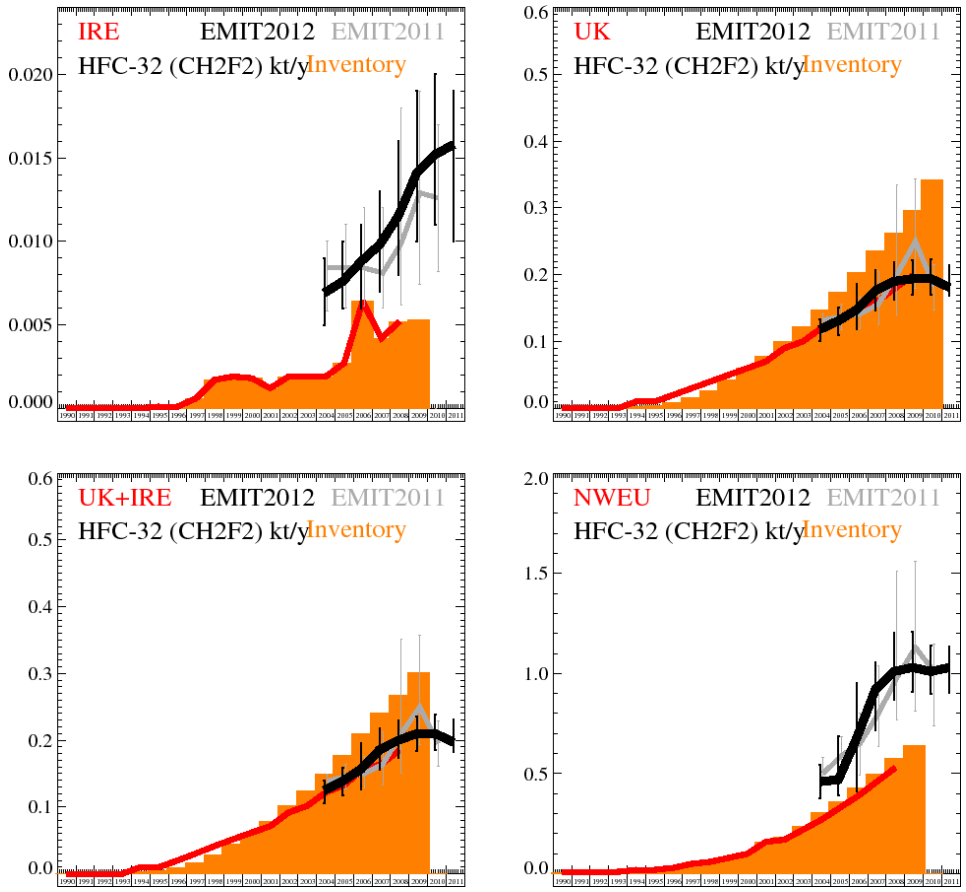

Figure 101: Inversion emission estimates for IRE, UK, IRE+UK and NWEU. Uncertainty bars represent the 5th and 95th percentiles. Orange bars represent UNFCCC emission estimates from the 2012 inventory. Grey (EMIT) and red (UNFCCC) are emissions as estimated last year.

Unit	Year	IRE	(5th-95th)	UK	(5th-95th)	UK+IRE	(5th-95th)	NWEU	(5th-95th)	Number
t/y	2004	6.9	(5.- 9.)	118	(100.- 133.)	125	(106.- 139.)	460	(375.- 543.)	480
t/y	2005	7.6	(6.- 10.)	131	(109.- 151.)	139	(117.- 159.)	470	(394.- 687.)	2400
t/y	2006	8.8	(6.- 11.)	148	(119.- 186.)	157	(127.- 195.)	680	(413.- 951.)	4000
t/y	2007	9.8	(7.- 13.)	176	(147.- 207.)	186	(156.- 218.)	920	(717.-1058.)	4000
t/y	2008	11.5	(8.- 16.)	190	(163.- 218.)	200	(174.- 230.)	1010	(868.-1206.)	4000
t/y	2009	14.1	(10.- 19.)	194	(170.- 221.)	210	(184.- 236.)	1030	(906.-1208.)	4000
t/y	2010	15.2	(11.- 20.)	194	(170.- 223.)	210	(186.- 239.)	1010	(896.-1140.)	2080
t/y	2011	15.8	(10.- 19.)	181	(168.- 215.)	197	(183.- 231.)	1030	(903.-1134.)	160

Table 18: Emission estimates for UK, IRE and NWEU with uncertainty (5th – 95th %ile).

5.2.3.7 HFC-365mfc

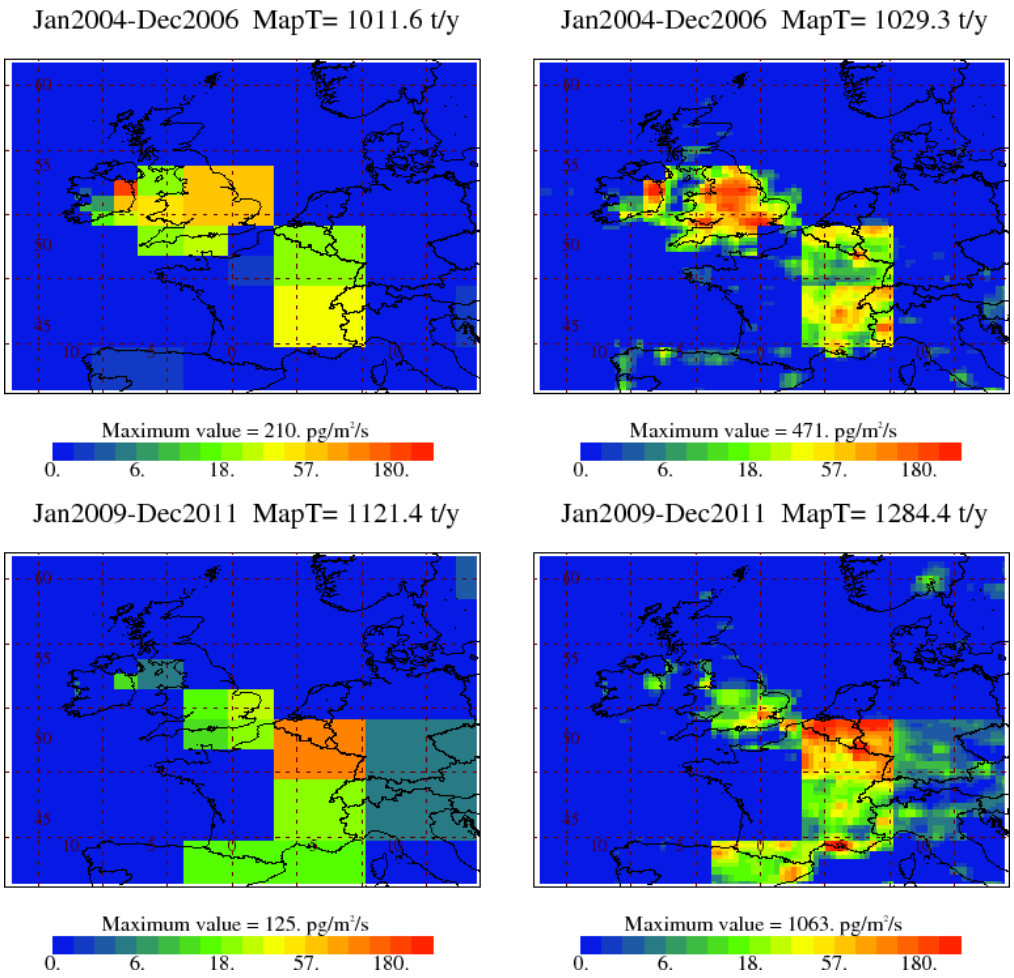

Figure 102: NAME-inversion emission estimates for 1990-92 (upper) and 2009-11 (lower). On the right hand side the emissions per grid box have been re-distributed based on population.

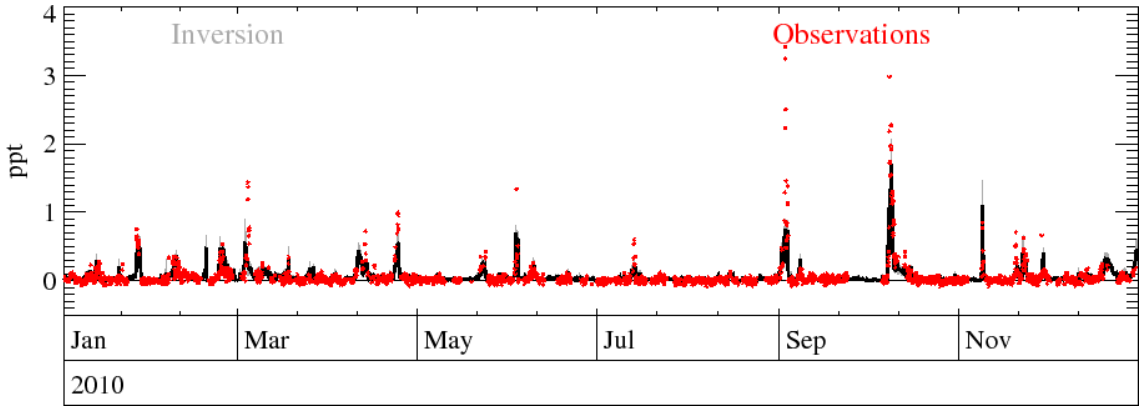

Figure 103: Example time-series of observations Vs. model using best-fit emission estimates.

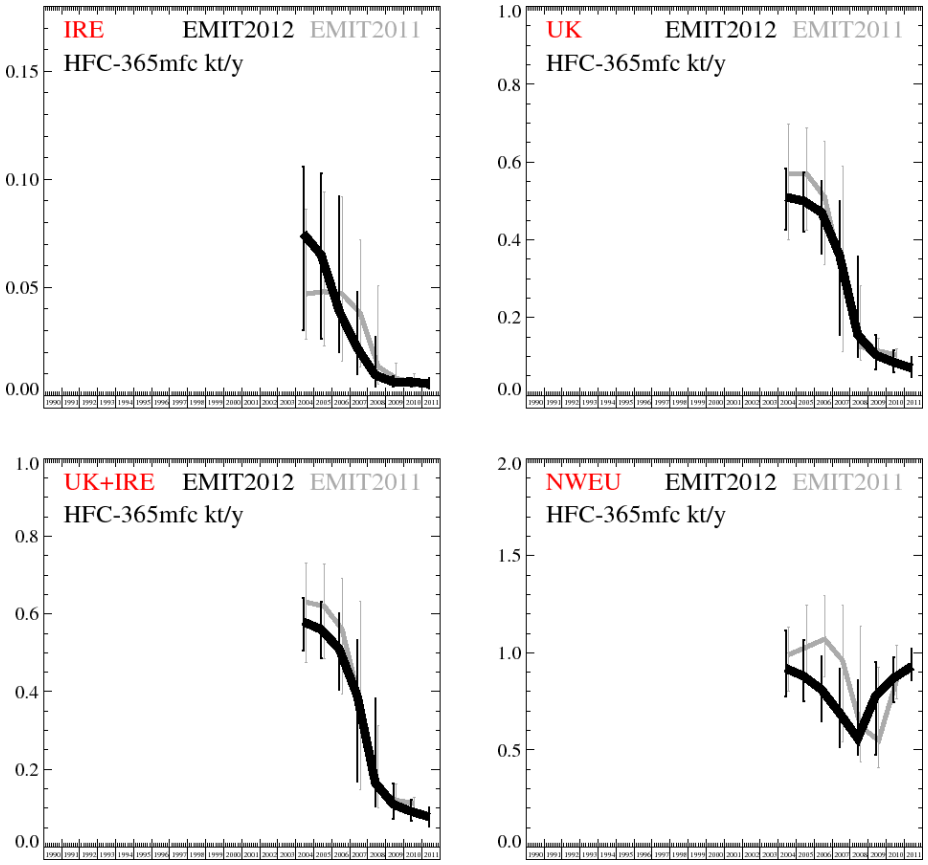

Figure 104: Emission estimates for IRE, UK, IRE+UK and NWEU. The uncertainty bars represent the 5th and 95th percentiles. Grey emissions are estimates from last year.

Unit	Year	IRE	(5th-95th)	UK	(5th-95th)	UK+IRE	(5th-95th)	NWEU	(5th-95th)	Number
t/y	2004	75	(30.- 106.)	510	(426.- 583.)	580	(507.- 640.)	920	(773.-1113.)	1440
t/y	2005	65	(26.- 103.)	500	(422.- 574.)	560	(486.- 631.)	880	(749.-1066.)	3360
t/y	2006	39	(20.- 92.)	470	(365.- 551.)	510	(404.- 602.)	810	(647.- 984.)	4000
t/y	2007	22	(10.- 48.)	360	(156.- 499.)	390	(168.- 534.)	690	(513.- 918.)	4000
t/y	2008	9.4	(4.- 27.)	156	(99.- 357.)	166	(104.- 384.)	560	(475.- 860.)	4000
t/y	2009	6.2	(4.- 9.)	104	(67.- 155.)	110	(73.- 164.)	780	(477.- 955.)	4000
t/y	2010	6.3	(4.- 8.)	85	(60.- 115.)	92	(67.- 121.)	870	(747.- 979.)	2080
t/y	2011	5.3	(3.- 8.)	70	(48.- 98.)	78	(53.- 103.)	930	(857.-1023.)	160

Table 19: Emission estimates for UK, IRE and NWEU with uncertainty (5th – 95th %ile).

5.2.3.8 HFC-227ea

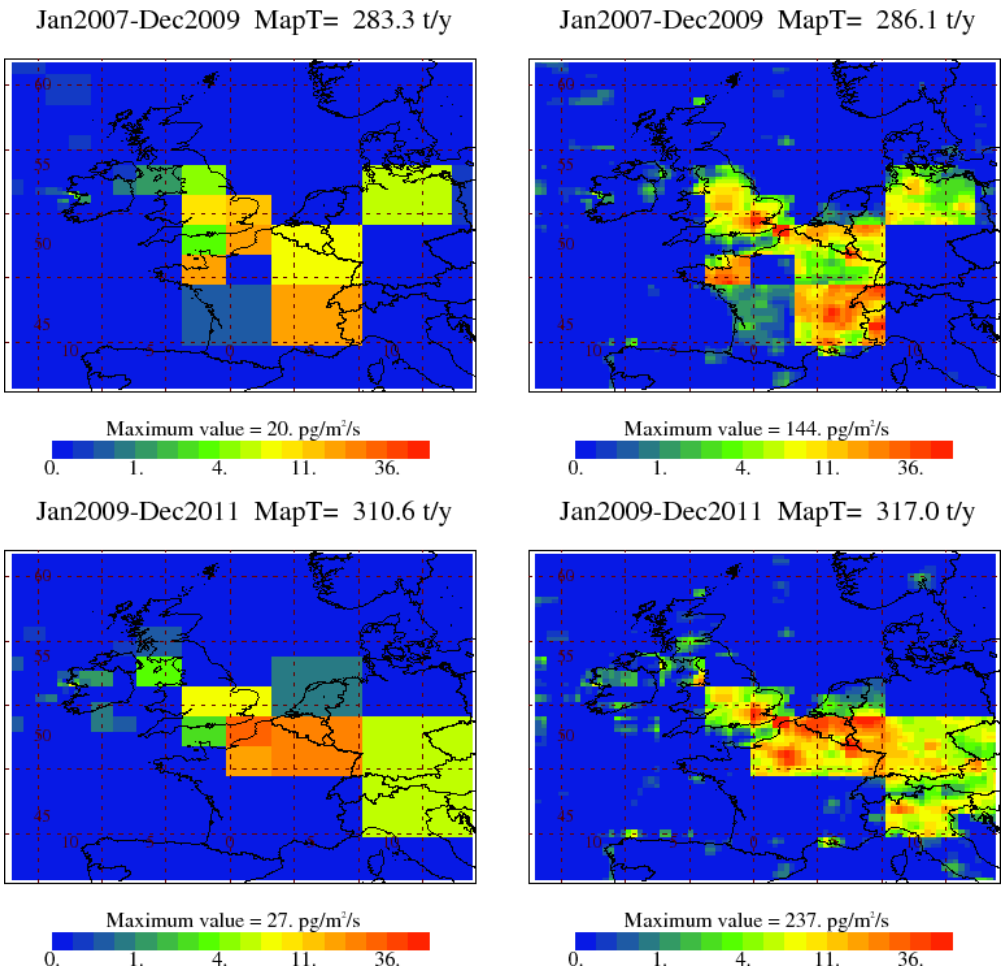

Figure 105: NAME-inversion emission estimates for 1990-92 (upper) and 2009-11 (lower). On the right hand side the emissions per grid box have been re-distributed based on population.

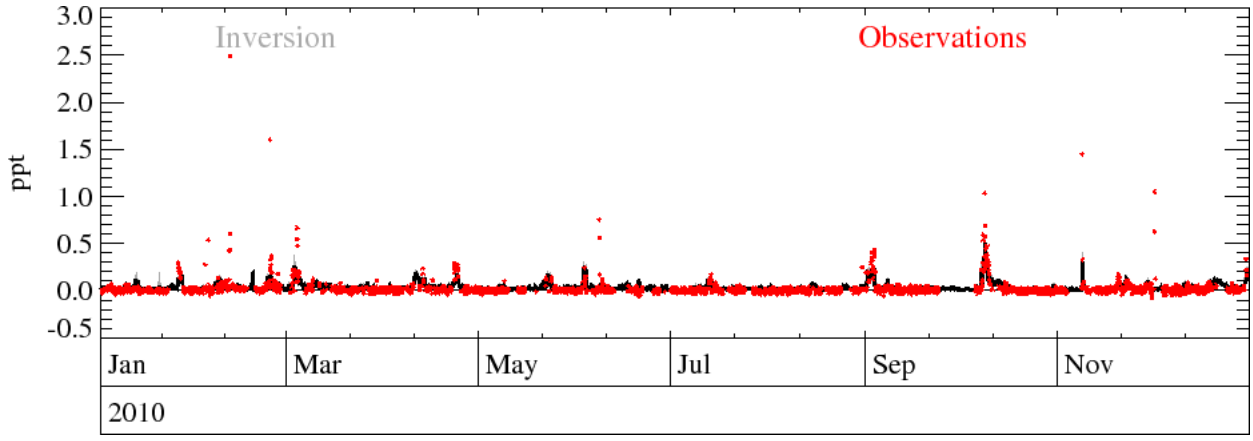

Figure 106: Example time-series of observations Vs. model using best-fit emission estimates.

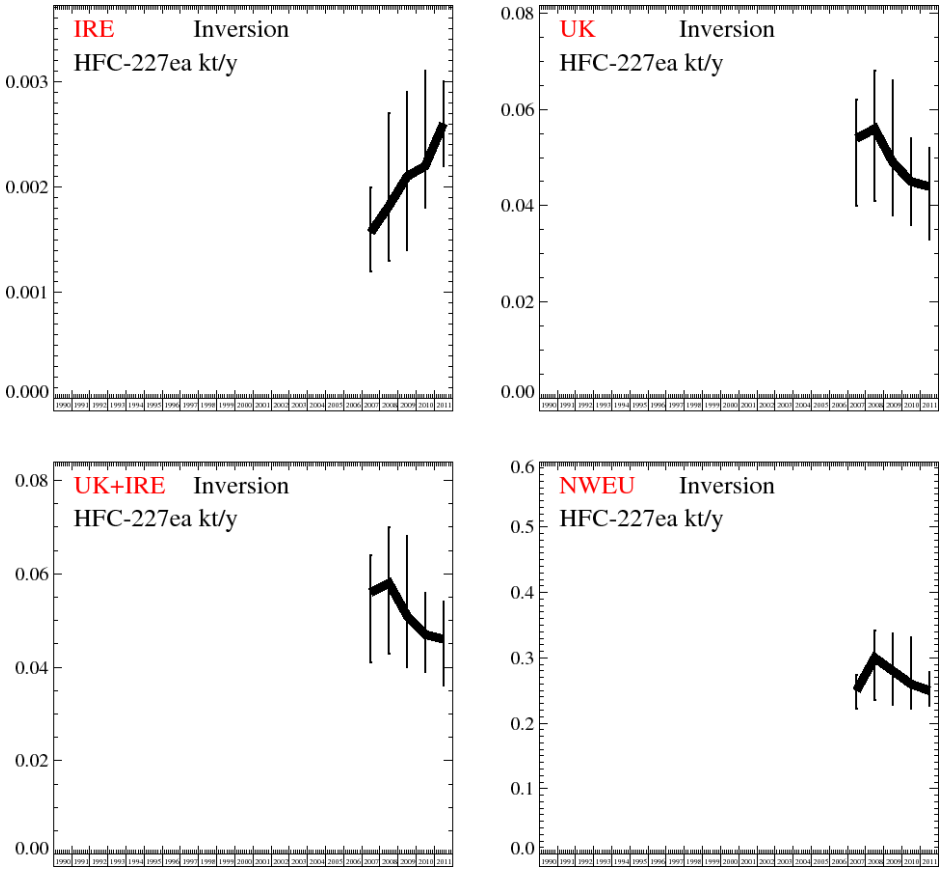

Figure 107: Emission estimates for IRE, UK, IRE+UK and NWEU. The uncertainty bars represent the 5th and 95th percentiles. Grey emissions are estimates from last year.

Unit	Year	IRE	(5th-95th)	UK	(5th-95th)	UK+IRE	(5th-95th)	NWEU	(5th-95th)	Number
t/y	2007	1.57	(1.2- 2.0)	54	(40.- 62.)	56	(41.- 64.)	250	(223.- 274.)	640
t/y	2008	1.82	(1.3- 2.7)	56	(41.- 68.)	58	(43.- 70.)	300	(235.- 342.)	2560
t/y	2009	2.1	(1.4- 2.9)	49	(38.- 66.)	51	(40.- 68.)	280	(228.- 338.)	4000
t/y	2010	2.2	(1.8- 3.1)	45	(36.- 54.)	47	(39.- 56.)	260	(222.- 332.)	2080
t/y	2011	2.6	(2.2- 3.0)	44	(33.- 52.)	46	(36.- 54.)	250	(227.- 279.)	160

Table 20: Emission estimates for UK, IRE and NWEU with uncertainty (5th – 95th %ile).

5.2.3.9 HFC-236fa

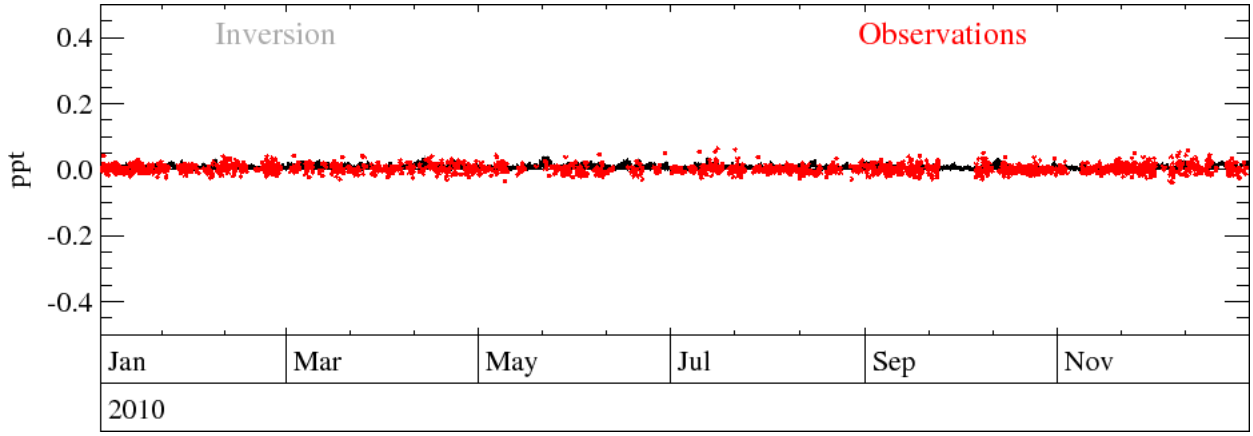

Figure 108: Example time-series of observations Vs. model using best-fit emission estimates.

As can be seen from the above plot there are no significant pollution events of this gas at Mace Head. This implies there are, at most, very few emissions within western Europe. The inversion results confirm this with emission estimates of fewer than 10 t/y across the whole of NWEU.

Unit	Year	IRE	(5th-95th)	UK	(5th-95th)	UK+IRE	(5th-95th)	NWEU	(5th-95th)	Number
t/y	2007	0.71	(0.50- 0.9)	2.9	(2.5- 3.4)	3.6	(3.2- 4.0)	4.9	(4.2- 6.)	640
t/y	2008	0.71	(0.53- 0.9)	3.2	(2.6- 3.8)	3.9	(3.4- 4.5)	6.2	(4.5- 9.)	2560
t/y	2009	0.73	(0.55- 0.9)	3.3	(2.7- 3.9)	4	(3.5- 4.6)	8.1	(5.4- 11.)	4000
t/y	2010	0.75	(0.59- 0.9)	3.3	(2.8- 3.9)	4.1	(3.5- 4.7)	9.3	(7.6- 11.)	2080
t/y	2011	0.79	(0.70- 1.0)	3.4	(2.6- 3.9)	4.2	(3.4- 4.7)	8.6	(7.5- 10.)	160

Table 21: Emission estimates for UK, IRE and NWEU with uncertainty (5^{th} – 95^{th} %ile).

5.2.3.10 HFC-245fa

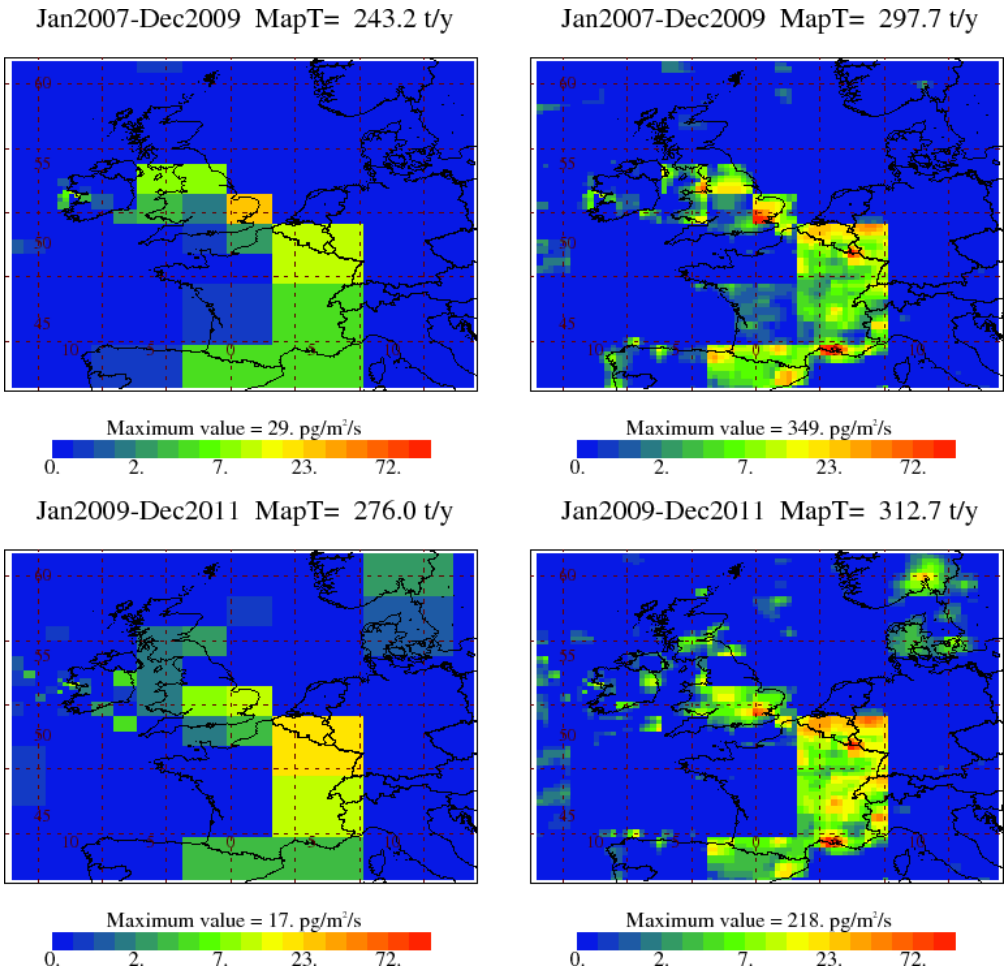

Figure 109: NAME-inversion emission estimates for 1990-92 (upper) and 2009-11 (lower). On the right hand side the emissions per grid box have been re-distributed based on population.

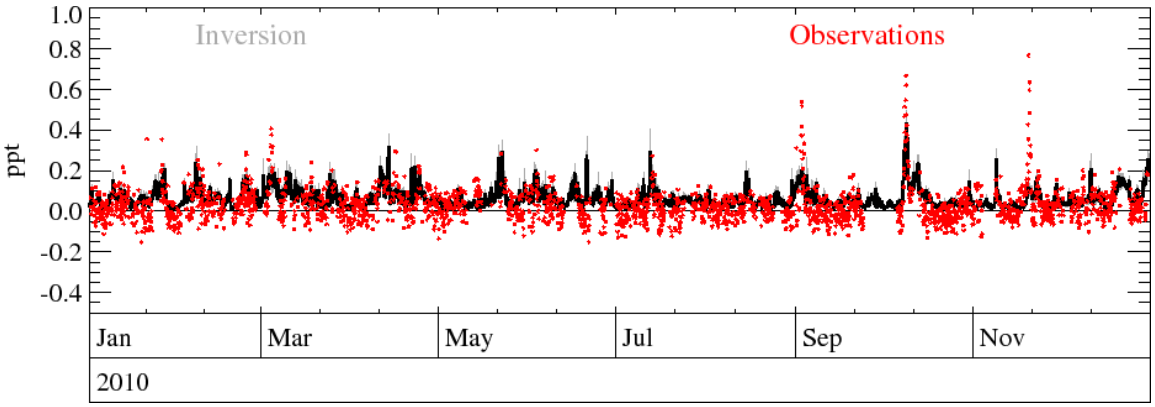

Figure 110: Example time-series of observations Vs. model using best-fit emission estimates.

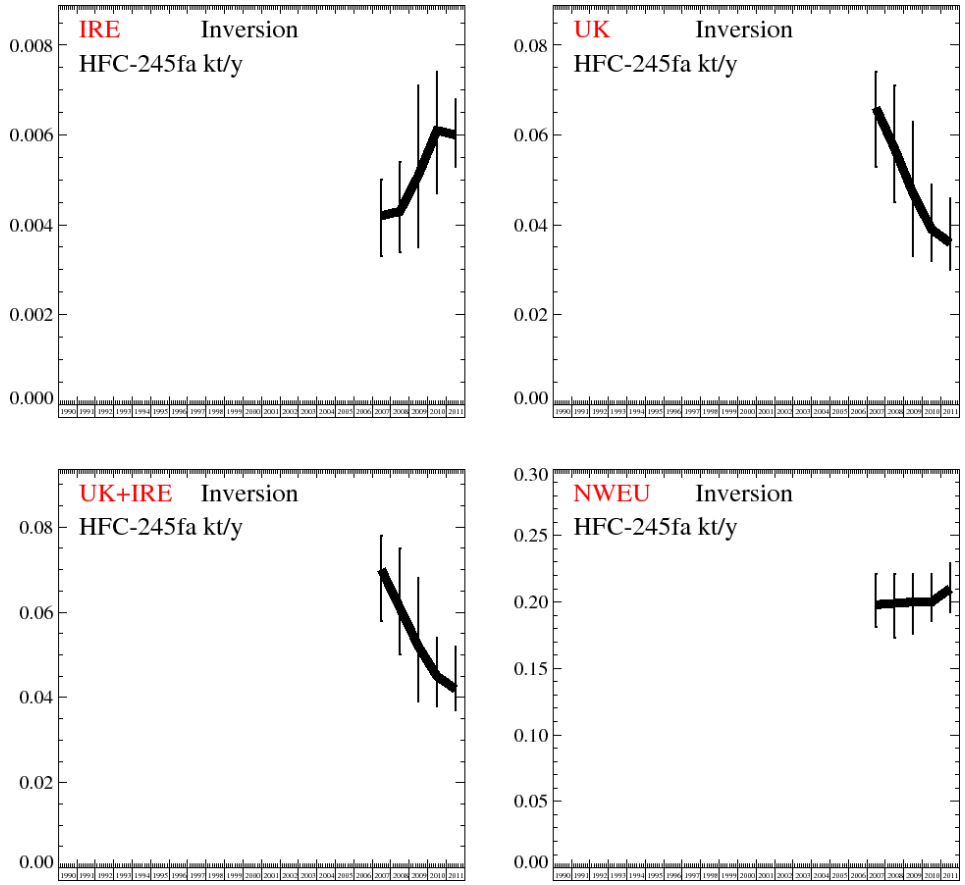

Figure 111: Emission estimates for IRE, UK, IRE+UK and NWEU. The uncertainty bars represent the 5th and 95th percentiles. Grey emissions are estimates from last year.

Unit	Year	IRE	(5th-95th)	UK	(5th-95th)	UK+IRE	(5th-95th)	NWEU	(5th-95th)	Number
t/y	2007	4.2	(3.3- 5.0)	66	(53.- 74.)	70	(58.- 78.)	198	(181.- 221.)	480
t/y	2008	4.3	(3.4- 5.4)	57	(45.- 71.)	61	(50.- 75.)	199	(173.- 221.)	2400
t/y	2009	5.1	(3.5- 7.1)	47	(33.- 63.)	52	(39.- 68.)	200	(176.- 221.)	4000
t/y	2010	6.1	(4.7- 7.4)	39	(32.- 49.)	45	(38.- 54.)	200	(186.- 221.)	2080
t/y	2011	6	(5.3- 6.8)	36	(30.- 46.)	42	(37.- 52.)	210	(192.- 229.)	160

Table 22: Emission estimates for UK, IRE and NWEU with uncertainty (5th – 95th %ile).

5.2.4 PFC

5.2.4.1 PFC-14

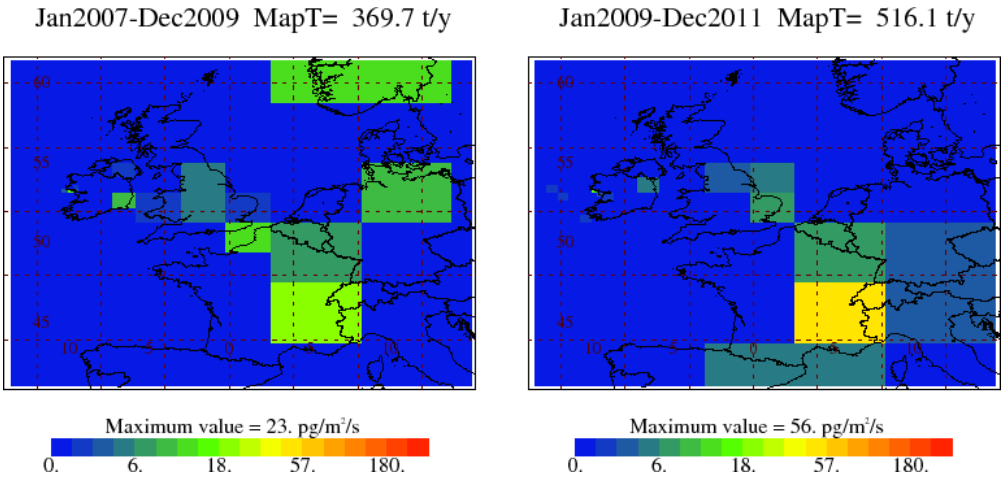

Figure 112: NAME-inversion emission estimates for 1990-92 (left) and 2009-11 (right)

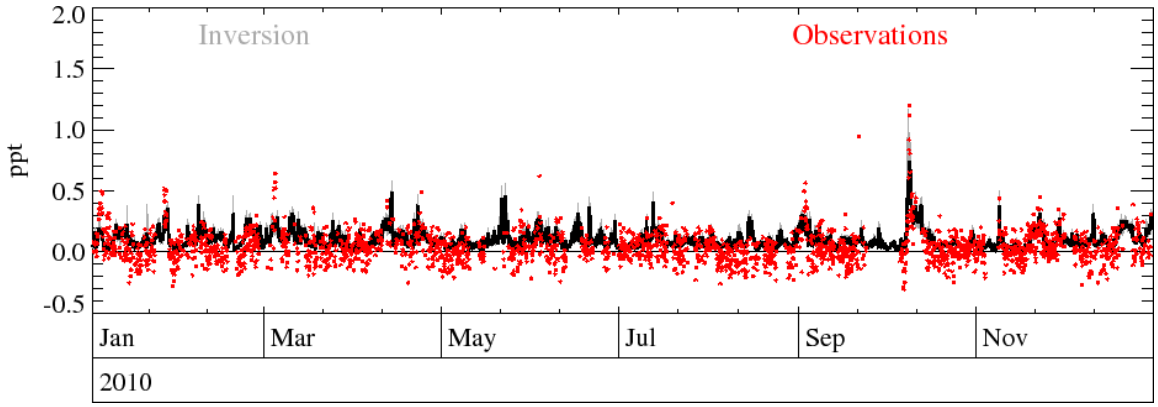

Figure 113: Example time-series of observations Vs. model using best-fit emission estimates.

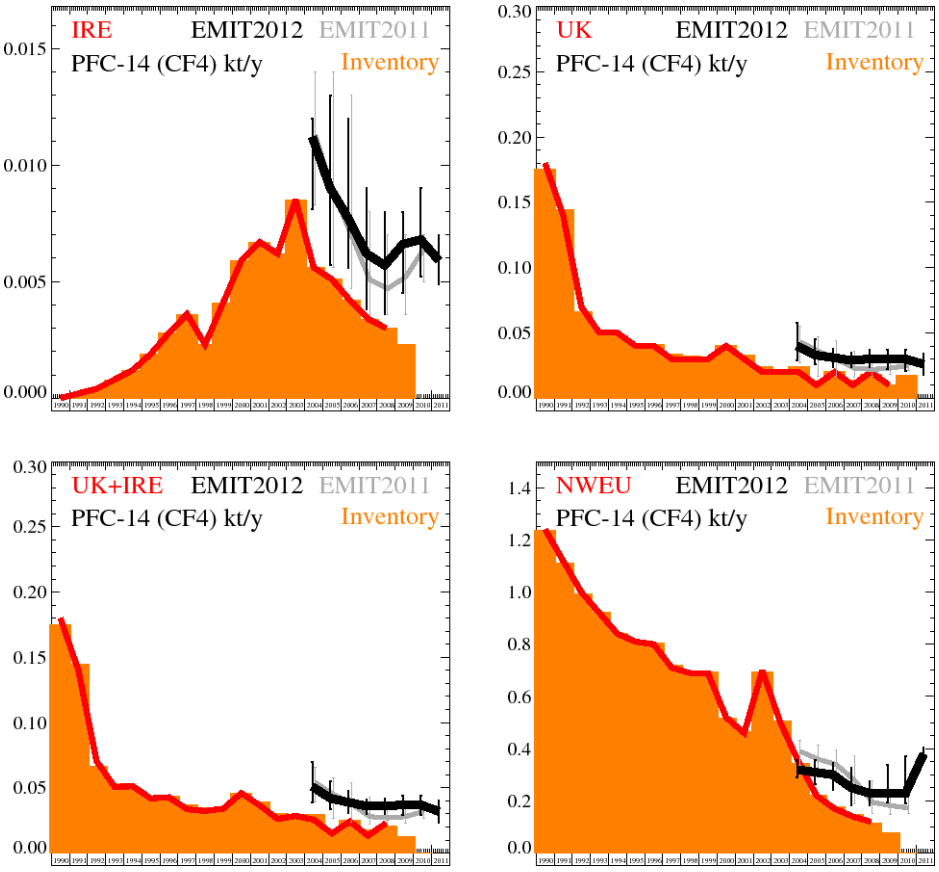

Figure 114: Inversion emission estimates for IRE, UK, IRE+UK and NWEU. Uncertainty bars represent the 5th and 95th percentiles. Orange bars represent UNFCCC emission estimates from the 2012 inventory. Grey (EMIT) and red (UNFCCC) are emissions as estimated last year.

Unit	Year	IRE	(5th-95th)	UK	(5th-95th)	UK+IRE	(5th-95th)	NWEU	(5th-95th)	Number
t/y	2004	11.2	(8.1- 12.)	40	(29.- 58.)	51	(39.- 70.)	320	(289.- 358.)	320
t/y	2005	9	(5.7- 13.)	33	(26.- 45.)	42	(34.- 55.)	310	(266.- 356.)	2240
t/y	2006	7.7	(5.6- 12.)	31	(24.- 38.)	39	(31.- 48.)	300	(242.- 346.)	4000
t/y	2007	6.2	(3.8- 9.)	29	(24.- 35.)	36	(30.- 41.)	250	(185.- 327.)	4000
t/y	2008	5.7	(3.6- 8.)	30	(24.- 37.)	36	(30.- 42.)	230	(185.- 274.)	4000
t/y	2009	6.6	(4.5- 8.)	30	(22.- 37.)	37	(29.- 44.)	230	(194.- 338.)	4000
t/y	2010	6.8	(5.2- 9.)	30	(21.- 37.)	37	(29.- 44.)	230	(191.- 372.)	2080
t/y	2011	5.9	(4.9- 7.)	26	(18.- 34.)	32	(23.- 40.)	380	(349.- 405.)	160

Table 23: Emission estimates for UK, IRE and NWEU with uncertainty (5th – 95th %ile).

5.2.4.2 PFC-116

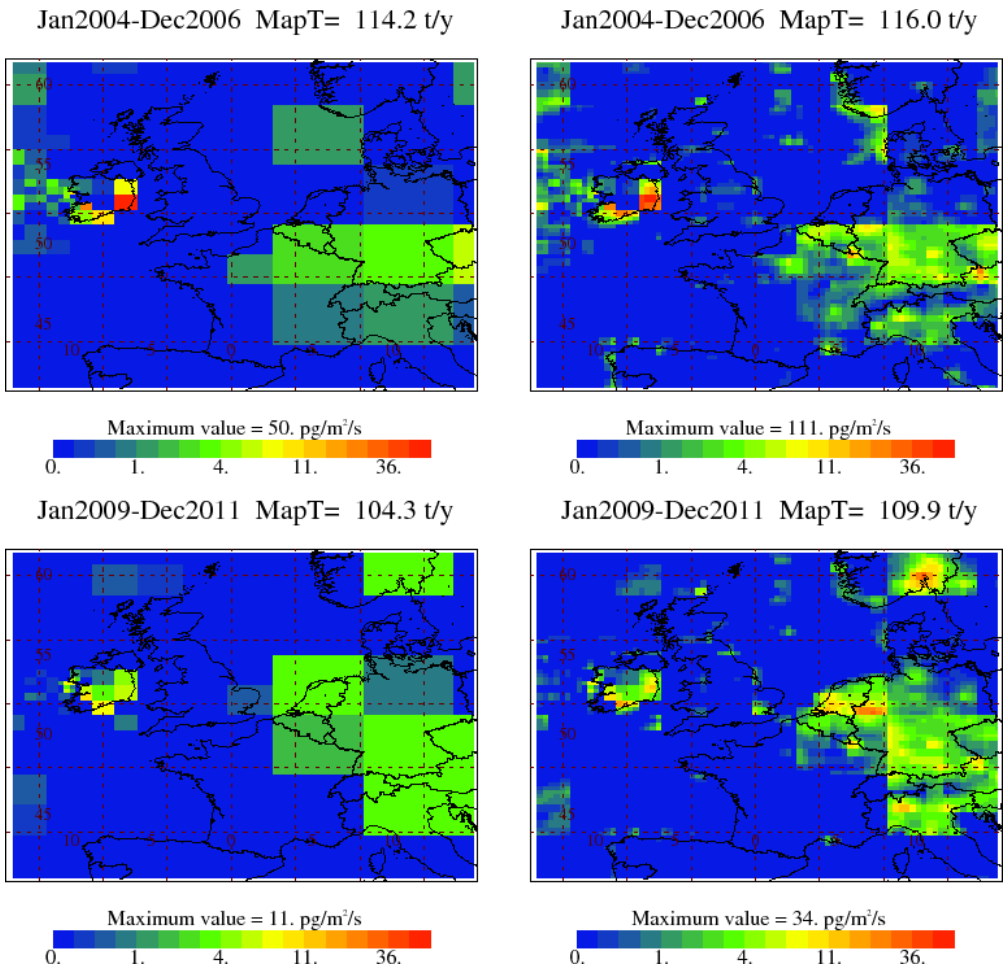

Figure 115: NAME-inversion emission estimates for 1990-92 (upper) and 2009-11 (lower). On the right hand side the emissions per grid box have been re-distributed based on population.

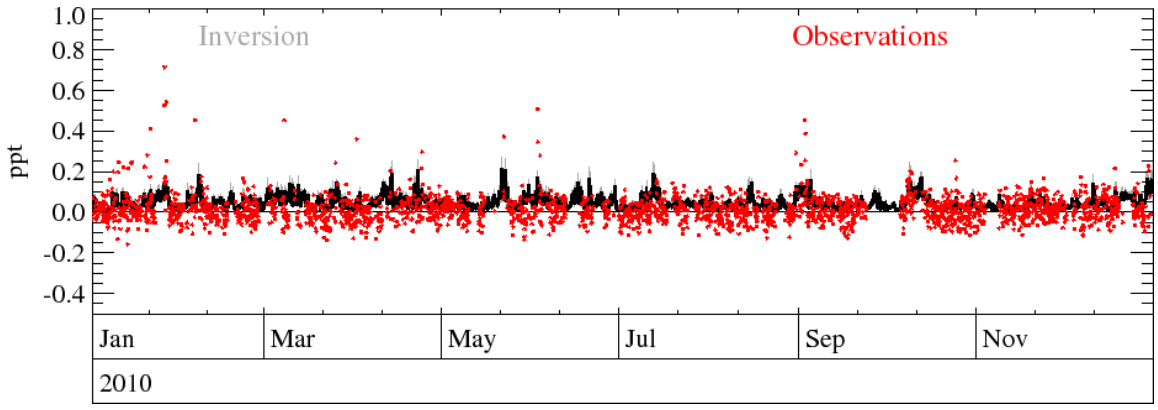

Figure 116: Example time-series of observations Vs. model using best-fit emission estimates.

Note the poor fit of the modelled time-series to the measured mass mixing ratios.

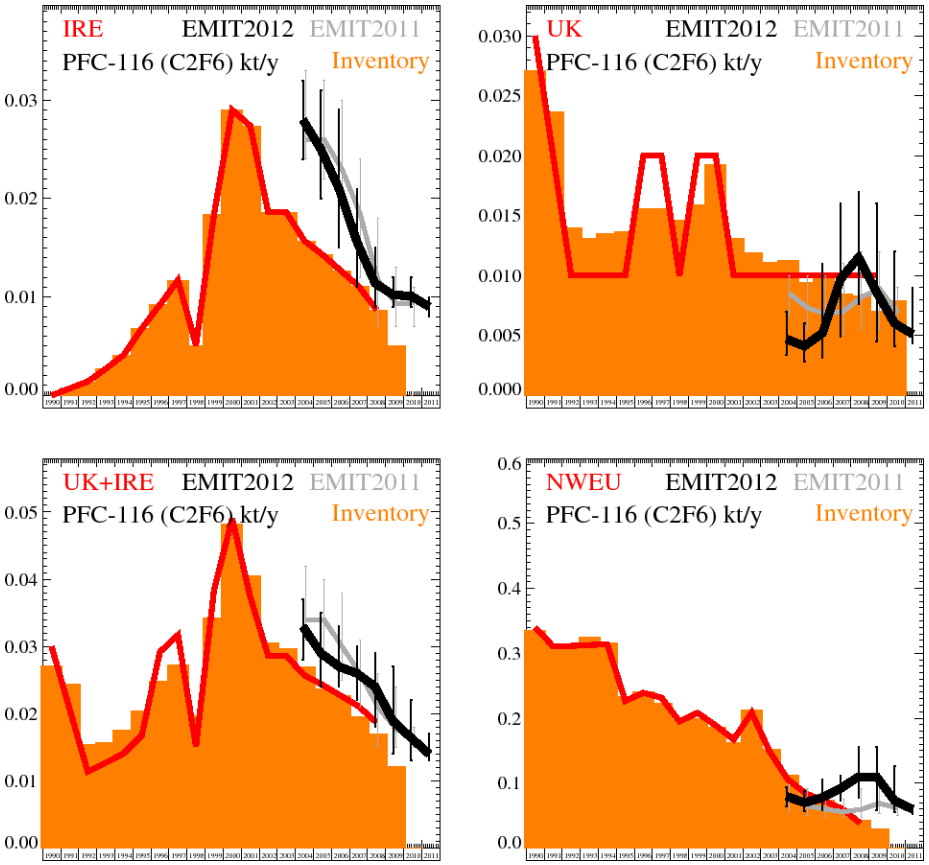

Figure 117: Inversion emission estimates for IRE, UK, IRE+UK and NWEU. Uncertainty bars represent the 5th and 95th percentiles. Orange bars represent UNFCCC emission estimates from the 2012 inventory. Grey (EMIT) and red (UNFCCC) are emissions as estimated last year.

Unit	Year	IRE	(5th-95th)	UK	(5th-95th)	UK+IRE	(5th-95th)	NWEU	(5th-95th)	Number
t/y	2004	28	(24.- 32.)	4.7	(3.4- 7.)	33	(28.- 37.)	80	(64.- 94.)	480
t/y	2005	25	(20.- 31.)	4.1	(2.8- 6.)	29	(24.- 35.)	70	(57.- 88.)	2400
t/y	2006	21	(15.- 29.)	5.2	(3.1- 11.)	27	(24.- 33.)	78	(59.- 105.)	4000
t/y	2007	15.6	(11.- 21.)	9.7	(4.9- 16.)	26	(22.- 30.)	92	(73.- 112.)	4000
t/y	2008	11.4	(9.- 15.)	11.5	(7.6- 17.)	24	(18.- 29.)	110	(78.- 156.)	4000
t/y	2009	10.2	(9.- 12.)	8.6	(4.5- 16.)	18.9	(14.- 27.)	110	(59.- 156.)	4000
t/y	2010	10.1	(9.- 12.)	6	(4.1- 12.)	16.4	(13.- 22.)	73	(56.- 126.)	2080
t/y	2011	9	(8.- 10.)	5.1	(4.3- 9.)	14	(13.- 17.)	60	(52.- 66.)	160

Table 24: Emission estimates for UK, IRE and NWEU with uncertainty (5th – 95th %ile).

5.2.4.3 PFC-218

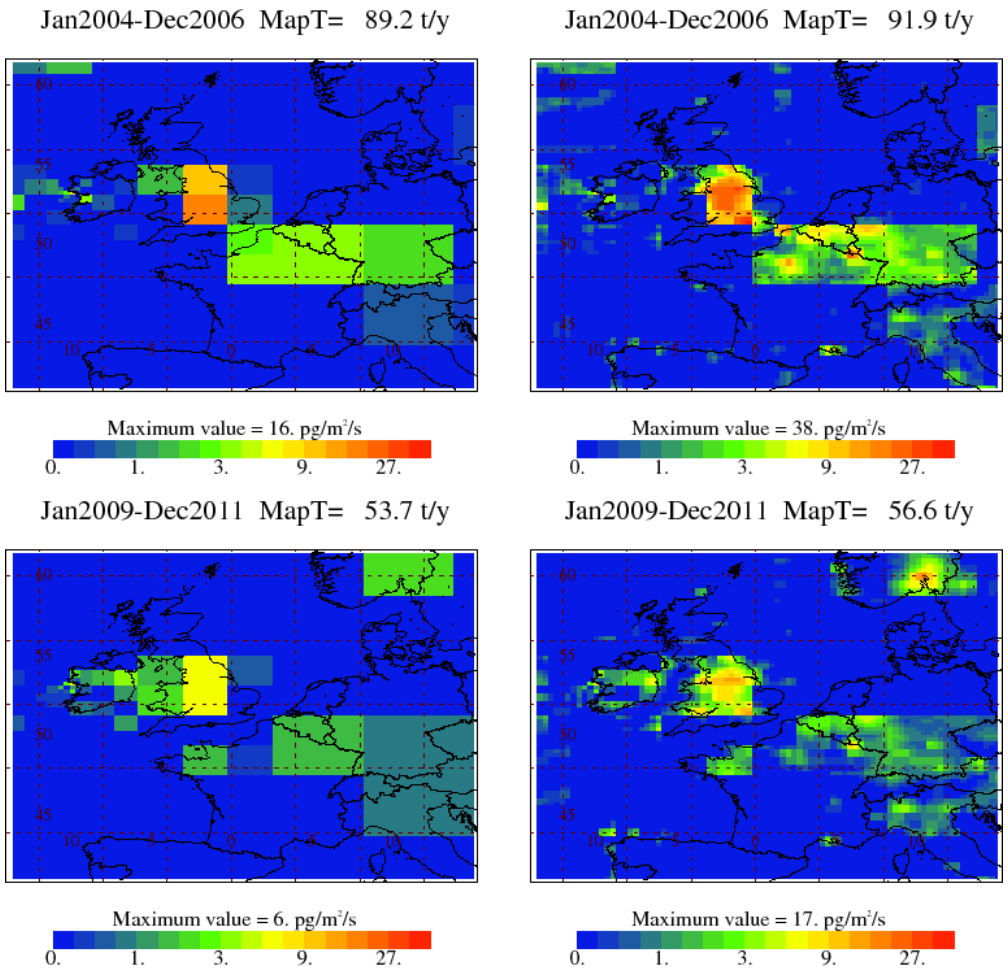

Figure 118: NAME-inversion emission estimates for 1990-92 (upper) and 2009-11 (lower). On the right hand side the emissions per grid box have been re-distributed based on population.

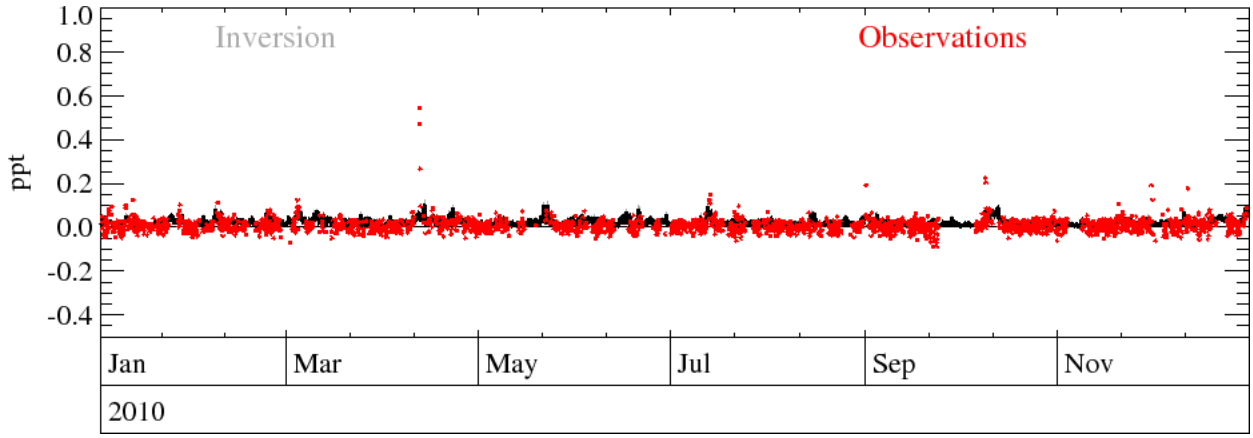

Figure 119: Example time-series of observations Vs. model using best-fit emission estimates.

Note the poor fit of the modelled time-series to the measured mass mixing ratios. The number of pollution events seen at Mace Head is low and these are not well resolved by the modelled emissions. The inversion results should therefore be treated with significant caution.

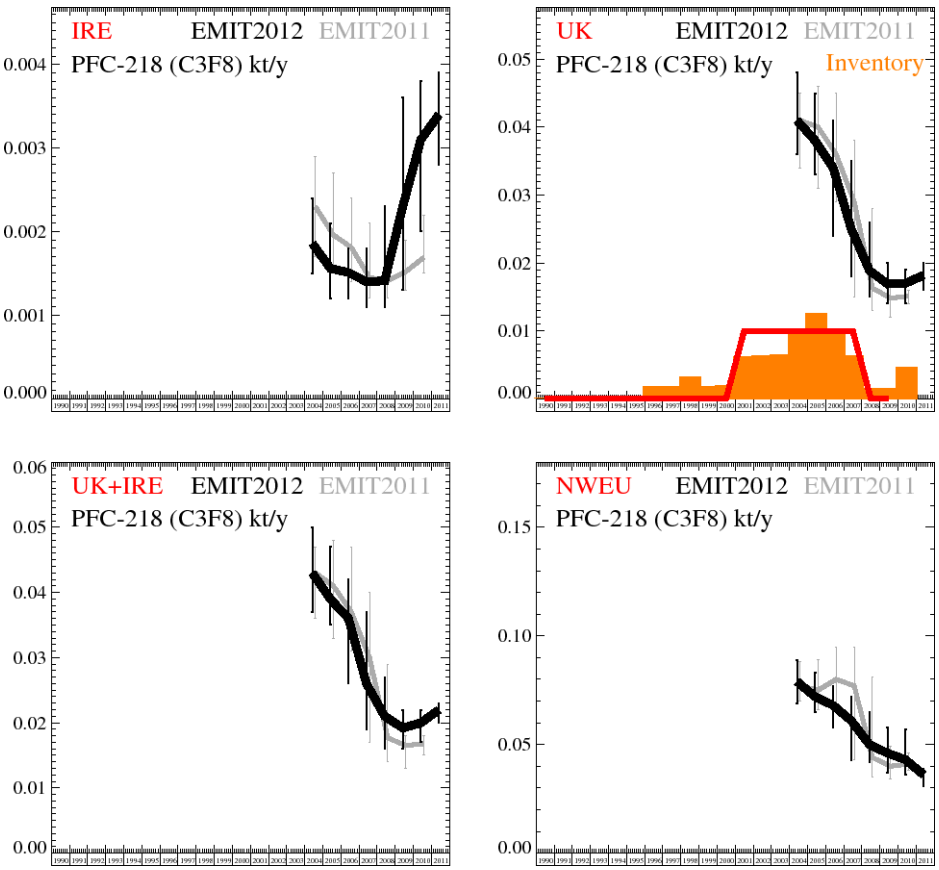

Figure 120: Inversion emission estimates for IRE, UK, IRE+UK and NWEU. Uncertainty bars represent the 5th and 95th percentiles. Orange bars represent UNFCCC emission estimates from the 2012 inventory. Grey (EMIT) and red (UNFCCC) are emissions as estimated last year.

Unit	Year	IRE	(5th-95th)	UK	(5th-95th)	UK+IRE	(5th-95th)	NWEU	(5th-95th)	Number
t/y	2004	1.86	(1.5- 2.4)	41	(36.- 48.)	43	(37.- 50.)	79	(69.- 89.)	480
t/y	2005	1.56	(1.2- 2.1)	38	(33.- 45.)	39	(35.- 47.)	72	(65.- 83.)	2400
t/y	2006	1.51	(1.2- 1.8)	34	(24.- 41.)	36	(26.- 42.)	68	(58.- 77.)	4000
t/y	2007	1.4	(1.1- 1.8)	25	(18.- 35.)	26	(19.- 37.)	61	(43.- 72.)	4000
t/y	2008	1.41	(1.1- 2.3)	18.9	(15.- 26.)	21	(16.- 27.)	50	(42.- 65.)	4000
t/y	2009	2.3	(1.3- 3.6)	16.9	(14.- 20.)	19.2	(16.- 22.)	46	(37.- 58.)	4000
t/y	2010	3.1	(2.0- 3.8)	17	(14.- 19.)	20	(17.- 22.)	43	(36.- 57.)	2080
t/y	2011	3.4	(2.8- 3.9)	18.2	(16.- 20.)	22	(20.- 23.)	36	(31.- 39.)	160

Table 25: Emission estimates for UK, IRE and NWEU with uncertainty (5th – 95th %ile).

5.2.4.4 SF_6

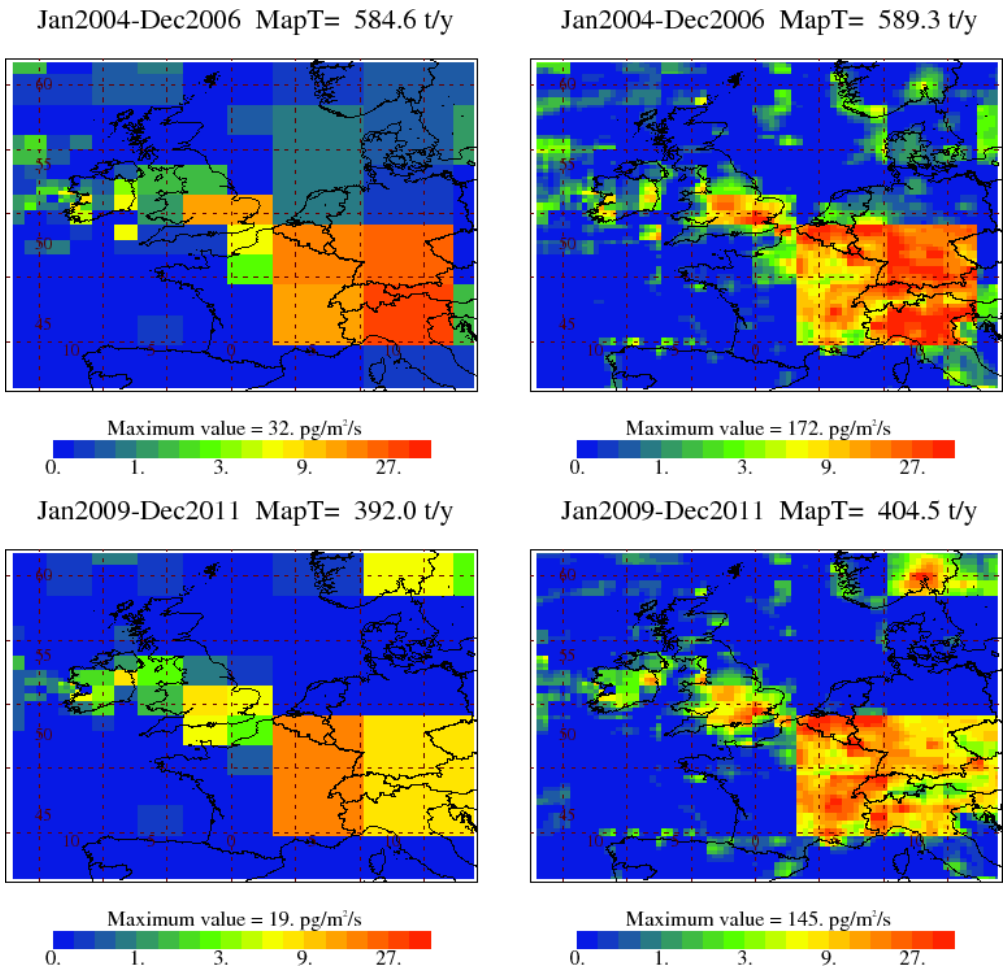

Figure 121: NAME-inversion emission estimates for 1990-92 (upper) and 2009-11 (lower). On the right hand side the emissions per grid box have been re-distributed based on population.

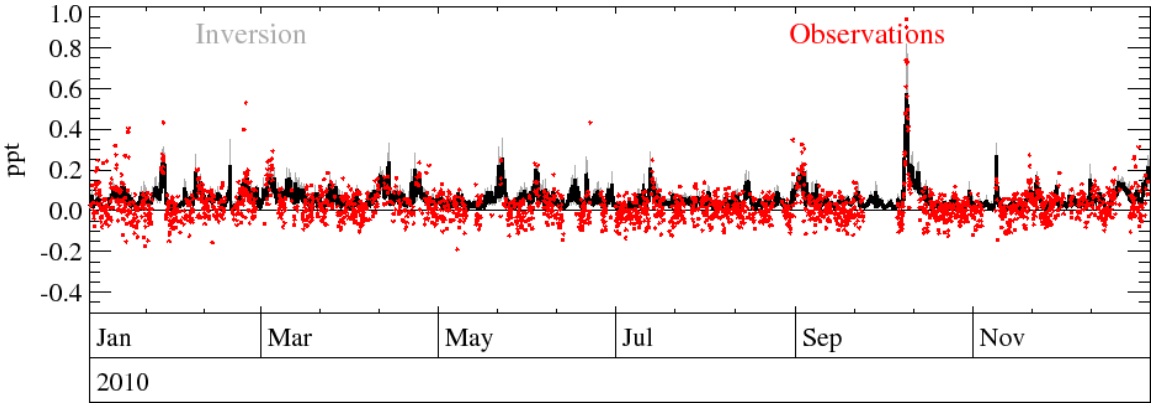

Figure 122: Example time-series of observations Vs. model using best-fit emission estimates.

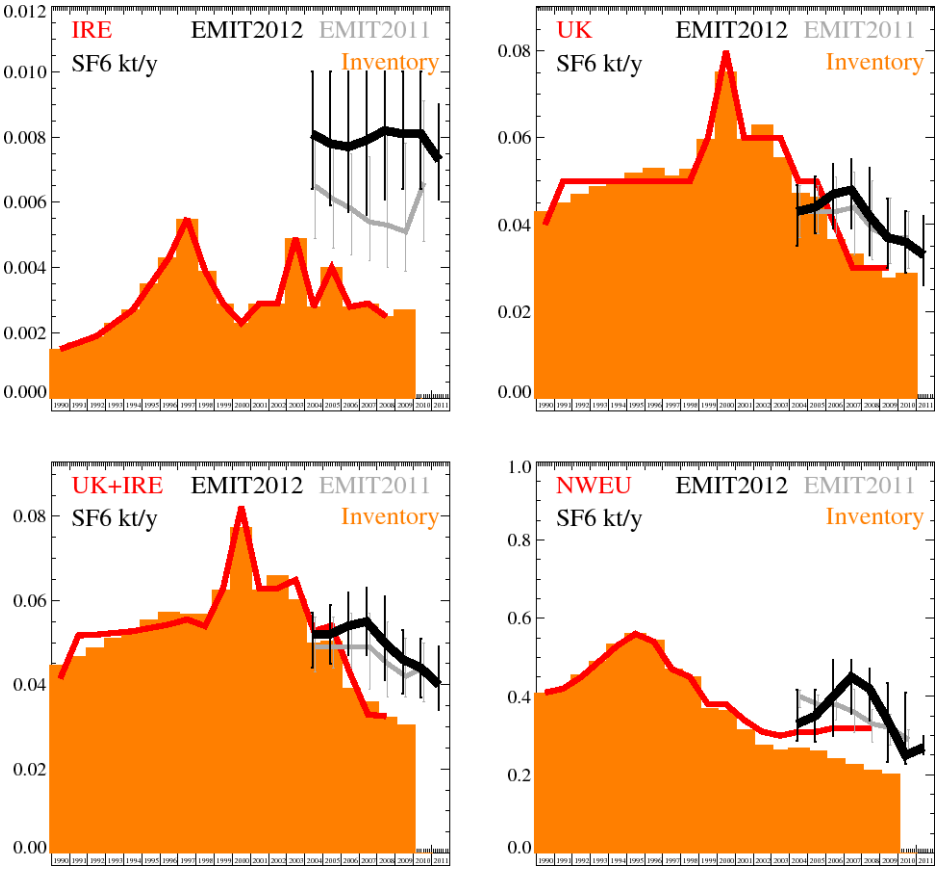

Figure 123: Inversion emission estimates for IRE, UK, IRE+UK and NWEU. Uncertainty bars represent the 5th and 95th percentiles. Orange bars represent UNFCCC emission estimates from the 2012 inventory. Grey (EMIT) and red (UNFCCC) are emissions as estimated last year.

Unit	Year	IRE	(5th-95th)	UK	(5th-95th)	UK+IRE	(5th-95th)	NWEU	(5th-95th)	Number
t/y	2004	8.1	(6.4- 10.)	43	(35.- 49.)	52	(44.- 57.)	330	(286.- 418.)	480
t/y	2005	7.8	(5.9- 10.)	44	(38.- 51.)	52	(45.- 59.)	350	(285.- 418.)	2400
t/y	2006	7.7	(5.7- 10.)	47	(39.- 54.)	54	(47.- 62.)	400	(298.- 493.)	4000
t/y	2007	7.9	(5.6- 10.)	48	(39.- 55.)	55	(47.- 63.)	450	(355.- 494.)	4000
t/y	2008	8.2	(6.1- 10.)	42	(33.- 53.)	50	(41.- 61.)	420	(339.- 471.)	4000
t/y	2009	8.1	(6.4- 10.)	37	(30.- 46.)	46	(38.- 53.)	340	(234.- 434.)	4000
t/y	2010	8.1	(6.4- 10.)	36	(29.- 43.)	44	(37.- 51.)	250	(229.- 409.)	2080
t/y	2011	7.3	(6.1- 9.)	33	(26.- 42.)	40	(34.- 49.)	270	(253.- 298.)	160

Table 26: Emission estimates for UK, IRE and NWEU with uncertainty (5th – 95th %ile).

5.2.5 Chlorine compounds

5.2.5.1 CH_3Cl (methyl chloride)

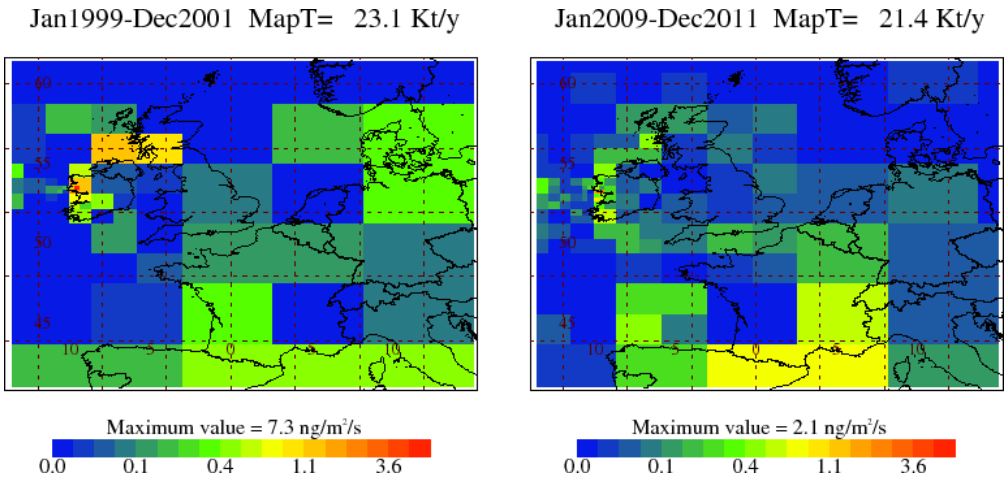

Figure 124: NAME-inversion emission estimates for 1990-92 (left) and 2009-11 (right).

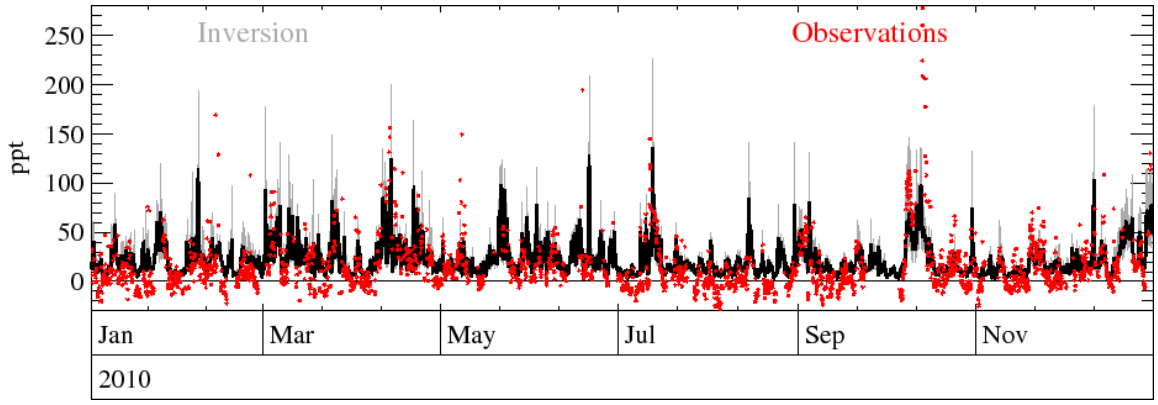

Figure 125: Example time-series of observations Vs. model using best-fit emission estimates.

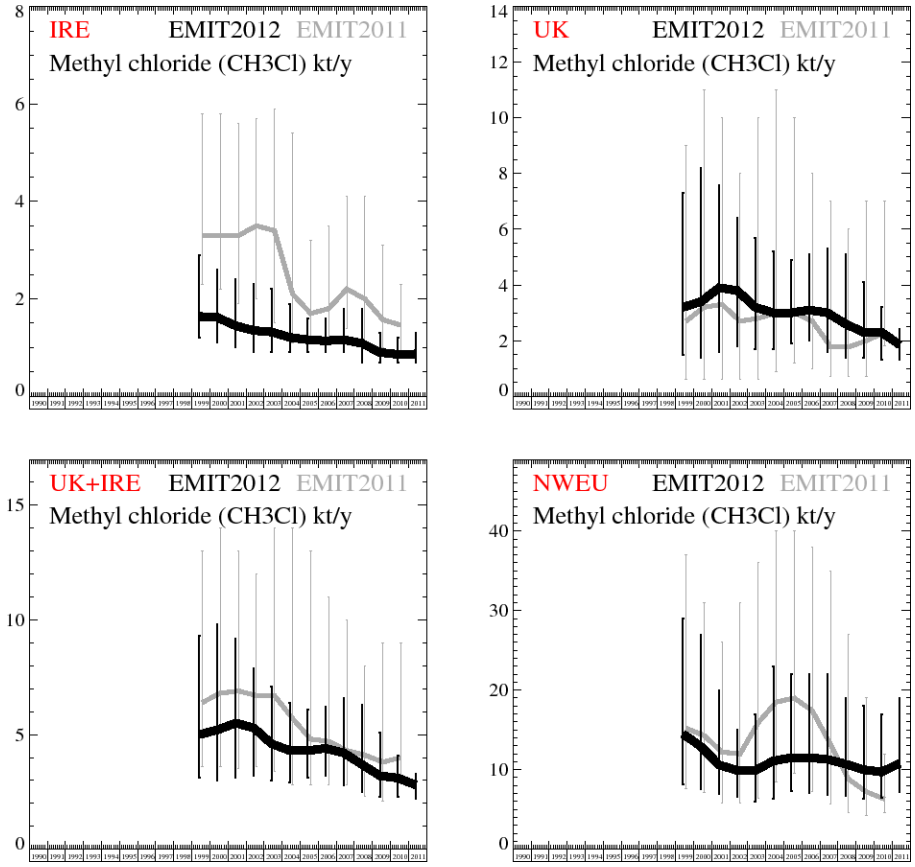

Figure 126: Emission estimates for IRE, UK, IRE+UK and NWEU. The uncertainty bars represent the 5th and 95th percentiles. Grey emissions are estimates from last year.

Unit	Year	IRE	(5th-95th)	UK	(5th-95th)	UK+IRE	(5th-95th)	NWEU	(5th-95th)	Number
kt/y	1999	1.64	(1.2- 2.9)	3.2	(1.5- 7.3)	5	(3.1- 9.3)	14.5	(8.1- 29.)	1920
kt/y	2000	1.62	(1.1- 2.6)	3.4	(1.4- 8.2)	5.2	(3.0- 9.8)	12.9	(7.6- 27.)	3840
kt/y	2001	1.45	(1.0- 2.4)	3.9	(1.6- 7.6)	5.5	(3.1- 9.2)	10.6	(6.9- 20.)	4000
kt/y	2002	1.35	(0.9- 2.3)	3.8	(1.8- 6.4)	5.3	(3.2- 7.9)	9.9	(6.6- 15.)	4000
kt/y	2003	1.32	(0.9- 2.2)	3.2	(1.7- 5.7)	4.6	(3.0- 7.1)	9.9	(6.0- 17.)	4000
kt/y	2004	1.21	(0.9- 1.9)	3	(1.7- 5.2)	4.3	(2.9- 6.4)	11.1	(6.4- 23.)	4000
kt/y	2005	1.16	(0.9- 1.6)	3	(1.9- 4.9)	4.3	(3.1- 6.1)	11.5	(7.3- 22.)	4000
kt/y	2006	1.14	(0.9- 1.6)	3.1	(2.0- 5.1)	4.4	(3.2- 6.2)	11.5	(7.1- 22.)	4000
kt/y	2007	1.16	(0.9- 1.8)	3	(1.6- 5.3)	4.2	(2.8- 6.6)	11.3	(6.8- 22.)	4000
kt/y	2008	1.09	(0.7- 1.8)	2.6	(1.4- 5.1)	3.7	(2.5- 6.3)	10.7	(6.7- 19.)	4000
kt/y	2009	0.9	(0.7- 1.3)	2.3	(1.4- 4.1)	3.2	(2.3- 5.1)	10	(6.4- 18.)	4000
kt/y	2010	0.86	(0.7- 1.2)	2.3	(1.3- 3.2)	3.1	(2.3- 4.1)	9.7	(6.5- 17.)	2080
kt/y	2011	0.87	(0.7- 1.3)	1.85	(1.3- 2.4)	2.8	(2.2- 3.3)	10.8	(7.2- 19.)	160

Table 27: Emission estimates for UK, IRE and NWEU with uncertainty (5th – 95th %ile).

5.2.5.2 CH_2Cl_2 (methylene dichloride)

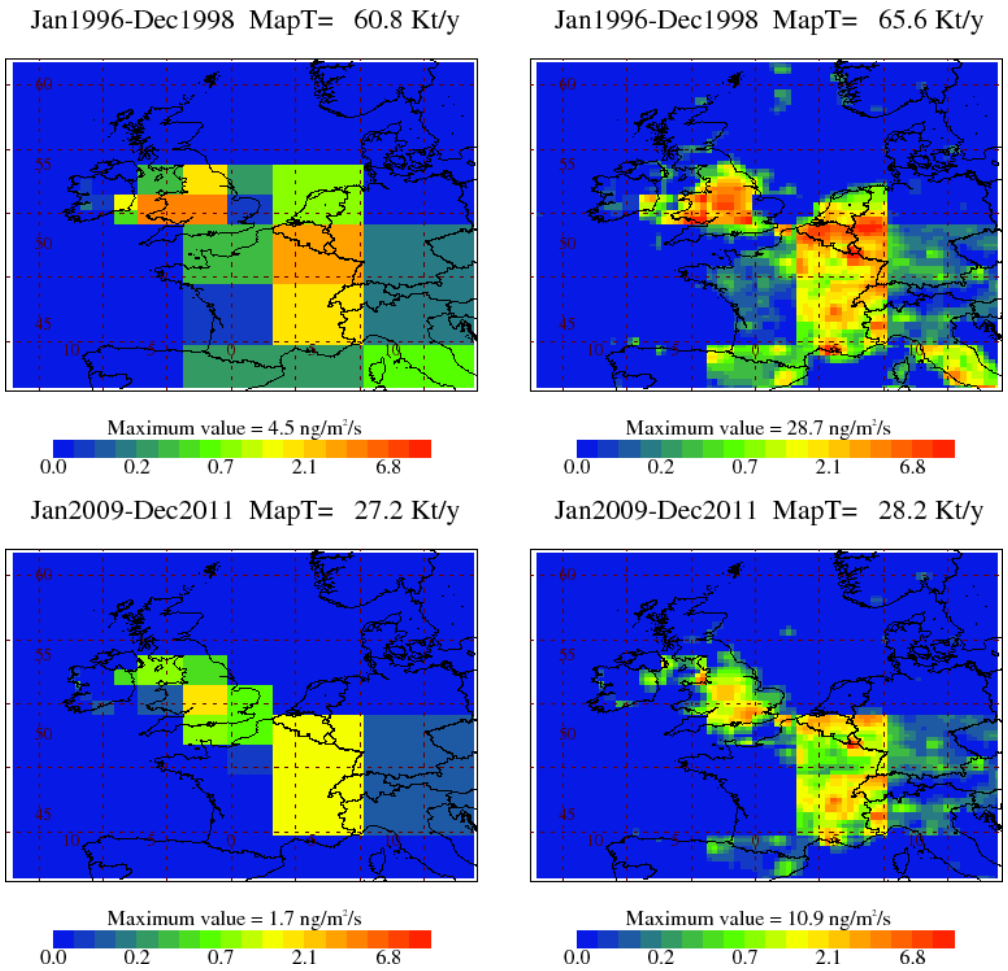

Figure 127: NAME-inversion emission estimates for 1990-92 (upper) and 2009-11 (lower). On the right hand side the emissions per grid box have been re-distributed based on population.

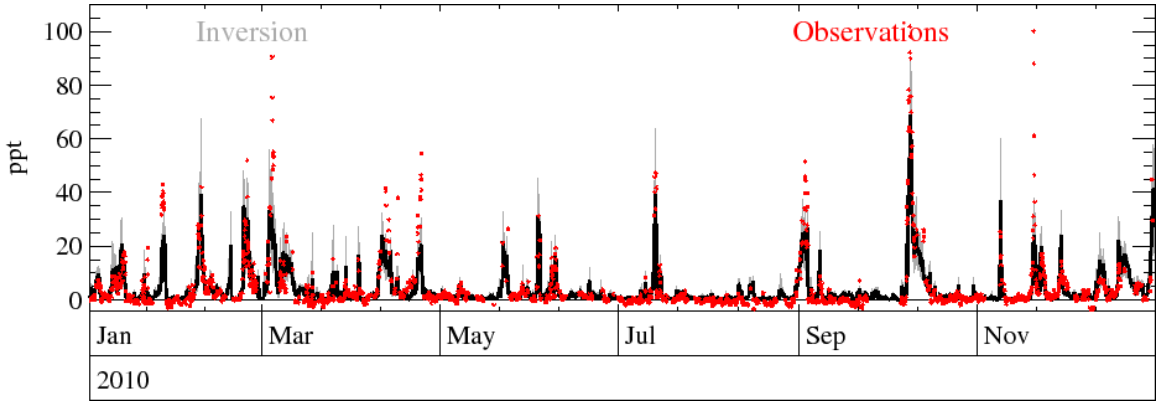

Figure 128: Example time-series of observations Vs. model using best-fit emission estimates.

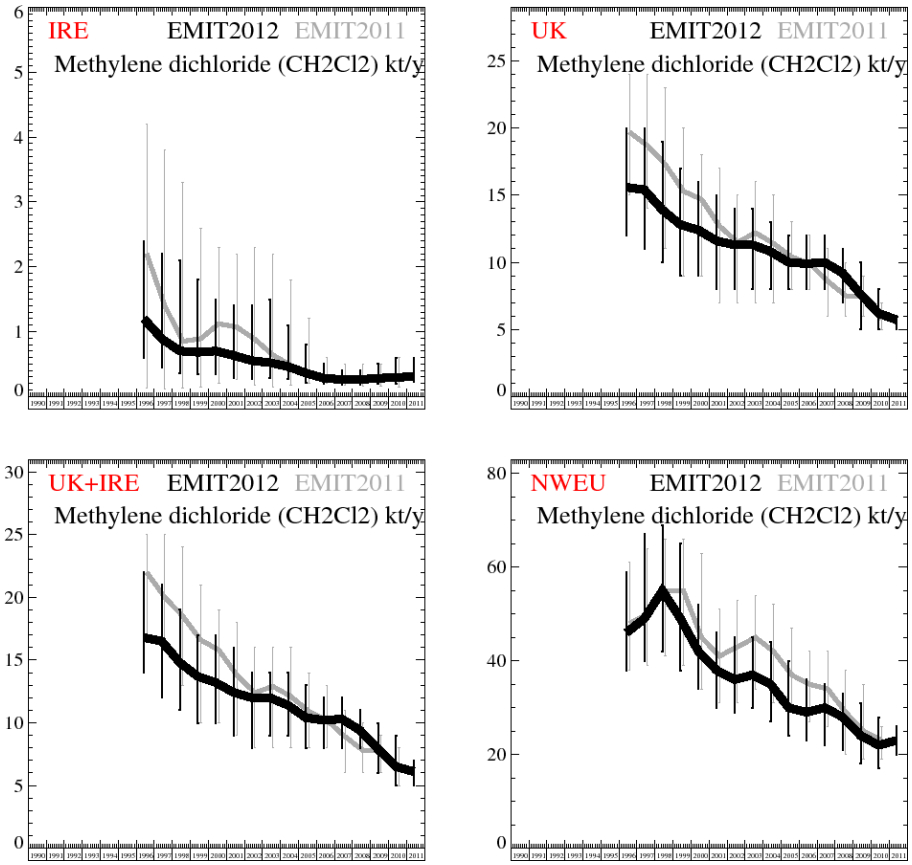

Figure 129: Emission estimates for IRE, UK, IRE+UK and NWEU. The uncertainty bars represent the 5th and 95th percentiles. Grey emissions are estimates from last year.

Unit	Year	IRE	(5th-95th)	UK	(5th-95th)	UK+IRE	(5th-95th)	NWEU	(5th-95th)	Number
kt/y	1996	1.2	(0.59- 2.4)	15.6	(12.- 20.)	16.8	(14.- 22.)	46	(38.- 59.)	1600
kt/y	1997	0.89	(0.45- 2.2)	15.4	(11.- 20.)	16.5	(12.- 21.)	49	(40.- 67.)	3520
kt/y	1998	0.7	(0.35- 2.1)	13.9	(10.- 19.)	14.8	(11.- 19.)	55	(42.- 69.)	4000
kt/y	1999	0.68	(0.34- 1.8)	12.8	(9.- 17.)	13.7	(10.- 17.)	49	(38.- 65.)	4000
kt/y	2000	0.7	(0.34- 1.5)	12.4	(9.- 16.)	13.2	(10.- 17.)	42	(34.- 52.)	4000
kt/y	2001	0.63	(0.29- 1.4)	11.6	(8.- 15.)	12.4	(9.- 16.)	38	(30.- 46.)	4000
kt/y	2002	0.55	(0.27- 1.4)	11.3	(8.- 14.)	12	(8.- 14.)	36	(29.- 45.)	4000
kt/y	2003	0.52	(0.28- 1.5)	11.3	(8.- 14.)	12	(9.- 14.)	37	(30.- 45.)	4000
kt/y	2004	0.46	(0.27- 1.1)	10.8	(8.- 13.)	11.4	(9.- 14.)	35	(27.- 44.)	4000
kt/y	2005	0.36	(0.21- 0.8)	10	(8.- 12.)	10.4	(8.- 13.)	30	(24.- 40.)	4000
kt/y	2006	0.28	(0.19- 0.5)	9.9	(8.- 12.)	10.2	(8.- 12.)	29	(23.- 36.)	4000
kt/y	2007	0.26	(0.18- 0.4)	10	(8.- 12.)	10.3	(8.- 12.)	30	(22.- 35.)	4000
kt/y	2008	0.26	(0.18- 0.4)	9.2	(7.- 11.)	9.4	(8.- 11.)	28	(21.- 33.)	4000
kt/y	2009	0.28	(0.19- 0.5)	7.6	(5.- 10.)	7.9	(6.- 10.)	24	(18.- 31.)	4000
kt/y	2010	0.29	(0.19- 0.6)	6.2	(5.- 8.)	6.5	(5.- 9.)	22	(17.- 28.)	2080
kt/y	2011	0.31	(0.23- 0.6)	5.7	(5.- 6.)	6.1	(5.- 7.)	23	(20.- 26.)	160

Table 28: Emission estimates for UK, IRE and NWEU with uncertainty (5th – 95th %ile).

5.2.5.3 Chloroform

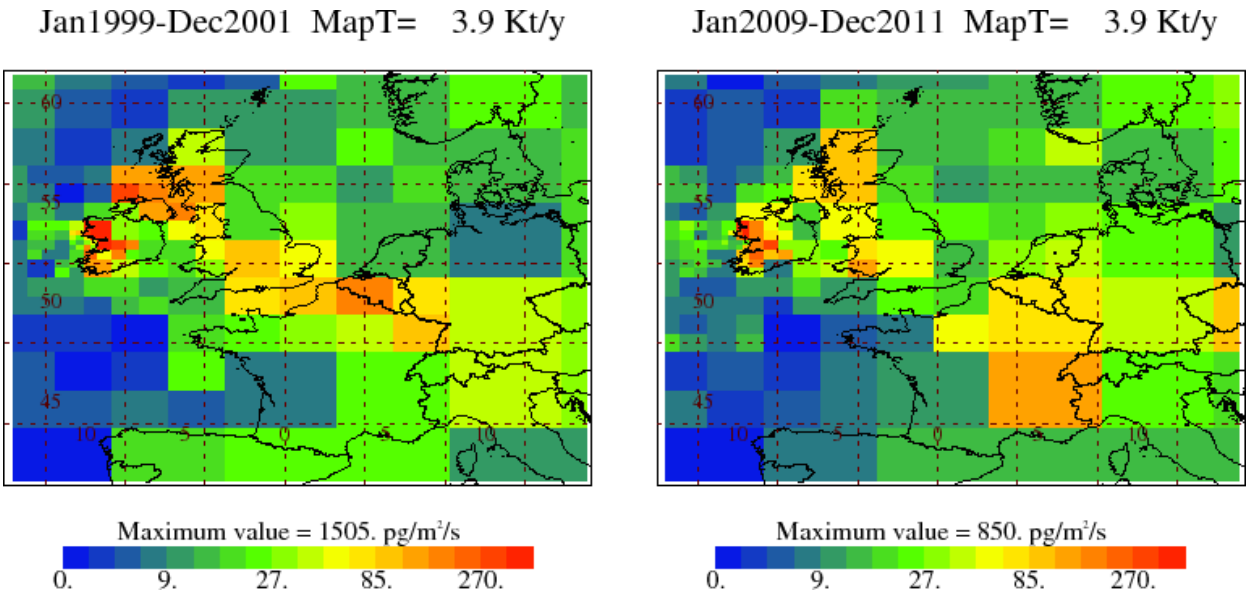

Figure 130: NAME-inversion emission estimates for 1999-2001 (left) and 2009-11 (right).

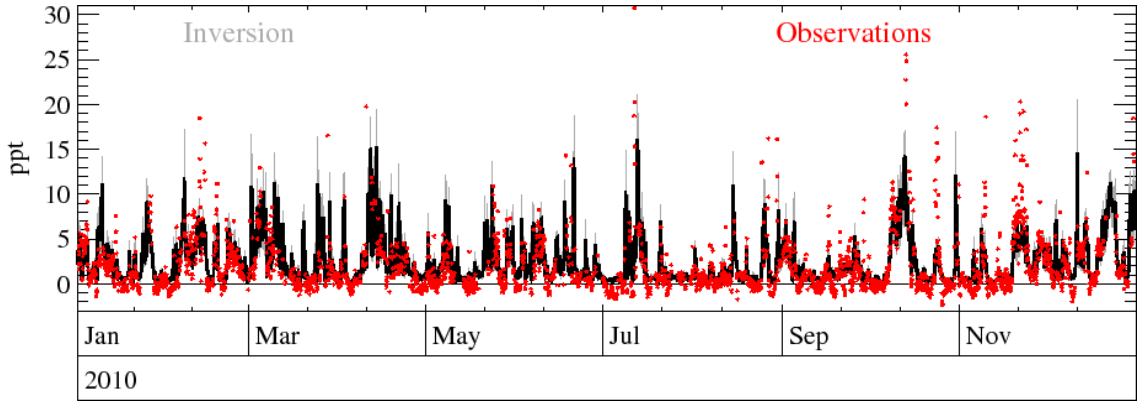

Figure 131: Example time-series of observations Vs. model using best-fit emission estimates.

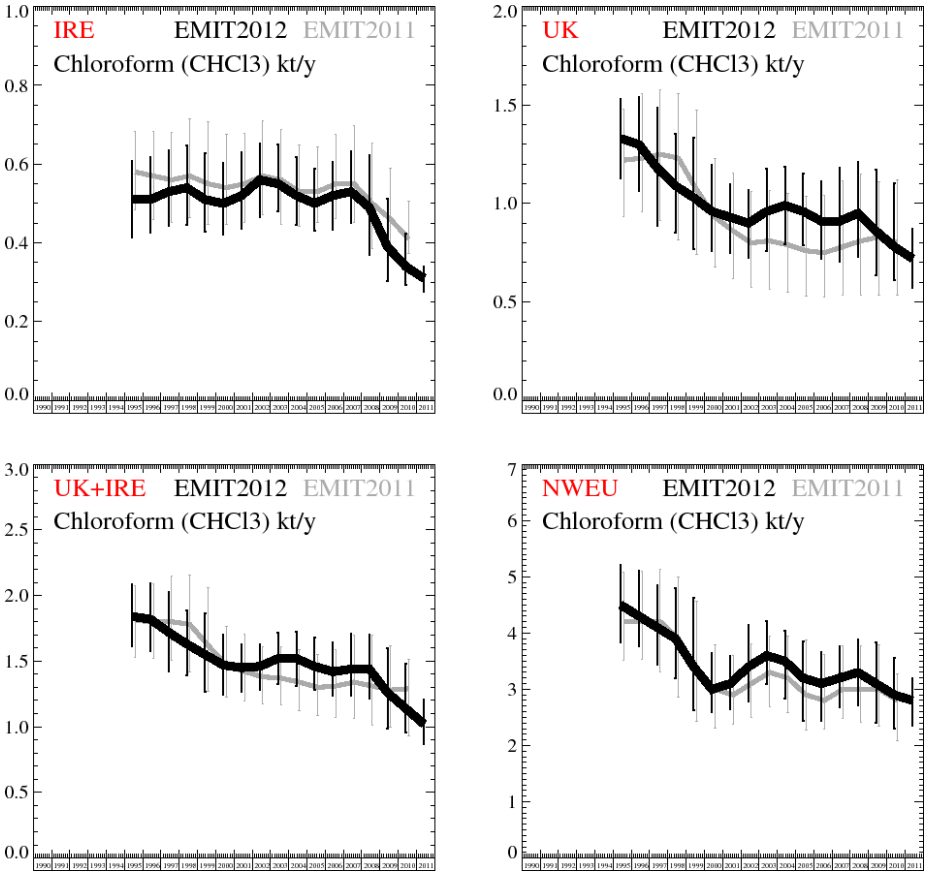

Figure 132: Emission estimates for IRE, UK, IRE+UK and NWEU. The uncertainty bars represent the 5th and 95th percentiles. Grey emissions are estimates from last year.

Unit	Year	IRE	(5th-95th)	UK	(5th-95th)	UK+IRE	(5th-95th)	NWEU	(5th-95th)	Number
t/y	1995	510	(413.- 608.)	1330	(1127.-1531.)	1840	(1612.-2087.)	4500	(3841.-5219.)	1920
t/y	1996	510	(425.- 617.)	1300	(1064.-1541.)	1820	(1576.-2095.)	4300	(3757.-5114.)	3840
t/y	1997	530	(444.- 636.)	1180	(888.-1484.)	1720	(1423.-2030.)	4100	(3436.-4849.)	4000
t/y	1998	540	(445.- 647.)	1090	(854.-1352.)	1630	(1389.-1885.)	3900	(3191.-4792.)	4000
t/y	1999	510	(429.- 627.)	1030	(770.-1332.)	1550	(1269.-1863.)	3400	(2630.-4631.)	4000
t/y	2000	500	(420.- 602.)	960	(757.-1194.)	1470	(1247.-1701.)	3000	(2597.-3645.)	4000
t/y	2001	520	(437.- 629.)	930	(747.-1098.)	1450	(1265.-1625.)	3100	(2649.-3601.)	4000
t/y	2002	560	(465.- 652.)	900	(725.-1070.)	1460	(1283.-1629.)	3400	(2787.-4136.)	4000
t/y	2003	550	(480.- 651.)	960	(759.-1179.)	1520	(1323.-1716.)	3600	(3091.-4205.)	4000
t/y	2004	520	(446.- 619.)	990	(795.-1188.)	1520	(1310.-1721.)	3500	(2832.-4035.)	4000
t/y	2005	500	(430.- 588.)	960	(786.-1154.)	1460	(1280.-1681.)	3200	(2441.-3846.)	4000
t/y	2006	520	(433.- 606.)	910	(719.-1114.)	1420	(1239.-1641.)	3100	(2441.-3657.)	4000
t/y	2007	530	(451.- 633.)	910	(704.-1181.)	1440	(1238.-1710.)	3200	(2679.-3763.)	4000
t/y	2008	490	(369.- 623.)	950	(731.-1209.)	1440	(1218.-1703.)	3300	(2717.-3883.)	4000
t/y	2009	390	(303.- 511.)	860	(637.-1171.)	1260	(988.-1601.)	3100	(2412.-3840.)	4000
t/y	2010	340	(294.- 424.)	780	(613.-1101.)	1140	(954.-1479.)	2900	(2295.-3552.)	2080
t/y	2011	310	(275.- 341.)	720	(573.- 873.)	1020	(867.-1210.)	2800	(2357.-3204.)	160

Table 29: Emission estimates for UK, IRE and NWEU with uncertainty (5th – 95th %ile).

5.2.5.4 Methyl chloroform

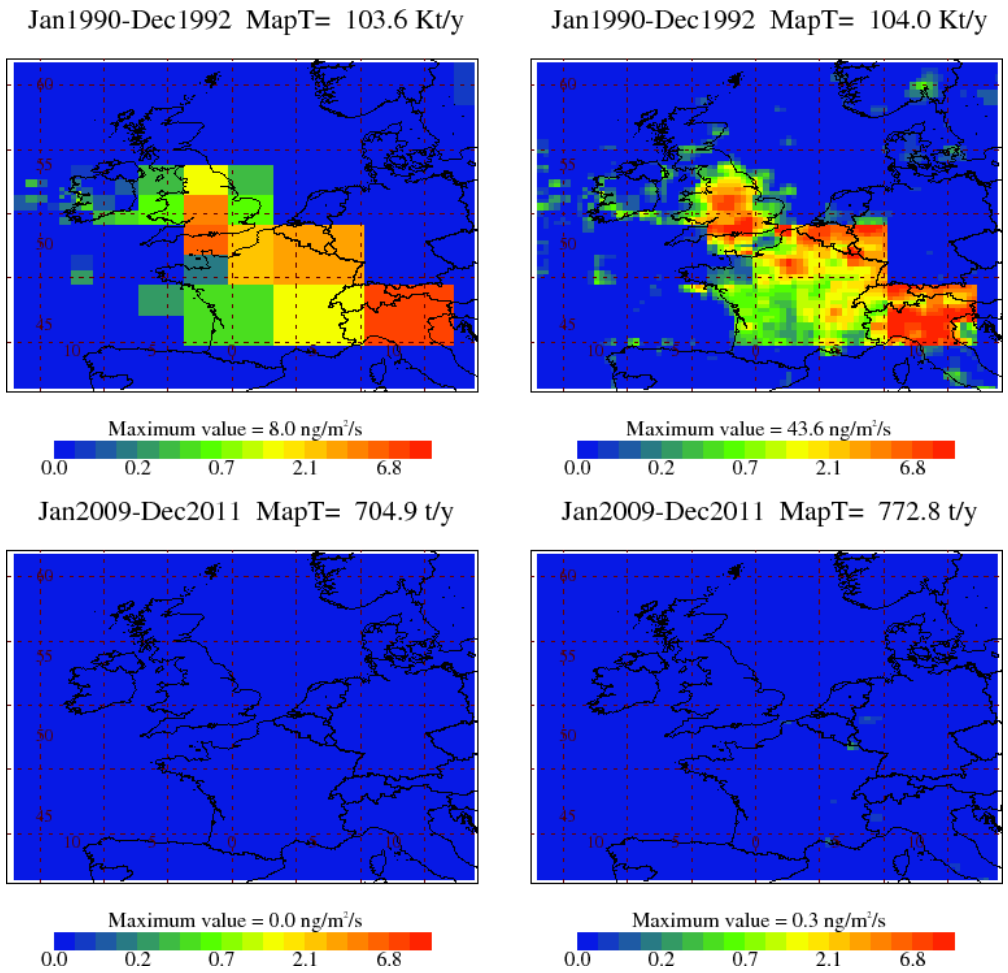

Figure 133: NAME-inversion emission estimates for 1990-92 (upper) and 2009-11 (lower). On the right hand side the emissions per grid box have been re-distributed based on population.

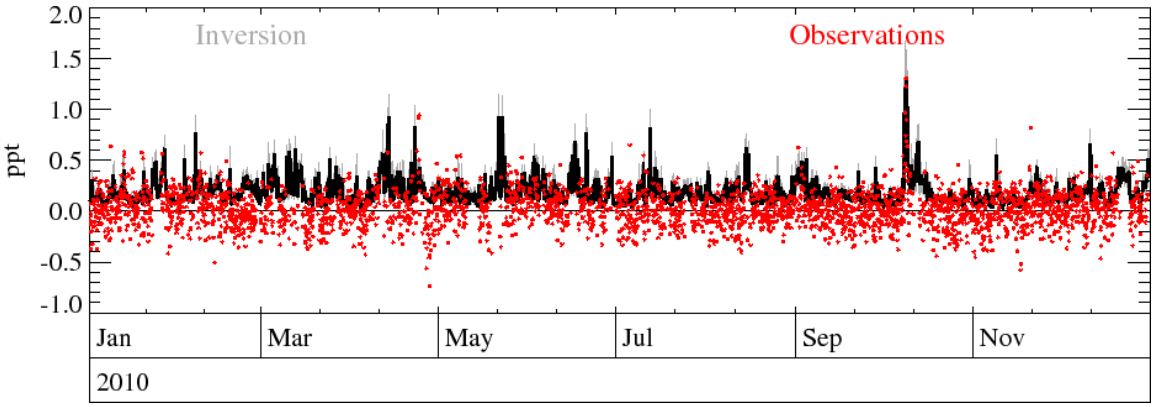

Figure 134: Example time-series of observations Vs. model using best-fit emission estimates.

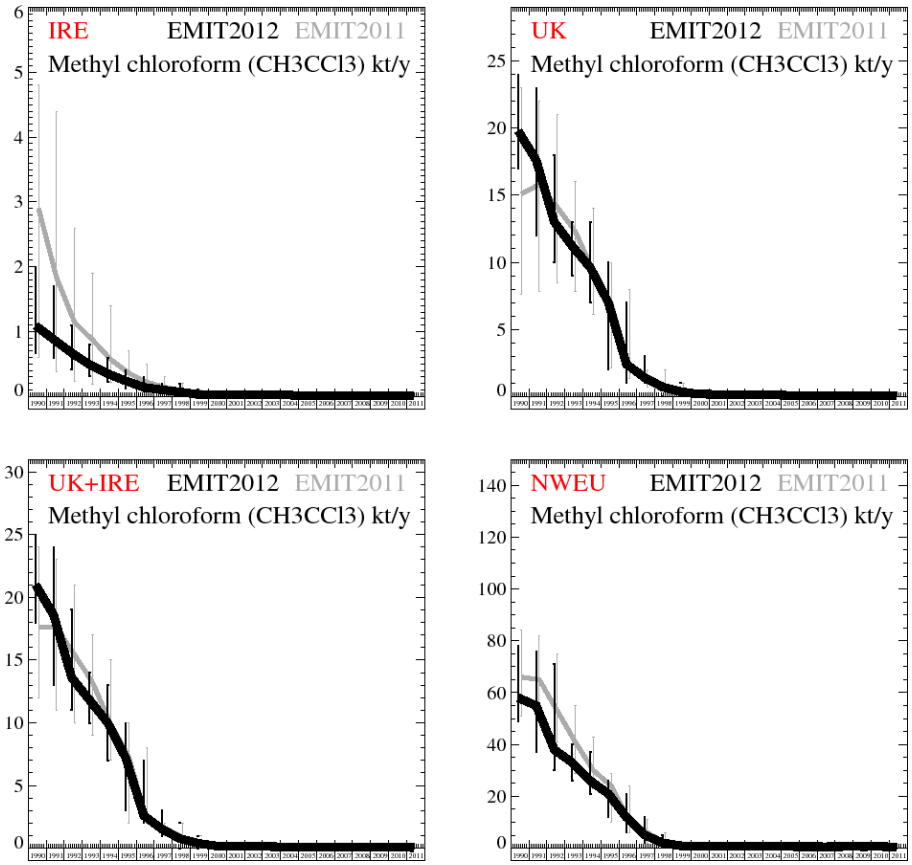

Figure 135: Emission estimates for IRE, UK, IRE+UK and NWEU. The uncertainty bars represent the 5th and 95th percentiles. Grey emissions are estimates from last year.

Unit	Year	IRE	(5th-95th)	UK	(5th-95th)	UK+IRE	(5th-95th)	NWEU	(5th-95th)	Number
kt/y	1990	1.09	(0.66- 2.0)	19.8	(17.- 24.)	21	(18.- 25.)	58	(49.- 78.)	1920
kt/y	1991	0.88	(0.59- 1.7)	17.6	(12.- 23.)	18.6	(13.- 24.)	55	(37.- 76.)	3840
kt/y	1992	0.67	(0.41- 1.1)	13	(10.- 18.)	13.6	(11.- 19.)	38	(30.- 71.)	4000
kt/y	1993	0.49	(0.32- 0.8)	11.2	(9.- 13.)	11.8	(10.- 14.)	33	(26.- 40.)	4000
kt/y	1994	0.35	(0.22- 0.6)	9.6	(7.- 13.)	10	(7.- 13.)	26	(21.- 37.)	4000
kt/y	1995	0.24	(0.12- 0.4)	7	(2.- 10.)	7.2	(3.- 10.)	21	(12.- 26.)	4000
kt/y	1996	0.14	(0.08- 0.3)	2.4	(1.- 7.)	2.6	(2.- 7.)	11.9	(6.- 21.)	4000
kt/y	1997	0.1	(0.07- 0.2)	1.41	(1.- 3.)	1.54	(1.- 3.)	5.1	(2.- 12.)	4000
kt/y	1998	0.07	(0.03- 0.2)	0.7	(0.- 1.)	0.76	(0.- 2.)	2.1	(1.- 5.)	4000
kt/y	1999	0.03	(0.02- 0.1)	0.36	(0.- 1.)	0.4	(0.- 1.)	0.96	(1.- 2.)	4000
kt/y	2000	0.02	(0.0- 0.0)	0.17	(0.- 0.)	0.19	(0.- 0.)	0.84	(1.- 1.)	4000
kt/y	2001	0.02	(0.0- 0.0)	0.15	(0.- 0.)	0.17	(0.- 0.)	0.83	(1.- 1.)	4000
kt/y	2002	0.02	(0.0- 0.0)	0.13	(0.- 0.)	0.15	(0.- 0.)	0.78	(1.- 1.)	4000
kt/y	2003	0.02	(0.0- 0.0)	0.11	(0.- 0.)	0.13	(0.- 0.)	0.72	(1.- 1.)	4000
kt/y	2004	0.02	(0.0- 0.0)	0.1	(0.- 0.)	0.11	(0.- 0.)	0.67	(0.- 1.)	4000
kt/y	2005	0.01	(0.0- 0.0)	0.08	(0.- 0.)	0.1	(0.- 0.)	0.64	(0.- 1.)	4000
kt/y	2006	0.01	(0.0- 0.0)	0.08	(0.- 0.)	0.09	(0.- 0.)	0.6	(0.- 1.)	4000
kt/y	2007	0.01	(0.0- 0.0)	0.08	(0.- 0.)	0.09	(0.- 0.)	0.59	(0.- 1.)	4000
kt/y	2008	0.01	(0.0- 0.0)	0.08	(0.- 0.)	0.09	(0.- 0.)	0.6	(0.- 1.)	4000
kt/y	2009	0.01	(0.0- 0.0)	0.07	(0.- 0.)	0.08	(0.- 0.)	0.61	(0.- 1.)	4000
kt/y	2010	0.01	(0.0- 0.0)	0.06	(0.- 0.)	0.07	(0.- 0.)	0.66	(0.- 1.)	2080
kt/y	2011	0.01	(0.0- 0.0)	0.05	(0.- 0.)	0.05	(0.- 0.)	0.53	(0.- 1.)	160

Table 30: Emission estimates for UK, IRE and NWEU with uncertainty (5th – 95th %ile).

5.2.5.5 Carbon tetrachloride

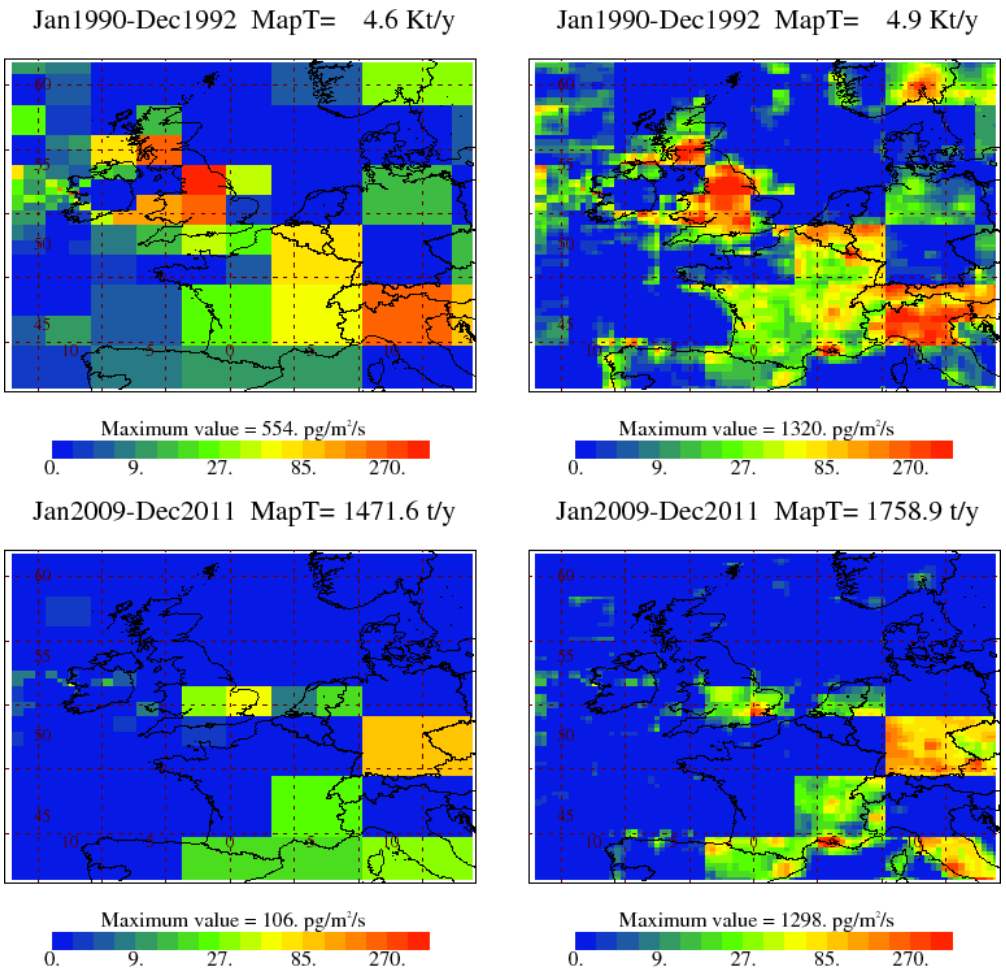

Figure 136: NAME-inversion emission estimates for 1990-92 (upper) and 2009-11 (lower). On the right hand side the emissions per grid box have been re-distributed based on population.

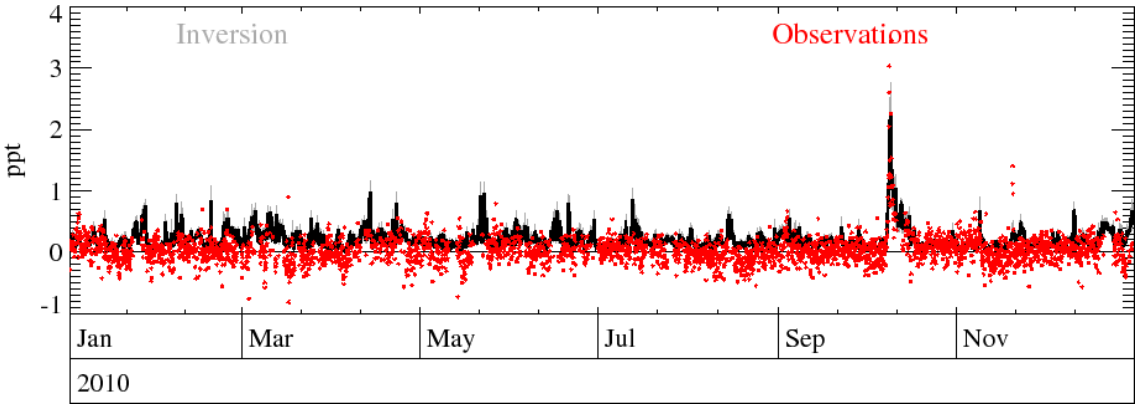

Figure 137: Example time-series of observations Vs. model using best-fit emission estimates.

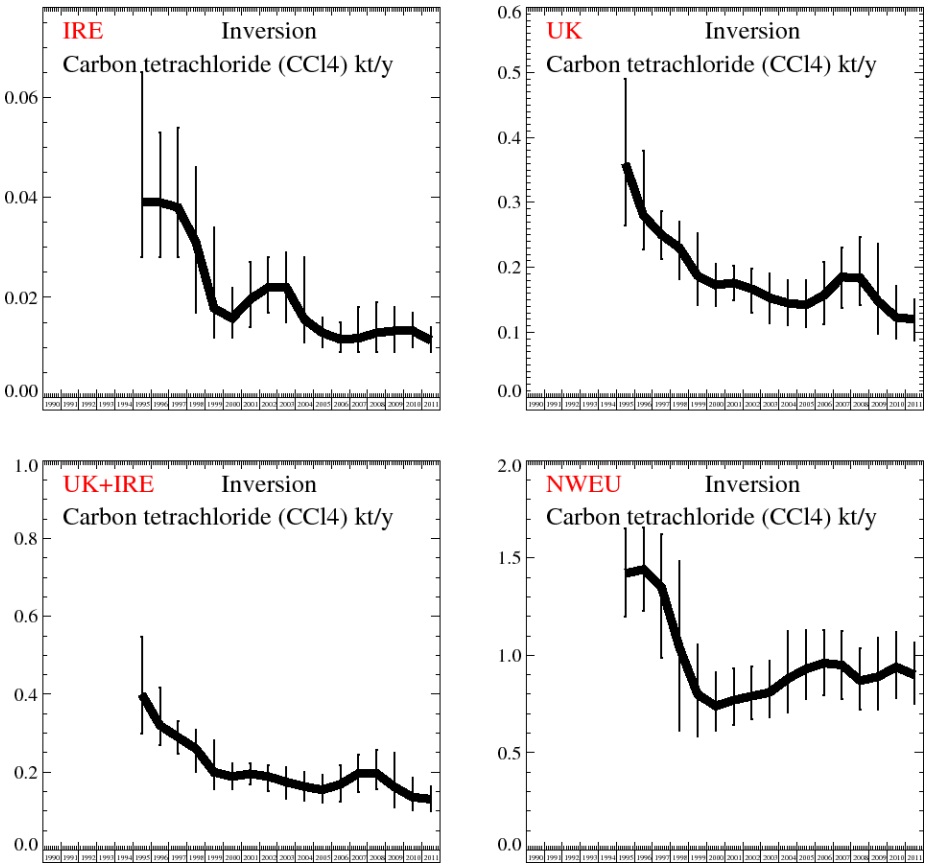

Figure 138: Emission estimates for IRE, UK, IRE+UK and NWEU. The uncertainty bars represent the 5th and 95th percentiles. Grey emissions are estimates from last year.

Unit	Year	IRE	(5th-95th)	UK	(5th-95th)	UK+IRE	(5th-95th)	NWEU	(5th-95th)	Number
t/y	1995	39	(28.- 65.)	360	(264.- 490.)	400	(298.- 547.)	1420	(1199.-1652.)	4000
t/y	1996	39	(28.- 53.)	280	(228.- 380.)	320	(270.- 417.)	1440	(1228.-1655.)	4000
t/y	1997	38	(28.- 54.)	250	(213.- 287.)	290	(247.- 331.)	1350	(989.-1620.)	4000
t/y	1998	31	(17.- 46.)	230	(182.- 271.)	260	(200.- 309.)	1040	(612.-1485.)	4000
t/y	1999	17.8	(12.- 34.)	187	(142.- 252.)	200	(156.- 281.)	800	(583.-1054.)	4000
t/y	2000	15.8	(12.- 22.)	173	(141.- 205.)	189	(156.- 223.)	740	(612.- 914.)	4000
t/y	2001	19.6	(14.- 27.)	176	(149.- 203.)	196	(168.- 223.)	770	(644.- 931.)	4000
t/y	2002	22	(17.- 28.)	167	(130.- 198.)	189	(152.- 219.)	790	(670.- 941.)	4000
t/y	2003	22	(15.- 29.)	153	(114.- 191.)	175	(133.- 213.)	810	(684.- 970.)	4000
t/y	2004	15.6	(11.- 28.)	145	(111.- 181.)	163	(126.- 201.)	880	(705.-1125.)	4000
t/y	2005	12.9	(10.- 16.)	142	(108.- 180.)	155	(121.- 193.)	930	(774.-1132.)	4000
t/y	2006	11.6	(9.- 15.)	157	(113.- 208.)	169	(125.- 218.)	960	(793.-1129.)	4000
t/y	2007	11.8	(9.- 18.)	185	(137.- 231.)	197	(149.- 244.)	950	(773.-1125.)	4000
t/y	2008	12.9	(9.- 19.)	184	(142.- 246.)	197	(156.- 258.)	870	(720.-1034.)	4000
t/y	2009	13.3	(9.- 18.)	148	(98.- 237.)	162	(110.- 249.)	890	(722.-1092.)	4000
t/y	2010	13.3	(10.- 17.)	123	(91.- 172.)	136	(103.- 186.)	940	(778.-1121.)	2080
t/y	2011	11.4	(9.- 14.)	120	(88.- 151.)	131	(101.- 163.)	900	(753.-1066.)	160

Table 31: Emission estimates for UK, IRE and NWEU with uncertainty (5th – 95th %ile).

5.2.5.6 $CHClCCl_2$ (trichloroethylene)

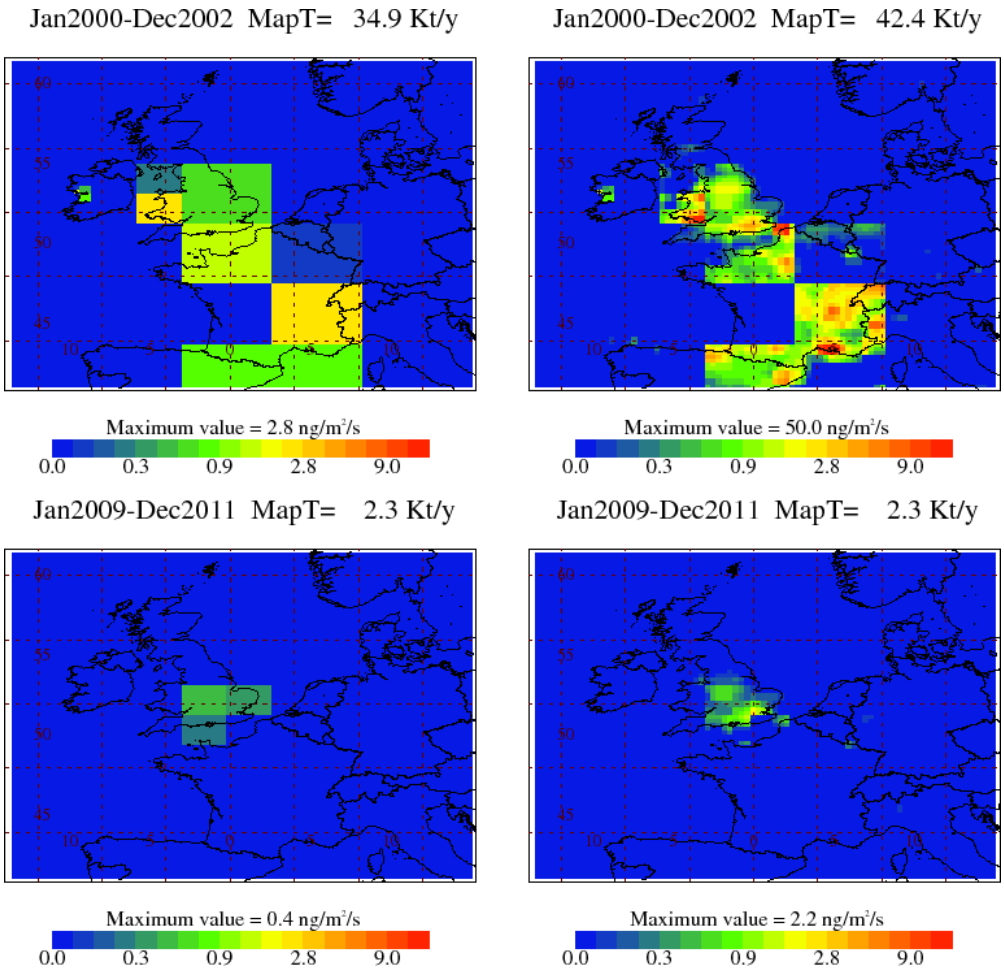

Figure 139: NAME-inversion emission estimates for 1990-92 (upper) and 2009-11 (lower). On the right hand side the emissions per grid box have been re-distributed based on population.

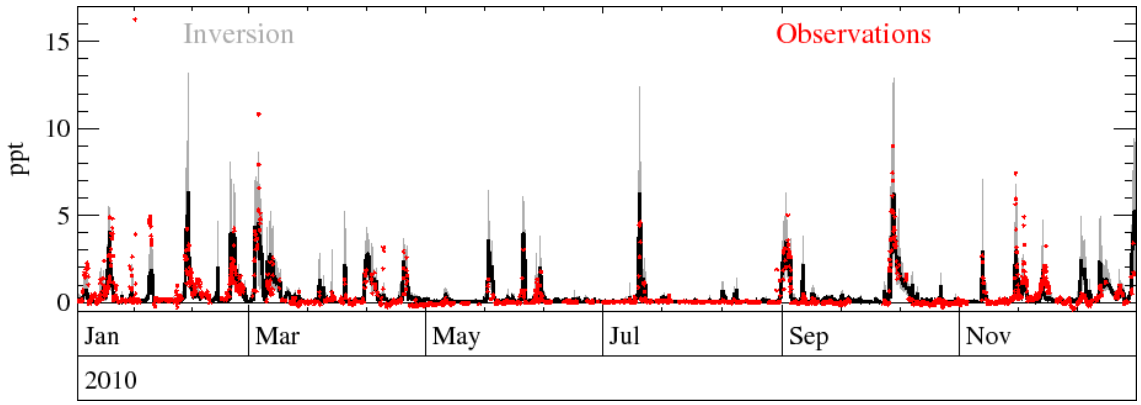

Figure 140: Example time-series of observations Vs. model using best-fit emission estimates.

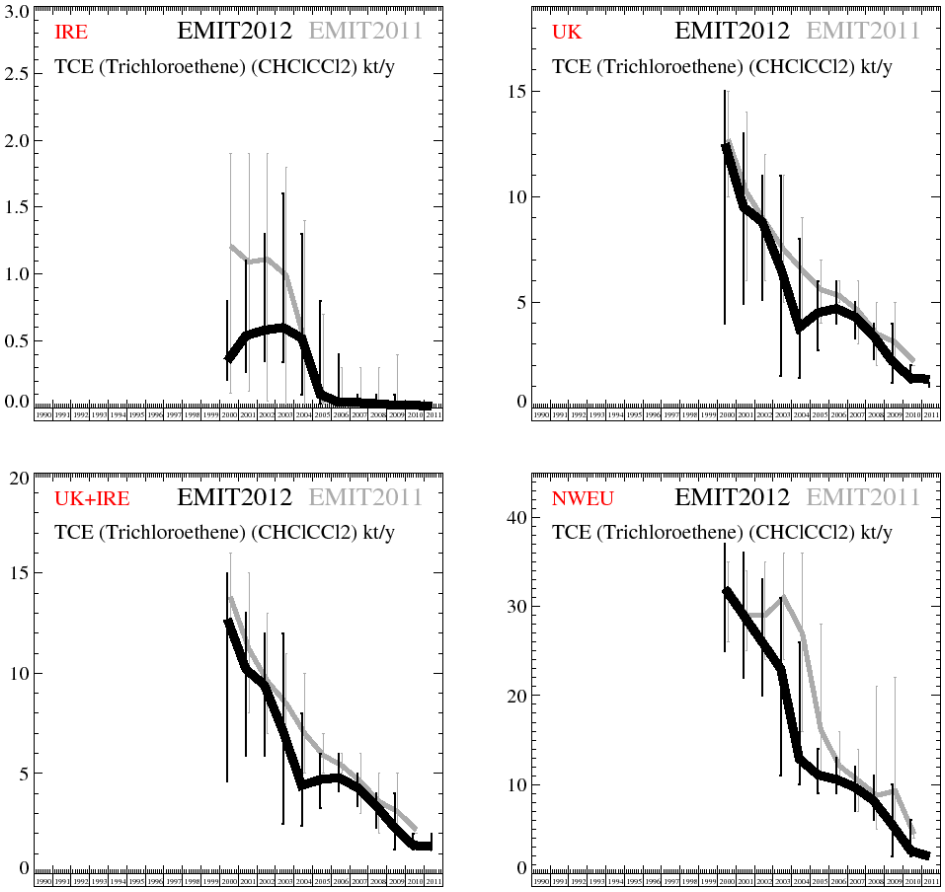

Figure 141: Emission estimates for IRE, UK, IRE+UK and NWEU. The uncertainty bars represent the 5th and 95th percentiles. Grey emissions are estimates from last year.

Unit	Year	IRE	(5th-95th)	UK	(5th-95th)	UK+IRE	(5th-95th)	NWEU	(5th-95th)	Number
kt/y	2000	0.35	(0.21- 0.8)	12.5	(4.0- 15.)	12.7	(4.6- 15.)	32	(25.- 37.)	640
kt/y	2001	0.54	(0.27- 1.1)	9.5	(4.9- 13.)	10.2	(5.9- 13.)	29	(22.- 36.)	2560
kt/y	2002	0.58	(0.35- 1.3)	8.8	(5.1- 11.)	9.4	(5.9- 12.)	26	(20.- 33.)	4000
kt/y	2003	0.6	(0.34- 1.6)	6.6	(1.5- 11.)	7.1	(2.5- 12.)	23	(11.- 31.)	4000
kt/y	2004	0.52	(0.10- 1.3)	3.8	(1.4- 8.)	4.4	(2.4- 8.)	12.9	(10.- 26.)	4000
kt/y	2005	0.1	(0.03- 0.8)	4.5	(2.7- 6.)	4.7	(3.3- 6.)	11.1	(9.- 14.)	4000
kt/y	2006	0.04	(0.03- 0.4)	4.7	(4.0- 6.)	4.8	(4.1- 6.)	10.6	(9.- 13.)	4000
kt/y	2007	0.04	(0.03- 0.1)	4.3	(3.3- 5.)	4.3	(3.4- 5.)	9.7	(7.- 12.)	4000
kt/y	2008	0.03	(0.01- 0.1)	3.4	(2.3- 4.)	3.4	(2.3- 4.)	8.2	(6.- 11.)	4000
kt/y	2009	0.02	(0.01- 0.1)	2.2	(1.2- 4.)	2.3	(1.2- 4.)	5.5	(2.- 10.)	4000
kt/y	2010	0.02	(0.01- 0.0)	1.4	(1.2- 2.)	1.42	(1.2- 2.)	2.6	(2.- 6.)	2080
kt/y	2011	0.01	(0.01- 0.0)	1.35	(1.2- 1.)	1.36	(1.2- 2.)	1.94	(2.- 2.)	160

Table 32: Emission estimates for UK, IRE and NWEU with uncertainty (5th – 95th %ile).

5.2.5.7 CCl_2CCl_2 (tetrachloroethylene)

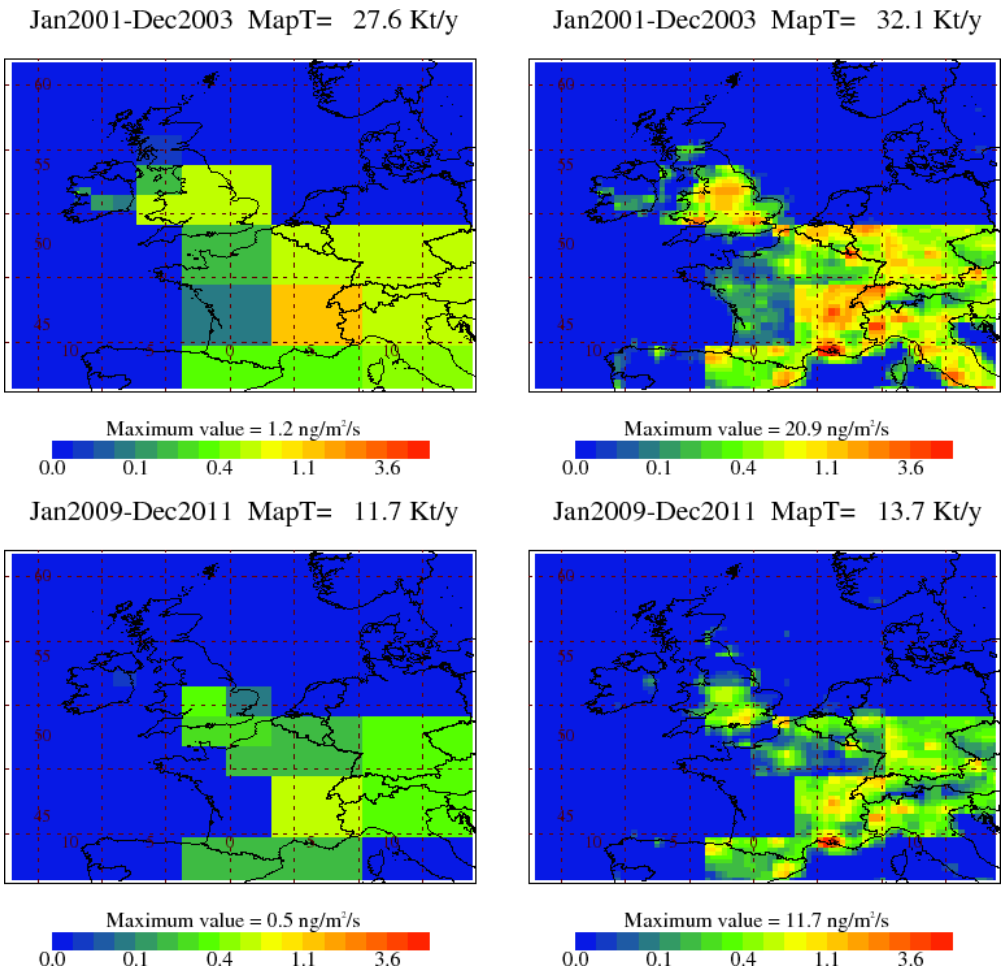

Figure 142: NAME-inversion emission estimates for 1990-92 (upper) and 2009-11 (lower). On the right hand side the emissions per grid box have been re-distributed based on population.

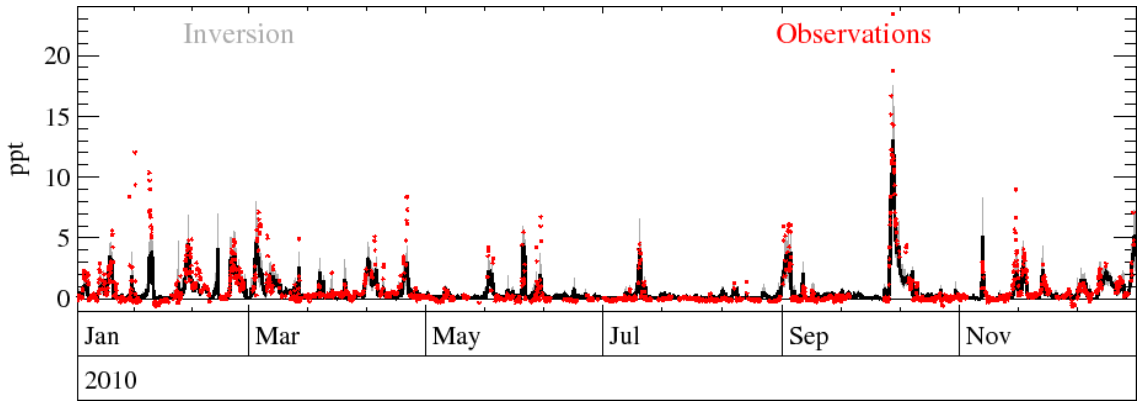

Figure 143: Example time-series of observations Vs. model using best-fit emission estimates.

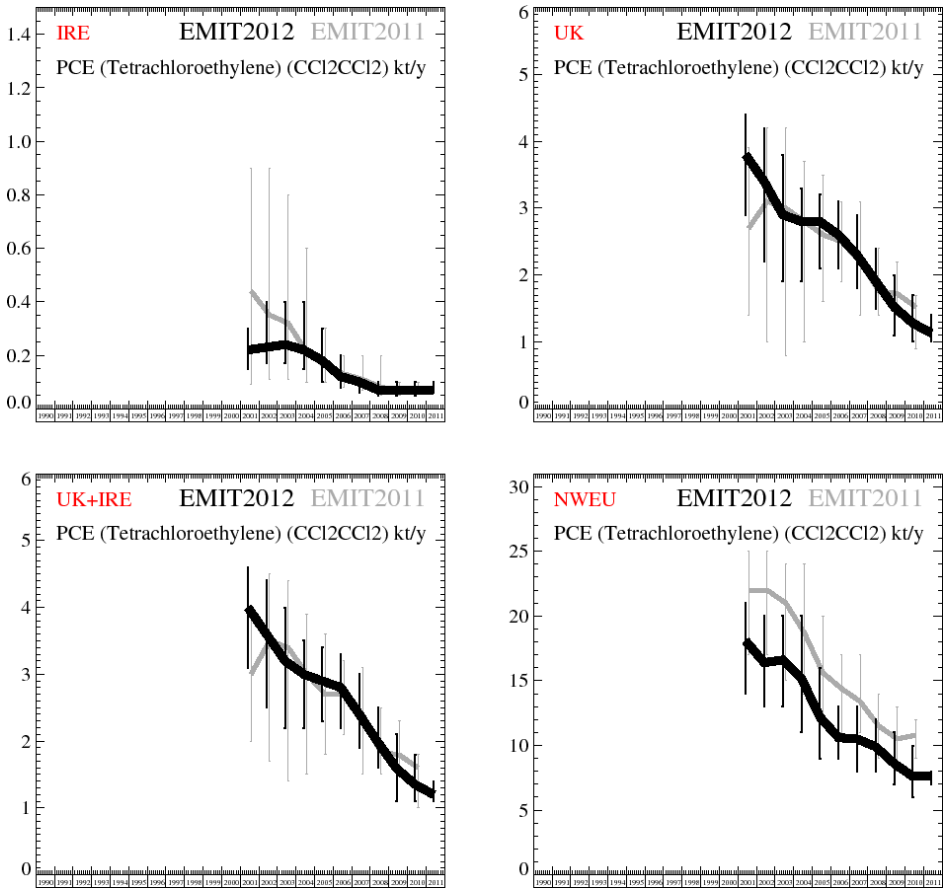

Figure 144: Emission estimates for IRE, UK, IRE+UK and NWEU. The uncertainty bars represent the 5th and 95th percentiles. Grey emissions are estimates from last year.

Unit	Year	IRE	(5th-95th)	UK	(5th-95th)	UK+IRE	(5th-95th)	NWEU	(5th-95th)	Number
kt/y	2001	0.22	(0.15- 0.3)	3.8	(2.9- 4.4)	4	(3.1- 4.6)	18.1	(14.- 21.)	640
kt/y	2002	0.23	(0.17- 0.4)	3.4	(2.2- 4.2)	3.6	(2.5- 4.4)	16.4	(13.- 20.)	2560
kt/y	2003	0.24	(0.17- 0.4)	2.9	(1.9- 3.8)	3.2	(2.2- 4.0)	16.6	(13.- 20.)	4000
kt/y	2004	0.22	(0.15- 0.4)	2.8	(1.9- 3.3)	3	(2.2- 3.5)	15.2	(11.- 20.)	4000
kt/y	2005	0.18	(0.10- 0.3)	2.8	(2.1- 3.2)	2.9	(2.3- 3.4)	12.2	(9.- 16.)	4000
kt/y	2006	0.12	(0.08- 0.2)	2.6	(2.1- 3.1)	2.8	(2.2- 3.3)	10.6	(9.- 13.)	4000
kt/y	2007	0.1	(0.06- 0.1)	2.3	(1.8- 2.9)	2.4	(1.9- 3.0)	10.5	(8.- 13.)	4000
kt/y	2008	0.07	(0.05- 0.1)	1.91	(1.5- 2.4)	1.98	(1.6- 2.5)	9.9	(8.- 12.)	4000
kt/y	2009	0.07	(0.05- 0.1)	1.52	(1.1- 2.0)	1.59	(1.1- 2.1)	8.6	(7.- 11.)	4000
kt/y	2010	0.07	(0.05- 0.1)	1.28	(1.0- 1.7)	1.35	(1.1- 1.8)	7.6	(6.- 10.)	2080
kt/y	2011	0.07	(0.06- 0.1)	1.13	(1.0- 1.4)	1.2	(1.1- 1.4)	7.6	(7.- 8.)	160

Table 33: Emission estimates for UK, IRE and NWEU with uncertainty (5th – 95th %ile).

5.2.6 Bromine compounds

5.2.6.1 Halon-1211

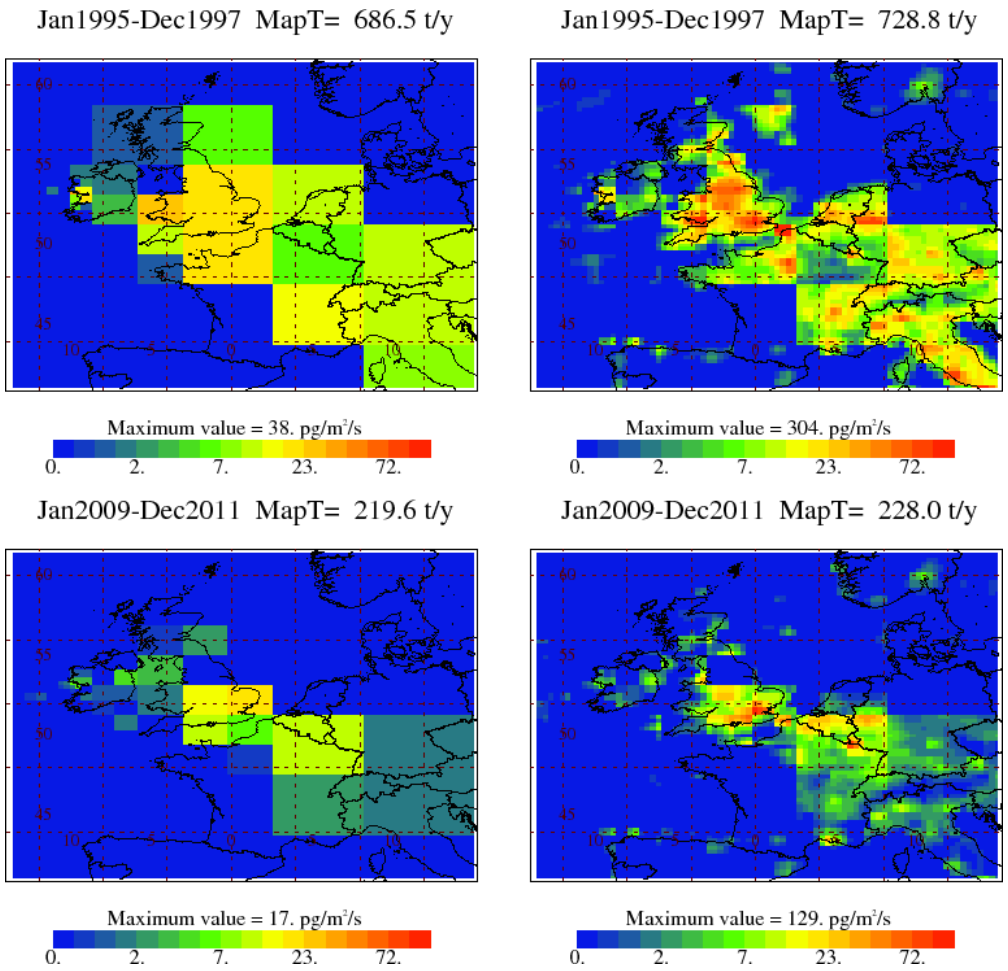

Figure 145: NAME-inversion emission estimates for 1990-92 (upper) and 2009-11 (lower). On the right hand side the emissions per grid box have been re-distributed based on population.

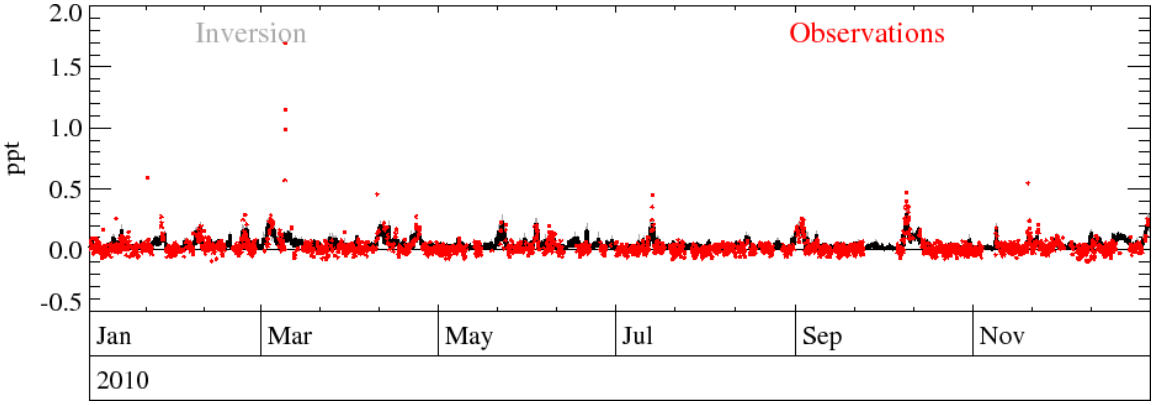

Figure 146: Example time-series of observations Vs. model using best-fit emission estimates.

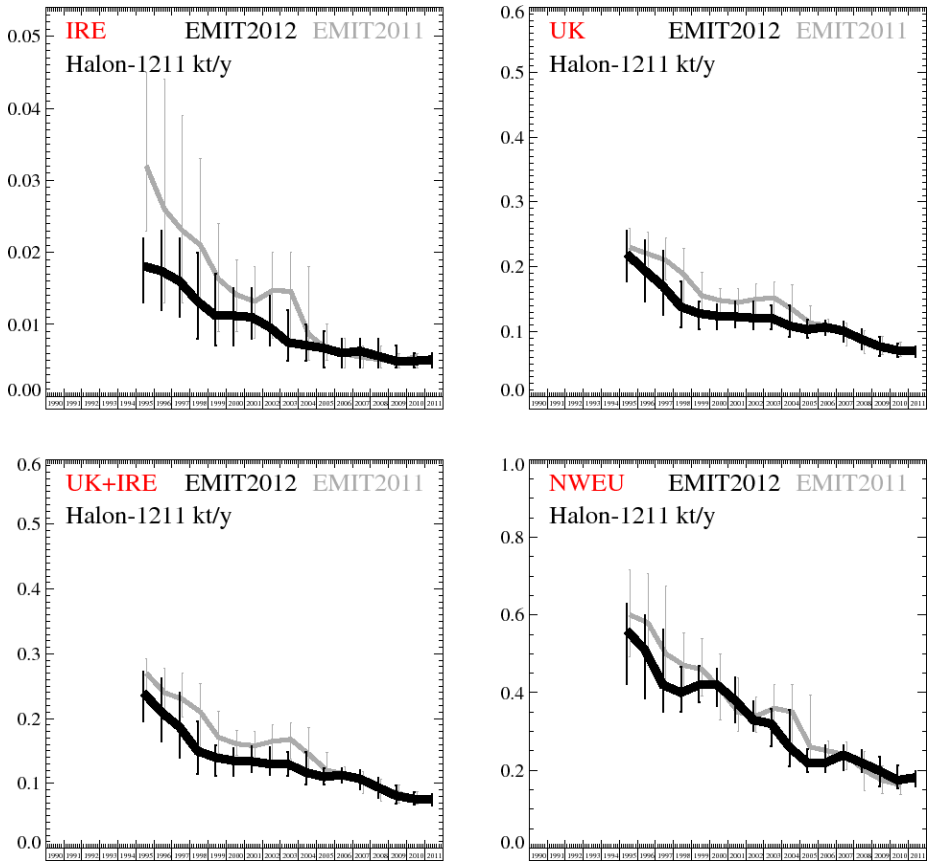

Figure 147: Emission estimates for IRE, UK, IRE+UK and NWEU. The uncertainty bars represent the 5th and 95th percentiles. Grey emissions are estimates from last year.

Unit	Year	IRE	(5th-95th)	UK	(5th-95th)	UK+IRE	(5th-95th)	NWEU	(5th-95th)	Number
t/y	1995	18.1	(13.- 22.)	220	(178.- 256.)	240	(196.- 272.)	560	(421.- 628.)	640
t/y	1996	17.4	(12.- 23.)	194	(146.- 241.)	210	(165.- 262.)	510	(386.- 600.)	2560
t/y	1997	16	(11.- 22.)	170	(126.- 224.)	187	(140.- 240.)	420	(350.- 563.)	4000
t/y	1998	13.2	(8.- 20.)	138	(106.- 178.)	150	(115.- 195.)	400	(350.- 466.)	4000
t/y	1999	11.2	(7.- 17.)	128	(103.- 147.)	140	(111.- 159.)	420	(375.- 470.)	4000
t/y	2000	11.2	(7.- 15.)	124	(103.- 142.)	135	(111.- 155.)	420	(365.- 461.)	4000
t/y	2001	11	(8.- 15.)	123	(107.- 146.)	134	(118.- 157.)	380	(323.- 440.)	4000
t/y	2002	9.6	(7.- 14.)	121	(104.- 146.)	130	(113.- 156.)	330	(301.- 379.)	4000
t/y	2003	7.5	(5.- 12.)	121	(104.- 141.)	130	(111.- 149.)	320	(262.- 358.)	4000
t/y	2004	7.1	(5.- 10.)	109	(92.- 141.)	117	(99.- 148.)	260	(210.- 357.)	4000
t/y	2005	6.7	(4.- 9.)	103	(91.- 118.)	110	(98.- 124.)	220	(197.- 255.)	4000
t/y	2006	6	(4.- 8.)	107	(95.- 117.)	113	(101.- 123.)	220	(197.- 264.)	4000
t/y	2007	6.3	(4.- 8.)	101	(85.- 116.)	107	(91.- 121.)	240	(201.- 265.)	4000
t/y	2008	5.6	(4.- 8.)	88	(73.- 103.)	94	(78.- 109.)	220	(196.- 253.)	4000
t/y	2009	4.9	(4.- 7.)	77	(63.- 92.)	81	(69.- 97.)	199	(159.- 235.)	4000
t/y	2010	4.9	(4.- 6.)	71	(61.- 82.)	76	(67.- 87.)	175	(155.- 212.)	2080
t/y	2011	5.1	(4.- 6.)	71	(61.- 77.)	76	(66.- 83.)	182	(159.- 199.)	160

Table 34: Emission estimates for UK, IRE and NWEU with uncertainty (5th – 95th %ile).

5.2.6.2 Halon-1301

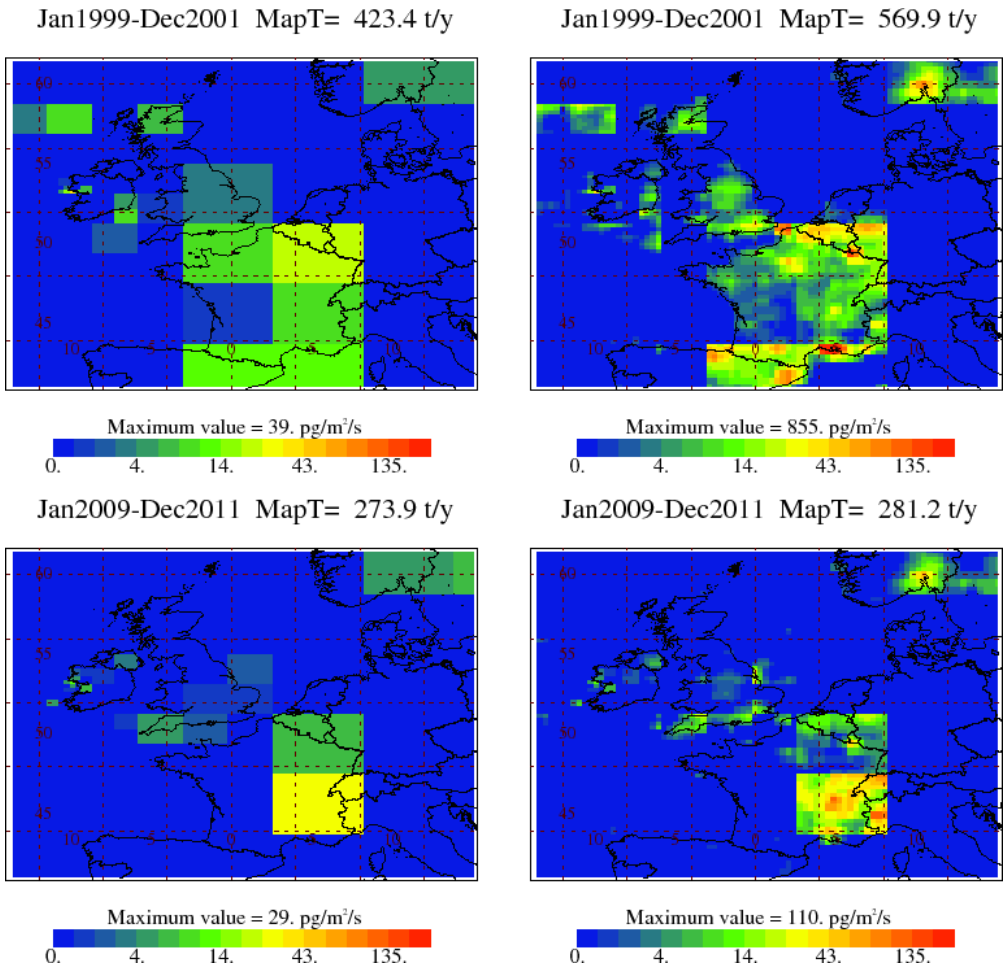

Figure 148: NAME-inversion emission estimates for 1990-92 (upper) and 2009-11 (lower). On the right hand side the emissions per grid box have been re-distributed based on population.

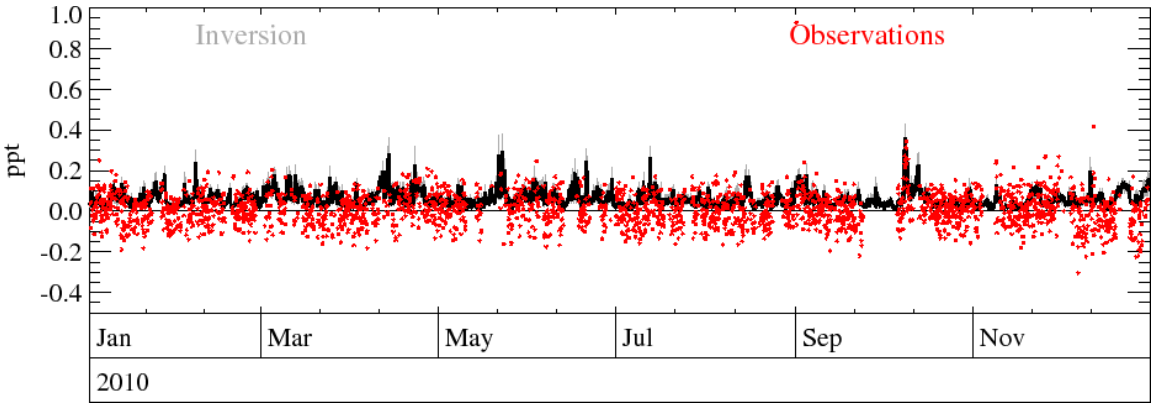

Figure 149: Example time-series of observations Vs. model using best-fit emission estimates.

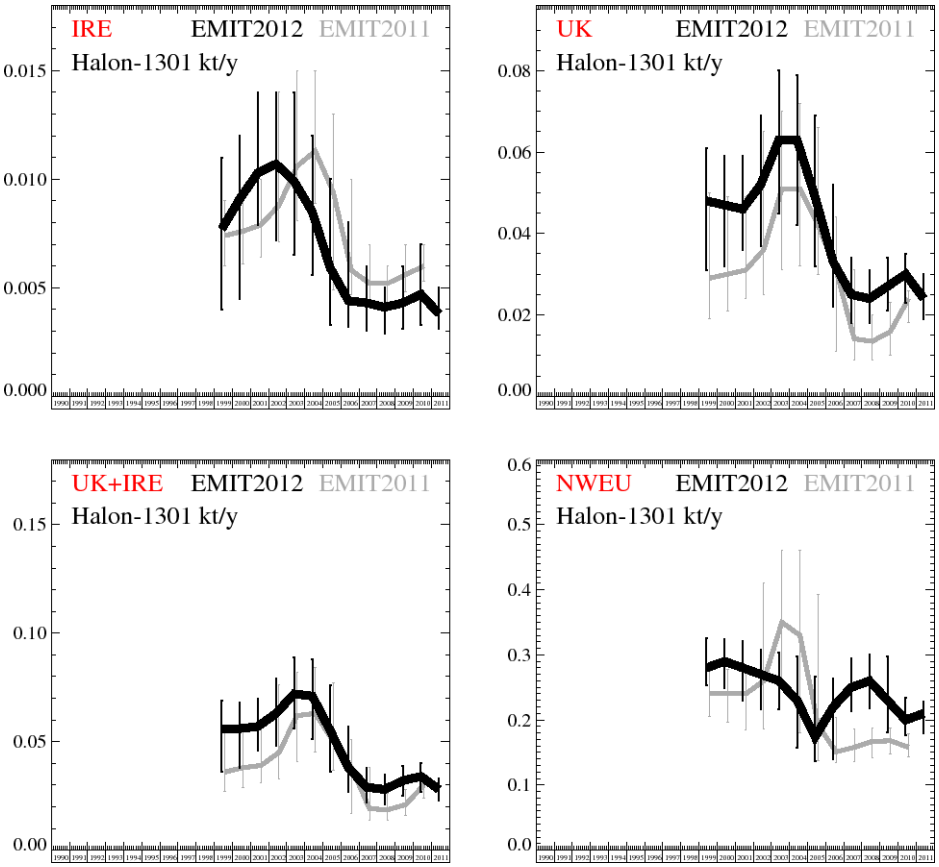

Figure 150: Emission estimates for IRE, UK, IRE+UK and NWEU. The uncertainty bars represent the 5th and 95th percentiles. Grey emissions are estimates from last year.

Unit	Year	IRE	(5th-95th)	UK	(5th-95th)	UK+IRE	(5th-95th)	NWEU	(5th-95th)	Number
t/y	1999	7.7	(4.0- 11.)	48	(31.- 61.)	56	(36.- 69.)	280	(254.- 326.)	1920
t/y	2000	9.1	(4.5- 12.)	47	(32.- 59.)	56	(38.- 68.)	290	(249.- 324.)	3840
t/y	2001	10.3	(7.9- 14.)	46	(36.- 59.)	57	(46.- 70.)	280	(229.- 321.)	4000
t/y	2002	10.7	(7.2- 14.)	52	(37.- 69.)	63	(48.- 79.)	270	(217.- 308.)	4000
t/y	2003	9.9	(6.5- 14.)	63	(45.- 80.)	72	(56.- 89.)	260	(217.- 304.)	4000
t/y	2004	8.5	(5.6- 12.)	63	(42.- 79.)	71	(51.- 88.)	230	(157.- 297.)	4000
t/y	2005	5.9	(3.3- 10.)	49	(32.- 69.)	55	(36.- 76.)	174	(137.- 267.)	4000
t/y	2006	4.4	(3.2- 8.)	33	(22.- 52.)	38	(27.- 57.)	220	(140.- 263.)	4000
t/y	2007	4.3	(3.0- 6.)	25	(18.- 34.)	29	(22.- 38.)	250	(213.- 294.)	4000
t/y	2008	4.1	(2.9- 5.)	24	(18.- 31.)	28	(21.- 35.)	260	(218.- 300.)	4000
t/y	2009	4.3	(3.1- 6.)	27	(21.- 34.)	32	(25.- 39.)	230	(181.- 297.)	4000
t/y	2010	4.7	(3.3- 7.)	30	(23.- 35.)	34	(27.- 40.)	200	(176.- 234.)	2080
t/y	2011	3.8	(3.1- 5.)	24	(19.- 30.)	28	(23.- 33.)	210	(180.- 228.)	160

Table 35: Emission estimates for UK, IRE and NWEU with uncertainty (5th – 95th %ile).

5.2.7 Hydrocarbons

5.2.7.1 CH_4 (methane)

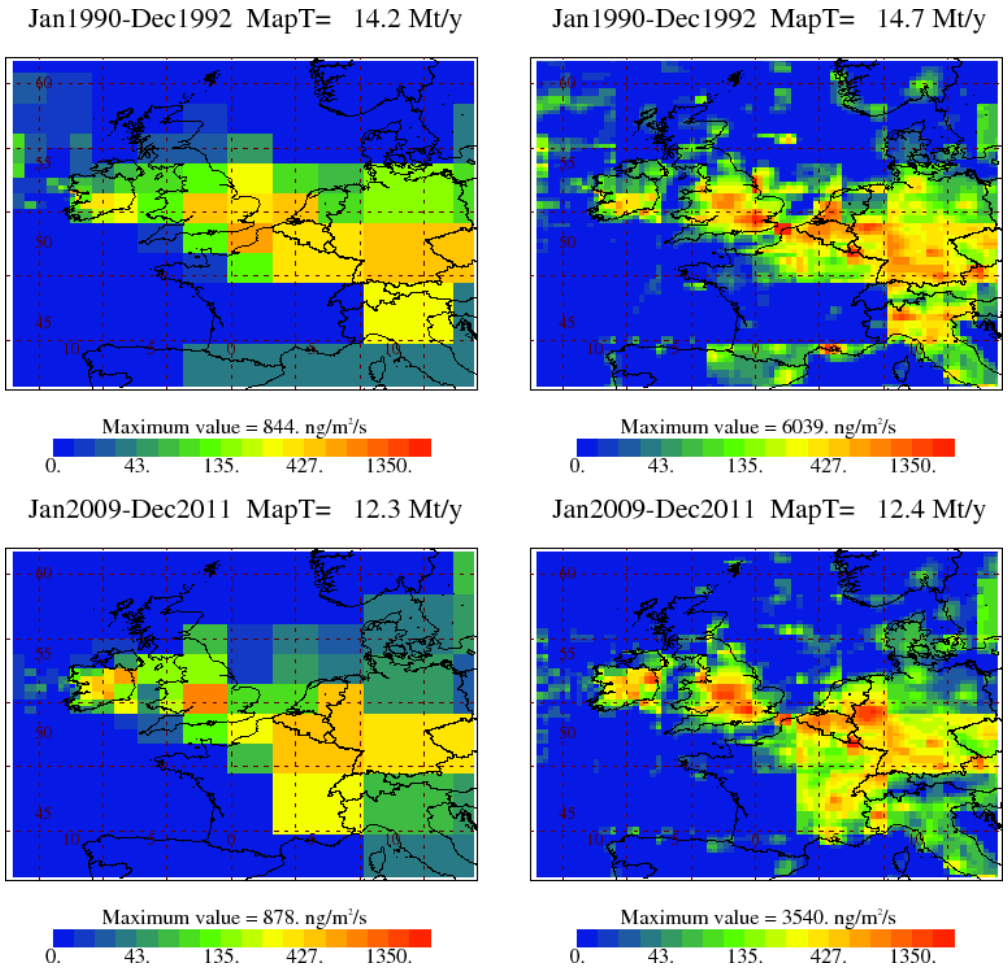

Figure 151: NAME-inversion emission estimates for 1990-92 (upper) and 2009-11 (lower). On the right hand side the emissions per grid box have been re-distributed based on population.

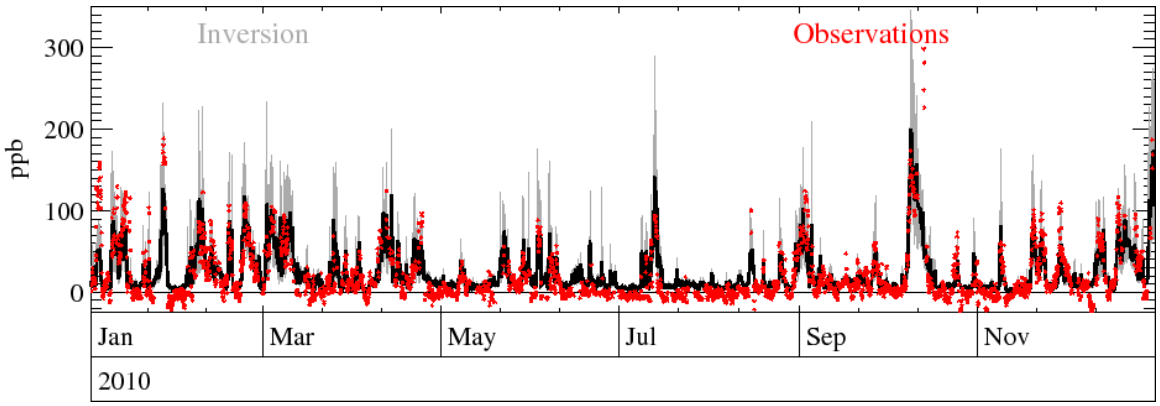

Figure 152: Example time-series of observations Vs. model using best-fit emission estimates.

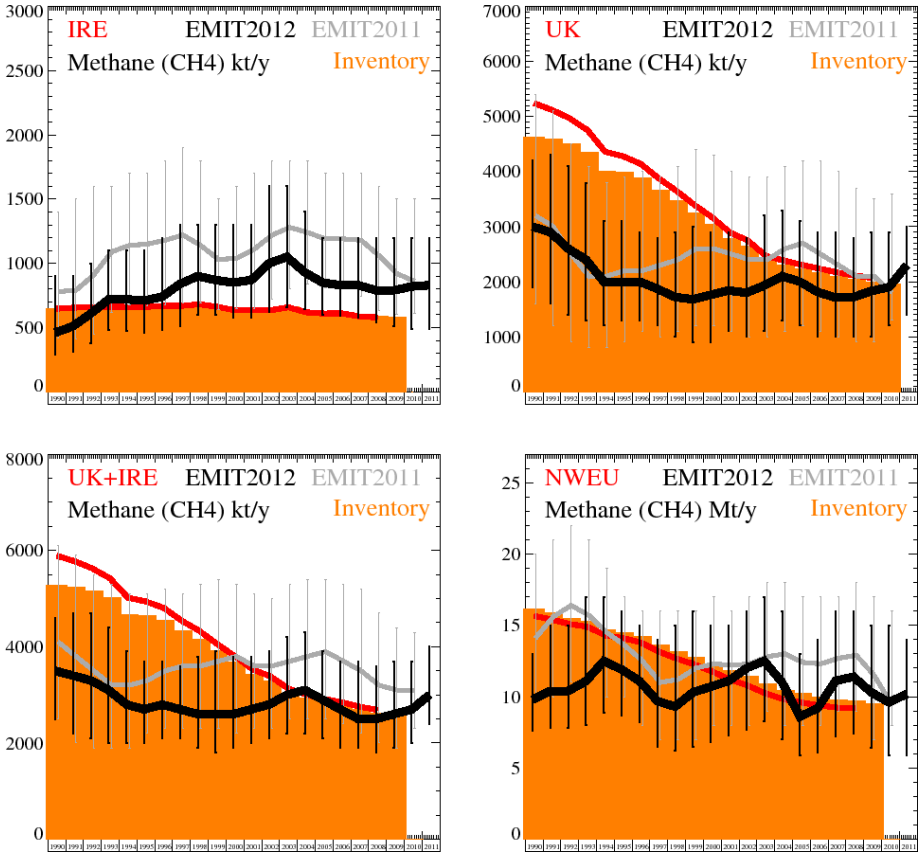

Figure 153: Inversion emission estimates for IRE, UK, IRE+UK and NWEU. Uncertainty bars represent the 5th and 95th percentiles. Orange bars represent UNFCCC emission estimates from the 2012 inventory. Grey (EMIT) and red (UNFCCC) are emissions as estimated last year.

Unit	Year	IRE	(5th-95th)	UK	(5th-95th)	UK+IRE	(5th-95th)	NWEU	(5th-95th)	Number
Mt/y	1990	0.46	(0.29- 0.9)	3	(1.9- 4.2)	3.5	(2.5- 4.6)	9.8	(7.6- 13.)	1920
Mt/y	1991	0.51	(0.31- 0.9)	2.9	(1.6- 4.3)	3.4	(2.2- 4.7)	10.4	(7.8- 15.)	3840
Mt/y	1992	0.61	(0.38- 1.0)	2.6	(1.4- 4.1)	3.3	(2.1- 4.7)	10.4	(7.8- 15.)	4000
Mt/y	1993	0.72	(0.48- 1.1)	2.4	(1.3- 3.8)	3.1	(2.0- 4.4)	11.1	(8.0- 17.)	4000
Mt/y	1994	0.72	(0.47- 1.1)	2	(1.2- 3.1)	2.8	(2.0- 3.9)	12.5	(8.9- 17.)	4000
Mt/y	1995	0.71	(0.46- 1.1)	2	(1.3- 3.1)	2.7	(2.0- 3.7)	11.9	(8.7- 16.)	4000
Mt/y	1996	0.74	(0.48- 1.2)	2	(1.3- 2.9)	2.8	(2.1- 3.7)	11.1	(8.2- 15.)	4000
Mt/y	1997	0.84	(0.51- 1.3)	1.87	(1.2- 2.8)	2.7	(2.1- 3.6)	9.7	(6.5- 14.)	4000
Mt/y	1998	0.9	(0.60- 1.3)	1.72	(1.0- 2.9)	2.6	(1.9- 3.8)	9.3	(6.2- 15.)	4000
Mt/y	1999	0.87	(0.60- 1.3)	1.68	(0.9- 3.0)	2.6	(1.8- 3.9)	10.3	(6.5- 16.)	4000
Mt/y	2000	0.85	(0.58- 1.3)	1.76	(0.9- 2.9)	2.6	(1.9- 3.8)	10.7	(6.8- 15.)	4000
Mt/y	2001	0.87	(0.58- 1.3)	1.84	(1.1- 2.9)	2.7	(2.0- 3.8)	11.1	(7.3- 15.)	4000
Mt/y	2002	1	(0.62- 1.6)	1.8	(1.0- 2.8)	2.8	(2.1- 3.9)	12	(7.7- 16.)	4000
Mt/y	2003	1.05	(0.66- 1.6)	1.93	(1.1- 3.2)	3	(2.2- 4.2)	12.5	(8.3- 17.)	4000
Mt/y	2004	0.93	(0.64- 1.4)	2.1	(1.3- 3.3)	3.1	(2.2- 4.3)	11	(7.0- 16.)	4000
Mt/y	2005	0.85	(0.60- 1.2)	2	(1.2- 3.1)	2.9	(2.1- 3.9)	8.6	(5.9- 13.)	4000
Mt/y	2006	0.83	(0.59- 1.2)	1.81	(1.0- 2.9)	2.7	(1.9- 3.7)	9.2	(6.1- 14.)	4000
Mt/y	2007	0.83	(0.58- 1.2)	1.71	(1.0- 2.9)	2.5	(1.9- 3.7)	11.1	(7.2- 16.)	4000
Mt/y	2008	0.79	(0.54- 1.2)	1.72	(1.0- 2.8)	2.5	(1.8- 3.6)	11.4	(7.4- 16.)	4000
Mt/y	2009	0.79	(0.51- 1.2)	1.83	(1.0- 2.9)	2.6	(1.9- 3.7)	10.3	(6.4- 15.)	4000
Mt/y	2010	0.82	(0.49- 1.2)	1.9	(1.2- 2.9)	2.7	(2.0- 3.7)	9.6	(5.9- 15.)	2080
Mt/y	2011	0.83	(0.49- 1.2)	2.3	(1.4- 3.0)	3	(2.4- 4.0)	10.2	(5.9- 14.)	160

Table 36: Emission estimates for UK, IRE and NWEU with uncertainty (5th – 95th %ile).

5.2.8 Oxides of carbon

5.2.8.1 CO (carbon monoxide)

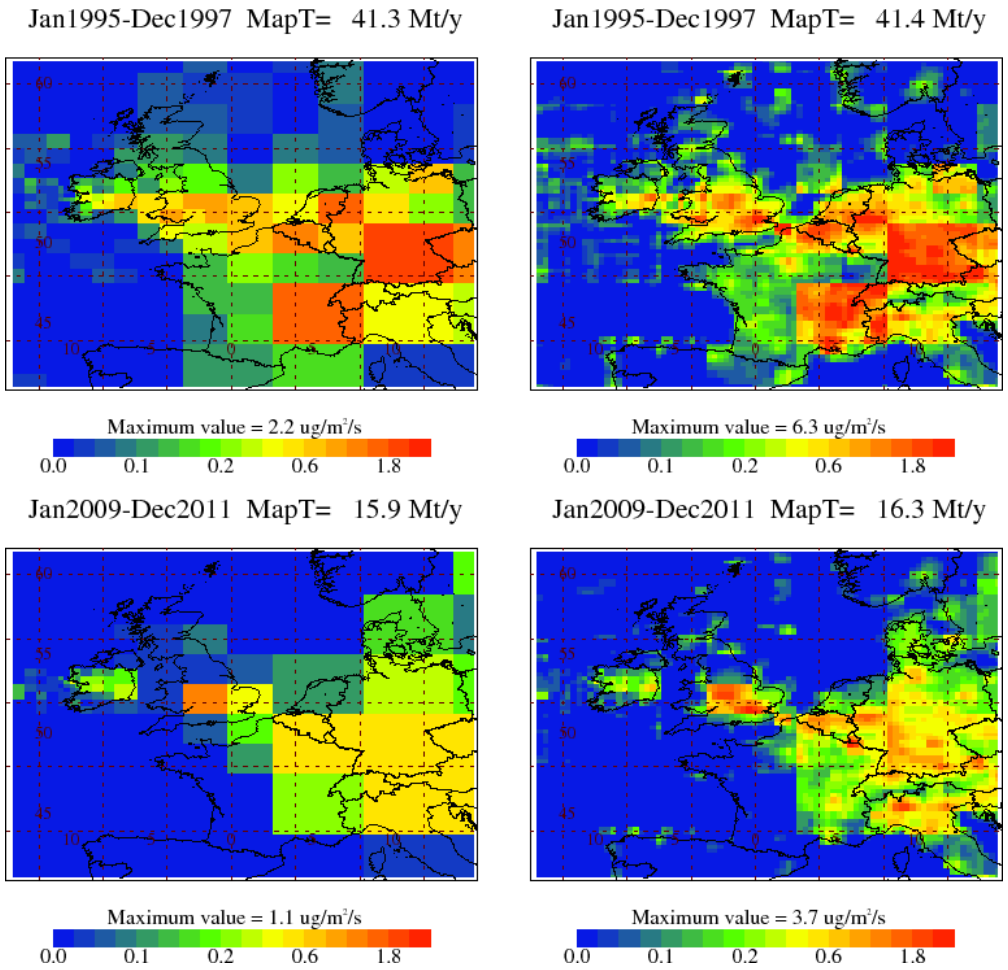

Figure 154: NAME-inversion emission estimates for 1990-92 (upper) and 2009-11 (lower). On the right hand side the emissions per grid box have been re-distributed based on population.

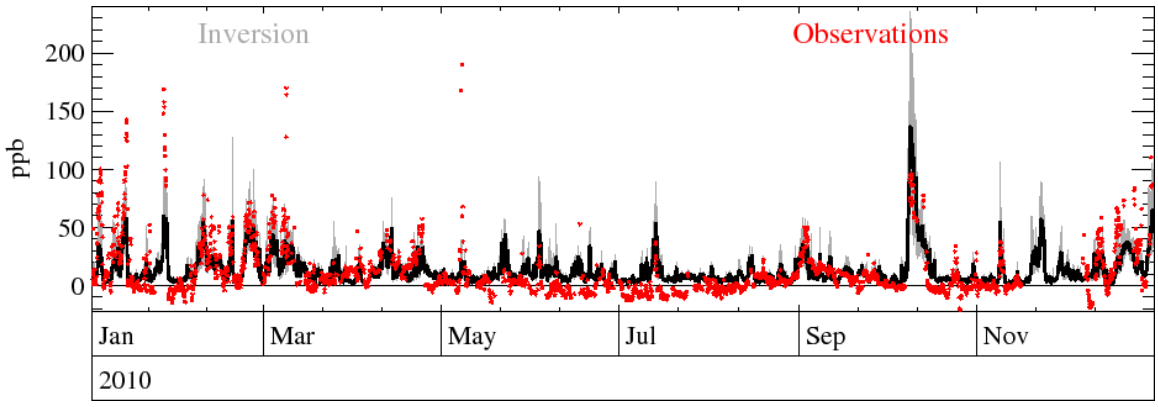

Figure 155: Example time-series of observations Vs. model using best-fit emission estimates.

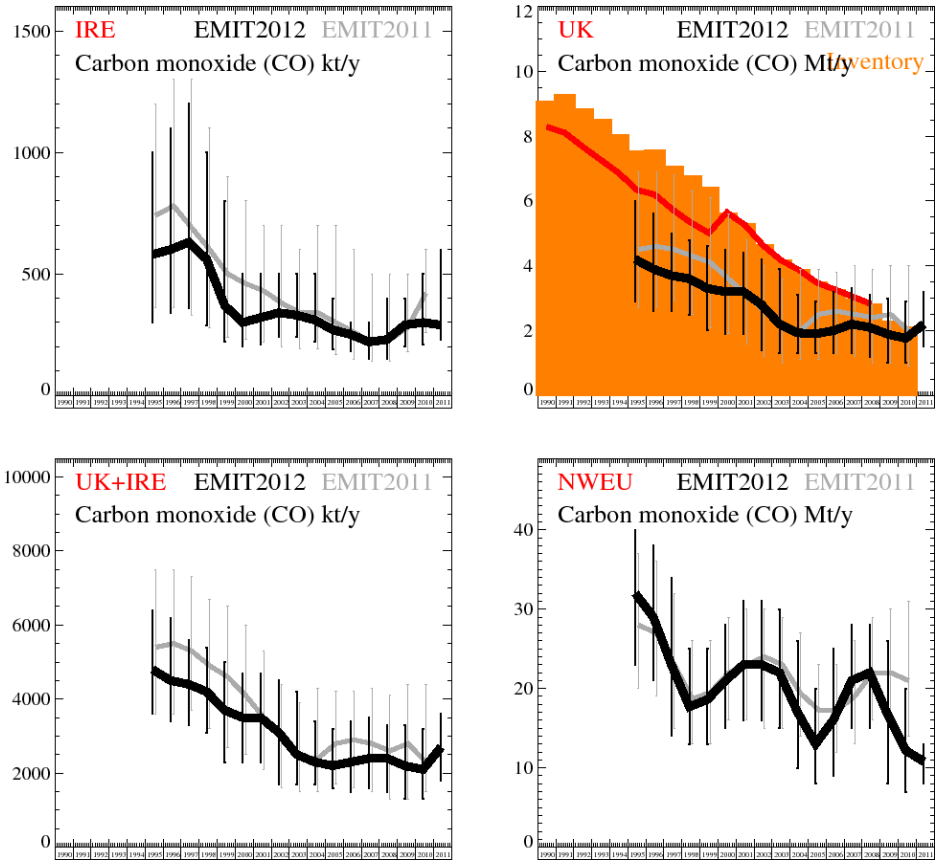

Figure 156: Inversion emission estimates for IRE, UK, IRE+UK and NWEU. Uncertainty bars represent the 5th and 95th percentiles. Orange bars represent EMEP emission estimates from the 2012 inventory. Grey (EMIT) and red EMEP) are emissions as estimated last year.

Unit	Year	IRE	(5th-95th)	UK	(5th-95th)	UK+IRE	(5th-95th)	NWEU	(5th-95th)	Number
Mt/y	1995	0.58	(0.30- 1.0)	4.2	(2.9- 6.0)	4.8	(3.6- 6.4)	32	(23.- 40.)	1920
Mt/y	1996	0.6	(0.34- 1.1)	3.9	(2.6- 5.6)	4.5	(3.4- 6.2)	29	(21.- 38.)	3840
Mt/y	1997	0.63	(0.36- 1.2)	3.7	(2.6- 5.0)	4.4	(3.3- 5.6)	23	(14.- 34.)	4000
Mt/y	1998	0.56	(0.29- 1.0)	3.6	(2.5- 4.8)	4.2	(3.1- 5.4)	17.7	(13.- 25.)	4000
Mt/y	1999	0.37	(0.22- 0.8)	3.3	(2.0- 4.6)	3.7	(2.3- 5.0)	18.6	(13.- 25.)	4000
Mt/y	2000	0.3	(0.20- 0.5)	3.2	(1.9- 4.5)	3.5	(2.3- 4.7)	21	(15.- 28.)	4000
Mt/y	2001	0.32	(0.21- 0.5)	3.2	(1.9- 4.4)	3.5	(2.3- 4.7)	23	(16.- 31.)	4000
Mt/y	2002	0.34	(0.24- 0.5)	2.8	(1.4- 4.2)	3.1	(1.7- 4.5)	23	(16.- 31.)	4000
Mt/y	2003	0.33	(0.24- 0.5)	2.2	(1.3- 3.9)	2.5	(1.7- 4.2)	22	(15.- 30.)	4000
Mt/y	2004	0.31	(0.22- 0.5)	1.93	(1.3- 3.1)	2.3	(1.7- 3.4)	17	(10.- 26.)	4000
Mt/y	2005	0.27	(0.19- 0.4)	1.9	(1.3- 2.9)	2.2	(1.6- 3.2)	13	(8.- 20.)	4000
Mt/y	2006	0.25	(0.18- 0.3)	2	(1.3- 3.2)	2.3	(1.5- 3.4)	16.1	(9.- 25.)	4000
Mt/y	2007	0.22	(0.15- 0.3)	2.2	(1.3- 3.3)	2.4	(1.6- 3.5)	21	(15.- 28.)	4000
Mt/y	2008	0.23	(0.15- 0.4)	2.1	(1.2- 3.1)	2.4	(1.5- 3.3)	22	(15.- 28.)	4000
Mt/y	2009	0.29	(0.20- 0.4)	1.89	(1.0- 3.0)	2.2	(1.3- 3.3)	16.7	(8.- 26.)	4000
Mt/y	2010	0.3	(0.21- 0.5)	1.76	(1.0- 2.9)	2.1	(1.3- 3.2)	12.2	(7.- 20.)	2080
Mt/y	2011	0.29	(0.23- 0.6)	2.2	(1.5- 3.2)	2.7	(1.8- 3.6)	10.8	(8.- 13.)	160

Table 37: Emission estimates for UK, IRE and NWEU with uncertainty (5th – 95th %ile).

5.2.8.2 CO_2 (carbon dioxide)

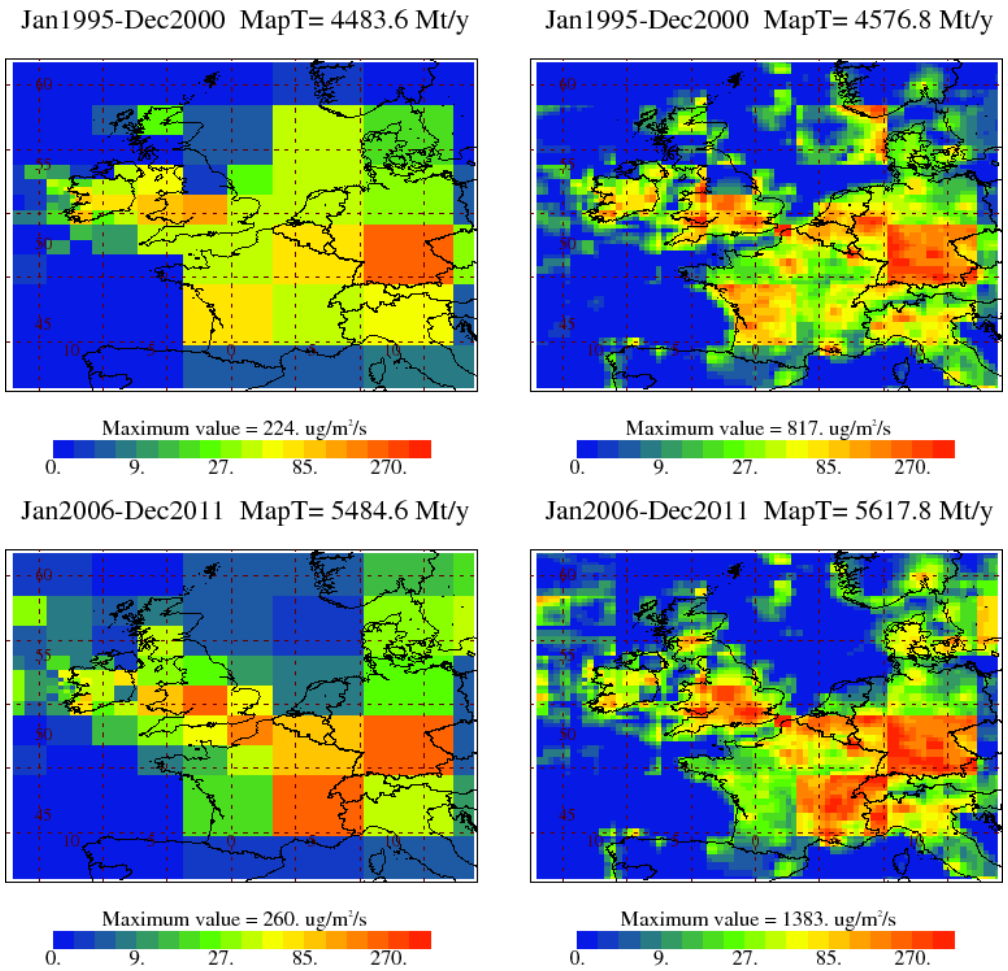

Figure 157: NAME-inversion emission estimates for 1990-92 (upper) and 2009-11 (lower). On the right hand side the emissions per grid box have been re-distributed based on population.

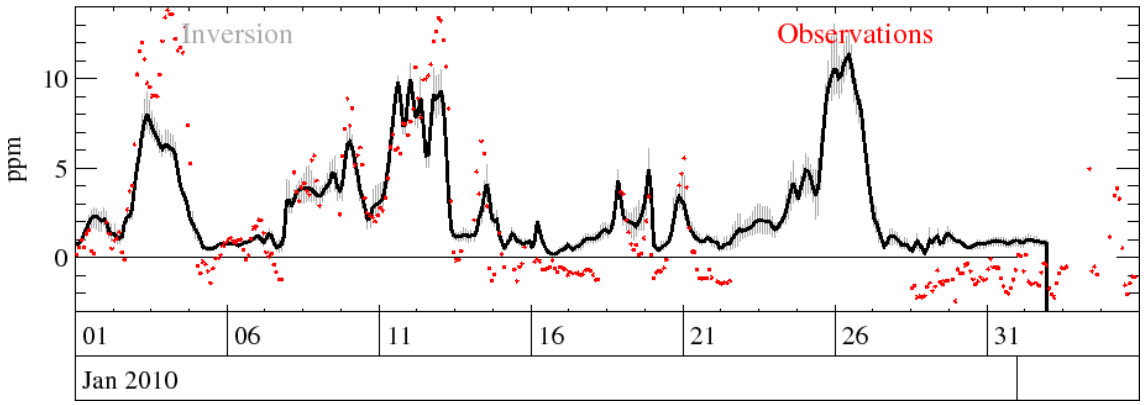

Figure 158: Example time-series of observations Vs. model using best-fit emission estimates.

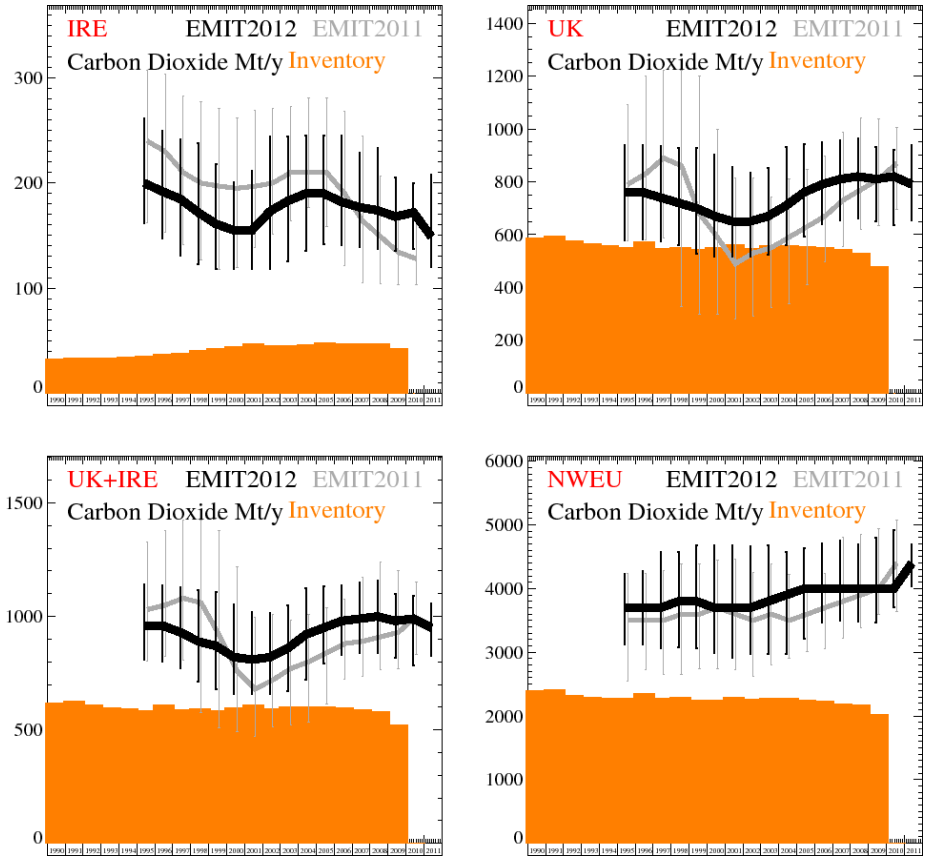

Figure 159: Inversion emission estimates for IRE, UK, IRE+UK and NWEU. Uncertainty bars represent the 5th and 95th percentiles. Orange bars represent UNFCCC emission estimates from the 2012 inventory. Grey (EMIT) and red (UNFCCC) are emissions as estimated last year.

Unit	Year	IRE	(5th-95th)	UK	(5th-95th)	UK+IRE	(5th-95th)	NWEU	(5th-95th)	Number
Mt/y	1995	200	(162.- 262.)	760	(577.- 939.)	960	(811.-1141.)	3700	(3128.-4234.)	4320
Mt/y	1996	192	(147.- 250.)	760	(583.- 940.)	960	(799.-1136.)	3700	(3131.-4283.)	6240
Mt/y	1997	185	(131.- 242.)	740	(573.- 936.)	930	(771.-1127.)	3700	(3061.-4573.)	8160
Mt/y	1998	172	(123.- 238.)	720	(560.- 929.)	890	(713.-1117.)	3800	(3074.-4577.)	9760
Mt/y	1999	161	(118.- 218.)	700	(529.- 929.)	870	(681.-1106.)	3800	(3060.-4681.)	9760
Mt/y	2000	155	(118.- 201.)	670	(516.- 903.)	820	(660.-1054.)	3700	(2995.-4681.)	9760
Mt/y	2001	155	(118.- 212.)	650	(516.- 857.)	810	(660.-1018.)	3700	(2920.-4681.)	9760
Mt/y	2002	173	(118.- 244.)	650	(516.- 835.)	820	(660.-1015.)	3700	(2967.-4669.)	9760
Mt/y	2003	183	(125.- 244.)	670	(525.- 853.)	860	(670.-1048.)	3800	(2977.-4681.)	9760
Mt/y	2004	190	(135.- 245.)	710	(559.- 931.)	920	(723.-1123.)	3900	(2979.-4572.)	9760
Mt/y	2005	190	(142.- 245.)	760	(592.- 943.)	950	(791.-1132.)	4000	(3212.-4632.)	9760
Mt/y	2006	182	(141.- 245.)	790	(639.- 949.)	980	(829.-1135.)	4000	(3461.-4707.)	9760
Mt/y	2007	177	(139.- 229.)	810	(655.- 958.)	990	(838.-1149.)	4000	(3492.-4757.)	7840
Mt/y	2008	174	(137.- 233.)	820	(661.- 964.)	1000	(837.-1157.)	4000	(3483.-4702.)	5920
Mt/y	2009	168	(135.- 205.)	810	(650.- 933.)	980	(819.-1098.)	4000	(3461.-4800.)	4000
Mt/y	2010	172	(137.- 200.)	820	(635.- 919.)	990	(784.-1091.)	4000	(3700.-4921.)	2080
Mt/y	2011	149	(120.- 208.)	790	(655.- 939.)	950	(827.-1059.)	4400	(4044.-4700.)	160

Table 38: Emission estimates for UK, IRE and NWEU with uncertainty (5th – 95th %ile).

5.2.9 Nitrous oxide

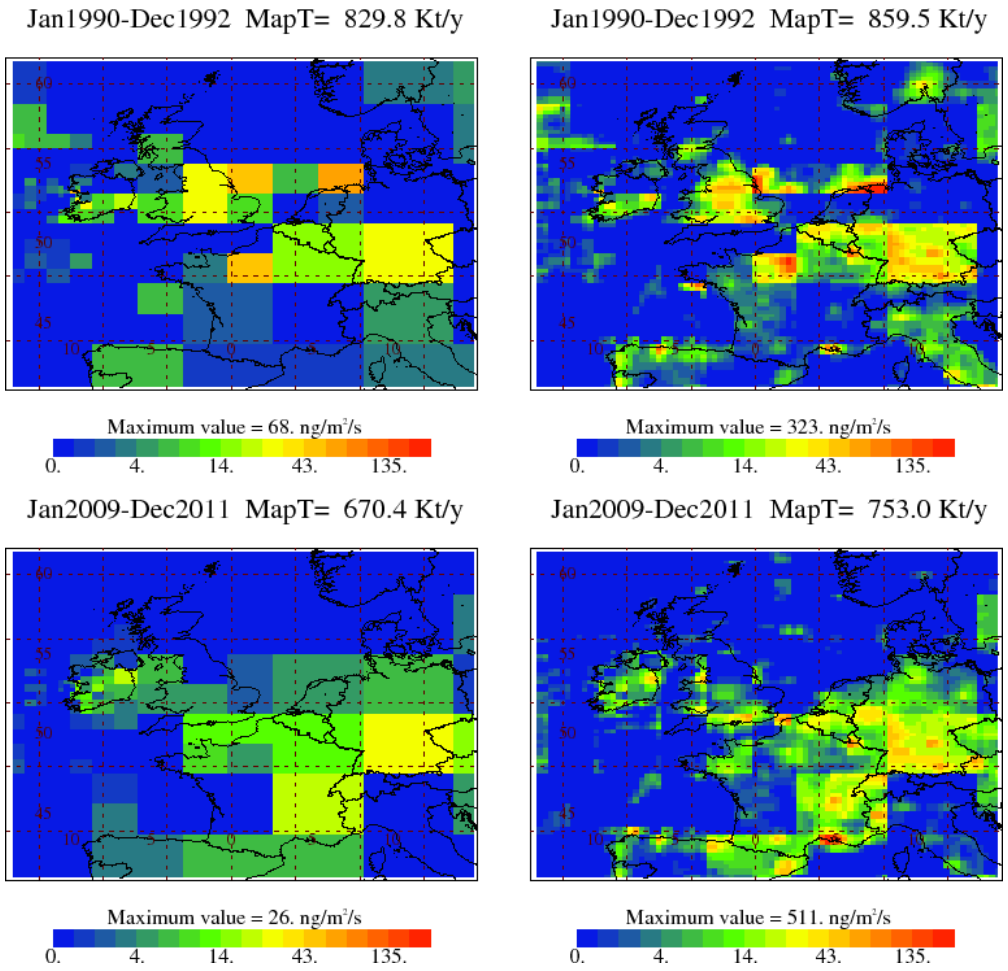

Figure 160: NAME-inversion emission estimates for 1990-92 (upper) and 2009-11 (lower). On the right hand side the emissions per grid box have been re-distributed based on population.

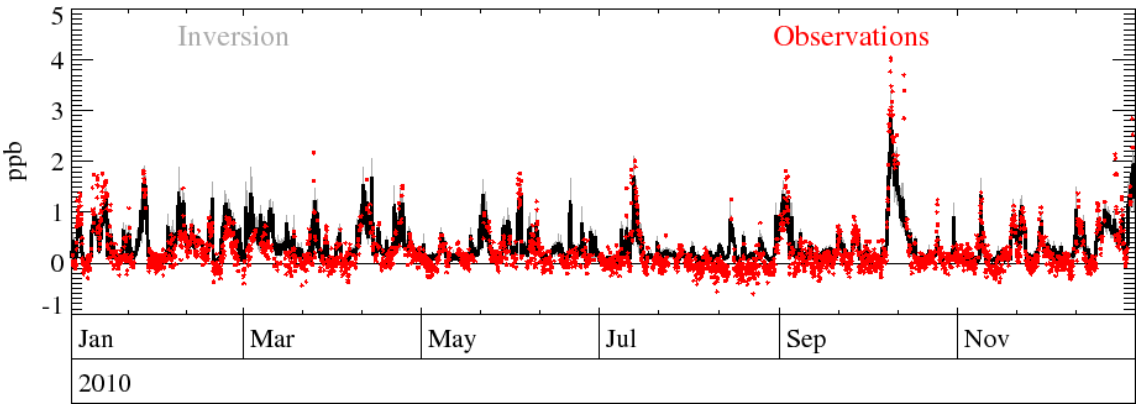

Figure 161: Example time-series of observations Vs. model using best-fit emission estimates.

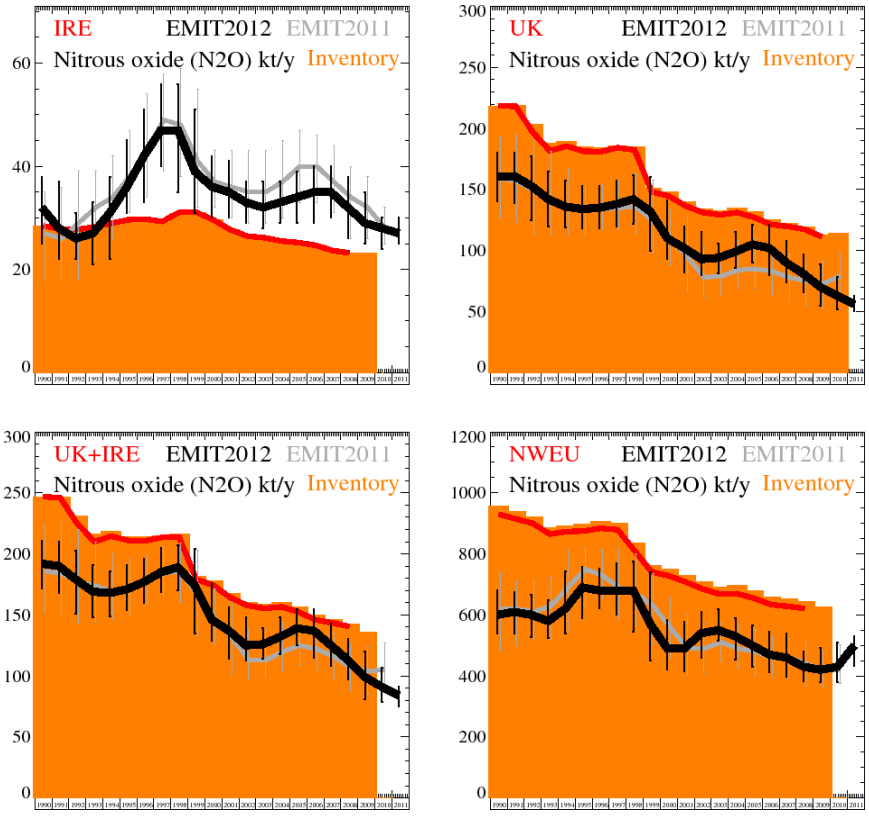

Figure 162: Inversion emission estimates for IRE, UK, IRE+UK and NWEU. Uncertainty bars represent the 5th and 95th percentiles. Orange bars represent UNFCCC emission estimates from the 2012 inventory. Grey (EMIT) and red (UNFCCC) are emissions as estimated last year.

Unit	Year	IRE	(5th-95th)	UK	(5th-95th)	UK+IRE	(5th-95th)	NWEU	(5th-95th)	Number
kt/y	1990	32	(25.- 38.)	161	(140.- 180.)	192	(172.- 211.)	600	(540.- 682.)	1920
kt/y	1991	28	(22.- 37.)	161	(139.- 180.)	190	(168.- 210.)	610	(540.- 676.)	3840
kt/y	1992	26	(22.- 31.)	153	(125.- 177.)	179	(151.- 203.)	600	(527.- 665.)	4000
kt/y	1993	27	(21.- 33.)	142	(120.- 165.)	169	(148.- 191.)	580	(523.- 649.)	4000
kt/y	1994	31	(22.- 38.)	136	(119.- 157.)	168	(149.- 186.)	620	(539.- 743.)	4000
kt/y	1995	36	(31.- 45.)	134	(118.- 153.)	171	(154.- 191.)	690	(590.- 757.)	4000
kt/y	1996	42	(33.- 51.)	135	(118.- 153.)	177	(160.- 196.)	680	(621.- 753.)	4000
kt/y	1997	47	(40.- 56.)	138	(120.- 157.)	185	(169.- 205.)	680	(602.- 770.)	4000
kt/y	1998	47	(35.- 56.)	142	(122.- 162.)	189	(170.- 207.)	680	(545.- 774.)	4000
kt/y	1999	39	(31.- 51.)	132	(100.- 160.)	174	(135.- 204.)	570	(450.- 739.)	4000
kt/y	2000	36	(30.- 42.)	110	(93.- 141.)	146	(129.- 176.)	490	(420.- 582.)	4000
kt/y	2001	35	(30.- 41.)	102	(82.- 120.)	137	(114.- 156.)	490	(416.- 577.)	4000
kt/y	2002	33	(29.- 37.)	93	(80.- 115.)	125	(113.- 148.)	540	(460.- 609.)	4000
kt/y	2003	32	(28.- 37.)	94	(81.- 106.)	126	(114.- 139.)	550	(515.- 620.)	4000
kt/y	2004	33	(29.- 37.)	99	(86.- 115.)	132	(118.- 148.)	530	(454.- 589.)	4000
kt/y	2005	34	(29.- 39.)	105	(90.- 121.)	139	(125.- 155.)	500	(430.- 566.)	4000
kt/y	2006	35	(29.- 40.)	102	(80.- 121.)	137	(115.- 155.)	470	(413.- 546.)	4000
kt/y	2007	35	(30.- 40.)	90	(74.- 108.)	125	(108.- 143.)	460	(397.- 538.)	4000
kt/y	2008	32	(26.- 38.)	81	(66.- 97.)	113	(97.- 130.)	430	(384.- 480.)	4000
kt/y	2009	29	(25.- 35.)	70	(55.- 89.)	99	(81.- 120.)	420	(379.- 493.)	4000
kt/y	2010	28	(24.- 30.)	63	(52.- 78.)	91	(79.- 107.)	430	(379.- 509.)	2080
kt/y	2011	27	(25.- 30.)	56	(50.- 63.)	84	(75.- 91.)	500	(433.- 531.)	160

Table 39: Emission estimates for UK, IRE and NWEU with uncertainty (5th – 95th %ile).

6 Aircraft GEOmon data analysis and validation

6.1 Introduction

This work employs vertical profiles of methane from aircraft measurements over three European locations along with modelled profiles to validate surface emissions in an independent way. At the same time, further knowledge is gained about the transport model and processes affecting and influencing the inversion methodology employed for the estimation of surface emissions of methane on a European scale. From all available aircraft profiles, 41 have been analysed. These are profiles with three or more observations and no recorded errors. From these, 28 are shown and discussed in this work.

The European emissions used in the estimation of modelled mixing ratio perturbations (above baseline), are two types: From inversion modelling and from bottom-up methods (EDGARv4.1 in this case). In the comparison of measured and modelled profiles, it is important to remember that the aircraft data reflect the emissions transported from the surface over the previous few days, whereas the modelled estimates use surface emissions that are annual averages and do not capture transient episodes. Another thing to consider in the validation process and analysis, is that the there are two components in the modelling process. One is obtaining the modelled perturbations, the second obtaining the background (baseline) mixing ratio values. Errors or bias in either of these processes can result in discrepancy between the observed and modelled values.

Many of the modelled profiles manage to capture the shape and values of the observations.

Categories of cases:

A. Good agreement: GRI profiles of 12/10/06, 01/12/06, 06/12/06, 02/02/07 associated with westerly or northerly flow from a clean air sector. The ORL profiles of 13/03/06, 06/06/06 and 21/07/06 have good agreement and the approaching flow is from three completely different directions. HNG profile of 04/03/07.

B. Cases of upper level influence: GRI profiles of 06/06/06 and 08/06/06. Stratospheric intrusion and mixing more than a week earlier affected free troposphere mixing ratios on these days.

C. Orographic and other processes associated with complex flow: GRI profile of 15/09/06, ORL profiles of 24/01/06 and 19/07/06, HNG profiles of 02/12/06 and 23/07/06.

D. Unresolved cases with no clear plausible explanation found: GRI profile of 22/09/06, ORL profile of 05/09/06, 19/07/06, HNG profile 25/05/06.

E. Cases where background in possible error: ORL 11/04/06, 11/05/06, 09/08/06, HNG 31/01/07, 22/04/07.

F. Or other kind of transport: HNG 23/09/06 and 03/04/07.

G. Indicative of surface emissions in error: ORL profiles of 10/02/06, 02/06/06, 07/09/06.

As a final note, transient or time dependent emissions are not captured in the modelling. As a result of these effects, discrepancies between the measurements and modelled profiles cannot be deciphered in absence of further independent information.

6.2 Methodology and data

6.2.1 Aircraft data

Vertical profiles of CH_4 were collected as part of the CARBO-EUROPE project (http://www.ce-atmosphere.cnrs-gif.fr/), using small aircraft at a frequency of 1 to 3 flights per month. Typically, air samples were collected at 10 altitude levels from 100 m above the surface up to 3 km and

were analyzed at the LSCE facility with a gas chromatographic system [*Ramonet et al., 2002*, *Schmidt et al.*, 2006]. Profiles over three European locations, for years 2006 and 2007, are used in this work:

- **GRI** (Griffin Scotland 56.55° N, 2.98° W). The flights of this campaign are over Angus Tower station (535 m asl): 222 m above ground on a hill 313 m on mountainous terrain.
- **ORL** (Orleans France 47.83° N, 2.5° E). About 100 km South of Paris. GIF_SUR_YVETTE (48.71° N, 2.15° E)
- **HNG** (Hungary 46.95° N, 16.35° E). These flights are above the tall tower Hegyhatsal in Hungary. The instrument is at 96 m above ground on a hill 248 m (total altitude 344 m asl).

All aircraft profiles have been recalibrated for this work to the NOAA04 scale to enable comparison with modelled data. Table 40 gives a list of dates and stations used in the model comparison and validation. The total number of available data is more than those listed in table 40. For the analysis, validation and further discussion, only profiles with at least three measurements and no recorded errors were considered.

6.2.2 Modelling set-up & assumptions

Modelled concentrations $\mathbf{O_m}$ at each point in the aircraft profile were obtained from:

$$\mathbf{O_m = B + O' = B + M \times E} \quad \ldots(3)$$

In (3), **M** is the transport matrix that describes the way surface emissions are diluted from source to a measurement point [*Manning et al.*, 2011]. To obtain the transport or dilution matrix, a unit mass is released from each point in the profile that there is a measurement (Figure 163a), running back in time for 13 days using the Met Office Lagrangian dispersion model NAME [*Jones et al.*, 2007], with meteorology from the Met Office Unified model (UM) at global (0.56° × 0.37° in 2006) and higher resolution (0.11° × 0.11°) over Europe. **E** represents the matrix of surface CH_4 emissions and **B** the background concentration values. Surface emissions used in this analysis were obtained from top-down inversion modelling [*Athanassiadou et al.*, 2011] and inventories using bottom-up methodology (EDGARv4.1).

Figure 164 shows surface emissions maps of methane for 2006 and 2007 from the inversion technique (left) and also the a-priori emission maps from the inventory, for the same years (right). Overall, there are similarities between the two emission set, such as high emissions in the Benelux area. There are two differences though, of somewhat importance. The less important one is that the emissions map from the inversion has some emissions over the sea on the western boundary. The other, and more important, is the absence of emissions over the south-western part of the European Alps, an area where the bottom-up inventory has high emissions. This results from unresolved processes in the transport model near orography and is a key issue that effects emission estimation in the inversion process. Some implications of this are highlighted in the discussion of certain profile cases described later in this section.

Multiplication of the transport matrix with the regional emissions only provides modelled perturbations. In order to be able to compare with the measurements, a suitable background field is needed. The background (baseline) values were obtained here from specific runs of the TM5 model [*Bergamaschi et al*., 2010, *Corazza et al.*, 2011, *Meirink et al.*, 2008] using the method described in [*Rödenbeck et al.,* 2009]. The driving meteorological data for TM5 are from ECMWF ERA-Interim archive (http://www.ecmwf.int/research/era/), with the original resolution coarsened both in the vertical (25 levels from original 60), and in the horizontal (6°×4°on the global domain, and 1°×1° over Europe).

NAME was also used to produce air history (dilution) maps from the 0-5 km, 5-10 km and 10-18 km layers, Figure 163b. These were obtained by running the model backwards with thousands of particles from each measurement location for 13 days and outputting two types of time integrated concentrations [gs/m^3]: (a) time integral taken oven the whole run and (b) 24 hr integrals of concentrations for each day, representing the locus of thousands of back-trajectories in that 24 hr period. Overlap of these with the relative position of high PV areas (representative of stratospheric air) was used to identify and trace air of stratospheric origin within the troposphere. Parameters such as PV, water vapour and O_3 mixing ratios, were retrieved from the ECMWF operational analysis archives (T799L91 model, ca 25 km horizontal resolution, at 00UTC, 06UTC, 12UTC and 18UTC), for the period of interest and used to identify the location and structure of the tropopause, stratospheric intrusions and thus areas of potential mixing.

To facilitate the discussion of various cases, the following terminology is adopted: Modelled mixing ratios using emission maps from inversion and from the bottom-up inventory will be referred to as R2a and Ev4.1 respectively.

6.3 Discussion of cases

6.3.1 GRI profiles

In half of the GRI profiles shown, the differences between the observed and modelled mixing ratios are less than 10 ppb and the overall shape of the measured profile is capture well by the modelling. These are late autumn and winter cases and the approaching flow is from a westerly narrow path from the Atlantic or from a clean northerly sector. The other half of the cases though are different, here the modelled and observed profiles do not agree albeit for different reasons. These are discussed below. All GRI profiles are shown in Figure 165.

15/09/06: In this case, the modelled data from both R2a and Ev4.1 overestimate the observations below 1600 m and underestimate them above this level. A big difference is also observed between the modelled values at 800 m, with the Ev4.1 overestimating observations by more than 30 ppb over R2a (20 ppb higher than observed mixing ratio). In order to find a plausible explanation, we look at air history maps i.e., at the surface contribution to the various levels, Figure 168. Examination of air history for the 800 m level shows strong contributions from three areas. One is the area south of the Alps (N. Italy, Ligurian Sea) where the emissions from the inversion are much less than in EDGAR. This explains the big difference between the modelled values at 800 m. The air history at 1100 m is very similar to that seen at 800 m but with the Alpine area contribution slightly reduced. This is consistent with the smaller difference between the modelled values at 1100 m. There is not much surface contribution to the upper levels and the underestimation of the observed mixing ratios (10 ppb or less) is more difficult to explain. It could be party due to unresolved processes in relation to orography or upper level transport not captured in the background values.

22/09/06: This profile is a week later and in this case, the modelled mixing ratios underestimate the observations at all levels, by 10-20 ppb. Air history maps (Figure 168) show that at low levels the strongest contribution is from a south-west area that covers the Midlands, Wales, Bay of Biscay before splitting into two distinct parts. One is coming directly from a narrow strip with a westerly orientation and the second from the south along Portugal and Gibraltar area. Unless there is upper level transport from somewhere, the other possibility is that the TM5_b baseline is rather low in this case of southerly and westerly transport.

06/06/06 – 08/06/06: On 6th June, high mixing ratios are observed closer to the ground which are reduced rapidly to a constant with height profile with values 70 ppb less than the values near the surface. The observed values above 1600 m are much less than typical mixing ratios of free troposphere methane for these latitudes. On the 8th, the near surface and 3 km values are equal, but the minimum at 1600 m in the observed profile has the same low values as 2

days earlier. The modelled data fail to capture the shape of the observed profiles, especially on the 8th June. Surface air history maps (Figure 169), show that the air approaches GRI on a circular path with main contributions up to 1600 m from an area to the west and south-west of the UK.

Further back runs were conducted in this case, to identify contribution to the various levels from different layers in the atmosphere (not just surface), Figure 163b. Figure 170, shows the contribution from the 0 - 5 km to the 3100 m level for the 6th and 8th June (bottom row). The top and middle rows of Figure 170, show the contribution from the 5 – 10 km layer to the 3100 m and 1600 m respectively, for the 6th and 8th June. The grey shaded areas around 37° N and from 40° W to 20° W, is where a stratospheric intrusion has mixed down low methane concentrations 6-9 days before the observed low values. The stratospheric intrusion areas are shown in Figure 171 as areas of high potential vorticity (PV) on the 250mb surface. The more in depth investigation has revealed that this is a case of stratospheric intrusion influencing the mid troposphere concentrations. Mixing resulting from this kind of process is not captured by the coarse meteorology used in TM5 model.

6.3.2 ORL profiles

Most of the profiles are characterised by a well mixed (constant with height mixing ratios) boundary layer (BL), and sharp transition to constant with height but lower mixing ratio values aloft. The BL height ranges from 500 m to 1500 m depending on the time and season of the measurements. The aircraft measurements start quite low (200 m) in this campaign, enabling us to observe inside/outside the BL as well as transition zones. In most of the ORL cases, the modelled profiles capture this basic shape of the measured profiles reasonably well. Of the 12 cases shown, good agreement is found between observations and modelled results for 3, whereas further 4 agree well in parts of the profile, usually in the BL. In 3, the modelled profiles overestimate the observations (usually in the BL), whereas in another they underestimate the observations. Finally, there is one profile which is very difficult to explain (discussed later).

In most of the cases when shape of the observed profile is captured (and the BL from the UM is a good estimate of the real BL height), the air flow history has two distinct regimes: At low levels (inside BL) the air is of polluted origin whereas higher up it comes from a clean area or void of surface contributions. In these cases, the agreement, over or under –estimation of the measured profile will depend on the accuracy of emissions along the path followed en route to ORL. Out of the 12 cases shown, 3 diverge from this pattern with the flow being from the same direction at all heights, albeit reduced.

24/01/06: In this case, the modelled profiles agree in the overall shape of the profile with the observations, but there is under-prediction in the modelled mixing rations compared with the observations (as much as 60 ppb inside the BL). Examination of air history (Figure 172), shows that at low levels (up to 800 m), the air comes mainly from a relatively thin strip north and east of the Alps. Higher up there is little contribution from the surface and what there is, is from the Atlantic. The discrepancy between modelled and observed mixing ratios close to the ground can therefore attributed to not well defined processes and emissions near large orographic features. The latter is further supported by the fact that modelled perturbations using emissions from the inversion (R2a), further underestimates observations by 20 ppb compared to the ones from EDGAR (Ev4.1).

10/02/06: At low levels, most of the contribution is from a relatively narrow strip in a straight NNW line from ORL and Eastern cost of UK. The influence diminishes with height. In the BL, the R2a modelled profiles over-estimate the observed one by 10 ppb, whereas as the Ev4.1 by 40 ppb. There is no surface influence at 2500 m or 2000 m and this is captured well by both modelled solutions. It is postulated at this point that the bottom-up emissions inventory is too high for the East UK.

13/03/06: This is a case where the modelled and observed profiles agree very well, even to small detail as in the kick at 2000 m. From near the surface to 1000 m, the origin of air is the same and from a thin almost E-W oriented strip across Central Europe and a much broader area across Eastern Europe (Figure 173). Higher up, the flow is from the Atlantic. At first glance, this case has similarities, in terms if air history, with the one of 24/01/06. Closer inspection thought shows that the flow is not connected to the Alps in this case, making the case for influence/unresolved processes near orography in the case of 24/01/06 stronger.

11/04/06: This is similar to the 10/02/06 case in terms of NNW air origin (Figure 173). In this case thought the contribution is from a bit further to the East, off the coast of UK rather than the east UK itself. As a result, the modelled and observed profiles are in perfect agreement in the BL. Air history is identical from low down to 1500 m, northerly. At 2000 m the origin is similar but with reduced 'strength'. There is no surface influence above 2000 m. Consistent with the transport picture, the modelled perturbations are only slightly reduced at 2000 m, compared to near surface values, and almost zero above 2000 m. Most likely, the TM5_b fails to capture the sharp decrease at 2km, being as a result of too high value and therefore contributing to the discrepancy between modelled and observed profiles.

11/05/06: This is a case of 'wrong BL in the model' resulting to under/over estimation of observations below/above the true BL height. Otherwise, the comparison between modelled and observed profiles is not that bad. The air in this case approaches from the same easterly direction, and in a scorpion like shape, at all heights. At low levels, up to 1 km, there is also a contribution from a westerly direction along the English Channel and SW England. The 10 ppb difference between R2a and Ev4.1 is attributed to higher emissions in the latter, along the air history path.

02/06/06: This is case 'between' the 10/2/06 and 11/04/06 ones and is discussed here to provide extra evidence to the arguments presented in these two cases. The flow is again from a NNW direction with most of the influence from off the UK coast, apart from a little blob over the Central East England (Figure 175). As a result, the R2a modelled values agree well with the observations whereas the Ev4.1 ones overestimate them.

06/06/06: This case is only shown here because of the GRI one on the same day. Otherwise it is the same as the previous ones with NNW flow (fig 175), were the modelled and observed profiles agree very well.

19/07/06: Now this is a corker one where the modelled profiles and observations seem to relate to a different case. The air history (Figure 176), shows flow from around the Alps. At low levels most of the contribution is from the south and eastern parts, whereas higher up the contribution from north of the Alps becomes stronger. The case merits further investigation.

21/07/06: Easterly flow in this case with most of the contribution from eastern part of France and Spain, Figure 176. Model and observations agree reasonably well.

09/08/06: Yet another one with predominant influence from eastern UK where the R2a modelled profiles agree with the observations and the Ev4.1 ones over-estimate. Modelled perturbations are almost constant with height up to 1000 m, then virtually zero above that height. It can be argued therefore that above 1000 m, the TM5_b is too high and does not capture the slope of decrease with height of the observations. As a result, the modelled mixing ratios are much higher than the observations.

05/09/06: From surface to 1000 m the major contribution is from a narrow strip with EW orientation, and no much surface contribution above that (Figure 178). Both R2a and Ev4.1 modelled profiles overestimate the observations inside the BL. The TM5_b seems to be a bit too high in this case too.

07/09/06: Generally westerly influence over a broad area covering southern UK and bay of Biscay. Modelled mixing ratios overestimate the observations by about 20 ppb near the surface to 60-70 ppb at 1500 m. This is because the BL height is too high in the model. Moreover, the surface contribution at 1500 m is as strong as at 200 m, according to the model and consistent with the modelled mixing ratios.

6.3.3 HNG profiles

Aircraft and modelled profiles for the HNG campaign are shown in Figure 169. In many cases the modelled profiles represent the measurements reasonable well. Small discrepancies can be attributed to differences between the actual and model boundary layer or TM5 baselines been too high at upper levels (31/1/07). The case of 22/04/07 is similar to the ORL 09/08/06, where TM5_b fails to model the transition from high to low values at about 1500 m, resulting in the modelled profiles overestimating the observations above this height. All HNG profiles are shown in Figure 167. A selection of cases are discussed below.

25/05/06: In this case, the observed profiles show little variation with height (less than 10 ppb). The modelled profiles agree well up to 1.5 km, but slightly underestimate the observed profiles from 1.5 – 3 km. The air history maps show a rather consistent pattern with height (Figure 179), with a strong surface contribution along an East-West oriented narrow band that crosses Austria, South Germany and Northern France before turning straight north to the west of UK. The source of underestimation of the modelled data in the 1.5-3 km layer is not clear at this point.

23/09/06: This case is an interesting one of *Eastern pollution transport.* From surface to 1500 m, the air history (Figure 179), has a hook shape with the major contributions from Hungary, Romania, Ukraine, Russia before turning west over Baltic Sea, North Sea, North England, Northern Ireland. At 1250 m there is second maximum contribution from Russia, at the edge of our domain. This becomes more pronounced at 2250 m. Surface emissions from Eastern Europe are major contributors at all heights. As a result, the observed profile is rather uniform with height. The modelled mixing ratios underestimate the observed ones by about 20 ppb inside the BL. Higher up, the modelled mixing ratios decrease with height and as a result, the difference with observations increases to 50 ppb. Although there is indication in the transport of surface emissions from Eastern Europe, the model fails to capture the full magnitude. It is interesting that in this case, the modelled perturbations show significant signal up to 3250 m (usually the become zero above the BL). The case of 3/4/07 (not shown) is also one where the modelled mixing ratios are less than the observed ones in the BL (low levels anyway) and this is also a case where the air has come from eastern direction. The first thought is that surface emissions from that sector (both from the inversion and the inventories) are too low. But there is also the possibility that the TM5 baseline is also a bit too low when the air is from an eastern direction. Finally, it is unfortunate that the major emission contributor is at the edge and outside our domain's eastern boundary. So there is a possibility that this is the reason we underestimate the mixing ratios, especially at high levels were the main contribution is from Russia (eastern boundary and outside).

02/12/06: This is yet another interesting case. The observed profile shows very high mixing ratios in the BL (~800m) with a very sharp decrease and constant low values above that. Although the modelled profiles get the overall shape well, there are a couple of points worth mentioning that are what makes this case interesting. Usually, the modelled perturbations using surface emissions from inversion solutions and from inventories, agree within 5-10 ppb and when they do not, the perturbations using bottom-up are larger. It is interesting that in this case, that although the modelled perturbations from both surface emissions collapse to zero above 1750 m they differ by 60 ppb inside the BL. Moreover, perturbations from the inversion solution overestimate the observed values whereas the ones from bottom up inventories underestimate them by similar amount. At 1250 m, both types of perturbation estimates, overestimate the observations by the same amount (40 ppb). Examination of the air history

maps (Figure 180), show strong contributions from a relatively local area between the surrounding orography (basin formed by the Alps, Dinaric Alps, Balkan Mountains, Carpathian mountains) up to 1250 m. Above this level, there is very little surface contribution. If anything, there is more surface contribution at 3250 m than at 2250m. Closer inspection of surface emissions in the area of strong contribution shows that those obtained from the inversion solution are higher than those in the bottom up inventory. This explains the higher modelled values from top down emissions than bottom up ones. The discrepancy at 1250 m between the observations and modelled values could be attributed to missing, or not well captured orographic processes in the transport model.

23/07/07: This is a case of *Alpine circumvention*. It is similar and relates to the ORL 19-21/07/06 one. At low the lower levels (up to 1250 m), the flow approaches HNG from both the south and north sides of the Alps, the later being the dominant contribution. There is also a strong contribution from the English Channel, Channel Islands region. Further up, the main contribution is from the region south of the Alps and in particular the North Italy and Ligurian Sea, with a second contribution from Iberian Peninsula. The higher modelled profile from bottom up inventory is due to the higher surface emissions in this than the one from the inversion solution, along the path of air history. In particular, at levels above 1250 m there is a big difference between the two emission maps especially in the Po valley where the flow in not well represented in the transport model used for the inversion. The flow from Po valley does not reach stations used in the inversion. Over the Iberian Peninsula, the lack of stations also makes the emissions from the inversion not that reliable.

6.4 Summary

In this work, vertical profiles of methane obtained from various aircraft campaigns (GEOmon data) are compared with modelled profiles using annual average surface emissions from both inversion methods and from bottom-up inventories. In many cases there is reasonably good agreement between the aircraft measurements and modelled profiles. This gives us further confidence both in the modelling approach and the surface emissions estimated using the inversion modelling. Nevertheless, there are specific cases where significant differences occur between the modelled and observed profiles. These can be attributed (relate) to instances (reasons) where the various assumptions in the modelling process fall short. These are summarised and discussed below.

- Upper level stratospheric intrusions.
- Eastern pollution transport.
- Local effects due to complex flow in mountainous regions where transport is not well resolved.
- Baselines too high.
- Time dependency of emissions: In (1) we use emissions that are annual averages. Comparisons with aircraft measurements though, imply that the annual average emissions are representative at all times. Clearly, this is not always true.

Bottom-up inventories overestimate surface emissions over Eastern UK. On the other hand, emission estimates from the inversion methodology in the vicinity of the Alps, especially the southern and eastern sides, are unrealistic. It should be pointed out thought that this is an artefact of the stations set up and not the methodology itself. A suitable selection / availability of stations should significantly reduce this problem. Aircraft profiles can be used as an independent way to validate surface emissions and understand the physical processes in the inverse modelling.

Date	GRI	ORL	HNG	Special Runs
24/01/06		✓		
10/02/06		✓		
13/03/06		✓		
11/04/06		✓		
11/05/06		✓		
25/05/06			✓	
02/06/06		✓		
06/06/06	✓	✓		✓
08/06/06	✓			✓
19/07/06		✓		
21/07/06		✓		
09/08/06		✓		
22/08/06		✓		
01/09/06		✓		
05/09/06		✓		
07/09/06		✓		
15/09/06	✓			
22/09/06	✓			
23/09/06			✓	
05/10/06		✓		
12/10/06	✓			
17/10/06		✓		
15/11/06		✓		
01/12/06	✓			
02/12/06			✓	
06/12/06	✓			
15/12/06		✓		
26/01/07		✓		
31/01/07			✓	
02/02/07	✓			
04/03/07			✓	
03/04/07			✓	
19/04/07		✓		
22/04/07			✓	
06/07/07		✓		
09/07/07	✓			
23/07/07			✓	
24/07/07		✓		
08/08/07	✓			
09/12/07	✓			

Table 40: List of aircraft profiles

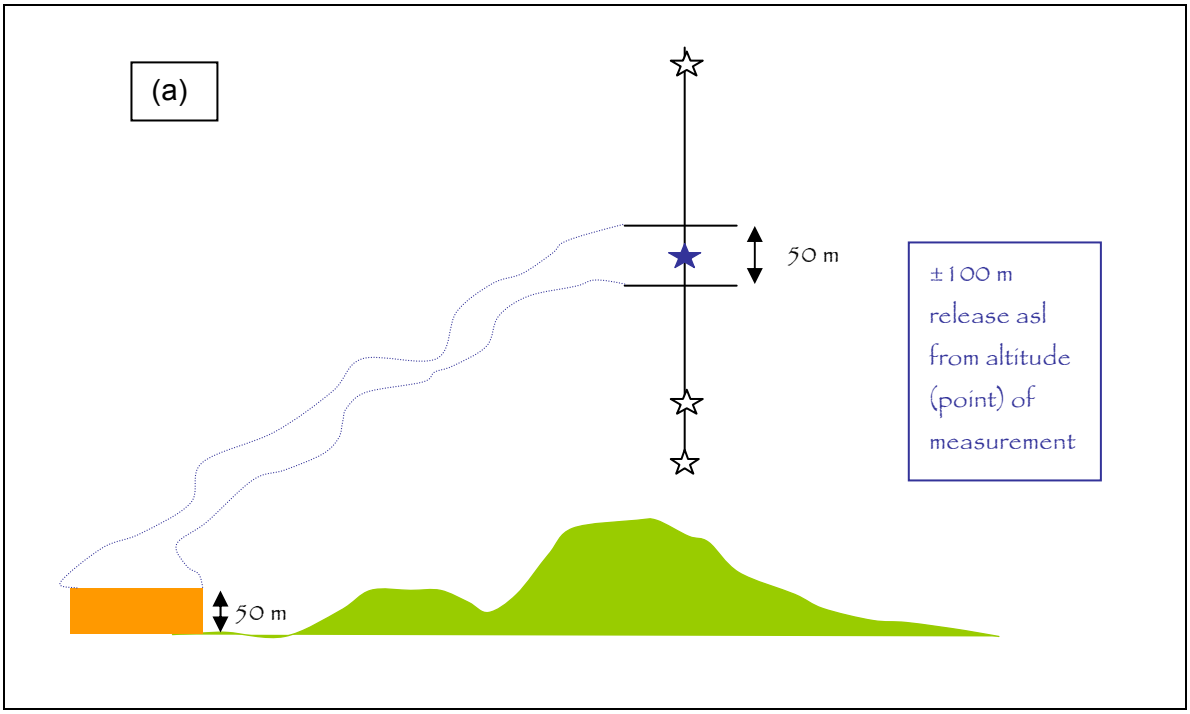

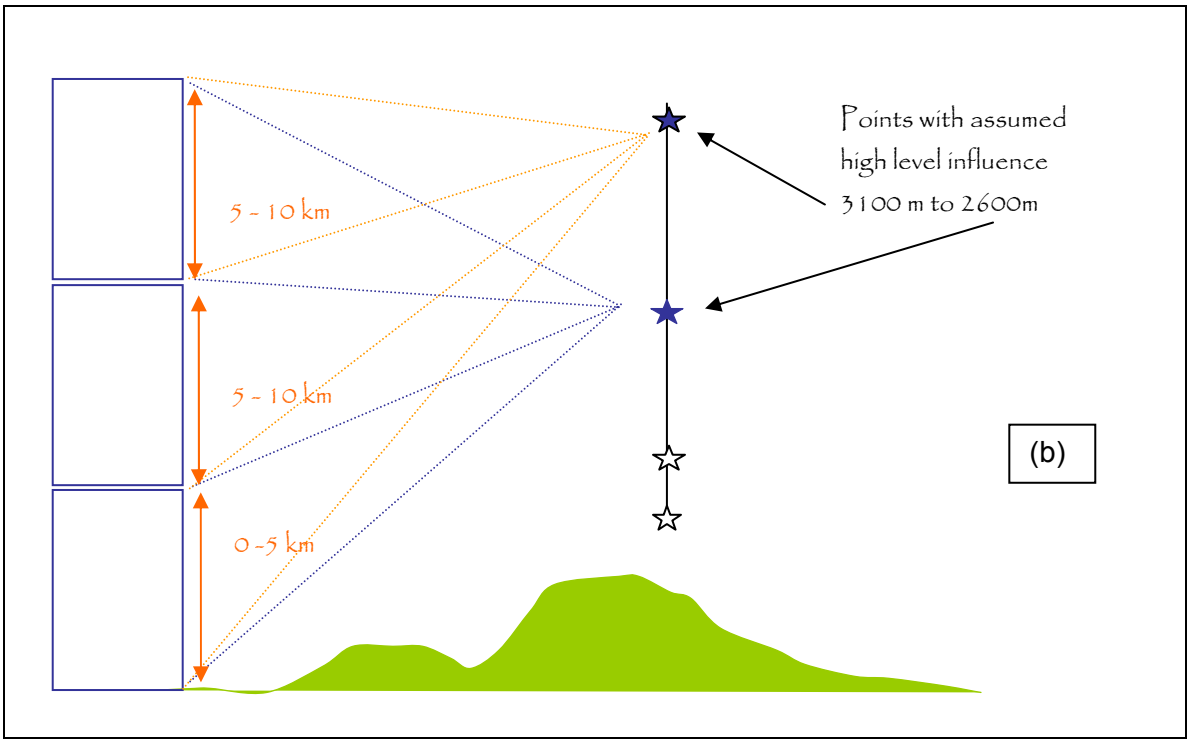

Figure 163: Schematic diagram of the back runs set-up. (a) Standard set-up, (b) schematic diagram of the special back runs GRI on 06/06/06 and 080606 and for ORL 060606.

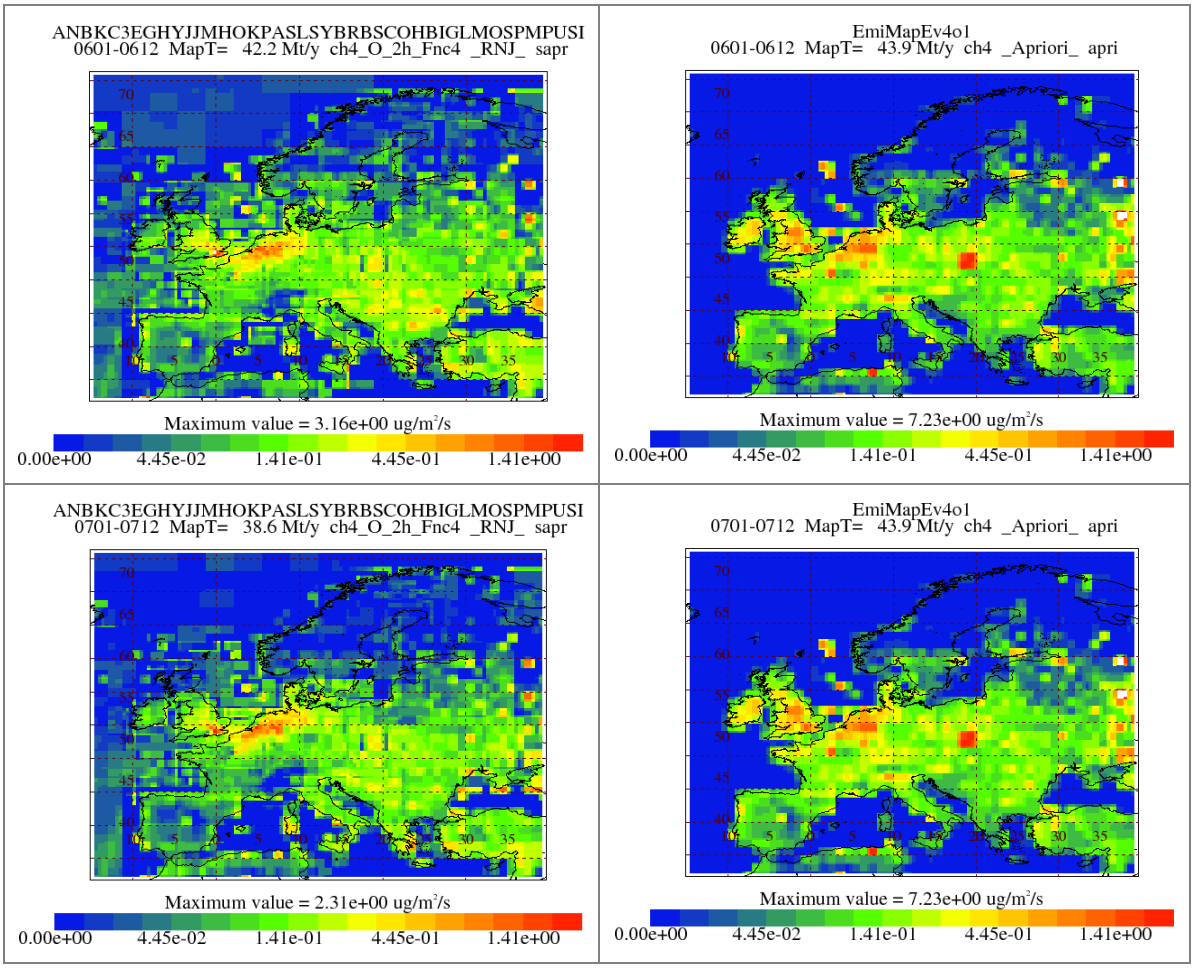

Figure 164: Surface emissions from inversion solution (left) and EDGARv4.1 (right). The top rows are for 2006, bottom 2007.

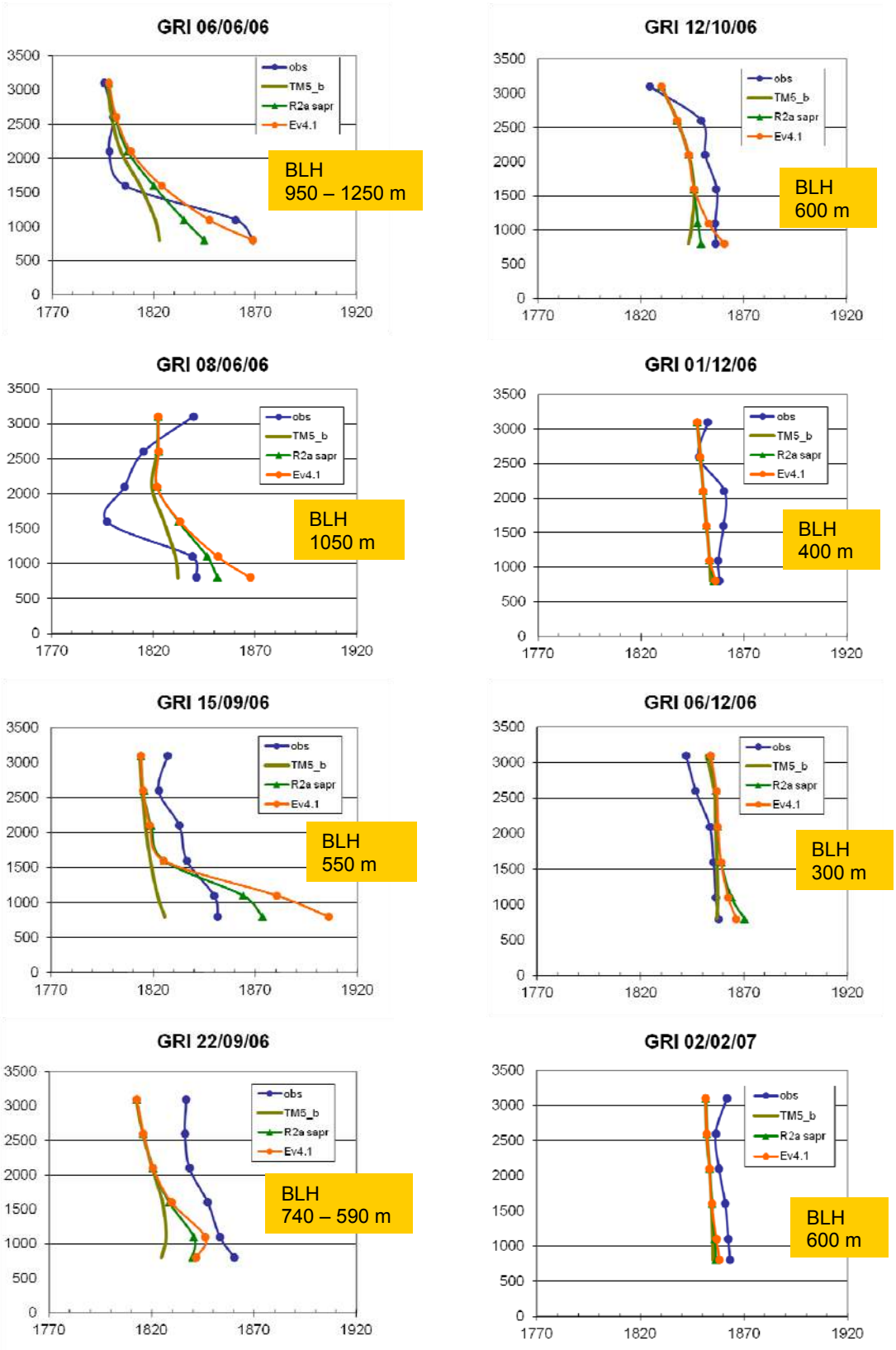

Figure 165: Mixing ratio profiles for GRI. Blue: Aircraft measurements, Tan: TM5 baseline, Green: Using surface emissions from inversion solution + TM5 baseline, Orange: Using EDGAR v4.1 surface emissions and TM5 baseline.

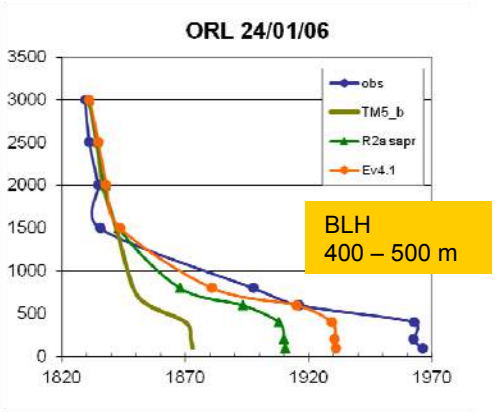
ORL 24/01/06
obs
TM5_b
R2a sapr
Ev4.1
BLH
400 – 500 m

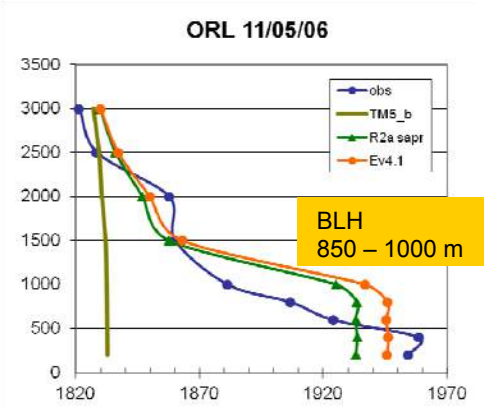
ORL 11/05/06
obs
TM5_b
R2a sapr
Ev4.1
BLH
850 – 1000 m

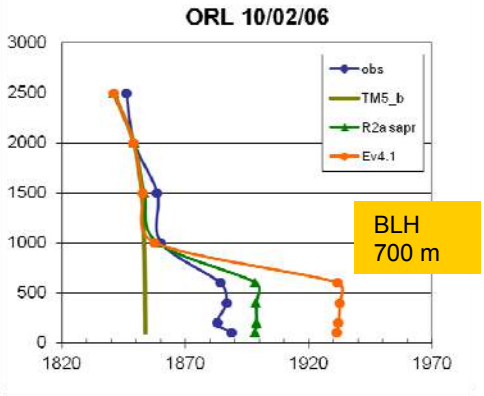
ORL 10/02/06
obs
TM5_b
R2a sapr
Ev4.1
BLH
700 m

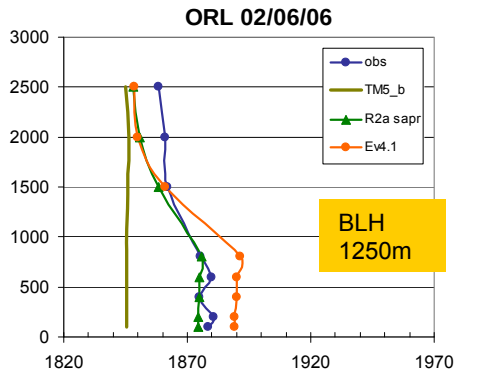
ORL 02/06/06
obs
TM5_b
R2a sapr
Ev4.1
BLH
1250m

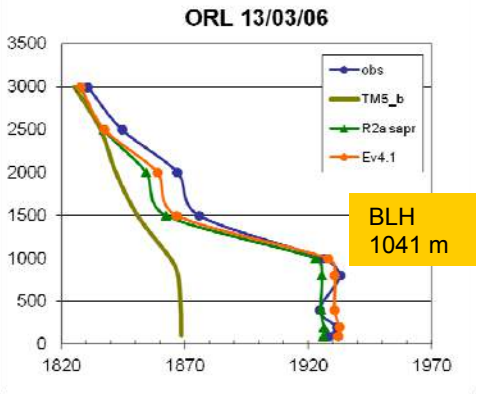
ORL 13/03/06
obs
TM5_b
R2a sapr
Ev4.1
BLH
1041 m

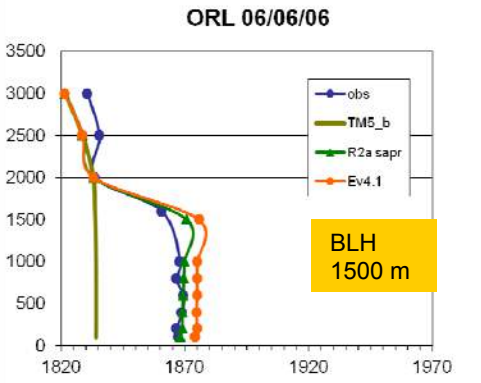
ORL 06/06/06
obs
TM5_b
R2a sapr
Ev4.1
BLH
1500 m

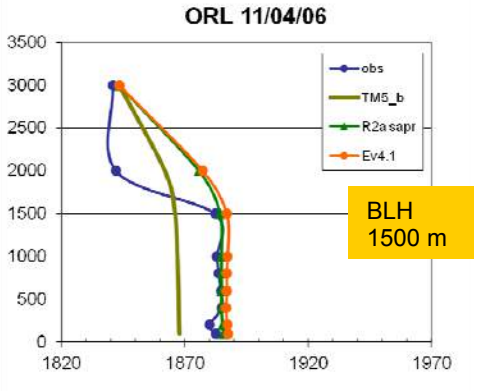
ORL 11/04/06
obs
TM5_b
R2a sapr
Ev4.1
BLH
1500 m

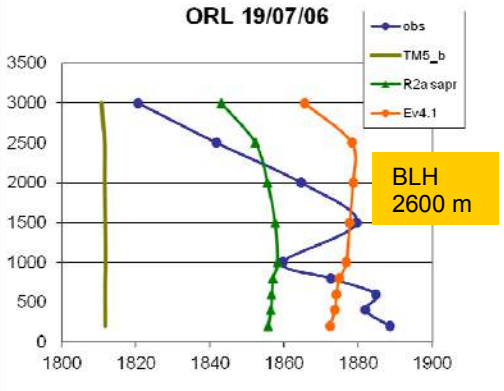
ORL 19/07/06
obs
TM5_b
R2a sapr
Ev4.1
BLH
2600 m

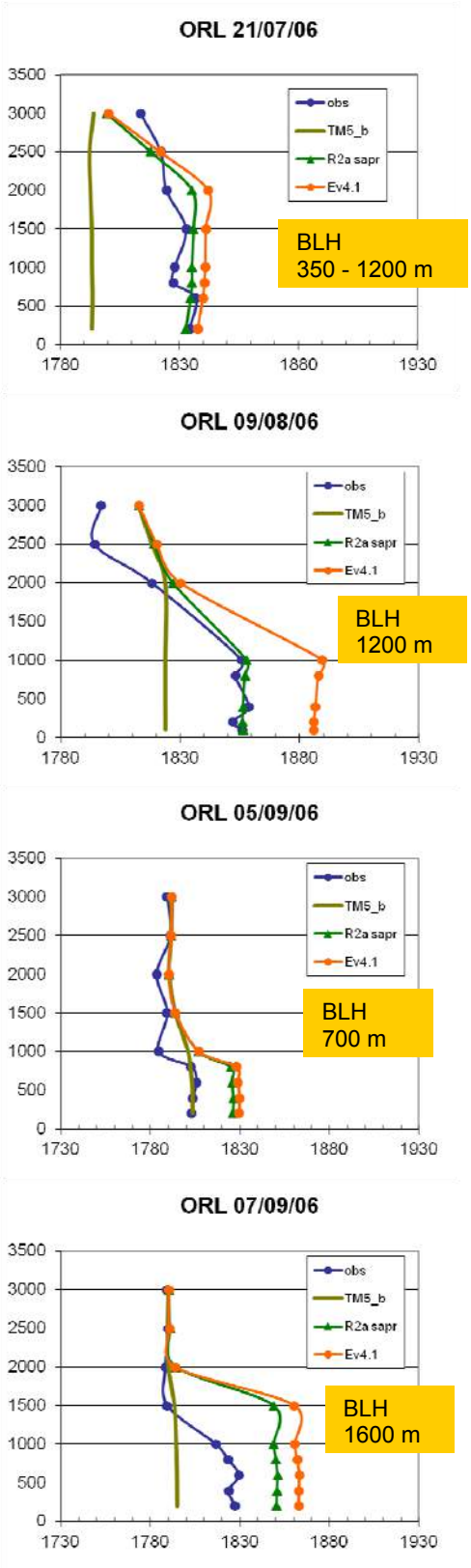

Figure 166: Mixing ratio profiles for ORL. Blue: Aircraft measurements, Tan: TM5 baseline, Green: Using surface emissions from inversion solution + TM5 baseline, Orange: Using EDGAR v4.1 surface emissions and TM5 baseline.

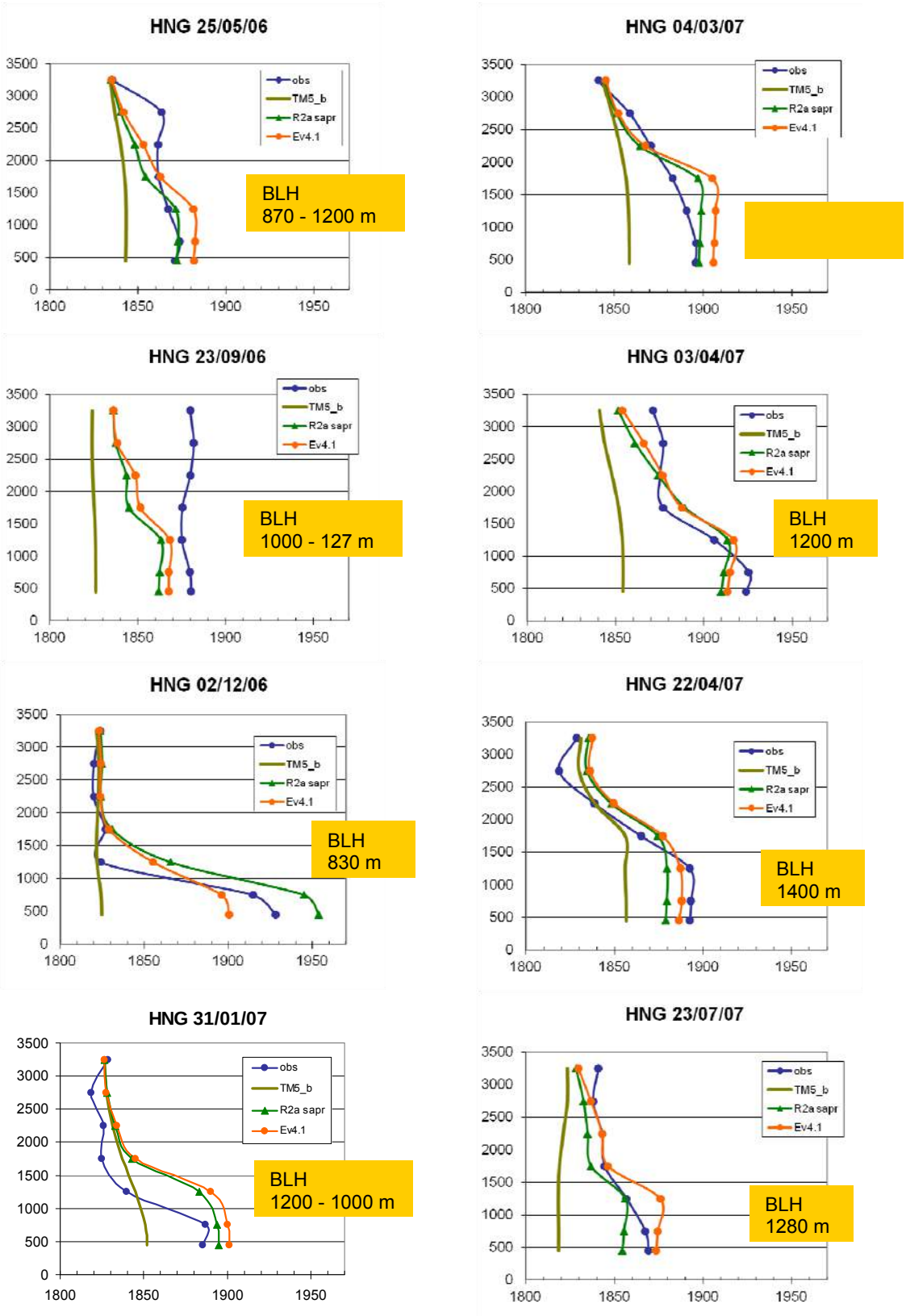

Figure 167: Mixing ratio profiles for HNG. Blue: Aircraft measurements, Tan: TM5 baseline, Green: Using surface emissions from inversion solution + TM5 baseline, Orange: Using EDGAR v4.1 surface emissions and TM5 baseline.

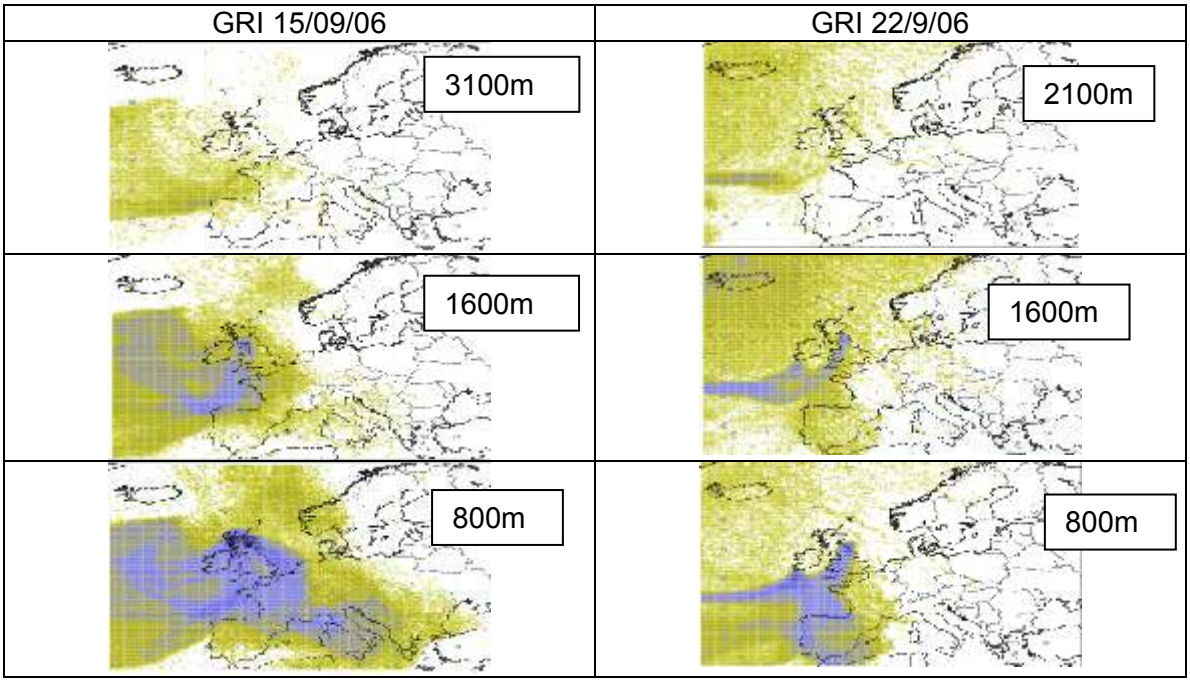

Figure 168: Surface contribution to various levels, for GRI on 15/9/06 and 22/9/06.

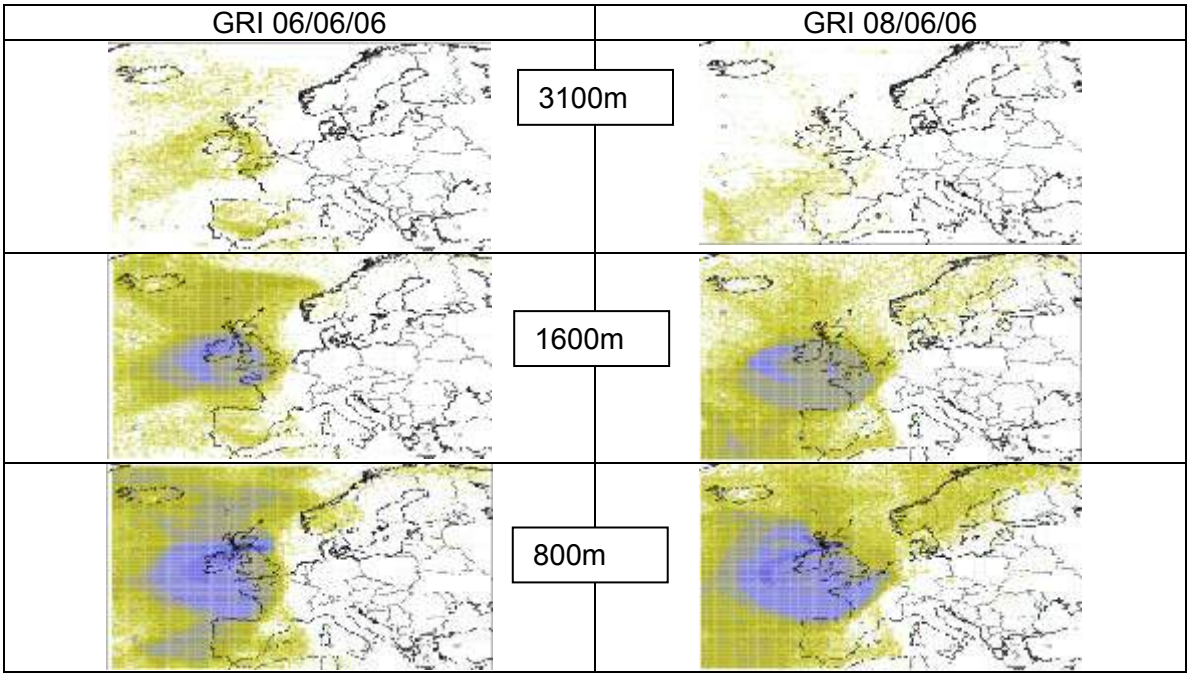

Figure 169: Surface contribution to various levels, for GRI on 06/06/06 and 08/06/06.

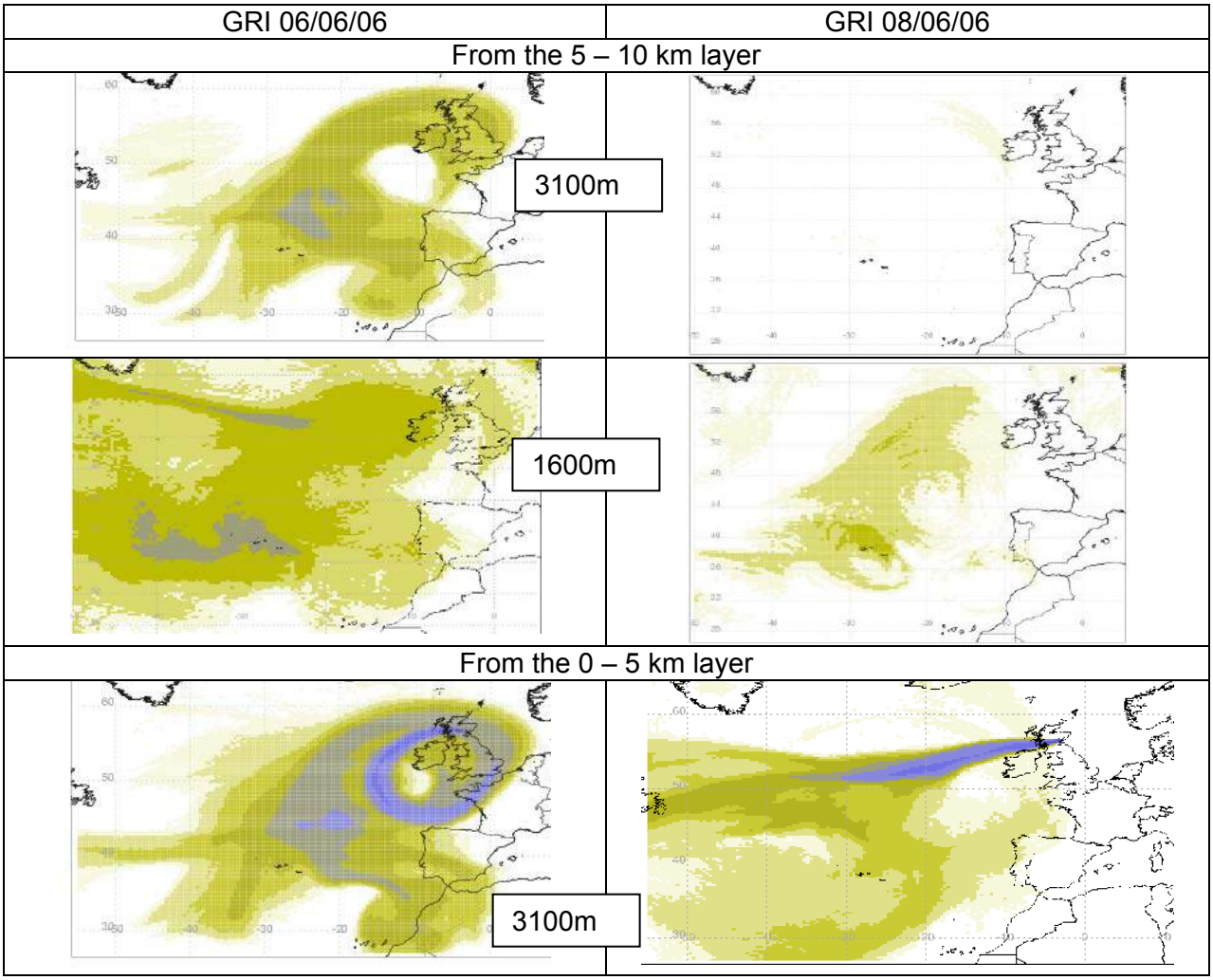

Figure 170: Contribution to 3100m and 1600 m levels from the 0 – 5 km and 5 – 10 km layers, for GRI on 06/06/06 and 08/06/06.

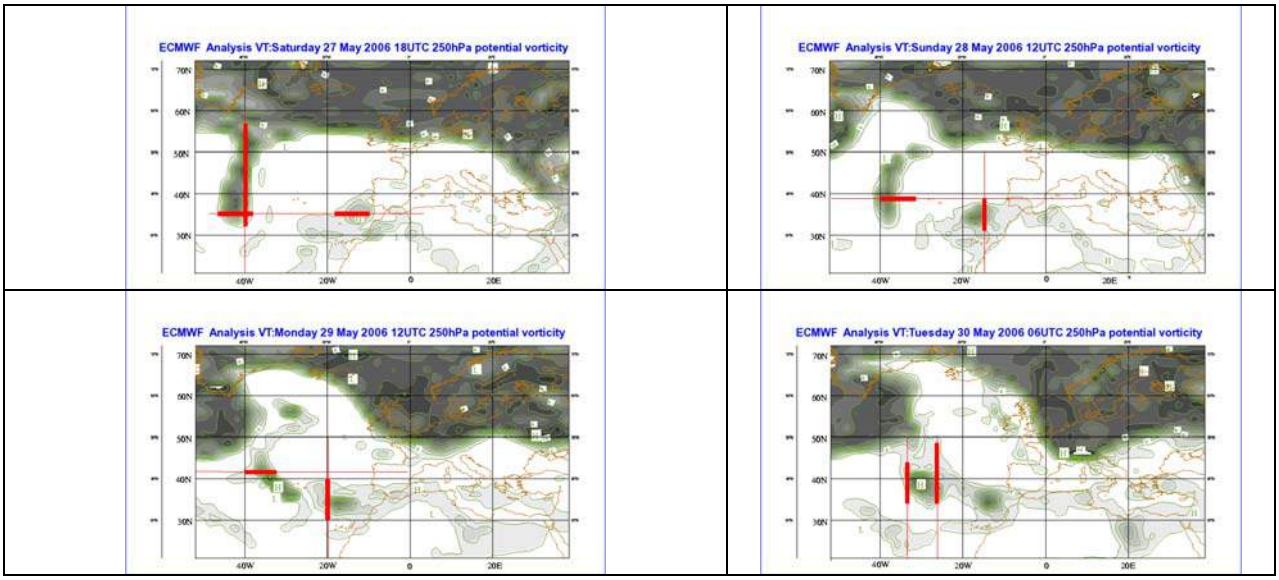

Figure 171: Potential vorticity on the 250 hPa surface for 27/5/06 (top left), 28/5/06 (top right), 29/5/06 (bottom left) and 30/5/06 (bottom right).

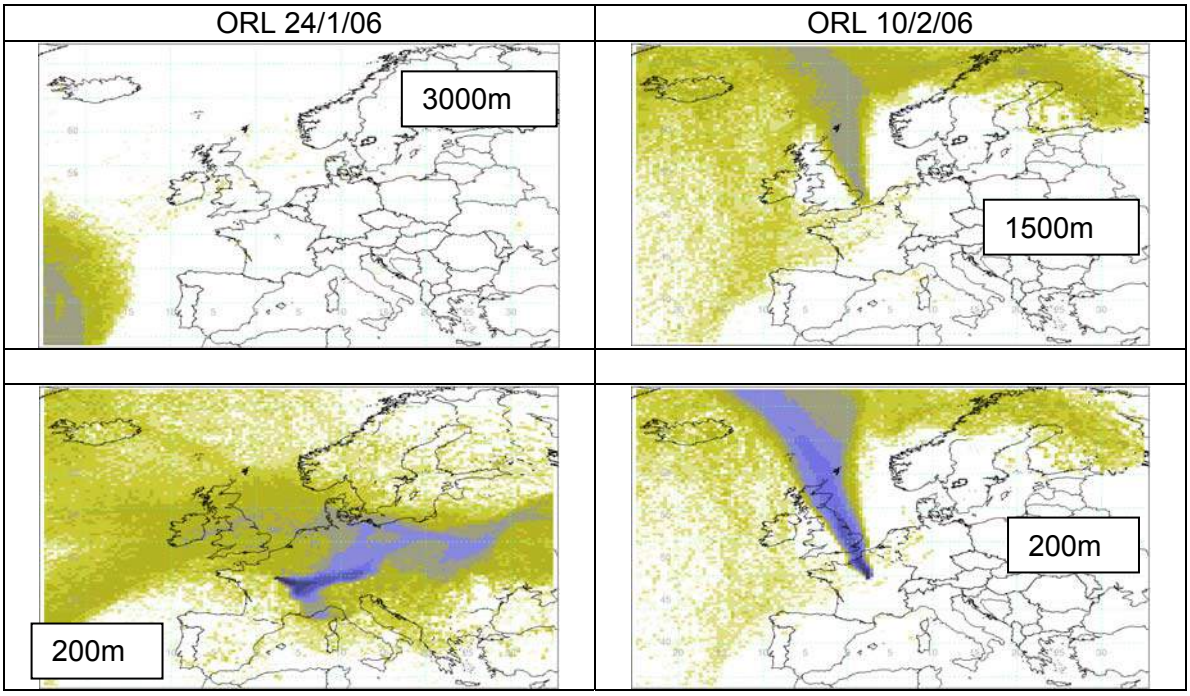

Figure 172: Surface origin of air to 3000m (top) and 200m (bottom) for ORL on 24/1/06 (left) and 13/3/06 (right).

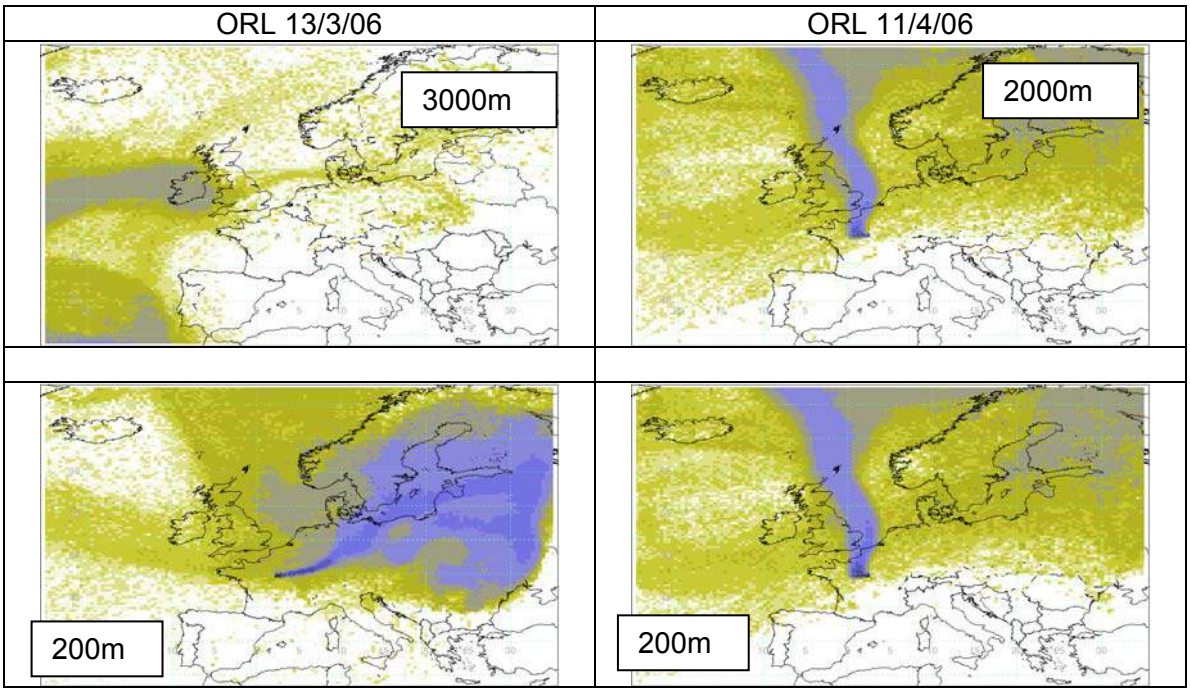

Figure 173: Surface origin of air to 3000m (top) and 200m (bottom) for ORL on 13/3/06 (left) and 11/4/06 (right).

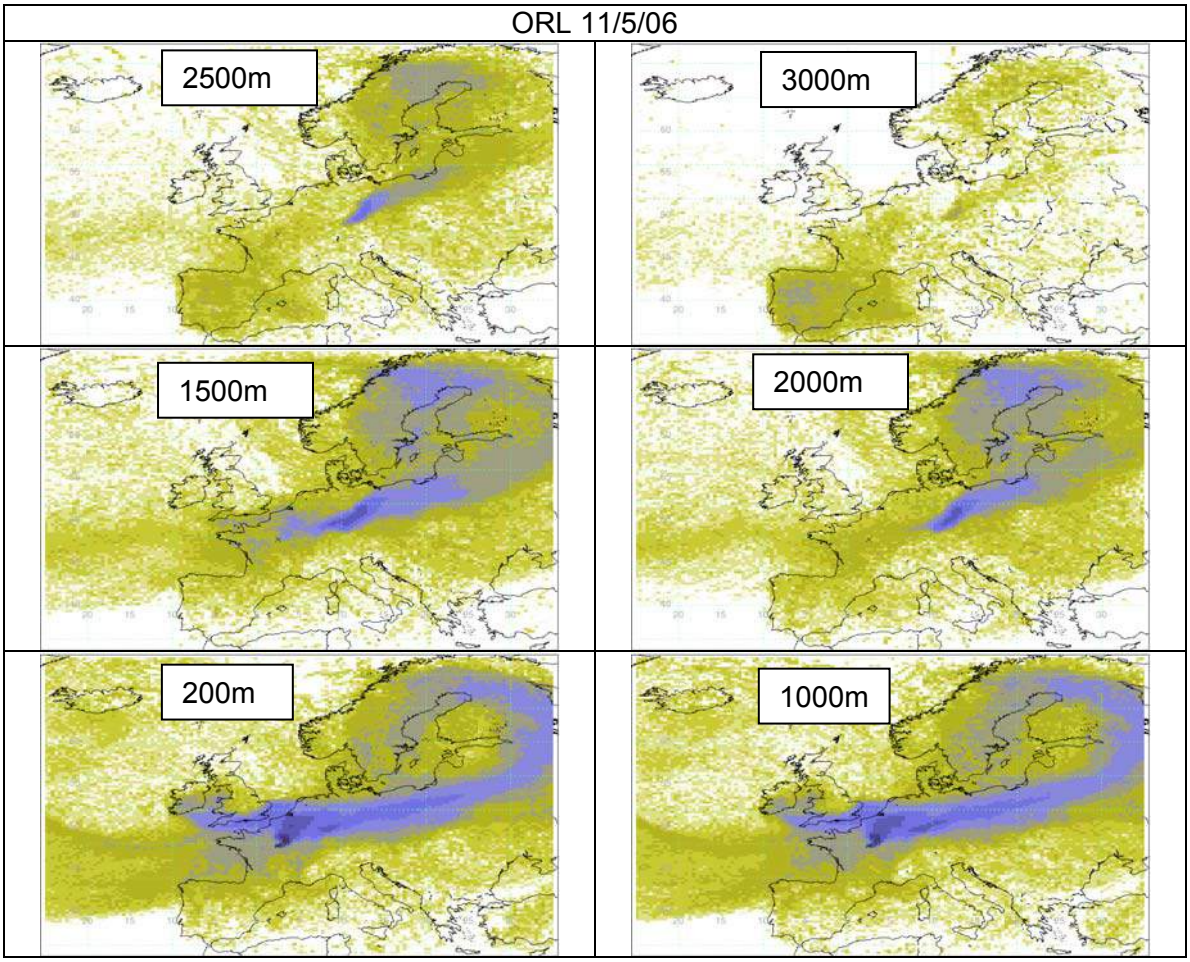

Figure 174: Surface origin of air to various heights for ORL on 11/5/06.

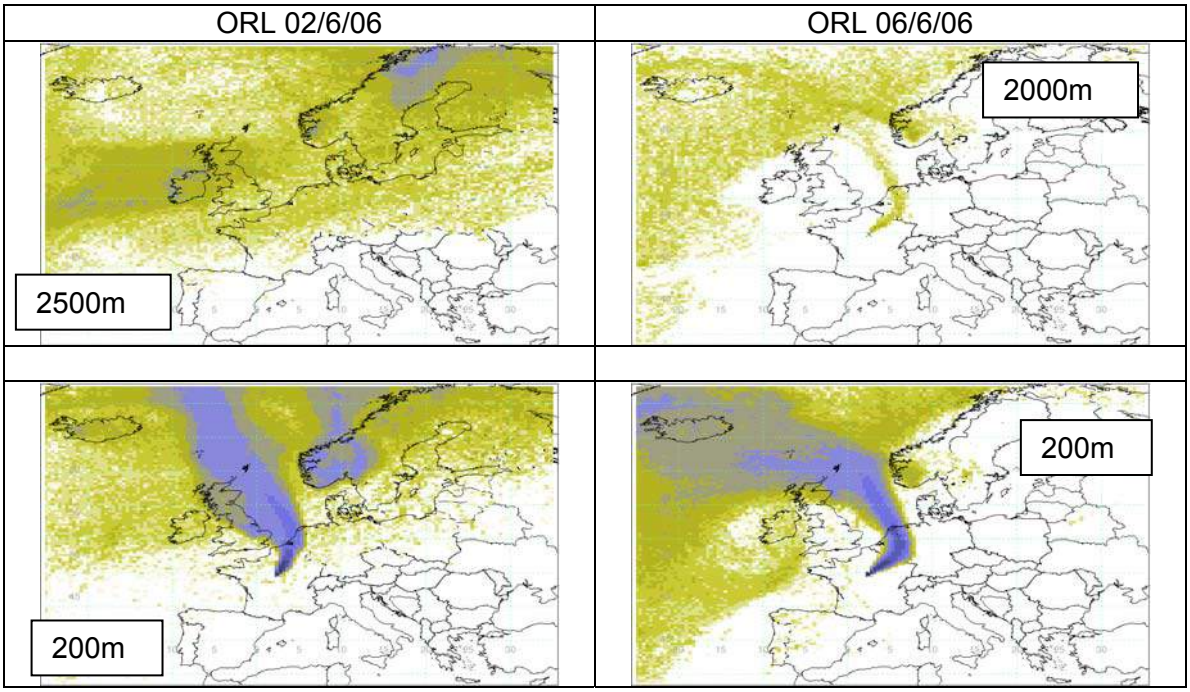

Figure 175: Surface origin of air to 3000m (top) and 200m (bottom) for ORL on 2/6/06 (left) and 6/6/06 (right).

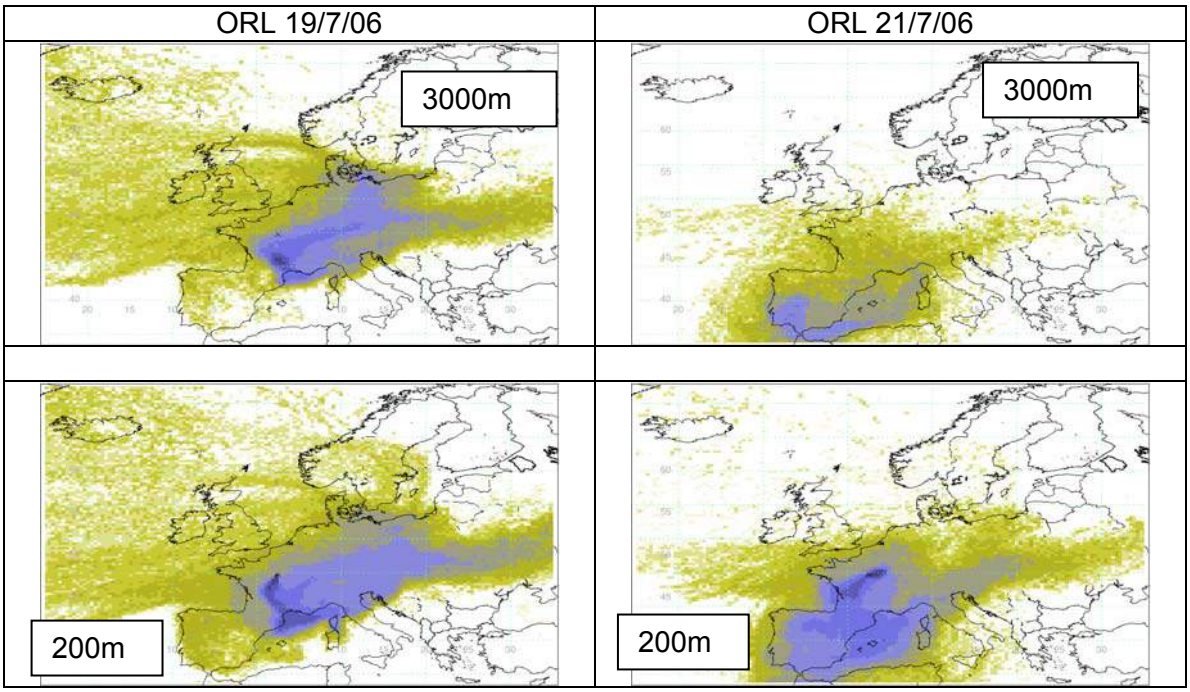

Figure 176: Surface origin of air to 3000m (top) and 200m (bottom) for ORL on 19/7/06 (left) and 21/7/06 (right).

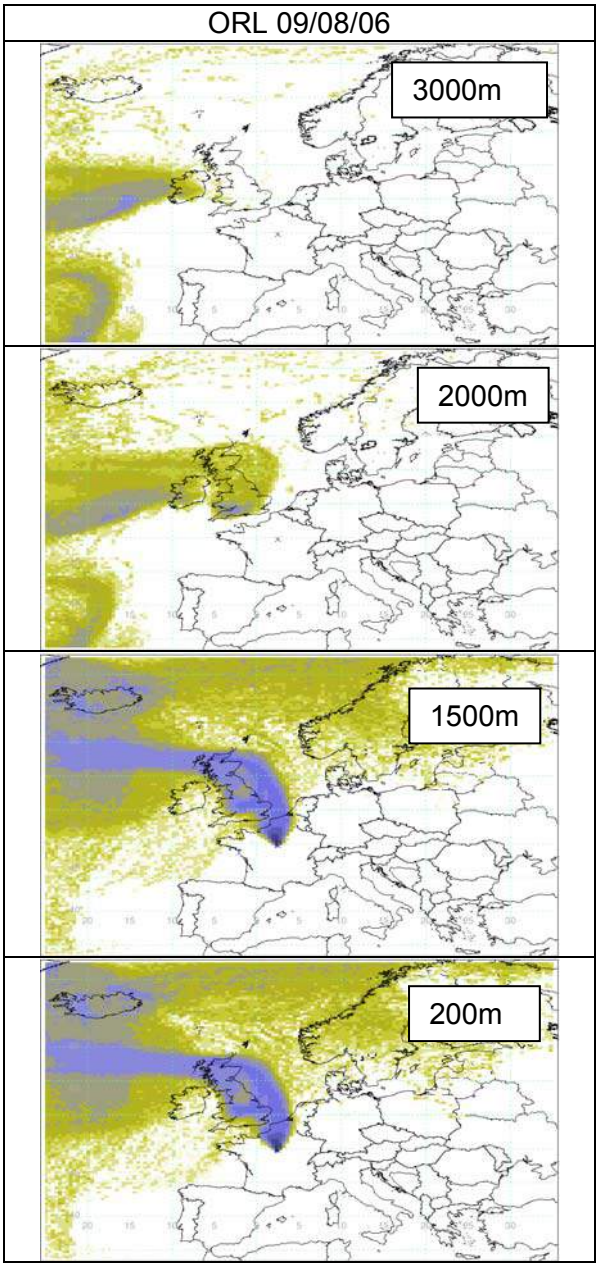

Figure 177: Surface origin of air for ORL on 9/8/06, at various heights.

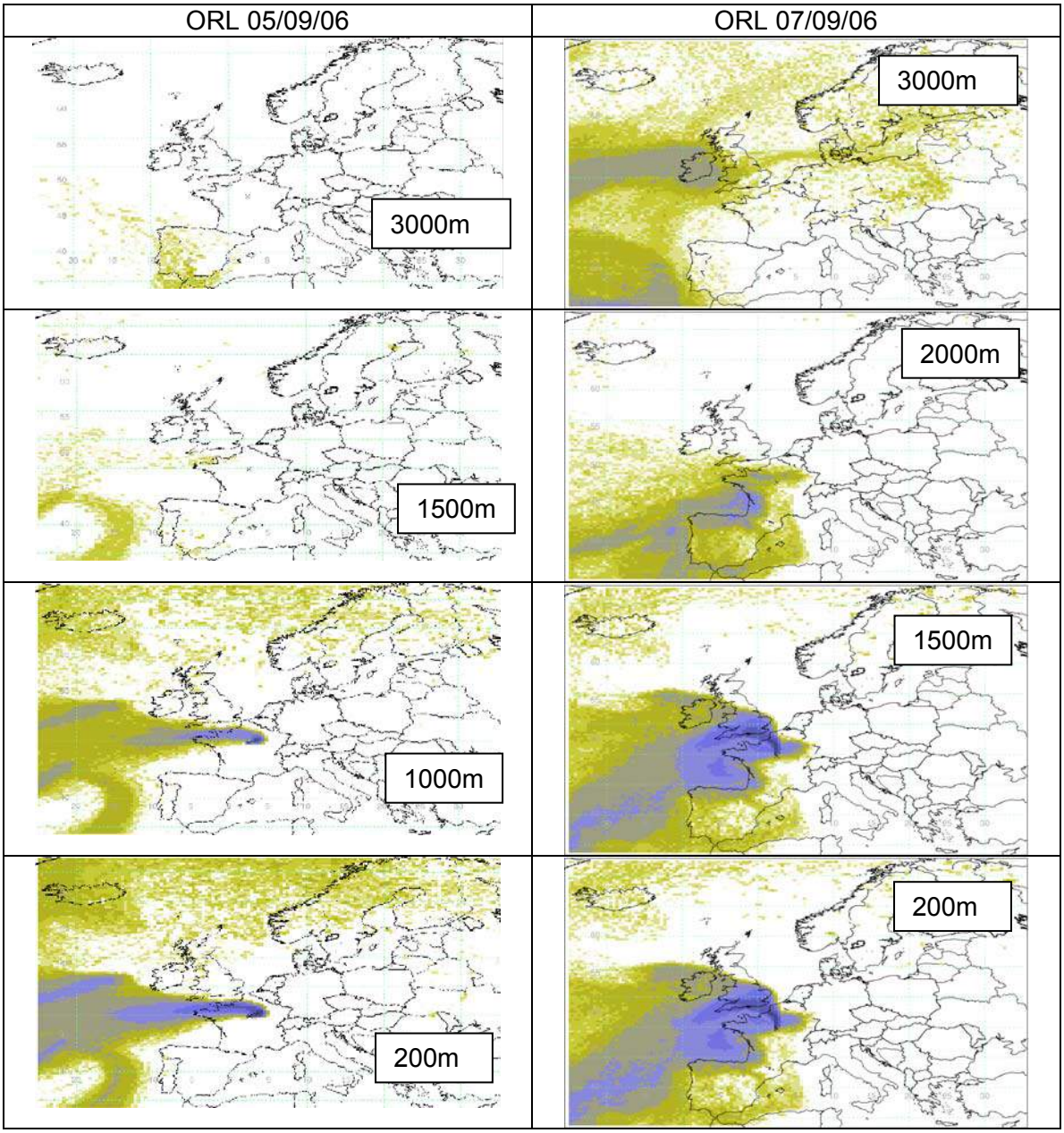

Figure 178: Surface origin of air for ORL on 5/9/06 (left) and 7/9/06 (right) at various heights.

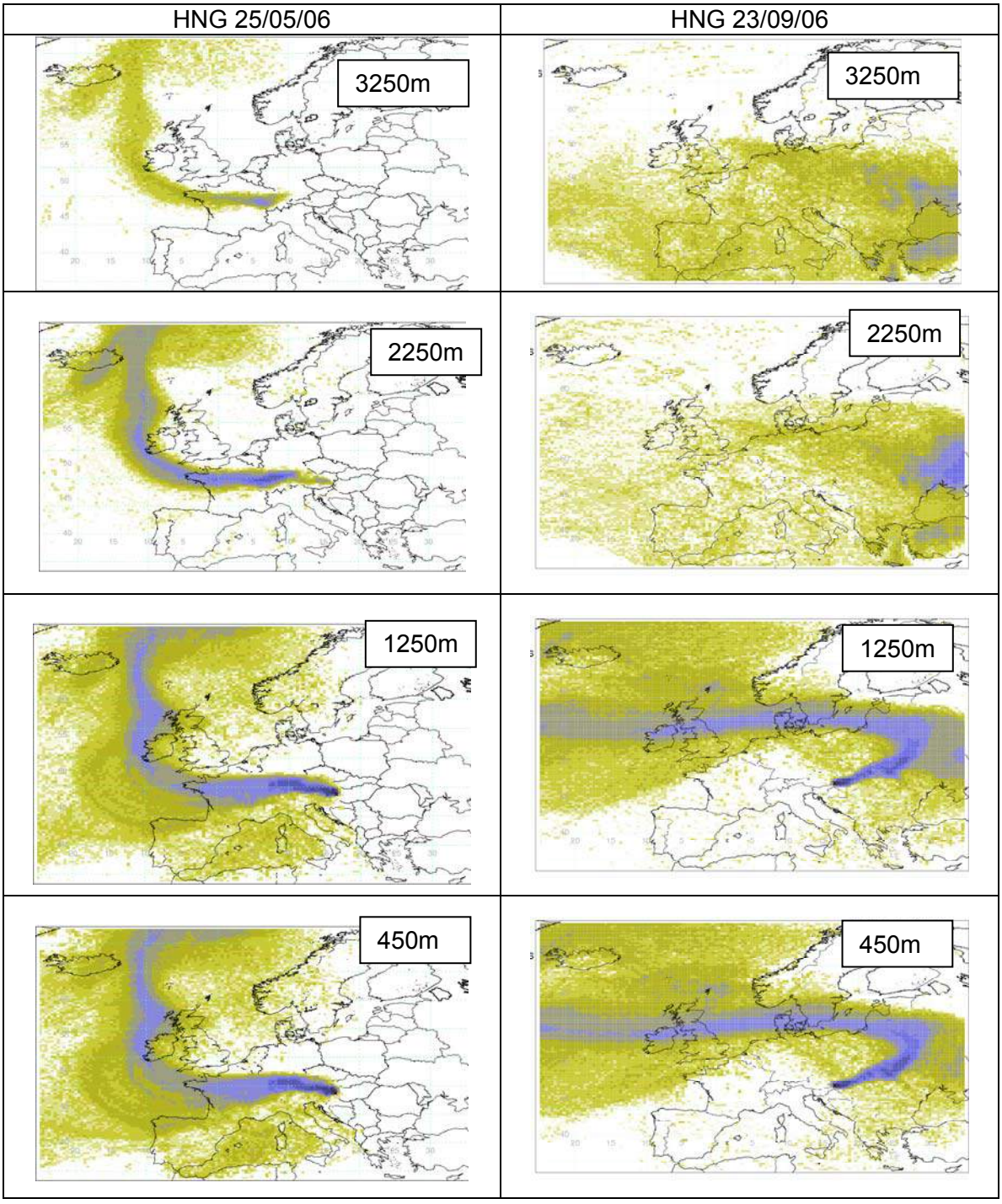

Figure 179: Surface contribution for HNG on 25/05/06 (left) and 23/9/06 (right) at various heights.

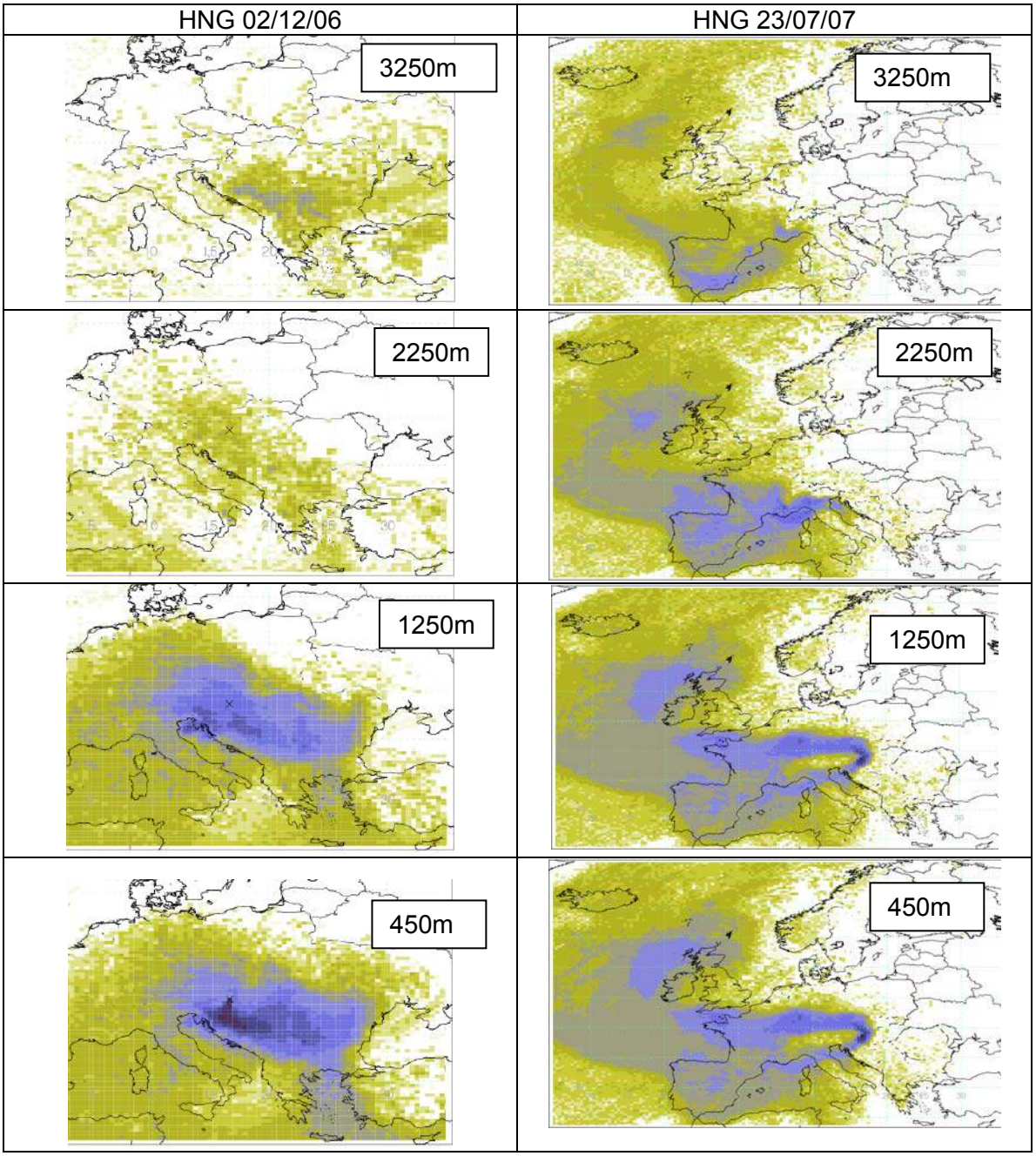

Figure 180: Surface contribution for HNG on 2/12/06 (left) and 23/7/07 (right) at various heights.

7 References

Athanassiadou, M., A. J. Manning, P. Bergamaschi, (2011), The NAME-Inversion Method in the Nitro Europe project, Proceedings of 14th Conference on Harmonisation within Atmospheric Dispersion Modelling for Regulatory Purposes – 2-6 October 2011, Kos, Greece, H14-248, p 627-631, http://www.harmo.org/conferences/Proceedings/_Kos/downloadItem.asp?CID=248

Baker, A. R., S. M. Turner, W. J. Broadgate, A. Thompson, G. B. McFiggans, O. Vesperini, P. D. Nightingale, P. S. Liss, and T. D. Jickells, Distribution and Sea-Air Fluxes of Biogenic Trace Gases in the Eastern Atlantic Ocean, *Global Biogeochemical Cycles*, *14*(3), 871–886, 2000.

Bassford, M. R., G. Nickless, P. G. Simmonds, A. C. Lewis, M. J. Pilling, and M. J. Evans, The concurrent observation of methyl iodide and dimethyl sulphide in marine air; implications for sources of atmospheric methyl iodide, *Atmospheric Environment*, *33*(15), 2373–2383, doi:10.1016/S1352-2310(98)00403-8, 1999.

Bergamaschi, P., M. Krol, J. F. Meirink, F. Dentener, A. Segers, J. van Aardenne, S. Monni, A. Vermeulen, M. Schmidt, M. Ramonet, C. Yver, F. Meinhardt, E. G. Nisbet, R. Fisher, S. O'Doherty, and E. J. Dlugokencky, (2010), Inverse modeling of European CH4 emissions 2001-2006, J. Geophys. Res., 115(D22309), doi:10.1029/2010JD014180.

Cohan, D. S., G. A. Sturrock, A. P. Biazar, and P. J. Fraser, Atmospheric Methyl Iodide at Cape Grim, Tasmania, from AGAGE Observations, *Journal of Atmospheric Chemistry*, *44*(2), 131–150, doi:10.1023/A:1022481516151, 2003.

Corazza, M., P. Bergamaschi, A. T. Vermeulen, T. Aalto, L. Haszpra, F. Meinhardt, S. O'Doherty, R. Thompson, J. Moncrieff, E. Popa, M. Steinbacher, A. Jordan, E. J. Dlugokencky, C. Brühl, M. Krol, and F. Dentener, (2011), Inverse modelling of European N2O emissions: Assimilating observations from different networks, Atmos. Chem. Phys., 11 (doi:10.5194/acp-11-2381-2011), 2381–2398.

Cox, M. L., G. A. Sturrock, P. J. Fraser, S. T. Siems, P. B. Krummel, and S. O'Doherty, Regional sources of methyl chloride, chloroform and dichloromethane identified from AGAGE observations at Cape Grim, Tasmania, 1998–2000, *Journal of Atmospheric Chemistry*, *45*(1), 79–99, 2003.

Daniel, J.S., and G.J.M Velders (Lead Authors), A.R. Douglass, P.M.D. Forster, D.A. Hauglustaine, I.S.A. Isaksen, L.J.M. Kuijpers, A. McCulloch, and T.J. Wallington, Halocarbon scenarios, ozone depletion potentials, and global warming potentials, Chapter 8 in Scientific Assessment of Ozone Depletion: 2006, Global Ozone Research and Monitoring Project—Report No. 50, 572 pp., World Meteorological Organization, Geneva, Switzerland, 2007.

European Union, DECISION No 455/2009/EC OF THE EUROPEAN PARLIAMENT AND OF THE COUNCIL of 6 May 2009 amending Council Directive 76/769/EEC as regards restrictions on the marketing and use of dichloromethane, *Official Journal of the European Union*, 2009.

Forster, P., V. Ramaswamy, (Coordinating Lead Authors), P. Artaxo, T. Berntsen, R. Betts, D.W. Fahey, J. Haywood, J. Lean, D.C. Lowe, G. Myhre, J. Nganga, R. Prinn, G. Raga, M. Schulz, and R. Van Dorland, Changes in atmospheric constituents and in radiative forcing, Chapter 2 in Climate Change 2007: The Physical Science Basis. Contribution of Working Group I to the Fourth Assessment Report of the Intergovernmental Panel on Climate Change, edited by S. Solomon, D. Qin, M. Manning, Z. Chen, M. Marquis, K.B. Averyt, M. Tignor, and H.L. Miller, 996 pp., Cambridge University Press, Cambridge, U.K., and New York, NY, U.S.A., 2007.

Fraser, P.J., D.E. Oram, C.E. Reeves, S.A. Penkett, and A. McCulloch, Southern Hemispheric halon trends (1978-1998) and global halon emissions, J. Geophys. Res., 104 (D13), 1598515999, 1999.

Jones, A.R., D.J. Thomson, M. Hort, and B. Devenish (2007), The U.K. Met Office's next-generation atmospheric dispersion model, NAME III, *Proceedings of the 27th NATO/CCMS International Technical Meeting on Air Pollution Modelling and its Application*, Springer, 580-589.

Keene, W., M. Khalil, D. Erickson, A. McCulloch, T. Graedel, J. Lobert, M. Aucott, S. Gong, D. Harper, G. Kleiman, P. Midgley, R. Moore, C. Seuzaret, W. Sturges, C. Benkovitz, V. Koropalov, L. Barrie, and Y. Li, Composite global emissions of reactive chlorine from anthropogenic and natural sources: Reactive Chlorine Emissions Inventory, *Journal of Geophysical Research-Atmospheres*, *104*(D7), 8429–8440, 1999.

Keller, C.A, D. Brunner, S. Henne, M.K. Vollmer, S. O'Doherty, S. Reimann, Evidence for under-reported Western European emissions of the potent greenhouse gas HFC-23, *Geophys. Res. Lett.,* **38**, L15808, doi:10.1029/2011GL047976, 2011.

Manning, A. J., S. O'Doherty, A. R. Jones, P. G. Simmonds, and R. G. Derwent (2011), Estimating UK methane and nitrous oxide emissions from 1990 to 2007 using an inversion modeling approach, *J.Geophys.Res.*, 116, D02305, doi:10.1029/2010JD014763.

Meirink, J. F., P. Bergamaschi, and M. Krol, (2008), Four-dimensional variational data assimilation for inverse modelling of atmospheric methane emissions: Method and comparison with synthesis inversion, Atmos. Chem. Phys., 8, 6341–6353.

Montzka, S. A., S. Reimann, A. Engel, K. Kruger, S. O'Doherty, W. T. Sturges, D. Blake, M. Dorf, P. Fraser, L. Froidevaux, K. Jucks, K. Kreher, M. J. Kurylo, A. Mellouki, J. Miller, O.-J. Nielsen, V. L. Orkin, R. G. Prinn, R. Rhew, M. L. Santee, A. Stohl, and D. Verdonik, Ozone-Depleting Substances (ODSs) and Related Chemicals, Chapter 1, in *Scientific Assessment of Ozone Depletion: 2010*, World Meteorological Organization, Geneva, Switzerland. 2011.

O'Doherty S, Cunnold, D.M Miller, B.R., Mühle, J. McCulloch, A. Simmonds, P.G. Manning, A.J. Reimann, S. Vollmer, M.K. Greally, B.R. Prinn, R.G. Fraser, P.J. Steele, L.P. Krummel P.B., Dunse, B.L. Porter, L.W. Lunder, C.R. Schmidbauer, N. Hermansen, O. Salameh, P.K. Harth, C.M. Wang R.H.J. and Weiss R.F., Global and regional emissions of HFC-125 (CHF_2CF_3) from in situ and air archive atmospheric observations at AGAGE and SOGE observatories J. Geophys. Res., J. Geophys. Res., 114, D23304, 2009.

Parrish, D.D., Law, K.S., Staehelin, J., Derwent, R.G., Cooper, O.R., Tanimoto, H., Volz-Thomas, A., Gilge, S., Scheel, H.-E., Steinbacher, M., Chan, E., 2012. Long-term changes in lower tropospheric baseline ozone concentrations at northern mid-latitudes. Atmos. Chem. Phys. Discussions, submitted.

Prinn, R.G., Weiss, R.F., Fraser P.J.,. Simmonds P.G, Cunnold D.M., Alyea F.N, O'Doherty S., Salameh P., Miller B.R., Huang J., Wang R.H.J., Hartley D.E., Harth C., Steele L.P., Sturrock G., Midgley P.M., and McCulloch A., A history of chemically and radiatively important gases in air deduced from ALE/GAGE/AGAGE: 1978-2000. J. Geophys. Res., 105, (2000), No. D14, 17751-17792.

Ramonet, M., P. Ciais, I. Nepomniachii, K. Sidorov, R.E.M. Neubert, U. Langendorfer, D. Picard, V. Kazan, S. Biraud, M. Gusti, O. Kolle, E.D. Schulze, and J. Lloyd, Three years of aircraft-based trace gas measurements over the Fyodorovskoye southern taiga forest, 300 km

north-west of Moscow, Tellus Series B-Chemical and Physical Meteorology, 54 (5), 713-734, 2002.

Rödenbeck, C., C.Gerbig, K.Trusilova, and M. Heimann, (2009), A two-step scheme for high-resolution regional atmospheric trace gas inversions based on independent models, *Atmos. Chem. Phys*., 9, 5331-5342.

Schmidt M., M. Ramonet, B. Wastine, M. Delmotte, P. Galdemard, V. Kazan, C. Messager, A. Royer, C. Valant, , I. Xueref and P. Ciais, (2006), RAMCES: The French Network of Atmospheric Greenhouse Gas Monitoring, WMO/GAW report 168, (http://www.wmo.int/pages/prog/arep/gaw/gaw-reports.html).

UNEP (United Nations Environment Program), *2002 Report of the Solvents, Coatings and Adhesives Technical Options Committee - 2002 Assessment (STOC 2002)*, edited by B. Ellis, UNEP Ozone Secretariat, Nairobi, Kenya. 2003.

WDCGG, 2012. Summary 36. GAW Data. Volume IV – Greenhouse gases and other atmospheric gases. World Data Center for Greenhouse Gases. Japan Meteorological Agency, Japan.

Weissflog, L., C. A. Lange, A. Pfennigsdorff, K. Kotte, N. Elansky, L. Lisitzyna, E. Putz, and G. Krueger, Sediments of salt lakes as a new source of volatile highly chlorinated C1/C2 hydrocarbons, *Geophysical Research Letters*, *32*(1), L01401, 2005.

WMO, 2011. Greenhouse gas bulletin No. 7, World Meteorological Organisation, Geneva, Switzerland.

Yokouchi, Y., Y. Nojiri, L. A. Barrie, D. Toom-Sauntry, and Y. Fujinuma, Atmospheric methyl iodide: High correlation with surface seawater temperature and its implications on the sea-to-air flux, *Journal of Geophysical Research*, *106*(D12), 12,661–12,668, doi:200110.1029/2001JD900083, 2001.